

January 2016

FAST-PYROLYSIS OF BIOMASS RELATED MODEL COMPOUNDS: A NOVEL APPROACH TO EXPERIMENTAL STUDY AND MODELING

John Charles Degenstein
Purdue University

Follow this and additional works at: https://docs.lib.purdue.edu/open_access_dissertations

Recommended Citation

Degenstein, John Charles, "FAST-PYROLYSIS OF BIOMASS RELATED MODEL COMPOUNDS: A NOVEL APPROACH TO EXPERIMENTAL STUDY AND MODELING" (2016). *Open Access Dissertations*. 1403.
https://docs.lib.purdue.edu/open_access_dissertations/1403

This document has been made available through Purdue e-Pubs, a service of the Purdue University Libraries. Please contact epubs@purdue.edu for additional information.

**PURDUE UNIVERSITY
GRADUATE SCHOOL
Thesis/Dissertation Acceptance**

This is to certify that the thesis/dissertation prepared

By John C. Degenstein

Entitled

FAST-PYROLYSIS OF BIOMASS RELATED MODEL COMPOUNDS: A NOVEL APPROACH TO EXPERIMENTAL STUDY AND MODELING

For the degree of Doctor of Philosophy

Is approved by the final examining committee:

Rakesh Agrawal

Co-chair

Fabio H. Ribeiro

Co-chair

W. Nicholas Delgass

Hilkka I. Kenttamaa

To the best of my knowledge and as understood by the student in the Thesis/Dissertation Agreement, Publication Delay, and Certification Disclaimer (Graduate School Form 32), this thesis/dissertation adheres to the provisions of Purdue University's "Policy of Integrity in Research" and the use of copyright material.

Approved by Major Professor(s): Fabio H. Ribeiro and Rakesh Agrawal

Approved by: John A. Morgan

Head of the Departmental Graduate Program

2/18/2016

Date

FAST-PYROLYSIS OF BIOMASS RELATED MODEL COMPOUNDS:
A NOVEL APPROACH TO EXPERIMENTAL STUDY AND MODELING

A Dissertation

Submitted to the Faculty

of

Purdue University

by

John C. Degenstein

In Partial Fulfillment of the

Requirements for the Degree

of

Doctor of Philosophy

May 2016

Purdue University

West Lafayette, Indiana

For my family and friends.

ACKNOWLEDGMENTS

I want to begin by thanking the many people who have helped me during my Ph.D. I have to start by thanking my co-advisors Professors Rakesh Agrawal, W. Nicholas Delgass and Fabio H. Ribeiro and my committee member, and close collaborator, Professor Hilkkka I. Kenttämäaa. Without their guidance and support, my Ph.D. would simply not have been possible and I feel very fortunate to have had all of them actively involved in my research.

Professor Agrawal was someone who taught me to think of the bigger picture impacts of even discoveries that might have seemed relatively small at first. He also taught me to keep an eye on the future, and never to be married inseparably from a particular approach.

Next I want to thank Prof. Delgass who brought a positive and encouraging attitude to every interaction I had with him. His technical sense in science was incredibly helpful and led me to suggest very significant changes to the course of my research project. The advice Prof. Delgass has given me during my time at Purdue will stick with me for the rest of my life, ranging in everything from the aforementioned scientific advice to how to manage interpersonal relationships.

Professor Ribeiro has been a fantastic teacher, and I often think back to how much my perception of the science of catalysis and Chemical Engineering has changed since coming to Purdue as a result of his teaching. Fabio was often a man of few words, but I quickly learned that his advice was often very well timed and accurate. From him, I also learned to approach the results of research with greater skepticism; that there is almost always an explanation for what you might observe that exists within the realm of existing knowledge. While this may sound as if Fabio is simply a nay-sayer I think it is a reflection of his high standards in research and his desire to make lasting

contributions to science. When I came to Purdue, I did not have a solid opinion of what fundamental research truly means, but I can say now that there is both enormous room and need for this approach to science.

I must also thank my committee member Professor Hilkka Kenttämä, who has treated me as one of her group from the very beginning of my time working with her. I have really appreciated the environment she has created in her group and I was able to really step outside of my comfort zone in expanding my areas of knowledge to include research related to both chemical analysis and organic chemistry. It was through her leadership that I was able to form a very important collaboration with Dr. John Nash and McKay Easton who have made extremely valuable contributions related to my research. I very much appreciate Prof. Kenttämä's frank and honest attitude and her support of both my research and me as a person.

Thank you to the staff of the School of Chemical Engineering as well. I would like to thank a few in particular, Debra Bowman, Katie Fields, Courtney Eddy, Corwin Green, and Beverly Johnson. A big thank you is also due to Yury Zvinevich for his dedicated help in troubleshooting and building reactors.

I must thank the ChE biomass group members that I have had the pleasure of working with, both past (Drs. Piotr Gawecki, Sara Yohe, Vinod Kumar Venkatakrishnan, Dharik Mallapragada, Dhairya Mehta, and Harshavardhan Choudhari) and present (Emre Gencer, McKay Easton, Richard Caulkins, Ian Smith, Taufik Ridha, Abhijit Talpade). Also I must thank the members of Hilkka's group both past (Drs. Matt Hurt, David Borton, Alex Dow, Huaming Sheng, Nelson Vinueza, Vanessa Gallardo, Jinshan Gao, Chris Marcum, Tiffany Jarrell, James Riedeman, and Linan Yang) and present (Priya Murria, Hanyu Zhu, Laurance Cain, and Joann Max). I have to give special thanks to Priya Murria, who has been a very close collaborator of mine that I have very much enjoyed working with, who has tirelessly driven our research to a higher level. I also have to give special thanks to Matt Hurt who I also worked with closely on this project and was also a great collaborator on this project. Next, a special thanks to McKay Easton who was a great collaborator with whom

I am very grateful for the synergy of his theoretical results with our experimental results. Also, thank you to Drs. Huaming Sheng and Jinshan Gao who contributed their valuable synthesis experience to synthesize very useful model compounds used in this study. I am so fortunate to have worked with such a large group of researchers with such diverse backgrounds!

To all of the catalysis group members I have worked with thank you for all the great presentations and discussions I have had the pleasure to attend. I must specially thank with the following catalysis group people; Paul Dietrich, Shane Bates, Vince Kispersky, Mike Detwiler, Amir Gharachorlou, Kaiwalya Sabnis, Atish Parekh, Jamie Harris, Yanran Cui, Viktor Cybulskis, Arthur Shih, and Shankali Pradhan.

I must also thank the fantastic friends I have made at Purdue, many of whom are already listed above. Here are a few of my great friends from Purdue that were not already mentioned; Nathan J. Davis, Brian Graeser, Dan Pohlman, Steven Mcleod, Aditya Baradwaj, George Weeden, Kevin Brew, Mark Koeper, Chuck Hages, Nathan Carter, Renay Su, and Betty Yang.

I must thank my family for their support and guidance through my doctorate. I am very fortunate for my family's love and support, which enabled me to pursue my passion for scientific research.

This work would not have been possible without the financial support from US Department of Energy and the National Science Foundation. I was supported, in part, by National Science Foundation Emerging Frontiers in Research and Innovation (EFRI) under Award #0938033. This research was also supported as part of the Center for Direct Catalytic Conversion of Biomass to Biofuels (C3Bio), an Energy Frontier Research Center funded by the U.S. Department of Energy (DOE), Office of Science, Basic Energy Sciences (BES), under Award #DE-SC0000997.

TABLE OF CONTENTS

	Page
LIST OF TABLES	x
LIST OF FIGURES	xiii
ABSTRACT	xxi
1 Introduction	1
1.1 Research Objectives	3
1.2 Thesis Objectives	3
2 On-Line Mass Spectrometric Methods for the Determination of the Primary Products of Fast Pyrolysis of Carbohydrates and for Their Gas-Phase Manipulation	5
2.1 Introduction	5
2.2 Experimental Section	7
2.2.1 Materials	7
2.2.2 Mass Spectrometry	7
2.2.3 Pyroprobe	8
2.2.4 Determination of the Primary Products of Fast Pyrolysis of Cellobiose	9
2.2.5 Apparatus for Exploring the Reactivity of the Primary Products of Fast Pyrolysis	9
2.3 Results and Discussion	10
2.4 Conclusions	20
2.5 Acknowledgements	22
3 High-pressure fast-pyrolysis, fast-hydroxy-pyrolysis and catalytic hydrodeoxygenation of cellulose: Production of liquid fuel from biomass	23
3.1 Introduction	23
3.2 Experimental Methods	25
3.2.1 Reactor Design	25
3.3 Experimental Approach	28
3.3.1 Liquid Product Analysis	32
3.3.2 Liquid-chromatography mass-spectrometry (LC-MS) method development	33
3.3.3 Materials	34
3.4 Results and Discussion	35

	Page	
3.4.1	High-pressure cellulose fast-pyrolysis products	35
3.4.2	Effect of temperature in high-pressure cellulose fast-pyrolysis	37
3.4.3	Effect of hydrogen in cellulose fast-hydroxylation and compar- ison of reactor performance with reaction pressure, at 480°C	39
3.4.4	Effect of hydrogen in cellulose fast-hydroxylation (25 bar H ₂) at 580°C	41
3.4.5	Effect of candidate catalysts for HDO of cellulose fast-hydro- xylation vapors	43
3.5	Conclusions	46
3.6	Acknowledgements	47
4	Mass Spectrometric Studies of Fast Pyrolysis of Cellulose	51
4.1	Introduction	51
4.2	Experimental Methods	53
4.3	Results and Discussion	53
4.4	Conclusions	58
4.5	Acknowledgments	58
5	Fast Pyrolysis of ¹³ C-Labeled Cellobioses: Gaining Insights into the Mecha- nisms of Fast Pyrolysis of Carbohydrates	60
5.1	Acknowledgements	67
6	Determination of the Primary Fast Pyrolysis Products of Synthetic G-Lignin Oligomers with β -O-4 linkages via On-Line Mass Spectrometry	69
6.1	Introduction	69
6.2	Results and Discussion	73
6.2.1	Comparison of the primary fast pyrolysis products of 1-4	75
6.2.2	Insights into the mechanisms of fast pyrolysis of β -O-4 lignin tetramer 3: concerted nonradical elimination mechanisms vs radical mechanisms	80
6.3	Conclusions	83
6.4	Experimental Methods	85
6.4.1	Materials	85
6.4.2	Mass Spectrometry	85
6.4.3	Pyrolysis	86
6.4.4	Determination of the primary products of fast pyrolysis of lignin model compounds	86
7	Fast Pyrolysis of Guaiacyl Lignin Model Compounds with β -O-4 Linkages	87
7.1	Introduction	87
7.2	Experimental Methods	90
7.2.1	Reactor Description	90
7.2.2	Loading and Reactor Operation	91
7.2.3	Product Identification and Quantification	93

	Page
7.2.4 Model Compound Synthesis	93
7.3 Results	93
7.3.1 Quantitative analysis of dimeric molecules using a GC/MS	93
7.3.2 Pyrolysis of Dimer 1	95
7.3.3 Pyrolysis of Trimer 2, Tetramer 3, Trimer 4 and Polymer 5	97
7.4 Discussion	99
7.4.1 Product distribution from lignin model compounds	99
7.4.2 Char Formation	102
7.4.3 Effect of Vapor Phase Residence Time	106
7.4.4 Primary Products of Lignin Pyrolysis	108
7.5 Conclusions	110
8 A Synergistic Biorefinery Based on Catalytic Conversion of Lignin Prior to Cellulose Starting from Lignocellulosic Biomass	111
8.1 Introduction	111
8.2 Selective Catalytic Conversion of Lignin	112
8.3 Carbohydrate Residue Retains its Value	116
8.4 Genetic Variants Control Products	118
8.5 Lignin-Derived Fuel and Chemical Platform	119
8.6 Conclusion	122
8.7 Materials and Methods	123
8.8 Acknowledgements	124
9 A Novel Theory of the Physical and Chemical Processes of Pyrolysis	125
10 Summary	129
BIBLIOGRAPHY	131
A Supporting Information for On-Line Mass Spectrometric Methods for the Determination of the Primary Products of Fast Pyrolysis of Carbohydrates and for Their Gas-Phase Manipulation	155
B Supporting Information for High-pressure fast-pyrolysis, fast-hydroxylation and catalytic hydrodeoxygenation of cellulose: Production of liquid fuel from biomass	157
B.1 Screw feeder design	157
B.2 High pressure reactor design	157
B.2.1 Fast-hydroxylation Reactor	157
B.2.2 Downstream fixed-bed vapor-phase hydrodeoxygenation (HDO) Reactor	158
B.2.3 Condenser and Gas/Liquid Separation	159
C Supporting Information for Mass Spectrometric Studies of Fast Pyrolysis of Cellulose	165
C.1 Pyrolysis Probe - Mass Spectrometer Residence Time Experimental	165

	Page
C.2 Pyrolysis Probe - Gas Chromatograph / Mass Spectrometer	167
D Supporting Information for Fast Pyrolysis of ¹³ C-Labeled Cellobioses: Gain- ing Insights into the Mechanisms of Fast Pyrolysis of Carbohydrates	169
D.1 Synthesis of Labeled Cellobioses.	169
E Supporting Information for Determination of the Primary Fast Pyrolysis Products of Synthetic G-Lignin Oligomers with β -O-4 linkages via On-Line Mass Spectrometry	175
F Supplementary Information for Fast Pyrolysis of Guaiacyl Lignin Model Compounds with β -O-4 Linkages	180
F.1 Estimation of Lights, CO, and CO ₂	180
F.2 Estimation of Water	180
F.3 Char Yield versus Coniferyl Alcohol	181
G Supplementary Information for A Synergistic Biorefinery Based on Catalytic Conversion of Lignin Prior to Cellulose Starting from Lignocellulosic Biomass	187
G.1 HPLC/MS Analysis	187
G.1.1 Instrumentation	187
G.1.2 High-performance liquid chromatography/high-resolution tan- dem mass spectrometry	187
G.1.3 Quantitation of aromatic products from lignin conversion	191
G.2 Determination of Lignin Content in Washed Biomass	192
G.2.1 Acetyl Bromide Soluble Lignin (ABSL)	193
G.3 Determination of Carbohydrates	194
G.3.1 Liquid Fraction	194
G.3.2 Solid Residue	194
G.4 Enzymatic Hydrolysis	195
G.4.1 Pd/C free solid residue	195
G.5 Pyrolysis of the Cellulosic Solid Residue from the Biomass	196
G.6 Hydrodeoxygenation Reaction of Dihydroeugenol to Hydrocarbons, Propy- l-cyclohexane and Propylbenzene - Continuous Vapor-Phase Reactor	197
G.6.1 Calculating % Yield	197
G.7 Hydrodeoxygenation Reaction of Dihydroeugenol and 2,6-Dimethoxy- 4-propylphenol to Hydrocarbons, Propylcyclohexane and Propylbenzene - Micro-Scale Pulse Reactor	199
VITA	201

LIST OF TABLES

Table	Page	
2.1	Approximated average relative molar abundances of the primary products of fast pyrolysis of cellobiose normalized to the most abundant product (with standard deviations based on three experiments).	16
3.1	Experimental conditions and product distribution [†] summary for experiments of cellulose fast-pyrolysis.	29
3.2	Experimental conditions and product distribution [†] summary for experiments of cellulose fast-hydrolysis without HDO catalyst.	30
3.3	Experimental conditions for experiments of catalytic HDO of cellulose fast-hydrolysis vapors and base case experiment without HDO catalyst.	31
3.4	Elemental analysis (carbon, hydrogen and oxygen), water content, H/C ratio, O/C ratio extent of deoxygenation (dry basis) from fast-hydrolysis experiments with candidate HDO catalysts and base case comparison with fast-hydrolysis experiment without HDO catalyst. Dry cellulose: (O/C) = 0.83, (H/C) = 1.67.	44
7.1	List of the GC columns tested with the relevant parameters.	92
7.2	Lumped pyrolysis products of dimer 1 as a function of the columns tested.	96
7.3	Lumped pyrolysis products of tetramer 3 as a function of the columns tested.	96
7.4	Quantified pyrolysis product distribution (wt% of starting model compound) of various lignin model compounds.	98
7.5	Relative abundances of identified monomeric pyrolysis products normalized with respect to coniferyl alcohol (4-(3-hydroxyprop-1-en-1-yl)-2-methoxyphenol).	103
8.1	Conversion of lignin starting with intact lignocellulosic biomass over Zn/Pd/C catalyst.	115
B.1	Chemical compounds identified and quantified for LC-MS analysis of liquid products from all experiments.	162
C.1	Quantitative pyrolysis product distribution produced from the Pyrolysis-GC/MS reactor for pyrolysis of cellotriosan and cellulose.	168

Table	Page
E.1 All major tetrameric, trimeric, dimeric and monomeric pyrolysis product ions of 1-3 with m/z, relative abundances and fragment sequences. Water (W) and formaldehyde (F) losses are also indicated. Ions in bold are parent fragment ions.	176
E.2 CAD of small lignin products produced upon pyrolysis of β -O-4 G-Lignin tetramer along with proposed structures.	177
F.1 Predicted boiling point of the lignin model compounds aim to show the relative volatility of the model compounds. Boiling point predicted via Joback fragmentation method modified by S.E. Stein.	182
F.2 Weight percentage of monomeric species based on the number of carbon atoms in the molecule.	182
F.3 Elution time for dimer 1 for each of the different columns tested.	182
F.4 Quantified lumped pyrolysis product distribution from coniferyl alcohol in wt% of the reactant.	183
F.5 Quantified pyrolysis product distribution from dimer 1 as a function of the vapor phase residence time in wt% of the reactant.	183
F.6 Quantified pyrolysis product distribution from polymer 5 as a function of the vapor phase residence time in wt% of the reactant.	184
F.7 Detailed pyrolysis product distribution produced from dimer 1 as a function of the vapor phase residence time in wt% of the reactant fed.	185
G.1 HPLC/MS quantitation of all soluble aromatic/phenolic products from lignin conversion and HDO over Zn/Pd/C catalyst in MeOH.	188
G.2 Reaction mass balance after catalytic cleavage and HDO of WT poplar lignin over Zn/Pd/C catalyst.	190
G.3 DFRC analysis of lignin composition for each of the biomass samples.	192
G.4 Acetyl bromide soluble lignin content analysis (ABSL).	193
G.5 Sugar content of the MeOH fraction after extraction of phenolic products from lignin.	194
G.6 Sugar content of the remaining cellulosic solid residue after lignin conversion over Zn/Pd/C as determined via acid hydrolysis with HPLC analysis.	195
G.7 Enzymatic Hydrolysis of Pd/C free biomass residue after reaction under catalytic HDO conditions.	196

Table	Page
G.8 (a) Product yields of the high-pressure, vapor-phase hydrodeoxygenation reaction of 2-methoxy-4-propylphenol (dihydroeugenol) at 100% conversion in the continuous reactor. (b) Comparison of product yields of the high-pressure, vapor-phase hydrodeoxygenation reaction of dihydroeugenol, 2,6-dimethoxy-4-propylphenol and a 50:50 mixture at 100% conversion in the micro-scale pulse reactor and the continuous reactor.	199

LIST OF FIGURES

Figure	Page
2.1 A cut away diagram of the ionization chamber in front of the LQIT. The pyroprobe (in blue) is shown in both the direct pyrolysis (left) orientation and within the flow tube (right). The direction of gas flow is indicated by the dashed arrow.	10
2.2 An APCI/ammonium hydroxide positive ion mass spectrum of an equimolar mixture of six model compounds introduced via direct injection (the molar ratio of glycolaldehyde is estimated to be between 0-2 due to the unknown extent of glycolaldehyde dimer breakdown). All model compounds were ionized but not equally efficiently.	13
2.3 An APCI/chloroform negative ion mass spectrum of an equimolar mixture of six model compounds introduced via the heated pyroprobe (the molar ratio of glycolaldehyde is estimated to be between 0-2 due to the unknown extent of glycolaldehyde dimer breakdown). Three model compounds were not ionized.	14
2.4 Mass spectra of the primary products of fast pyrolysis of cellobiose ionized using ammonium attachment in positive ion mode (top) and chloride attachment in negative ion mode (bottom). All elemental compositions were determined using high resolution data collected in an LQIT/FT-ICR. Ionized levoglucosan has m/z values of 163 and 180 in the top spectrum and m/z values of 161 and 197 in the bottom spectrum. All ions with m/z values lower than 170 correspond to protonated molecules in the top spectrum and deprotonated molecules in the bottom spectrum, and hence have m/z values that differ by two units. Protonated $C_4H_4O_2$ molecule (m/z 85) is only seen in the top spectrum, while deprotonated $C_5H_6O_3$ molecule (m/z 113) is only seen in the bottom spectrum. Otherwise, the spectra show the same ionized molecules. The most abundant product's ($C_8H_{14}O_7$) proposed structure is shown in the top spectrum.	15
2.5 Mass spectra collected after the primary products of fast pyrolysis of cellobiose were allowed to undergo reactions for 2 s at 300°C (top), 2s at 400°C (middle) and 11 s at 400°C (bottom) and ionized using ammonium attachment in positive ion mode. All elemental compositions were determined using high resolution data collected in an LQIT/FT-ICR. All ions with m/z values lower than 170 correspond to protonated molecules.	19

Figure	Page
2.6 CAD mass spectra measured for authentic cellotriosan ionized via chloride attachment in negative ion mode and the unknown trimer (ionized in the same manner) formed upon pyrolysis of cellobiose in the flow tube. The chloride attached cellotriosan and trimer (m/z 521) were isolated and subjected to CAD which resulted in HCl loss, forming fragment ions of m/z 485, corresponding to the deprotonated molecules of cellotriosan and the unknown trimer. These deprotonated molecules were subjected to CAD to obtain the mass spectra shown top left and bottom left, respectively. Both ions produced an abundant fragment ion corresponding to the loss of a molecule with MW 162 Da to yield an ion of m/z 323. The fragment ions of m/z 323 were isolated and subjected to CAD to produce the mass spectra shown top right and bottom right, respectively.	20
3.1 3D model sketch of the reactor system.	27
3.2 Schematic of overall cellulose conversion pathway.	32
3.3 (a) Bar graph showing typical liquid product composition data, from LC/MS analysis, of cellulose fast-pyrolysis at 27 bar total inert pressure in the cyclone-type reactor used in this study. (b) Bar graph showing liquid product composition data of cellulose fast-pyrolysis at 1 bar inert pressure in a fluidized bed reactor, from Patwardhan et al.[6]	36
3.4 Graph showing trends in content of light oxygenate molecules, levoglucosan and its isomers in the liquid products from cellulose fast-pyrolysis at 480°C, 520°C, 550°C and 580°C. All runs were at 25 bar in helium at a total inert pressure of 27 bar.	38
3.5 Variation of liquid and gas yields with pyrolysis temperature in high-pressure cellulose fast-pyrolysis and cellulose fast-hydrolysis at 27 bar total pressure.	39
3.6 Bar graph showing differences in liquid product composition between fast-pyrolysis (25 bar He, 50 bar He) and fast-hydrolysis (25 bar H ₂ , 50 bar H ₂) at 27 bar and 54 bar total pressure with 480°C pyrolysis temperature.	40
3.7 Graph showing differences in content of light oxygenate molecules, water, levoglucosan and its isomers in the liquid products from cellulose fast-pyrolysis and fast-hydrolysis at 580°C pyrolysis temperature.	42

Figure	Page
3.8 Comparison of (a) product yields and (b) gas phase compositions from fast-hydropyrolysis with no HDO catalyst and fast-hydropyrolysis with Al ₂ O ₃ , 2% Ru/Al ₂ O ₃ , 2% Pt/Al ₂ O ₃ candidate HDO catalysts. Reaction conditions: Base case experiment with no HDO catalyst: P _{H₂} = 17 bar, P _{total} = 27 bar, fast-hydropyrolysis temperature = 580°C; Experiments with candidate HDO catalysts: P _{H₂} = 9 bar, P _{total} = 27 bar, catalyst bed temperature = 375°C, weight hourly space velocity (WHSV) = 9 hr ⁻¹ , fast-hydropyrolysis temperature = 550°C.	48
3.9 Comparison of liquid product compositions from fast-hydropyrolysis with no HDO catalyst and fast-hydropyrolysis with Al ₂ O ₃ , 2% Ru/Al ₂ O ₃ , 2% Pt/Al ₂ O ₃ candidate HDO catalysts. Reaction conditions: Base case experiment with no HDO catalyst: P _{H₂} = 17 bar, P _{total} = 27 bar, fast-hydropyrolysis temperature = 580°C; Experiments with candidate HDO catalysts: P _{H₂} = 9 bar, P _{total} = 27 bar, catalyst bed temperature = 375°C, weight hourly space velocity (WHSV) = 9 hr ⁻¹ , fast-hydropyrolysis temperature = 550°C.	49
3.10 Comparison of conversions of levoglucosan and its isomers, glycolaldehyde and formic acid in fast-hydropyrolysis with Al ₂ O ₃ , 2% Ru/Al ₂ O ₃ and 2% Pt/Al ₂ O ₃ candidate HDO catalysts as compared to base case fast-hydropyrolysis with no HDO catalyst.	50
4.1 The carbohydrate molecules studied here contain two to six d-glucose units coupled to each other in a linear manner via β(1-4) linkages, just as in cellulose.	52
4.2 Positive ion mode mass spectra showing the primary products of the fast pyrolysis of cellobiose (top) and cellohexaose (bottom) ionized by APCI with ammonium hydroxide. The ions whose relative abundances differ the most are indicated with dotted lines. Two isomers of levoglucosan were observed, levoglucosan itself (ion of m/z 180) and another isomer (ion of m/z 163). All the structures shown for cellobiose have been identified [9] by CAD mass spectral comparison using authentic compounds.	55
4.3 Positive ion mode mass spectra showing the primary products of the fast pyrolysis of cellotriosan (top) and cellulose (bottom) ionized by APCI with ammonium hydroxide. Some of the ions having the same m/z ratio are indicated with a dotted line.	56
4.4 A positive ion mode mass spectrum showing the primary products of the fast pyrolysis of cellobiosan (m/z 342) ionized by APCI with ammonium hydroxide. The ions of m/z 85, 127, 145, 163, 180, and 195 are also formed for cellotriosan, cellopentosan and cellulose. The ion of m/z 324 results from the loss of H ₂ O from the ion of m/z 342.	57

Figure	Page
4.5	59
<p>A simple schematic of the major fast pyrolysis pathways proposed for oligosaccharides formed from cellulose during fast pyrolysis upon addition of water. The cleavages indicated in red are thought to occur in the middle of a cellulose chain. The cleavages indicated in blue and green likely occur only at the reducing terminals, which for long chains of cellulose represent a small overall fraction of the total units. Hence, they are minor pathways.</p>	
5.1	61
<p>Positive ion-mode mass spectra showing the initial fast-pyrolysis products (either as ammonium adducts or protonated molecules) of (a) glucopyranosyl[1-¹³C]glucose and (b) unlabeled cellobiose ionized by APCI with ammonium hydroxide dopant. The structures of the intact molecules are shown at the far right in each spectrum. The products that are ¹³C-labeled in the top spectrum are connected with red dotted lines to the corresponding unlabeled products in the lower spectrum.</p>	
5.2	65
<p>Positive ion-mode mass spectra showing the initial fast-pyrolysis products (either as ammonium adducts or protonated molecules) of (a)[1-¹³C]glucopyranosylglucose and (b) glucopyranosyl[3-¹³C]glucose ionized by APCI with ammonium hydroxide dopant. The structures of the intact molecules are shown at the far right in each spectrum. The only product that is labeled in the top spectrum but unlabeled in the bottom spectrum is glucose, as indicated by a red dotted line. The ion labeled with * corresponds to an unknown impurity.</p>	
5.3	67
<p>Calculated free energies (kcal mol⁻¹) of intermediates and transition states (square brackets) for the formation of levoglucosan from cellobiose via consecutive losses of one glycolaldehyde (GA) and two ethenediol (EDL) molecules (which are likely to eventually tautomerize to glycolaldehyde) at 600°C obtained at the M06-2X/6-311++G(d,p)//M06-2X/6-311++G(d,p) level of theory. The location of a ¹³C label at C-1 in the reducing end is indicated by a red circle, at C-3 by a blue circle, and at C-5 by a green circle. The mass-to-charge (m/z) ratios are for unlabeled cellobiose. . .</p>	
6.1	71
<p>The proposed phenyl-shift reaction for the β-radical of phenethyl phenyl ether during fast pyrolysis.[121]</p>	
6.2	72
<p>Four proposed routes for the initial decomposition of phenethyl phenyl ether during fast pyrolysis. Routes a and b involve free radical mechanisms. Routes c and d involve retroene and Maccoll reactions, respectively.[13]</p>	
6.3	74
<p>The lignin model compounds (1-4) used in this study. The β-O-4 linkages in compounds 1-3 are in trans relative configuration. Polymer 4 has a ratio of 1:1 for cis/trans β-O-4 linkages. The number n is about 20 for 4.</p>	

Figure	Page
6.4 The negative-mode APCI mass spectra (MS^1) measured for compounds 1-3 after fast pyrolysis.	76
6.5 Proposed structures for several monomeric fast pyrolysis products (detected as deprotonated molecules) of 3. Ion m/z 164 in the box is radical anion.	77
6.6 Dimeric fast pyrolysis products (detected as deprotonated molecules) of 3. Three key pyrolysis product with m/z 515 (a), m/z 391(b) and m/z 319 (c) as well as other pyrolysis products with different degrees of H_2O and CH_2O losses from the key products can be identified.	78
6.7 The negative-mode APCI mass spectrum (MS^1) measured for polymer 4 after fast pyrolysis and the comparison of the monomer and dimer regions for polymer 4 and tetramer 3. The ions of m/z 319 and 271 are not found in the mass spectrum of polymer 4 since 4 does not have the same end units as tetramer 3.	79
6.8 Proposed fast pyrolysis mechanisms for the cleavage of β -O-4 linkages and the elimination of water and formaldehyde. The energy barriers for these processes were calculated at the B3LYP/6-31G(d,p) level of theory.[30]	81
6.9 The top mass spectrum (MS^1) shows all the major primary fast pyrolysis products of compound 3 that were ionized under APCI negative mode. The bottom negative-mode APCI mass spectrum (MS^2) shows the CAD fragment ions of deprotonated 3 introduced into the mass spectrometer using direct injection. Ions marked in bold (m/z 587, 515, 391, 319 and 195) are key pyrolysis products formed through Maccoll elimination from deprotonated 3 without H_2O and CH_2O losses.	83
6.10 The proposed primary products for fast pyrolysis of 3. Compound 3 yields trimer, dimer and monomer fragments via concerted Maccoll elimination (E) upon rapid heating. Simultaneous water and formaldehyde losses also occur during this process. The resulting products are evaporated off the ribbon surface, ionized and detected by the mass spectrometer.	84
7.1 Lignin model compounds (1-5) used in this study. Numbers inside the rings are for notation purposes only, relevant end groups are highlighted in blue.	94
7.2 Two pathways observed during pyrolysis of dimer 1.	100
7.3 Structures of the major products from pyrolysis of lignin model compounds.	101
7.4 Transformation of trimer 2 to potential products via pathway 1.	104

Figure	Page
7.5 Char yield as a function of the degree of polymerization of the lignin model compounds.	105
7.6 Yield of products from pyrolysis of dimer 1 as a function of vapor phase residence time. Dimer 1 (squares), Monomeric species (triangles), Coniferyl alcohol(circles), 2-methoxy-4-(2-(2-methoxyphenoxy)vinyl)phenol (diamonds).	108
7.7 Yield of products from pyrolysis of polymer 5 as a function of vapor phase residence time. Dimeric species (squares), Monomeric species (triangles).	109
8.1 Selective depolymerization and hydrodeoxygenation (HDO) of lignin first from wood biomass to give a lignin-derived hydrocarbon platform and glucose from the carbohydrate residue.	113
8.2 Single ion monitoring ESI(-)/HPLC/MS of lignin products (m/z 165 and m/z 195) from (a) WT-717 poplar and (b) 717-F5H, a high-S transgenic line. CAD MS/MS of (c) deprotonated 2,6-dimethoxy-4-propylphenol and (d) deprotonated dihydroeugenol derived from WT-717 poplar.	114
8.3 Mass balance after catalytic cleavage and HDO of WT poplar lignin over Zn/Pd/C catalyst. *Mass of phenolic products includes all quantified phenolics and also accounts for the loss of O into H ₂ O during HDO. Liquid Phase sugars were quantified by HPLC analysis. The solid phase residue was hydrolyzed with acid. Then glucose, arabinose, and xylose were quantified by HPLC analysis.	117
8.4 Positive mode ammonium attachment Atmospheric Pressure Chemical Ionization mass spectra measured for fast pyrolysis [9] products of (a) WT-LORRE poplar, (b) carbohydrate residue from WT poplar after our one-step catalytic conversion of lignin over Zn/Pd/C, and (c) pure crystalline cellulose.	118
8.5 Pathways for the production of renewable fuels (in blue) and chemicals (in green) from the lignin portion of biomass. Methoxypropylphenols can be used as is for the fragrance industry (dihydroeugenol), or can be catalytically tailored to fuels (such as propylbenzene and toluene) or used for the production of chemicals (such as propane, methanol, benzene, cumene, para-xylene, ethylbenzene, styrene, phenol, and acetone).	121
9.1 A new model for pyrolysis that utilizes reactions in both the intermediate liquid and gas phases. The liquid droplet is assumed to be at a uniform temperature and composition and shrinks from an initial size due to evaporation and reaction, which is modeled by a semi-batch reactor. The gas-phase is also assumed to be at a uniform temperature and composition, but conforms more closely to a CSTR model due to the continuous gas flow. (Note: not drawn to scale)	127

Figure	Page
A.1 Mass spectra collected after the primary products of fast pyrolysis of cellobiose were allowed to undergo reactions for 2 s at 300°C (top), 2s at 400°C (middle) and 11 s at 400°C (bottom) and ionized using chloride attachment in negative ion mode. All elemental compositions were determined using high resolution data collected in an LQIT/FT-ICR. All ions with m/z values lower than 170 correspond to deprotonated molecules.	156
B.1 Picture of high pressure biomass screw feeder.	158
B.2 Cross section view of high-pressure cyclone-type fast-hydropyrolysis reactor.	159
B.3 Cross section view of downstream fixed-bed vapor-phase HDO reactor.	160
B.4 Process flow diagram of the complete reactor system along with the hydrogen safety systems like hydrogen detectors, automatic shut-off valves, excess flow valves, redundant pressure relief and emergency exhaust. . .	161
B.5 Simplified schematic of the LC-MS setup for the analysis of liquid products from all experiments. Model numbers of the Agilent LC-MS modules are shown below each unit. Relevant analysis method parameters are shown above each unit.	163
B.6 LC-MS calibrations of the 14 chemical compounds used for quantification	164
C.1 A block diagram showing the set-up for ex-situ temperature measurements for the pyroprobe.	165
C.2 A block diagram showing the set-up for in-situ residence plus analysis time measurements for the pyrolysis/MS setup.	166
D.1 Synthesis of Glucopyranosyl[3- ¹³ C]glucose	170
D.2 Synthesis of Glucopyranosyl[5- ¹³ C]glucose	172
E.1 The CAD pattern of m/z 319 isolated from the pyrolysis spectrum of 3 is the same as the CAD pattern of authentic dimer using direct inject. . .	175
E.2 The CAD pattern of m/z 271 isolated from the pyrolysis spectrum of 3 is the same as the CAD pattern of m/z 271 from authentic dimer using direct inject.	178
E.3 The CAD pattern of m/z 515 isolated from the pyrolysis spectrum of 3 is the same as the CAD pattern of m/z 515 from authentic 1 using direct inject.	179
F.1 Structure of lignin model compound Dimer 1 and predicted lignin fragment Dimer 6.	181

Figure	Page
F.2 Schematic of experimental setup (Py-GC/MS) for pyrolysis studies with Lignin model compounds. Red box indicates the heated zone (T=300°C).	186
F.3 Char yield and coniferyl alcohol fraction in the vapor phase pyrolysis products as a function of the degree of polymerization of the lignin model compounds.	186
G.1 (a) HPLC/MS and (b) HPLC/UV spectra of poplar WT-LORRE 225°C and 500 psig H ₂ in MeOH for 12 hours (c) HPLC/UV spectra of organosolv poplar.	191
G.2 Pyrolysis of unreacted raw eucalyptus WT (a) and eucalyptus WT residue (b) in Ammonium Positive Attachment mode.	197

ABSTRACT

Degenstein, John C. PhD, Purdue University, May 2016. Fast-Pyrolysis of Biomass Related Model Compounds: A Novel Approach to Experimental Study and Modeling. Major Professors: Rakesh Agrawal, W. Nicholas Delgass, and Fabio H. Ribeiro.

Fast pyrolysis is a potentially attractive method for converting biomass to a low energy-density liquid (bio-oil) that can be further upgraded for use as fuel. Currently there is no agreement concerning the reaction pathways and mechanisms for pyrolysis of any individual component of biomass. This information is important for optimization of the fast-pyrolysis process. The work was divided into four areas, 1–development and validation of analytical methods and reactors, 2–the utilization of these methods to study pyrolysis of biomass and related models, 3–use of available biomass conversion pathways to propose potential integration with the existing fuel and chemicals markets, and 4–a proposed kinetic and multiphase reactor model for the physical and chemical processes that occur during pyrolysis.

In the first area, mass spectrometric methodology was developed for the determination and manipulation of the initial products of fast-pyrolysis of carbohydrates and lignin-related molecules. A fast-pyrolysis probe/linear quadrupole ion trap mass spectrometer combination was used to study the quenched initial fast-pyrolysis products, those that first left the hot pyrolysis surface. The quenched products were ionized in an atmospheric pressure chemical ionization (APCI) source infused with one of two ionization reagents, chloroform or ammonium hydroxide, to aid in ionization. Liquid chromatography-mass spectrometry (LC-MS) methods were also developed and utilized for quantitative characterization of the liquid products from a lab-scale pyrolysis reactor.

In the second area, the aforementioned pyrolysis probe / mass spectrometric methodology was used to study pyrolysis of cellulose (and related models), of lignin model compounds, and of biomass. Based on several observations, the fast pyrolysis of cellulose is suggested to initiate predominantly via two competing processes: the formation of anhydro-oligosaccharides, such as cellobiosan, cellotriosan, and cellopen-tosan (major route), and the elimination of glycolaldehyde (or isomeric) units from the reducing end of oligosaccharides formed from cellulose during fast pyrolysis. Several products were shown to result entirely from fragmentation of the reducing end of cellobiose, leaving the nonreducing end intact in these products. These findings are in disagreement with mechanisms proposed previously.

Also, in the second area, fast-pyrolysis of several guaiacyl β -O-4 lignin model compounds was studied using both pyrolysis mass spectrometry and pyrolysis gas-chromatography mass spectrometry. The results indicate that the lignin oligomers undergo a number of different types of reaction pathways including Maccoll elimination, homolytic bond dissociation, and elimination of formaldehyde and water.

Also in the second area, a lab-scale, high-pressure, continuous-flow fast-hydro-pyrolysis and vapor-phase catalytic hydrodeoxygenation (HDO) reactor was tested with cellulose as a model biomass feedstock while varying temperature, pressure and gas composition. The major compounds in the liquid from cellulose fast-pyrolysis (27 bar, 520°C) are levoglucosan and its isomers, formic acid, glycolaldehyde, and water, constituting 51 wt%, 11 wt%, 8 wt% and 24 wt% of liquid respectively. The formation of permanent gases (CO, CO₂, CH₄) and glycolaldehyde and formic acid increased with increasing pyrolysis temperature in the range of 480°C-580°C in high-pressure cellulose fast-pyrolysis, in the absence of hydrogen. Our results showed that high pressures of hydrogen did not have a significant effect on the fast-hydro-pyrolysis of cellulose at 480°C but suppressed the formation of reactive light oxygenate species like glycolaldehyde and formic acid at 580°C.

In the third area, over 50% yield of oxygenated hydrocarbons was obtained from the lignin fraction of biomass using a novel Zn/Pd/C catalyst. Genetically modi-

fied poplar enhanced in syringyl (S) monomer content yielded only a single product, dihydroeugenol. Lignin-derived methoxyphenols can be deoxygenated further to propylcyclohexane. This effective conversion of lignin enables several newly proposed conversion pathways to useful fuels and chemicals based on conversion of lignin into intact hydrocarbons.

In the fourth area, a new kinetic and multiphase reactor model for the physical and chemical processes that occur during pyrolysis is proposed. This model helps explain the observed difference in average molecular weight between the pyrolysis probe / mass spectrometric reactor and reactors with higher gas-phase temperatures.

1. INTRODUCTION

With the environmental concerns associated with utilizing petroleum-based resources, new economically competitive sources of fuels and chemicals based upon renewable resources are needed. In addition to this, domestic energy security can be enhanced by utilizing renewable fuel resources, which is particularly important for countries that produce less fuel than they consume. There are several routes to produce fuels and/or chemicals from lignocellulosic biomass including gasification together with Fischer-Tropsch, enzymatic saccharification with fermentation, catalytic fast-pyrolysis, and fast-pyrolysis combined with downstream hydrodeoxygenation (HDO) among many others. Fast-pyrolysis, which is defined as the rapid heating of material in the absence of oxygen up to at least $\sim 400^{\circ}\text{C}$, is a potentially viable approach to produce both fuel and chemical precursors from lignocellulosic biomass. Fast-pyrolysis combined with HDO has been recently demonstrated as a capable process to produce drop-in hydrocarbons (some of which are in the fuel range) directly from biomass in as little as 20 seconds.[1]

Fast-pyrolysis also has several other advantages over the other aforementioned biomass conversion processes. Enzymatic saccharification and fermentation have the key disadvantages of typically producing ethanol which is not a drop-in fuel, they lose CO_2 sourced from lignocellulosic biomass during cell respiration and they only convert the cellulosic component of biomass. Furthermore, typical enzymatic saccharification processes utilize extremely long residence times of ~ 72 hours, which increases capital expenditures. Loss of CO_2 during cell respiration is a critical disadvantage which leads to overall carbon recoveries from biomass that are $\sim 35\%$. This means that in the long term, greater land resources are required to meet the world's transportation needs. Indeed, even the ability to utilize large amounts of ethanol is in question

in the United States since starch-based ethanol has reached the upper limit of the “blending wall” as a gasoline additive. This means that additional ethanol which is produced from new sources such as from lignocellulosic biomass has a limited and uncertain market and must directly compete with the existing starch-based ethanol producers. Drop-in hydrocarbon fuels, on the other hand, can compete directly with neat gasoline for which both the market and potential impact are much larger.

Biomass itself is composed of 3 major structural components; lignin, hemicellulose and cellulose. The structures of these components *in planta* may vary season-to-season, plant-to-plant and species-to-species. Cellulose is the largest component by weight of lignocellulosic biomass and also possesses the simplest polymeric structure, with between hundreds and thousands of dehydrated glucose building blocks linked together via glycosidic bonds.[2, 3] Thus, cellulose and related glucosaccharides are logical starting points for the study of biomass pyrolysis and as of 2016 have been the subject of numerous pyrolysis studies.[1, 4–11]

Lignin is another major component of biomass, and due to its relatively low carbon-to-oxygen ratio, contains the most carbon and has the highest energy density.[12] Furthermore, lignin is composed of monomers with aromatic rings which are desirable for both fuel and chemicals applications. Detailed studies of pyrolysis of lignin are still lacking due to the use of either model compounds that are too simple [13], extracted from biomass [14] or with a structure that is not the same as any linkage commonly found in plants [15]. Extracted lignin is not a good model for lignin *in planta* because it has been shown that the extraction process breaks many of the common β -O-4 linkages that are present in biomass.[16]

Lastly, hemicellulose is a cross linked polymeric network of 5 and 6-carbon sugars which are mainly xylose but also contain arabinose, glucose and galactose.[17] Studies concerning pyrolysis of hemicellulose are also lacking due to the use of extracted hemicellulose [18] and a lack of studies of pyrolysis of the related small oligomeric sugars, as was undertaken with cellulose/glucosaccharides. It is not known if the extraction process destroys the hemicellulose structure as has been shown with lignin, but the

substructural complexity of hemicellulose does indicate the need to perform more detailed studies of models that contain the different substructural features present *in planta*.

1.1 Research Objectives

Pyrolysis has been an active area of research for several decades, and many researchers have studied pyrolysis of cellulose in particular. Despite this enormous literature of prior experimental and some recent computational results we sought to learn more via both a novel experimental approach, but also in direct conjunction with theory. Our novel experimental approach has thus far involved use of an apparatus which quickly quenches and analyzes the products of pyrolysis. Our hypothesis is that being able to analyze volatile products of any size will allow us to gain insights into reaction pathways and mechanisms which heretofore were not possible. On top of this, we have utilized this methodology to readily ascertain the fate of isotopic labels selectively incorporated into model compounds.

1.2 Thesis Objectives

The primary goal of the research in this dissertation centers around furthering understanding pyrolysis of the various aforementioned components of biomass via an approach that involves the heavy use of surrogate model compounds with some of the same features as the *in planta* components. In Chapter 2 the development of the original methods for pyrolysis - mass spectrometry are described in detail as well as pyrolysis data from pyrolysis of cellobiose (a dimeric model for cellulose). Next, in Chapter 3 results of fast-hydrolysis and hydrodeoxygenation of cellulose was attempted using some initial candidate catalysts, and the lab-scale reactor system was described in detail. In Chapters 4 and 5 detailed study of a range of cellulose model compounds was performed, combining theory, experimental results and isotopic labeling. In Chapters 6 and 7, pyrolysis of several β -O-4 lignin model compounds is

reported using pyrolysis - mass spectrometry (along with a related new pyrolysis - mass spectrometry method) and pyrolysis - GC/MS in each chapter respectively. In Chapter 8 a new technology for extracting and upgrading lignin is reported, along with pyrolysis - mass spectrometry of the initial biomass and residues and a vision for using lignin in the existing fuel and chemicals markets. Lastly, in Chapter 9 a proposed kinetic multiphase model for pyrolysis of glucosaccharides is described.

2. ON-LINE MASS SPECTROMETRIC METHODS FOR THE DETERMINATION OF THE PRIMARY PRODUCTS OF FAST PYROLYSIS OF CARBOHYDRATES AND FOR THEIR GAS-PHASE MANIPULATION

2.1 Introduction

With declining light petroleum resources along with various environmental concerns of petroleum based energy, new fuel sources are needed.[19–21] Fast pyrolysis, the rapid heating of material in the absence of oxygen, is a potentially viable approach to produce fuels along with other valuable chemicals from lignocellulosic biomass.[2, 20–23] This is due to the ability of pyrolysis to break down vast polymers into smaller, volatile, carbon containing molecules that retain most of the energy-rich chemical bonds.[24, 25] Cellulose is the most abundant and simplest polymer in biomass, consisting of hundreds to thousands of dehydrated glucose building blocks (molecular weight (MW) 162 Da) linked together via glycosidic bonds.[2, 3] Thus, cellulose and related carbohydrates are a logical starting point for the study of biomass pyrolysis.

Most current carbohydrate fast pyrolysis reactors produce so-called bio-oils that are viscous liquids with several detrimental properties that prevent them from being used as a fuel, including their tendency to degrade over time.[2, 19, 20, 26–30] Bio-oils are complex, oxygen-rich mixtures with roughly half the heating value of gasoline.[26, 28] Hence, they require catalytic upgrading. The upgrading process is hindered by the complexity of bio-oils as well as their compositional dependence on the time and temperature that the primary pyrolysis products experience within the reactor.[29, 31, 32] The first compounds that leave the surface of the pyroprobe ribbon are considered here as the primary products.

To better understand the reactor parameters that lead to the complexity of bio-oils, the primary products of carbohydrate pyrolysis need to be determined. Further,

information on how they react within a pyrolysis reactor is also necessary. The fast pyrolysis reactors used to study carbohydrates have residence times that range from hundreds of milliseconds up to several seconds.[33, 34] Due to the length of these reaction times and the condensation of the products into a liquid oil, which is known to degrade over time, the final liquid pyrolysis products no longer resemble the primary products since they have undergone secondary gas-phase and solution reactions.[2, 32, 35] Previously, in order to address this problem, fast-pyrolysis experiments have been coupled with gas chromatography/mass spectrometry (GC/MS) to carry out on-line studies of primary pyrolysis products.[4–7, 18, 36, 37] Based on these and other studies, levoglucosan is widely believed to be the major primary product of cellulose fast pyrolysis although some studies suggest formation of other small molecules concurrently with the formation of levoglucosan.[4, 7, 38, 39] A serious limitation of the GC/MS approach is that it only allows the determination of relatively volatile and thermally stable compounds. Carbohydrates larger than a single monomeric unit (MW 162 Da) cannot be detected by GC/MS without derivatization.[27, 38, 40]

In order to address above problems, a different on-line mass spectrometric analysis method, without a GC, is needed. Further, this analytical method needs to be coupled with a device capable of very fast pyrolysis (preferably with up to $20,000^{\circ}\text{C} \times \text{s}^{-1}$ heating rate) in order to be able to observe and study the primary products. To achieve these goals, two fast pyrolysis/tandem mass spectrometry systems were devised, one to determine the primary products of carbohydrate fast pyrolysis and another one to study how changes in temperature and residence time change the extent of secondary reactions of the primary products in order to simulate a pyrolysis reactor. The results obtained using both systems for model compounds as well as cellobiose are described below.

2.2 Experimental Section

2.2.1 Materials

Hydroxyacetone (technical grade 90%; CAS 116-09-6), furfural (99%, CAS 98-01-1), 5-hydroxymethylfurfural (99%, CAS 67-47-0), levoglucosan (99%, CAS 498-07-7), chloroform (ChromasolvPlus for HPLC, 99.9% with amylene stabilizer, CAS 67-66-3), and glycolaldehyde dimer (CAS 23147-58-2) were purchased from Sigma Aldrich. Cellobiosan (>95%, CAS 35405-71-1) and cellobiose (~98%, CAS 528-50-7) were purchased from Carbosynth, methanol (Optima LC/MS ~99.9%, CAS 67-56-1) was purchased from Fisher Scientific, ammonium hydroxide (28-30% as NH₃, CAS 1336-21-6) was purchased from Mallinckrodt Chemicals, cellotriosan (98%, CAS 78797-67-8) was purchased from LC Scientific, and compressed nitrogen cylinder (~99.9%, CAS 7727-37-9) was purchased from Indiana Oxygen. All chemicals except for the glycolaldehyde dimer were used without further modification. Glycolaldehyde dimer was converted to monomers (CAS 141-46-8) via dissolving in water and heating at 65°C for 10 minutes.[41]

2.2.2 Mass Spectrometry

Detection and characterization of cellobiose fast pyrolysis products was performed using a Thermo Scientific (Waltham, MA) LTQ linear quadrupole ion trap (LQIT) mass spectrometer coupled with a Finnigan Surveyor Liquid Chromatograph (LC) MS Pump Plus. High resolution data to determine elemental compositions were collected using a 7 Tesla Thermo Scientific LTQ-FT-ICR. Solutions for direct injection experiments of model compounds were made at a concentration of 10⁻⁵ M in 3 mL methanol : water (50 : 50 v/v) with either 200 μL of chloroform for negative ion mode chloride attachment or 200 μL ammonium hydroxide for positive ion mode ammonium attachment. The solutions were pumped into an APCI source via the APCI probe at a rate of 3 μL/min with a solution of methanol : water (50 : 50 v/v) tee-infused from the LC at a rate of 100 μL/min. During pyrolysis experiments,

either chloroform : methanol (50 : 50 v/v) or ammonium hydroxide : water (50 : 50 v/v) solution was pumped into the APCI source via the APCI probe at a rate of 10 $\mu\text{L}/\text{min}$ with a solution of methanol : water (50 : 50 v/v) tee-infused from the LC at a rate of 100 $\mu\text{L}/\text{min}$. The instrumental variables of the LQIT were set to the following values for all experiments: discharge current 5.0 μA , vaporizer temperature 300°C, sheath gas (N_2) flow 40 arbitrary units, auxiliary gas flow (N_2) 10 arbitrary units, sweep gas flow (N_2) 0 arbitrary units, capillary temperature 250°C, capillary voltage -1 V, and tube lens voltage -105 V. Collisionally activated dissociation (CAD) experiments used an ion isolation window of ± 2 Daltons (Da), with the normalized collision energy ranging from 5 up to 30 arbitrary units and activation time being 30 ms. Data collection and processing was carried out using Xcalibur 2.1 software.

2.2.3 Pyroprobe

All pyrolysis experiments were performed using a Pyroprobe 5200 purchased from CDS Analytical (Oxford, PA). The pyroprobe uses a resistively heated platinum ribbon (2.1 mm x 35 mm x 0.1 mm) with the ability to heat at rates up to 20,000°C \times s⁻¹. Based on previous work in other laboratories, platinum is not acting as a catalyst during the pyrolysis experiments.[42, 43] Roughly tens to hundreds of micrograms of sample were loaded onto the platinum ribbon and held onto the surface via electrostatic attractions. This method of loading of the ribbon resulted in a submonolayer of sample on its surface. This was done to ensure rapid and uniform heat transfer to all particles. The ribbon was heated up to 600°C at a rate of 1,000°C \times s⁻¹ resulting in a heating time of 0.6 s. The pyroprobe was maintained at 600°C for 1 s. This final temperature and rate of temperature increase were selected due to minimal char formation (optical observation) under these conditions.

2.2.4 Determination of the Primary Products of Fast Pyrolysis of Cellobiose

The tip on the probe described above was inserted into the ionization chamber of the LQIT through a home-built adaptor that was placed into the unused atmospheric pressure photoionization (APPI) port. This adaptor positioned the platinum ribbon approximately 5 mm in front of and 5 mm below the skimmer cone/inlet of the LQIT. A diagram of this setup is shown in Figure 2.1. Once pyrolysis occurred, the evaporated products were immediately diluted via diffusion into the 2 L ionization chamber and subsequently quenched via collisions with nitrogen gas (at about 100°C), which prevented secondary reactions. The products were ionized and characterized by multi-stage tandem mass spectrometry experiments. For ammonium attachment in positive ion mode, the average standard deviations of the product ions' relative abundances were about 7%. For chloride attachment in negative ion mode, the average standard deviations of the product ions' relative abundances were about 5%.

2.2.5 Apparatus for Exploring the Reactivity of the Primary Products of Fast Pyrolysis

To explore the secondary reactions of the primary pyrolysis products, a home-built aluminum flow tube was constructed to prevent immediate quenching of the primary products. The tip of the pyroprobe was placed in the end of the heated aluminum tube. Preheated nitrogen gas was passed through the flow tube and over the platinum ribbon to sweep the products through the flow tube and into the ionization zone of the LQIT where they were quenched and ionized. A diagram of this setup is also shown in Figure 2.1. To adapt the instrument for the placement of the flow tube into the ionization area, the window in the front door of the ionization chamber was replaced with a piece of ceramic with a hole in the center that had the same diameter as the flow tube. The flow tube and nitrogen gas were kept at the same temperature by using a temperature control system. This configuration allowed the study of the effects of temperature and residence time on the reactions of the primary products

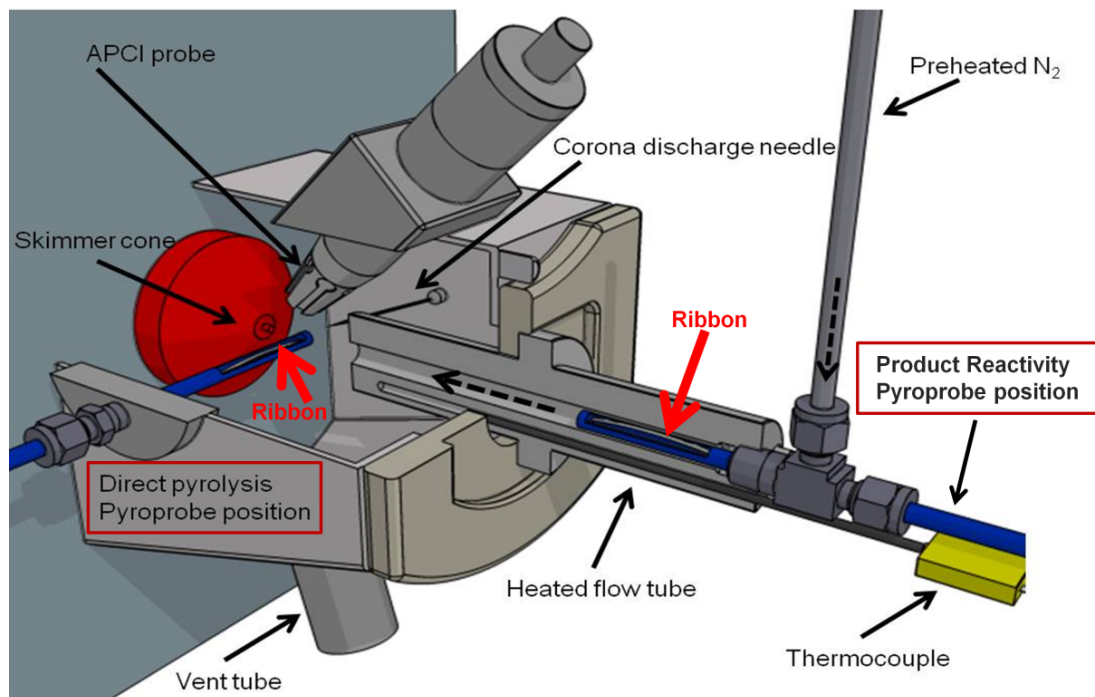


Figure 2.1. A cut away diagram of the ionization chamber in front of the LQIT. The pyroprobe (in blue) is shown in both the direct pyrolysis (left) orientation and within the flow tube (right). The direction of gas flow is indicated by the dashed arrow.

within the flow tube. The residence times were estimated by determining the time it takes for the gas with a known flow rate to pass through the flow tube with a known internal volume.

2.3 Results and Discussion

As discussed above, in order to develop methodology for the determination of the primary products of fast pyrolysis of carbohydrates, and to examine their secondary reactions, two pyrolysis probe setups were coupled with a LQIT mass spectrometer. In the setup for analysis of the primary pyrolysis products, the effluent from the pyroprobe was quenched and ionized by APCI immediately after evaporation into the ion source, followed by analysis of the ions in the LQIT mass spectrometer. In

the other setup, the pyrolysis products were provided time in a flow tube to undergo secondary and tertiary reactions before quenching and determination of the products.

Six model compounds commonly formed during carbohydrate pyrolysis,[3, 44] glycolaldehyde, hydroxyacetone, furfural, 5-hydroxymethylfurfural, levoglucosan, and cellobiosan, were first examined to select an appropriate APCI ionization method for the pyrolysis products. Negative ion mode APCI doped with chloroform has been reported to create chloride anions that readily add to carbohydrates with nearly equal efficiencies and without extensive fragmentation.[45–48] Hence, each of the six model compounds was introduced individually into the APCI source via direct injection while using chloroform dopant. The results obtained using direct injection show that although this method formed stable chloride anion adducts with no fragmentation for most compounds, it formed deprotonated hydroxyacetone instead of a chloride anion adduct and did not ionize glycolaldehyde and furfural.

Since negative ion mode chloride anion attachment could not be used to ionize all of the model compounds, a complementary ionization technique was tested. Ammonium hydroxide dopant in positive ion mode chemical ionization and APCI is known to form stable ammonium adducts with carbohydrate residues and to produce either protonated molecules or molecular ions of related low molecular weight molecules.[48–50] Hence, each of the six model compounds was individually introduced into the APCI source both via direct injection and by vaporizing them off the heated pyrolysis probe while using ammonium hydroxide dopant. This approach was found to ionize all six model compounds without fragmentation. However, the different analytes produced different types of ions (ammonium adducts, molecular ions and/or protonated molecules) when they were introduced via direct injection. The situation was better when the compounds were evaporated from the heated pyroprobe since then the ammonium adducts dominated for most model compounds. However, furfural, glycolaldehyde and 5-hydroxymethylfurfural still formed more than one type of ion and hydroxyacetone only produced a molecular ion. It is important to note that during heated pyroprobe introduction of glycolaldehyde, the ionized dimer was

observed for both ionization methods, indicating that the method that was used to break down the glycolaldehyde dimer did not cause complete dissociation or reassociation occurred on the pyroprobe as the solvent evaporated. This may be the reason for the inability to observe glycolaldehyde in some of the experiments.

Finally, an equimolar mixture of all six model compounds (the concentration of glycolaldehyde was not exactly known due to the incomplete conversion of its dimer to glycolaldehyde) was injected into the ion source and analyzed by using both ionization methods to determine whether the detection of some of the compounds may be hindered by the presence of compounds with greater ionization efficiencies. The mass spectrum obtained using positive ion mode with ammonium hydroxide dopant (Figure 2.2) shows that all six compounds can be observed if they are present in roughly equal proportions. Interestingly, only 5-hydroxymethylfurfural produced more than one ion (it produced two). The response factors of the compounds varied widely.

Chloride attachment APCI did not ionize glycolaldehyde, hydroxyacetone, and furfural in the mixture introduced via direct injection or by the heated pyroprobe. 5-Hydroxymethyl-furfural, levoglucosan, and cellobiosan produced solely chloride anion adducts. Levoglucosan and cellobiosan were evaporated and ionized with almost equal efficiency for both introduction methods (Figure 2.3). 5-Hydroxymethylfurfural yielded a very low signal due to its low chloride anion affinity (it contains only one hydroxyl group).

Once it was realized that the ammonium hydroxide dopant method can be used to ionize all six model compounds but not with equal response factors and that the chloroform dopant method yields semi-quantitative information for carbohydrates but not for smaller model compounds, both ionization methods were used to examine the primary products of fast pyrolysis of cellobiose by using the direct pyrolysis setup described above. Surprisingly, all but a few pyrolysis products were ionized by both methods (Figure 2.4). All compounds larger than levoglucosan demonstrated 100% ammonium or chloride attachment. Levoglucosan showed both adducts as well as

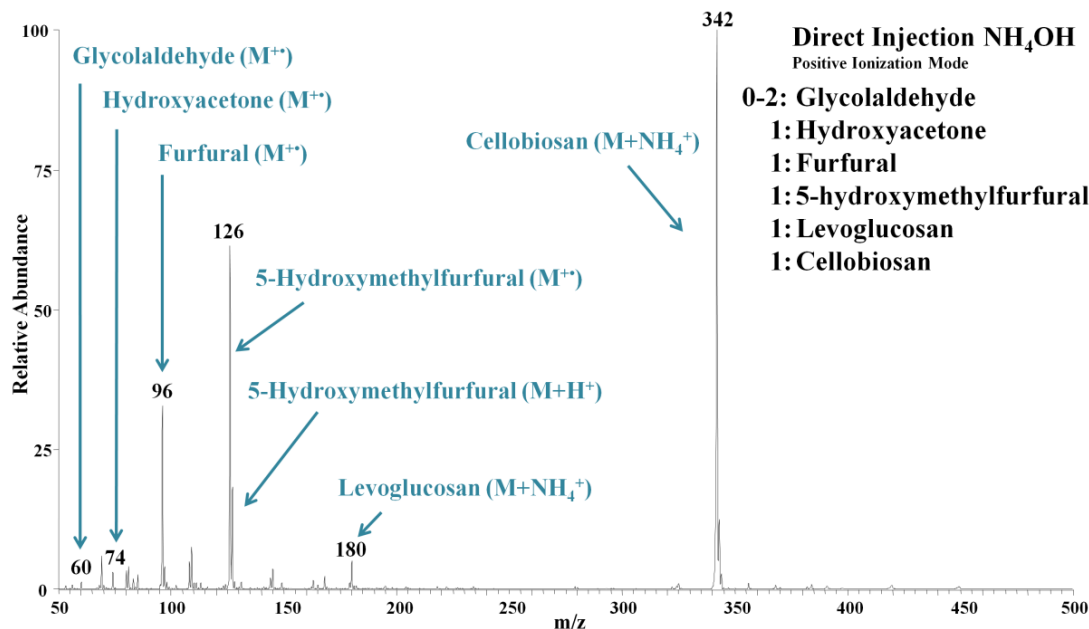


Figure 2.2. An APCI/ammonium hydroxide positive ion mass spectrum of an equimolar mixture of six model compounds introduced via direct injection (the molar ratio of glycolaldehyde is estimated to be between 0-2 due to the unknown extent of glycolaldehyde dimer breakdown). All model compounds were ionized but not equally efficiently.

protonated (positive ion mode) and deprotonated molecules (negative ion mode). The compounds smaller than levoglucosan did not show adducts but instead were either protonated (positive ion mode) or deprotonated (negative ion mode).

Several primary products were detected for fast pyrolysis of cellobiose (Figure 2.4). Their elemental compositions were determined by using high-resolution experiments. Many of these products arise from losses of water (18 Da), formaldehyde (30 Da) and glycolaldehyde (60 Da) in various combinations. Hence, although water, formaldehyde and glycolaldehyde were not efficiently detected in these experiments, their formation can be inferred from the reactions observed. In addition to these compounds, among the products observed, only levoglucosan (MW 162) and 5-hydroxymethylfurfural (MW 126) have been reported in the literature as major final fast pyrolysis products of cellobiose.[4, 7] This is not surprising since most previous studies have employed

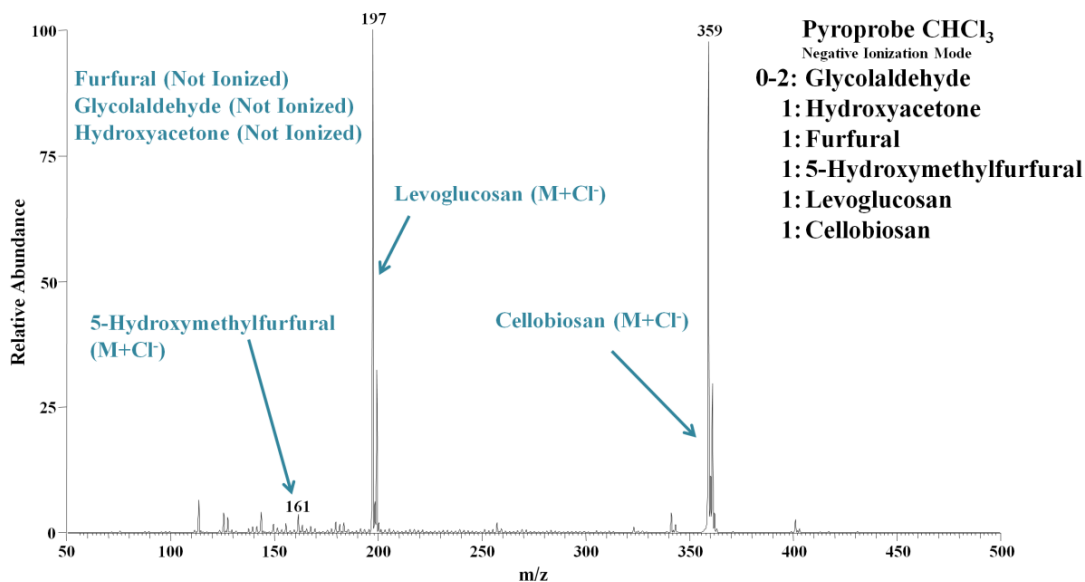


Figure 2.3. An APCI/chloroform negative ion mass spectrum of an equimolar mixture of six model compounds introduced via the heated pyroprobe (the molar ratio of glycolaldehyde is estimated to be between 0-2 due to the unknown extent of glycolaldehyde dimer breakdown). Three model compounds were not ionized.

GC-MS analysis. For example, the largest molecules observed in such previous studies were levoglucosan and its isomers.[4, 7] Hence, it is not unexpected that several products that had not been previously reported were observed to be present in large quantities (Table 2.1), including glucose, cellobiosan and cellobiose that has lost glycolaldehyde or an isomeric molecule. The most abundant product with an elemental composition of C₈H₁₄O₇ is likely to have the structure shown in Figure 2.4. This structure is proposed due to the similarity of the ionized molecule's CAD mass spectrum to that published for an authentic ion in a previous study.[51] Due to the semi-quantitative nature of the chloride attachment method,[46] approximate relative quantitation can be achieved for molecules with at least two hydroxyl groups by considering the relative abundances of their chloride adducts (Table 2.1). The relative molar percent for the molecules that do not form chloride anion adducts was

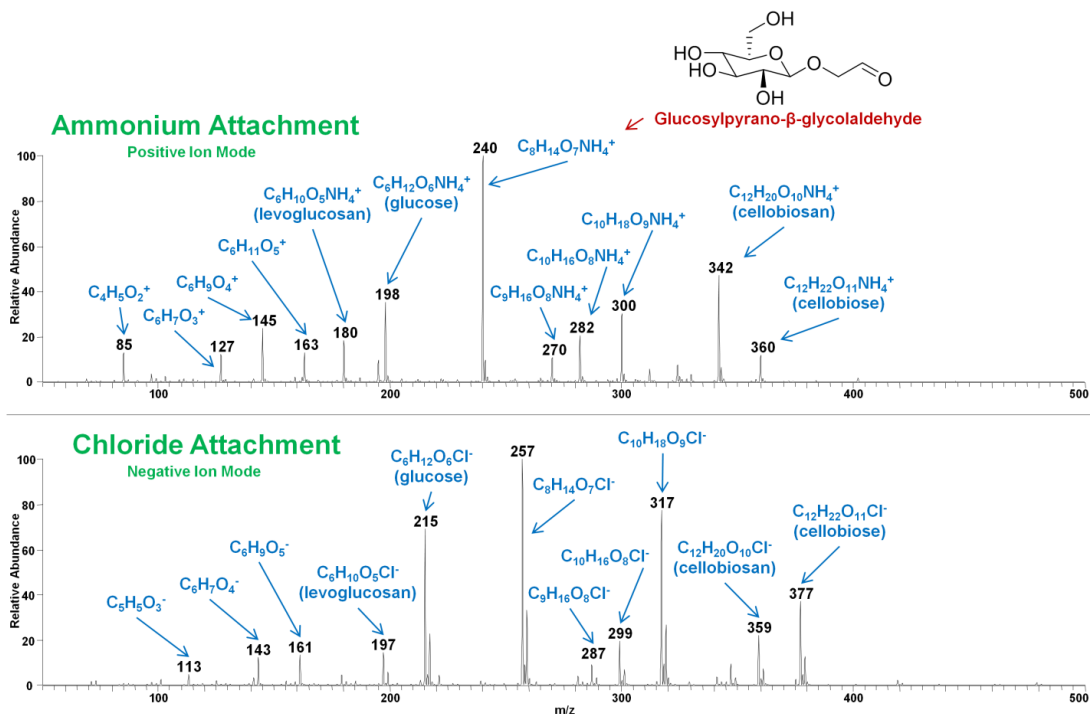


Figure 2.4. Mass spectra of the primary products of fast pyrolysis of cellobiose ionized using ammonium attachment in positive ion mode (top) and chloride attachment in negative ion mode (bottom). All elemental compositions were determined using high resolution data collected in an LQIT/FT-ICR. Ionized levoglucosan has m/z values of 163 and 180 in the top spectrum and m/z values of 161 and 197 in the bottom spectrum. All ions with m/z values lower than 170 correspond to protonated molecules in the top spectrum and deprotonated molecules in the bottom spectrum, and hence have m/z values that differ by two units. Protonated $C_4H_4O_2$ molecule (m/z 85) is only seen in the top spectrum, while deprotonated $C_5H_6O_3$ molecule (m/z 113) is only seen in the bottom spectrum. Otherwise, the spectra show the same ionized molecules. The most abundant product's ($C_8H_{14}O_7$) proposed structure is shown in the top spectrum.

estimated (Table 2.1) using relative ionization efficiencies for ammonium cation attachment determined for model compounds under the same conditions as in pyrolysis experiments. Deprotonated 5-hydroxymethylfurfural (m/z 127; identified based on the identical CAD mass spectra measured for the unknown ion and the deprotonated authentic 5-hydroxymethylfurfural) is considered first.

Table 2.1.

Approximated average relative molar abundances of the primary products of fast pyrolysis of cellobiose normalized to the most abundant product (with standard deviations based on three experiments).

MW	Elemental Composition	Average Relative Molar Abundance (%)
84	$C_4H_4O_2$	8 ± 7
114	$C_5H_6O_3$	Not Estimated
126	$C_6H_6O_3$	7 ± 3
144	$C_6H_8O_4$	13 ± 9
162 (no adduct formation)	$C_6H_{10}O_5$	Not Estimated
162	$C_6H_{10}O_5$	10 ± 4
180	$C_6H_{12}O_6$	70 ± 9
222	$C_8H_{14}O_7$	100 ± 0
252	$C_9H_{16}O_8$	11 ± 3
264	$C_{10}H_{16}O_8$	17 ± 4
282	$C_{10}H_{18}O_9$	61 ± 19
324	$C_{12}H_{20}O_{10}$	20 ± 3
342	$C_{12}H_{22}O_{11}$	34 ± 6

Based on the mass spectrum shown in Figure 2.2, the ionization efficiency of 5-hydroxymethylfurfural is $75 \pm 1\%$ of that of cellobiosan. To correct for this bias, the relative abundance measured for 5-hydroxymethylfurfural formed in fast pyrolysis of cellobiose and ionized by protonation upon ammonium APCI (ion of m/z 127; Figure 2.4, top) was multiplied by 1.33, resulting in a corrected relative molar abundance of $15 \pm 6\%$. This corrected relative molar abundance of 5-hydroxymethylfurfural was then divided by the relative abundance measured (using the same approach) for cellobiosan formed in pyrolysis of cellobiose in order to get the molar ratio of these two pyrolysis products: 0.3 ± 0.1 moles of 5-hydroxymethylfurfural for every mole of cellobiosan. The molar ratio (0.3) was then correlated back to the molecules that could be ionized by chloride attachment by multiplying it by the relative abundance measured by using chloride attachment mass spectrometry for cellobiosan produced upon fast pyrolysis of cellobiose ($26 \pm 3\%$ when taking into account the ^{37}Cl isotope) to obtain a value $7 \pm 3\%$. Hence, the approximate relative molar abundance of 5-hydroxymethyl furfural was found to be $7 \pm 3\%$ relative to the abundance of the ions of m/z 257 (most abundant ions in the bottom spectrum in Figure 2.4). Equation 1, given in supplementary information, illustrates how the calculation was carried out.

Based on their measured elemental compositions, the ions of m/z 145 and m/z 85 (Figure 2.4, top), derived from molecules formed upon fast pyrolysis of cellobiose and ionized by ammonium attachment, are furan derivatives. The ionization efficiencies of these molecules were assumed to be the same as for 5-hydroxymethylfurfural and their measured relative abundances were corrected in the same way as that of 5-hydroxymethylfurfural. The relative abundances of the deprotonated molecules of m/z 161 and 113 (negative ion mode) are not included in Table 2.1. The former is an isomer of levoglucosan (that does not form a chloride adduct like levoglucosan), not a furan derivative, and neither one is a chloride adduct; hence, it is not possible at this time to reasonably estimate their ionization efficiencies. The approximate relative abundances of the most abundant primary products of fast pyrolysis of cellobiose are listed in Table 2.1.

In order to determine the types of secondary reactions that may be expected for the primary fast pyrolysis products of cellobiose, it was pyrolyzed inside the flow tube (described in detail in the Experimental Section). The primary products of cellobiose were allowed to react for 2 s and 11 s at two different temperatures (300°C and 400°C). Similar product distributions were measured using both ionization methods. Hence, only results obtained using positive ion mode ionization are discussed below. The corresponding negative ion mode ionization mass spectra are presented in Figure A.1. Figure 2.5 shows that most of the primary fast pyrolysis products of cellobiose react away, ultimately producing anhydro-oligosaccharides up to cellopentosan or an isomer under the conditions used. The ability of anhydrosugars to polymerize is not a new phenomenon.[52–56] The most abundant primary product of cellobiose with the elemental composition $C_8H_{14}O_7$ (its ammonium adduct has the m/z value of 240) reacts away rapidly. Hence, it is not unexpected that this product has not been reported in the literature. These findings demonstrate that a method other than GC/MS is needed to detect many of the products formed upon reactions of the primary pyrolysis products of cellobiose (and other carbohydrates). These results also suggest that the larger anhydro-oligosaccharides (cellotetrosan, cellopentosan, etc., or their isomers) that have been detected in bio-oils via HPLC analysis are likely, to some extent, to be formed via polymerization reactions of the primary fast pyrolysis products as opposed to incomplete breakdown of the pyrolyzed carbohydrate.[40] This hypothesis was confirmed by measuring CAD mass spectra for selected fragment ions of authentic cellotriosan (MW 486 Da) after ionization by chloride attachment. These CAD mass spectra were compared to those measured for the analogous fragment ions of the unknown trimer pyrolysis product formed from cellobiose within the flow tube (m/z 521; Figure 2.5). The MS2 mass spectra of the chloride attached cellotriosan and unknown trimer (m/z 521) display solely HCl loss resulting in fragment ions of m/z 485. The ions of m/z 485 correspond to the deprotonated cellotriosan and unknown trimer molecules. They were isolated and subjected to further CAD to obtain the mass spectra presented in Figure 2.6, left. The deprotonated trimer produced

several fragment ions of various m/z values that are not produced during the CAD of authentic deprotonated cellotriosan (i.e., ions of m/z 467, 365, and 347) but both produced an abundant fragment ion of m/z 323 corresponding to the loss of a molecule with a MW of 162 Da. The fragment ions of m/z 323 were isolated and subjected to CAD to produce the spectra in Figure 2.6, right. Again, several new fragment ions were produced upon CAD of ions of m/z of 323 formed from the unknown trimer compared to those produced from authentic cellotriosan (i.e., ions of m/z 305, 275, and 203). From the CAD mass spectra presented in Figure 2.6, the unknown trimer is concluded to be a mixture of isomers, including cellotriosan.

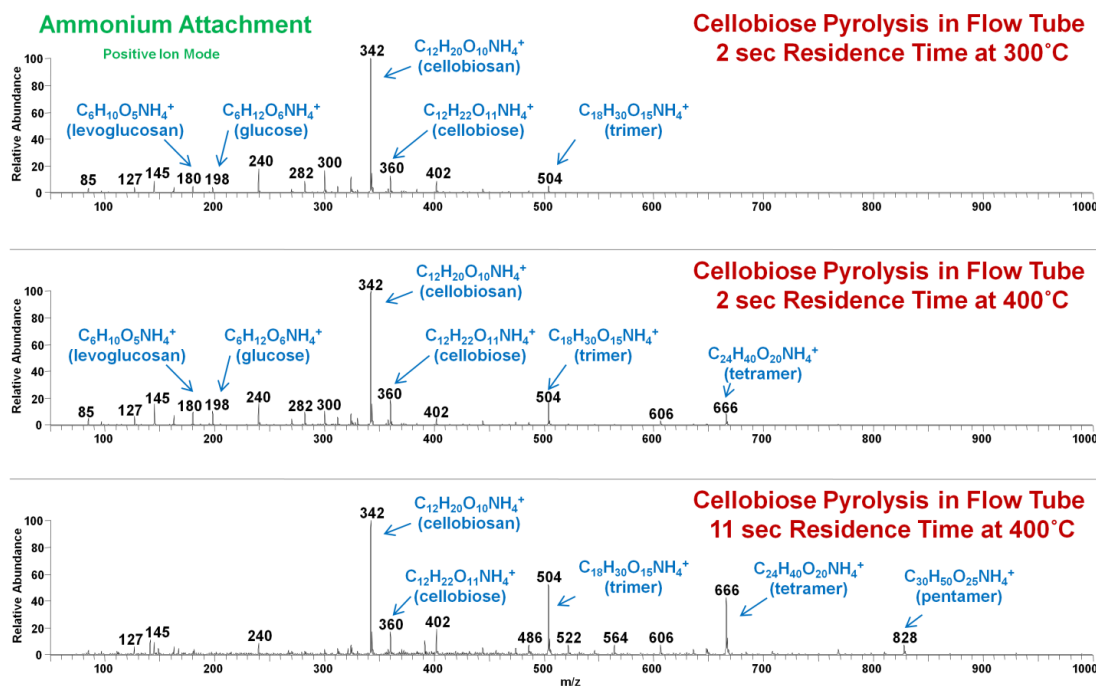


Figure 2.5. Mass spectra collected after the primary products of fast pyrolysis of cellobiose were allowed to undergo reactions for 2 s at 300°C (top), 2s at 400°C (middle) and 11 s at 400°C (bottom) and ionized using ammonium attachment in positive ion mode. All elemental compositions were determined using high resolution data collected in an LQIT/FT-ICR. All ions with m/z values lower than 170 correspond to protonated molecules.

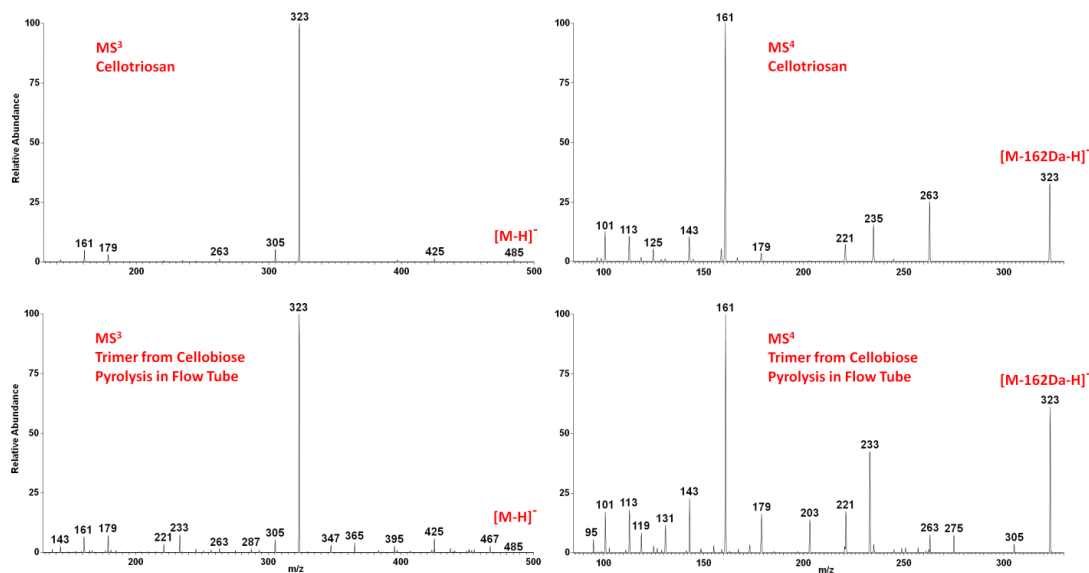


Figure 2.6. CAD mass spectra measured for authentic cellotriosan ionized via chloride attachment in negative ion mode and the unknown trimer (ionized in the same manner) formed upon pyrolysis of cellobiose in the flow tube. The chloride attached cellotriosan and trimer (m/z 521) were isolated and subjected to CAD which resulted in HCl loss, forming fragment ions of m/z 485, corresponding to the deprotonated molecules of cellotriosan and the unknown trimer. These deprotonated molecules were subjected to CAD to obtain the mass spectra shown top left and bottom left, respectively. Both ions produced an abundant fragment ion corresponding to the loss of a molecule with MW 162 Da to yield an ion of m/z 323. The fragment ions of m/z 323 were isolated and subjected to CAD to produce the mass spectra shown top right and bottom right, respectively.

2.4 Conclusions

Two fast pyrolysis/tandem mass spectrometry systems were devised, one to determine the primary products of fast pyrolysis of carbohydrates and another one to study how changes in temperature and residence time change the extent of secondary reactions of the primary products in order to simulate a pyrolysis reactor. Two complementary ionization methods were chosen to detect the pyrolysis products: APCI doped with chloroform in the negative ion mode and APCI doped with ammonium hydroxide in the positive ion mode. Examination of an equimolar mixture

of six model compounds commonly produced during carbohydrate pyrolysis (glycolaldehyde, hydroxyacetone, furfural, 5-hydroxymethylfurfural, levoglucosan, and cellobiosan) demonstrated that the positive ion mode APCI doped with ammonium hydroxide allows the detection of all these compounds but they do not have equal response factors. On the other hand, examination of the same mixture by using the negative ion mode APCI method revealed roughly equal ionization efficiency for compounds with at least two hydroxyl groups, consistent with previous studies for this method.[46] Hence, this ionization method allows semiquantitative analysis of carbohydrates produced during pyrolysis of oligosaccharides. However, this method cannot be used to detect pyrolysis products with fewer than two hydroxyl groups. A rough estimate of the relative molar abundances of the pyrolysis products that did not form chloride anion adducts was obtained using ionization efficiencies of model compounds determined using ammonium attachment in positive ion mode or chloride attachment in negative ion mode.

The fast pyrolysis/MS systems described above were used to examine fast pyrolysis of cellobiose. The primary fast pyrolysis products of cellobiose were determined to consist of only a handful of compounds that quickly polymerize to form anhydro-oligosaccharides when allowed to react at high temperatures for an extended period of time. The primary and secondary fast pyrolysis products of cellobiose include compounds that cannot be detected using GC/MS analysis that was employed in many previous studies.[7] These findings demonstrate that a method other than GC/MS is necessary to detect the primary, secondary and possibly also final products of fast pyrolysis of carbohydrates. Further, the results suggest that the complexity of bio-oils may arise, in part, from a variety of polymerization reactions of the primary pyrolysis products. Comparison of the CAD mass spectra measured for authentic deprotonated cellotriosan and the deprotonated unknown trimer formed in flow tube pyrolysis of cellobiose suggests that along with the formation of cellotriosan, other isomers are also formed in the flow tube, likely due to polymerization of the primary products. It should be noted here that while previous studies report that the composition of

bio-oil can be altered by changing process parameters (such as residence time), our work indicates that the complexity of the product distribution is generally lower at lower residence times and temperatures.[4, 40] Finally, the pyrolysis/MS methods developed here require only micrograms of sample and provide a fast approach for the examination of the influence of pyrolysis conditions and different feedstocks on the primary and secondary pyrolysis products of carbohydrates.

2.5 Acknowledgements

Reprinted with permission from M.R. Hurt, J.C. Degenstein, P. Gawecki, D.J. Borton II, N.R. Vinueza, L. Yang, et al., On-Line Mass Spectrometric Methods for the Determination of the Primary Products of Fast Pyrolysis of Carbohydrates and for Their Gas-Phase Manipulation, *Analytical Chemistry* 85 (2013) 10927–10934. doi:10.1021/ac402380h. Copyright 2013 American Chemical Society.

3. HIGH-PRESSURE FAST-PYROLYSIS, FAST-HYDROLYSIS AND CATALYTIC HYDRODEOXYGENATION OF CELLULOSE: PRODUCTION OF LIQUID FUEL FROM BIOMASS

3.1 Introduction

Traditionally, liquid transportation fuels have been produced from fossil-based petroleum sources. In the context of a petroleum-deprived future, it is imperative to look for sustainable carbon sources in conjunction with more efficient process pathways for producing high-energy-density liquid fuels. Sustainably available (SA) biomass comprised of crop and forest residues, agriculture and municipal waste, etc. is one such carbon source for producing liquid fuels to meet the large demand for transportation.[24, 57] Agrawal et al. suggested a sustainable H₂Bioil process for conversion of biomass to liquid fuels, where biomass is co-fed to a fast-hydrolysis and hydrodeoxygenation (HDO) reactor system along with H₂ produced from a carbon-free energy source like solar, to produce liquid fuels in a single step process.[58–60] This process seems practically realizable because of its modest estimated hydrogen consumption of 0.11 kg H₂/L oil, reasonably high estimated carbon efficiency (~70%) and estimated energy recovery (215 ege ton⁻¹).[24] This process is also economically attractive at a break-even crude oil price in the range of \$ 99/bbl to \$ 116/bbl, based on different economic scenarios.[61] Clearly, experimental demonstration of H₂Bioil based processes could have a significant impact on the transportation sector, which is primarily dependent on liquid fuels. This paper presents an experimental approach for the practical realization of the H₂Bioil process.

Fast-pyrolysis involves the rapid heating of biomass at near atmospheric pressure in an inert gas environment to temperatures of ~500°C and subsequent condensation of the vapors to form a liquid bio-oil.[62] This bio-oil is a high oxygen content, acidic

liquid product with energy content similar to that of the feed biomass and requires further hydroprocessing under severe conditions to be upgraded to transportation grade fuel.[19, 28] As an alternative to this two step approach, the H₂Bioil process is based on continuous-flow biomass fast-hydropyrolysis, which is the rapid heating of biomass at heating rates $>100^{\circ}\text{C}/\text{s}$ in the presence of high pressure hydrogen, to produce hydropyrolysis vapors which are upgraded in the vapor phase by catalytic HDO and quenched to form a high-energy-density, deoxygenated liquid product that can supplement petroleum-based liquid fuels or potentially be used directly as a fuel. This conversion process is envisioned to operate at high hydrogen partial pressures (up to 50 bar or higher) so the HDO reaction rates would be higher due to increased availability of hydrogen at high partial pressures.[63] Vapor phase catalytic upgrading is chosen to avoid secondary reactions during condensation and revaporization of the pyrolysis vapors.[63]

In the literature, there have been no systematic studies in a continuous-flow high-pressure lab-scale reactor for understanding the effect of process parameters and catalysts on fast-hydropyrolysis and direct downstream HDO. There have been some experimental demonstrations of fixed bed batch hydropyrolysis[64–68] and batch pressurized pyrolysis.[69–72] These studies have shown preliminary proof of the changes in pyrolysis products with high inert pressures and the deoxygenation capability of high pressures (>100 bar) of H₂ in presence of a suitable catalyst. Pindoria et al.[73] and Rocha et al. showed that a two stage approach combining hydropyrolysis and catalytic upgrading could lead to bio-oils with relatively low oxygen content in the presence of an appropriate catalyst in the second stage.[74] Zhang et al. and Meesuk et al. used fluidized bed reactors with batch mode biomass feed to show that presence of hydrogen atmosphere increased water content in the bio-oils and presence of a nickel catalyst improved deoxygenation, respectively.[75, 76] Work by Melligan and coworkers, with a micro-scale batch setup, showed that biomass hydropyrolysis along with catalytic upgrading increased yields of aromatic hydrocarbons.[77] Catalytic fast-pyrolysis, using fluidized bed and circulating fluidized bed reactors, with zeolite

catalysts leads to bio-oils with relatively low ($\sim 21\text{wt}\%$) oxygen content with $\sim 25\%$ carbon recovery as aromatics and light olefins.[78, 79] It has been proposed, however, that supplementary hydrogen would be required to further improve the carbon recovery and deoxygenation.¹ There have been studies on continuous-flow catalytic hydrolysis, which have claimed the production of a fungible hydrocarbon product from biomass using a fluidized bed reactor, but they do not use detailed liquid product composition characterization to look at the effects of high pressure (up to 50 bar), presence of hydrogen, hydrolysis temperature and catalysts.[80, 81]

In this study, we present the design and construction of a continuous-flow high-pressure reactor for fast-hydrolysis followed by a downstream vapor-phase catalytic HDO reactor. We also present results from experiments that were designed to systematically understand the effect of temperature on fast-pyrolysis, the presence of hydrogen in fast-hydrolysis, reactor performance with reaction pressure (25 bar and 50 bar), and the effect of different candidate downstream HDO catalysts. We have developed and used a liquid-chromatography-mass spectrometry (LC-MS) method for detailed characterization and quantitative analysis of the liquid products from the experiments. Cellulose, which constitutes about 35-50% of the whole lignocellulosic biomass,[2] was used as a biomass model compound for all the experiments reported in this paper. This reactor system has been successfully tested with real biomass feedstocks as well, but, cellulose as a feedstock produces a simpler set of pyrolysis products as compared to whole biomass, which aided in the systematic understanding of the effect of different reaction conditions on the products.

3.2 Experimental Methods

3.2.1 Reactor Design

The reactor system designed, built and used for this study is shown in Figure 3.1. The process flow diagram of the setup is shown in supplementary information (SI) Figure B.4. This is a continuous-flow, lab-scale, high-pressure fast-hydrolysis

(FHP) reactor with a downstream vapor-phase, fixed-bed catalytic hydrodeoxygenation (HDO) reactor. This reactor system was designed for use at high temperatures (up to 650°C for FHP reactor and up to 500°C for the HDO reactor) and high-pressures (up to 100 bar) with the capability of operating in an inert (He or He plus N₂) or hydrogen environment. The materials of construction are stainless steel grades 316, 316H and 324. All the connections that operate at high temperature are made with standard American Society of Mechanical Engineers (ASME) flanges rated above at least 100 bar at the highest operating temperature of the component. The reactor design is based on ASME B16.5 flange standards and B31.3 process piping codes. Hydrogen safety systems (Figure B.4) like hydrogen detectors, automatic shut-off valves, redundant pressure relief and emergency exhaust were included in the reactor system for safe use of high-pressure hydrogen.

The gas/vapor residence time in the fast-hydrolysis reactor is about 2-5 seconds and the overall residence time for the complete reactor system is about 15-35 seconds. Biomass or model biomass feedstock, such as cellulose, is fed to the reactor system using an in-house-built high-pressure biomass screw feeder capable of feeding at the rates of 0.1-20 g × min⁻¹. The feedstock is entrained in a flow of hydrogen and inert gases, with a total gas flow rate of ~30-40 std. L × min⁻¹, for feeding into the FHP reactor. The FHP reactor is an ablative cyclone-type pyrolysis reactor that is specially designed and optimized for high-pressure operation. Design factors for the cyclone reactor such as vapor residence time, particle residence time, reactor dimensions, inlet location and angle were optimized for best reactor performance based on the testing of a series of prototype reactors and work reported in the literature for near atmospheric-pressure fast-pyrolysis of biomass.[82] In the FHP reactor, the char is collected below the reactor in the char collector, and the vapors exit from the top of the reactor. The vapors then move through a transfer section to the downstream fixed-bed vapor-phase catalytic HDO reactor where they are upgraded. The upgraded vapor products are condensed with a concentric tube heat exchanger. Most of the products are condensed in the first stage, which is a coalescing filter. Residual

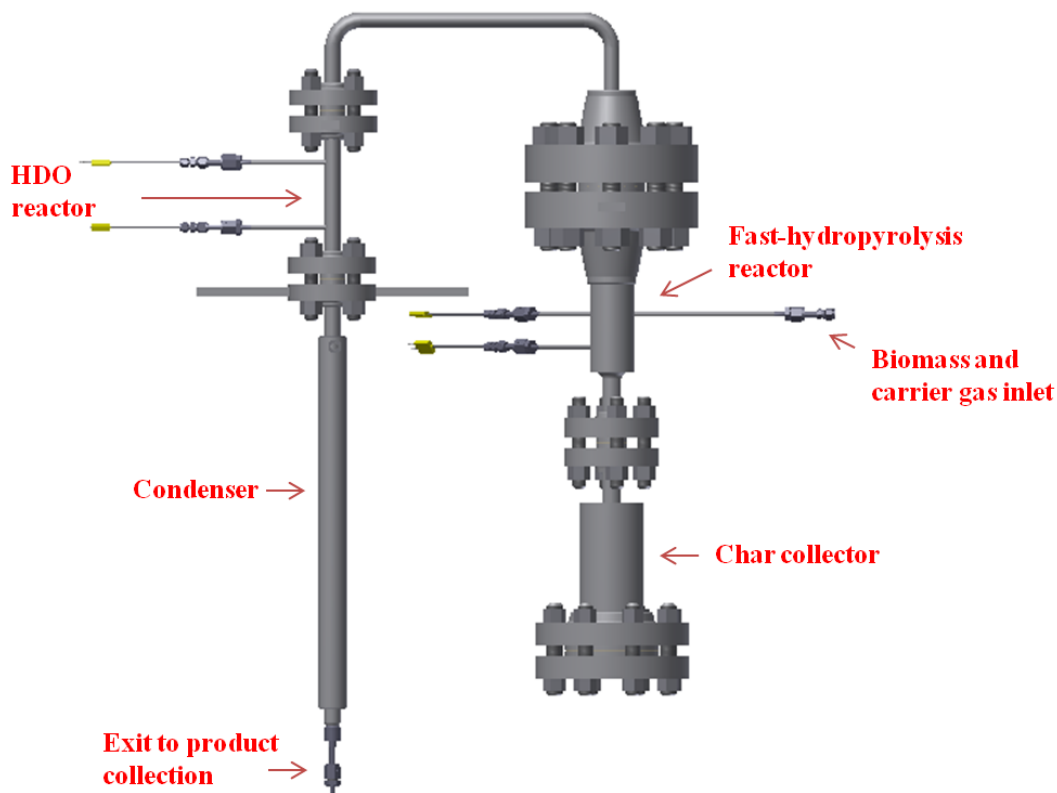


Figure 3.1. 3D model sketch of the reactor system.

vapors are condensed in the second stage, comprised of a liquid trap cooled with a mixture of ice and water. Liquids from both the collection stages are mixed together for analysis of the final liquid product. After liquid product separation, the remaining permanent gases are analyzed using an on-stream gas chromatograph (GC) with nitrogen as an internal standard. The reactor system is monitored and controlled by a custom in-house-built process control system based on LabVIEW. Detailed design information about the reactor system is available in the supplementary information of this publication. Full construction drawings of the reactor are available on request from the authors.

3.3 Experimental Approach

High-pressure cellulose fast-pyrolysis experiments (Table 3.1) were conducted at different temperatures (480°C to 580°C) at 27 bar pressure of inert gas (25 bar helium and 2 bar nitrogen as an internal standard for on-stream GC analysis). Experiments were also conducted at 54 bar of inert gas pressure to examine the effect of reaction pressure on reactor performance. High-pressure cellulose fast-hydrolysis experiments (Table 3.2) were conducted at 25 bar and 50 bar of hydrogen partial pressure (total pressure of 27 bar and 54 bar, respectively, including 2 bar and 4 bar nitrogen as an internal standard for on-stream GC analysis) at 480°C hydrolysis temperature. Experiments were also conducted at 580°C hydrolysis temperature to understand the effect of hydrogen at the highest temperature in the temperature range chosen. The gas/vapor residence time in the fast-hydrolysis reactor was ~ 2 seconds and ~ 4 seconds for all 27 bar and 54 bar experiments, respectively.

The experiments with vapor-phase downstream catalytic HDO (Table 3.3) were conducted at a fast-hydrolysis temperature of $\sim 550^\circ\text{C}$ and a catalyst bed temperature of $\sim 375^\circ\text{C}$. Commercially available candidate catalysts were chosen for comparison of extent of deoxygenation (Equation 1) and effect on the overall product distribution and yields. The catalysts tested were transition metals Ruthenium (Ru) and Platinum (Pt) supported on γ -alumina ($\gamma\text{-Al}_2\text{O}_3$, henceforth referred to as Al_2O_3). The catalysts were reduced in situ with flowing hydrogen at 375°C for 2 hours prior to each experiment. Al_2O_3 was also tested to understand the effect of support independently.

$$\text{Extent of deoxygenation (dry basis)/\%} = 100\% \times \frac{\left(\frac{\text{O}}{\text{C}}\right)_{\text{cellulose,dry}} - \left(\frac{\text{O}}{\text{C}}\right)_{\text{liquid,dry}}}{\left(\frac{\text{O}}{\text{C}}\right)_{\text{cellulose,dry}}} \quad (3.1)$$

The overall cellulose conversion pathway is shown in Figure 3.2. The cellulose feed rate was $\sim 0.8\text{-}0.9 \text{ g} \times \text{min}^{-1}$ in all the experiments. The overall mass balance in all the experiments was 80-95%. The unaccounted fraction is attributed to product collection losses during, and after, the high-pressure experiments due to gas/vapor product

Table 3.1.
 Experimental conditions and product distribution[†] summary for experiments of cellulose fast-pyrolysis.

	Run 1	Run 2	Run 3	Run 4	Run 5
Total pressure / bar	27	27	27	27	54
Helium partial pressure / bar	25	25	25	25	50
Nitrogen partial pressure / bar	2	2	2	2	4
Average fast-pyrolysis temperature / °C	480	520	550	580	480
Liquid yield / wt % of feed	69.2	68.7	68.6	63.7	56.5
Char yield / wt % of feed	7.7	11.8	9.3	10.6	20.4
Gas yield / wt % of feed	6.9	10.3	15.6	18.8	7.2
CO / wt % of feed	2.9	5.4	9.8	13.4	2.3
CO ₂ / wt % of feed	3.9	4.6	5.4	4.7	4.8
CH ₄ / wt % of feed	0.1	0.3	0.4	0.7	0.1
Overall Mass Balance / %	83.8	90.8	93.5	93.1	84.1

[†] Error in product distribution $\sim \pm 5-10\%$

Table 3.2.
 Experimental conditions and product distribution[†] summary for experiments of cellulose fast-hydrolysis without HDO catalyst.

	Run 6	Run 7	Run 8
Total pressure / bar	27	27	54
Hydrogen partial pressure / bar	25	17	50
Helium partial pressure / bar	0	9	0
Nitrogen partial pressure / bar	2	1	4
Average fast-hydrolysis temperature / °C	480	580	480
Liquid yield / wt % of feed	66.9	62.1	51.3
Char yield / wt % of feed	8.3	11	27.1
Gas yield / wt % of feed	5.5	15.6	8.3
CO / wt % of feed	2.1	9.6	2.6
CO ₂ / wt % of feed	3.2	5	5.5
CH ₄ / wt % of feed	0.2	1	0.2
Overall Mass Balance / %	80.7	88.7	86.7

[†] Error in product distribution $\sim \pm 5-10\%$

Table 3.3.

Experimental conditions for experiments of catalytic HDO of cellulose fast-hydrolysis vapors and base case experiment without HDO catalyst.

	Run 7	Run 9	Run 10	Run 11
Total pressure / bar	27	27	27	27
Hydrogen partial pressure / bar	17	9	9	9
Helium partial pressure / bar	9	15	15	15
Nitrogen partial pressure / bar	1	3	3	3
Average fast-hydrolysis temperature / °C	580	550	550	550
HDO catalyst	No Catalyst	Al ₂ O ₃	2% Ru/Al ₂ O ₃	2% Pt/Al ₂ O ₃
Weight hourly space velocity (WHSV) / hr ⁻¹	-	9	9	9
Average catalyst bed temperature / °C	-	375	375	375

dilution as a result of high feed gas standard condition flow rates needed for low reactor residence times. The typical experimental error in all the product distributions was $\sim\pm 5\text{-}10\%$ (standard deviation) based on duplicate repeats of experiments. The experiments were typically conducted for about 1 hour. After each experiment, the reactor was depressurized, liquid and solid products and the remainders of the feed in the screw feeder were weighed, and catalyst coke yield was measured through catalyst weight gain. All these data were used to check the overall mass balance. The total liquid product was the sum of liquid products collected in the two traps, weight change of coalescing filter element and liquid holdup in the reactor. The liquid holdup in the reactor system was calculated by flushing solvent (ethanol) through the reactor after each experiment and evaporating the solvent at room temperature to measure the residue.

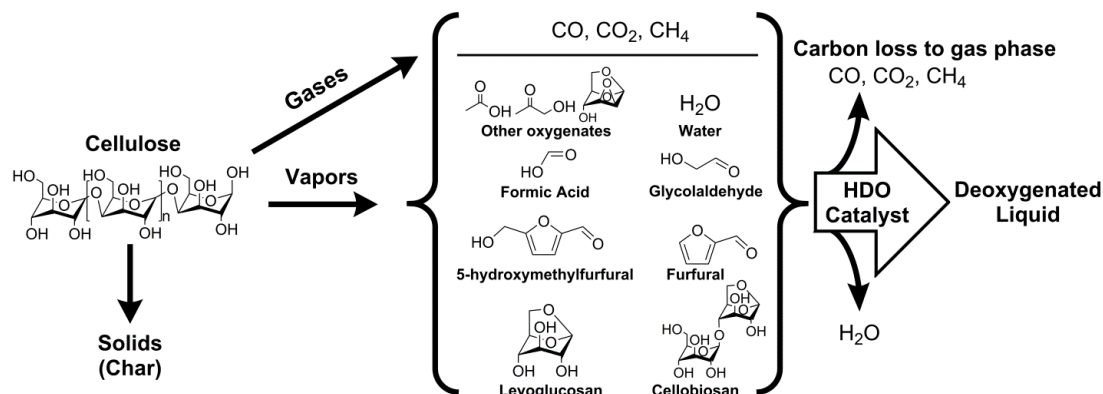


Figure 3.2. Schematic of overall cellulose conversion pathway.

3.3.1 Liquid Product Analysis

The liquid products from the different experiments were analyzed by several different analytical techniques. They were first analyzed for the elemental (C, H, O) composition and water content through Karl Fisher titration, both performed by Galbraith Laboratories (Knoxville, TN). The carbon and hydrogen contents were

measured by combustion techniques and the oxygen content was calculated based on difference. The elemental analysis and water content were used to calculate a dry basis elemental composition of the liquid products and for calculating the extent of deoxygenation on a dry basis. Then, for the quantitative characterization of the liquid product, we have developed a liquid chromatography-mass spectrometry (LC-MS) analytical method.

3.3.2 Liquid-chromatography mass-spectrometry (LC-MS) method development

Methods using gas chromatography-mass spectrometry (GC/MS) are excellent for performing analysis of compounds with atmospheric pressure boiling points of up to 300°C, but can cause thermal degradation during the volatilization of species that are non volatile at these temperatures. Thus methods in which these lower volatility species could be analyzed without degradation were desired. Indeed, several publications have indicated the presence of oligomeric anhydro-saccharides in the pyrolysis product distribution.[6, 32, 40] Hence, this LC-MS method was developed specifically for its ability to separate oligomeric sugars, monomeric sugars, and furan related compounds such as 5-hydroxymethylfurfural, and furfural, while remaining stable in the acidic medium typical of the cellulose fast-pyrolysis liquid products.²⁹ We have tested this method using oligomeric anhydro-saccharides up to 3 units in length (cellotriosan, 1,6-anhydro- β -D-cellobiose). This method was specifically developed for analysis of pyrolysis products from the cellulose fraction of whole biomass, and could also be useful with the hemicellulose pyrolysis product fraction. We note, however, that this method may not be applicable as-is for lignin pyrolysis products due to their lower polarity.

For the LC-MS analysis, an Agilent 1200 LC with a Ultraviolet/Visible (UV/VIS) diode array detector and a refractive index detector (RID) and an Agilent (Santa Clara, CA) single quadrupole mass spectrometer (MS 6975) with an atmospheric pressure chemical ionization source were used. A Rezex ROA LC column supplied by Phenomenex (Torrance, CA) with a 300mm column length (Part No. 00H-0138-K0)

was used with 0.1 wt% formic acid in water as the mobile phase. The recommended mobile phase for this column is 0.005N H₂SO₄ in high purity water, but to improve compatibility with the mass spectrometer, the acid was changed to 0.1wt% of formic acid (in high purity water) for enhanced volatility and reduced corrosivity. This mobile phase was pumped isocratically at 0.5 mL × min⁻¹, after vacuum degassing, through the column which was maintained at 80°C. The RID sample and reference cells were controlled at 55°C and the reference cell was purged before every analysis.

The chloride anion attachment based atmospheric pressure chemical ionization (APCI) method reported by Vinueza et al.[46] for analyzing sugar-based compounds has been used in this study for identification of compounds ionizable with this technique. The ionization conditions were defined by the APCI source operated at 300°C with a N₂ flow of 5 L × min⁻¹ in negative ionization mode, a corona current of 10 μA, capillary voltage of 3000 V, and fragmentor voltage of 2 V. Figure B.5 (Supplementary Information) shows the schematic of the LC-MS setup along with the syringe pump that was used for the injection of an equal volume mixture of methanol and chloroform for the chloride attachment of the ions. The RID was calibrated for 14 compounds as shown in Table B.1 and Figure B.6. The 14 compounds were chosen based on work in the literature that reported on the pyrolysis products of cellulose analyzed mainly with a gas-chromatography-mass-spectrometry (GC-MS) technique.[4, 6, 7, 83] The retention times of the compounds in the LC-MS, based on pure compound injections, and their mass spectra were used for identification of the compounds. All the experimental liquid product samples were diluted 100 times in the mobile phase and a 10 μL injection volume was used. All the samples were analyzed with duplicate repeats to calculate the analytical errors.

3.3.3 Materials

The cellulose feedstock used in all experiments was 50 μm microcrystalline cellulose from Sigma Aldrich (St Louis, MO). Ultra high purity (99.999%) grade hydrogen, high purity (99.995%) grade helium and high purity (99.995%) grade nitrogen were

used for the experiments. We note that in all experiments nitrogen is added as an internal standard gas. Catalysts used in this study were Al_2O_3 (Sasol, 1.8 mm diameter extrudates), 2% Pt/ Al_2O_3 (Alfa Aesar, 2.5 mm diameter trilobes) and 2% Ru/ Al_2O_3 (Alfa Aesar, 3.2 mm diameter extrudates). Pure compounds for LC-MS calibration viz. levoglucosan (1,6-anhydro- β -D-glucopyranose, $\geq 99\%$ purity), formic acid ($\geq 95\%$ purity), acetic acid ($\geq 99\%$ purity), glycolaldehyde dimer, hydroxyacetone ($\geq 90\%$ purity), furfural (2-furaldehyde, $\geq 99\%$ purity), 5-hydroxymethyl furfural (5-HMF, $\geq 99\%$ purity), acetone ($\geq 99.8\%$ purity), methanol ($\geq 99.9\%$ purity) and ethanol ($\geq 99.5\%$ purity) were purchased from Sigma Aldrich. Cellobiosan (1,6-anhydro- β -D-cellobiose, $\geq 95\%$ purity), levogalactosan (1,6-anhydro- β -D-galactopyranose, $\geq 97\%$ purity), 1,6:2,3-dianhydro- β -D-mannopyranose (DAMP, $\geq 98\%$ purity) and levoglucosenone ($\geq 95\%$ purity) were purchased from Carbosynth Limited (Compton, Berkshire, UK).

3.4 Results and Discussion

3.4.1 High-pressure cellulose fast-pyrolysis products

Figure 3.3 (a) shows a typical liquid product composition, based on the LC-MS analysis, from a high-pressure fast-pyrolysis experiment at 27 bar total inert pressure and 520°C pyrolysis temperature (Run 2 in Table 3.1). The most abundant compounds seen were levoglucosan and its isomers ($\sim 51\text{wt}\%$ of the liquid), light oxygenates like glycolaldehyde ($\sim 8\text{wt}\%$ of the liquid), formic acid ($\sim 11\text{wt}\%$ of the liquid), hydroxyacetone ($\sim 1\text{wt}\%$ of the liquid) and a small amount ($\sim 1\text{wt}\%$ of the liquid) of cellobiosan. No oligomers higher than the anhydrosugar dimer (cellobiosan) were seen in the liquid product. Water constituted $\sim 24\text{wt}\%$ of the total mass of the liquid product. With the 15 compounds (including water), about 95% of the total mass of the liquid product can be accounted for. The overall mass balance for this experiment was $\sim 91\%$ with a liquid yield of $\sim 69\text{ wt}\%$ of the feed cellulose, char yield

of ~ 12 wt% of the feed cellulose and permanent gas yield of ~ 10 wt% of the feed cellulose, shown in Table 3.1.

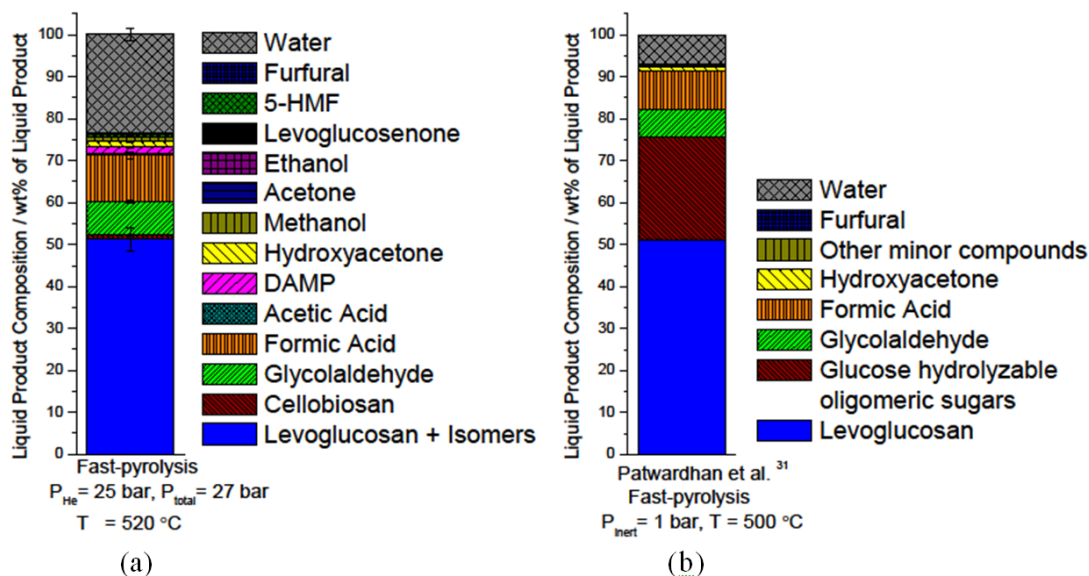


Figure 3.3. (a) Bar graph showing typical liquid product composition data, from LC/MS analysis, of cellulose fast-pyrolysis at 27 bar total inert pressure in the cyclone-type reactor used in this study. (b) Bar graph showing liquid product composition data of cellulose fast-pyrolysis at 1 bar inert pressure in a fluidized bed reactor, from Patwardhan et al.[6]

Figures 3.3 (a) and (b) show a comparison of the high-pressure (27 bar) cellulose fast-pyrolysis liquid product composition from this cyclone-type reactor with previously reported results on a fluidized bed reactor, at 1 bar reaction pressure, in Patwardhan et al.[6] The vapor residence time in the cyclone-type reactor, at 27 bar, is ~ 2 seconds and comparable to the vapor residence time in the fluidized bed reactor in Patwardhan et al.[6] The composition of levoglucosan, glycolaldehyde, formic acid, hydroxyacetone and furfural in the product agrees closely with the previously reported results despite the differences in the fast-pyrolysis reactor configurations and reaction pressure.[6] However, the composition of water and cellobiosan (anhydro sugar oligomers) in the liquid product differed from those reported in Patwardhan

et al.[6] The higher content of water in the liquid product from this reactor is due to higher char yield of ~ 12 wt% of feed cellulose versus ~ 2 wt% of feed cellulose in their study.[6] We note that this difference in char formation cannot be solely attributed to the difference in reaction pressure because the reactor configurations (cyclone-type vs. fluidized bed) could play an important role. In a later section, we provide a potential explanation for the increase in char yield (and corresponding increase in water yield) with increase in reaction pressure (25 bar to 50 bar) with this cyclone-type fast-pyrolysis reactor configuration. The higher production of oligomeric sugars in the previously reported fluidized bed reactor was explained by additional secondary reactions in their reactor as compared to the ablative cyclone-type reactor used in this study which produced a lower yield of oligomeric anhydro-sugars.[6] Moreover, the LC-MS technique developed and used for this study measures the content of oligomeric anhydro-sugars directly and does not rely on acid-hydrolysis for their measurement, as used in their study.[6] The liquid product from cellulose fast-pyrolysis is a complex mixture of reactive compounds, and thus acid-hydrolysis or derivatization may cause additional undesired reactions during analysis. Thus, the origin of these differences in the production of oligomers from different reactors and operating conditions needs further study.

3.4.2 Effect of temperature in high-pressure cellulose fast-pyrolysis

Figure 3.4 shows the increase in the formation of light oxygenate molecules like glycolaldehyde and formic acid and the decrease in the formation of levoglucosan and its isomers as the pyrolysis temperature increases from 480°C to 580°C . Figure 3.5 shows that the gas yield increases and the liquid yield decreases with increasing temperature of fast-pyrolysis or fast-hydrolysis. As shown in Figure 3.4 and Table 3.1, there was no trend in the char yield, and corresponding water yield, with the fast-pyrolysis temperature, within experimental error.

In this temperature range the formation of light oxygenates like glycolaldehyde and formic acid increases and formation of levoglucosan and its isomers decreases in high-

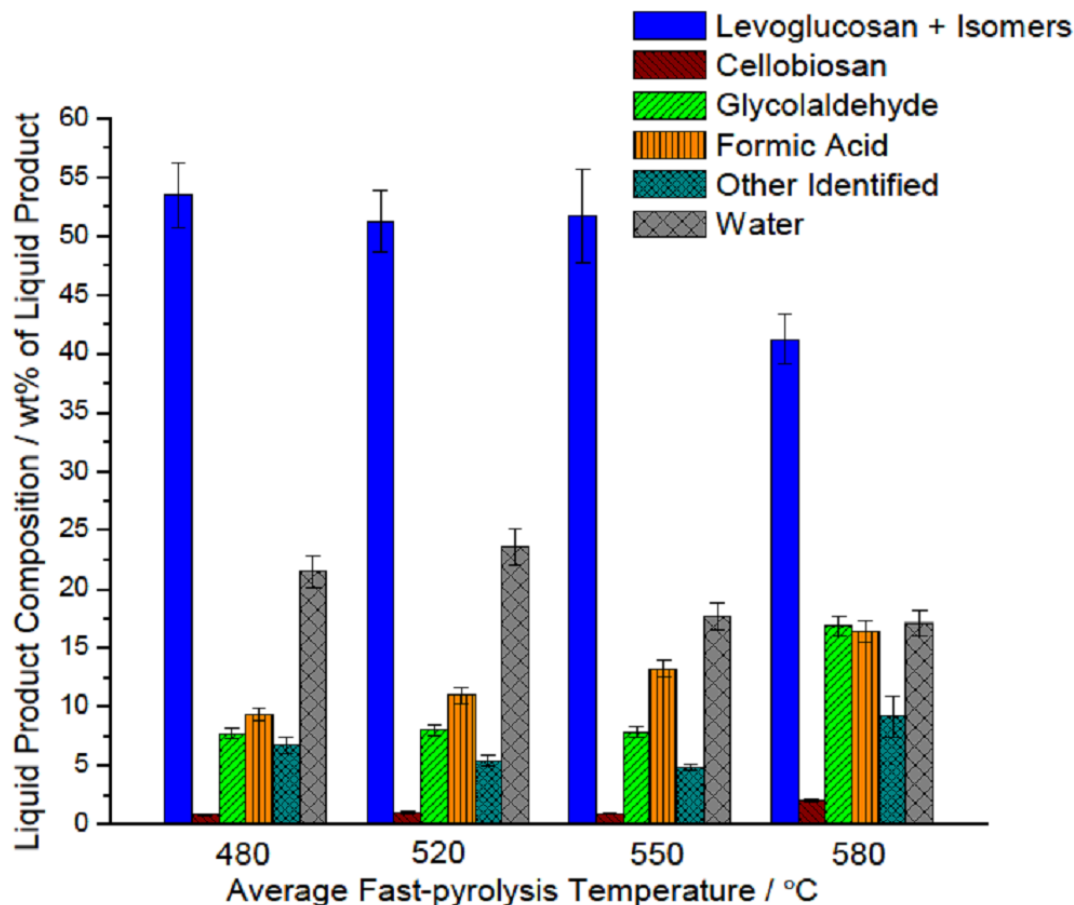


Figure 3.4. Graph showing trends in content of light oxygenate molecules, levoglucosan and its isomers in the liquid products from cellulose fast-pyrolysis at 480°C, 520°C, 550°C and 580°C. All runs were at 25 bar in helium at a total inert pressure of 27 bar.

pressure cellulose fast-pyrolysis (Figure 3.4), consistent with work in the literature on cellulose fast-pyrolysis at atmospheric pressure.[84] The corresponding increase in yield of permanent gases and decrease in the yield of liquid (Figure 3.5), is similar to results in the literature on atmospheric pressure fast-pyrolysis.[2] The increase in the yield of light oxygenates and permanent gases with increasing pyrolysis temperature has been attributed to secondary thermal cracking of the primary pyrolysis vapors.[2, 6, 62, 84]

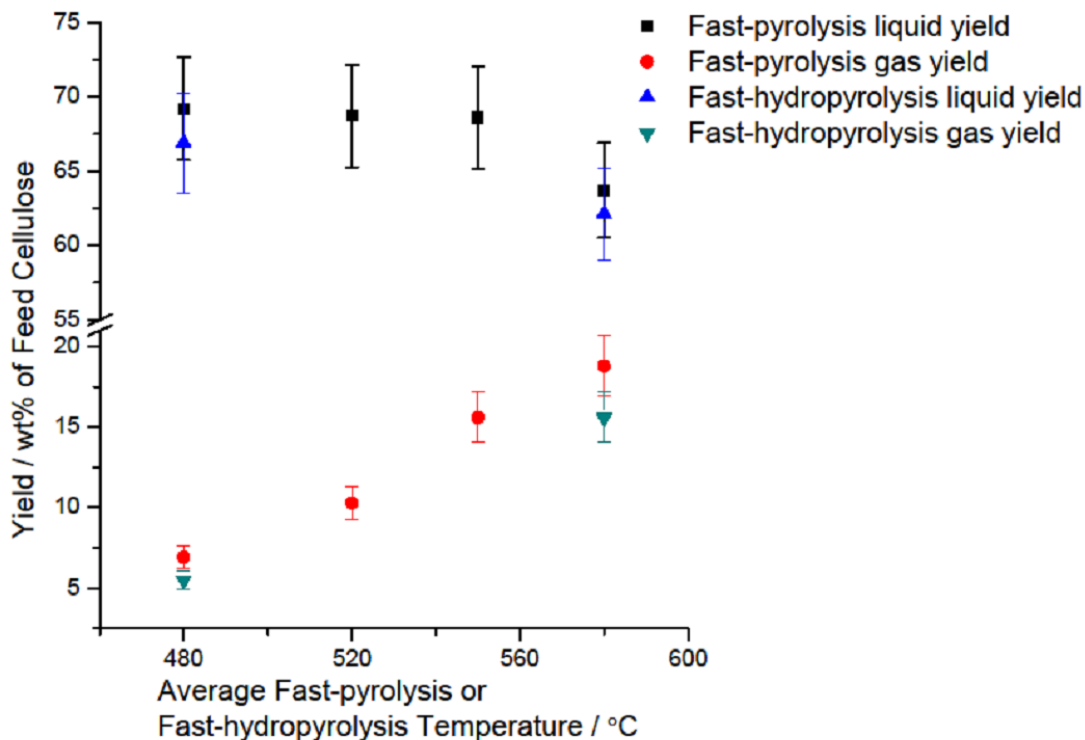


Figure 3.5. Variation of liquid and gas yields with pyrolysis temperature in high-pressure cellulose fast-pyrolysis and cellulose fast-hydrolysis at 27 bar total pressure.

3.4.3 Effect of hydrogen in cellulose fast-hydrolysis and comparison of reactor performance with reaction pressure, at 480°C

At 25 bar helium or hydrogen partial pressure and 480°C pyrolysis temperature, the LC-MS identification and quantification showed no significant differences in the composition of the liquid product from cellulose fast-pyrolysis versus fast-hydrolysis (Figure 3.6). Also, there are no significant differences, within experimental error, in the product yields of solids, liquids and gases (Tables 3.1 and 3.2) from the experiments at 25 bar helium or hydrogen partial and 480°C pyrolysis temperature.

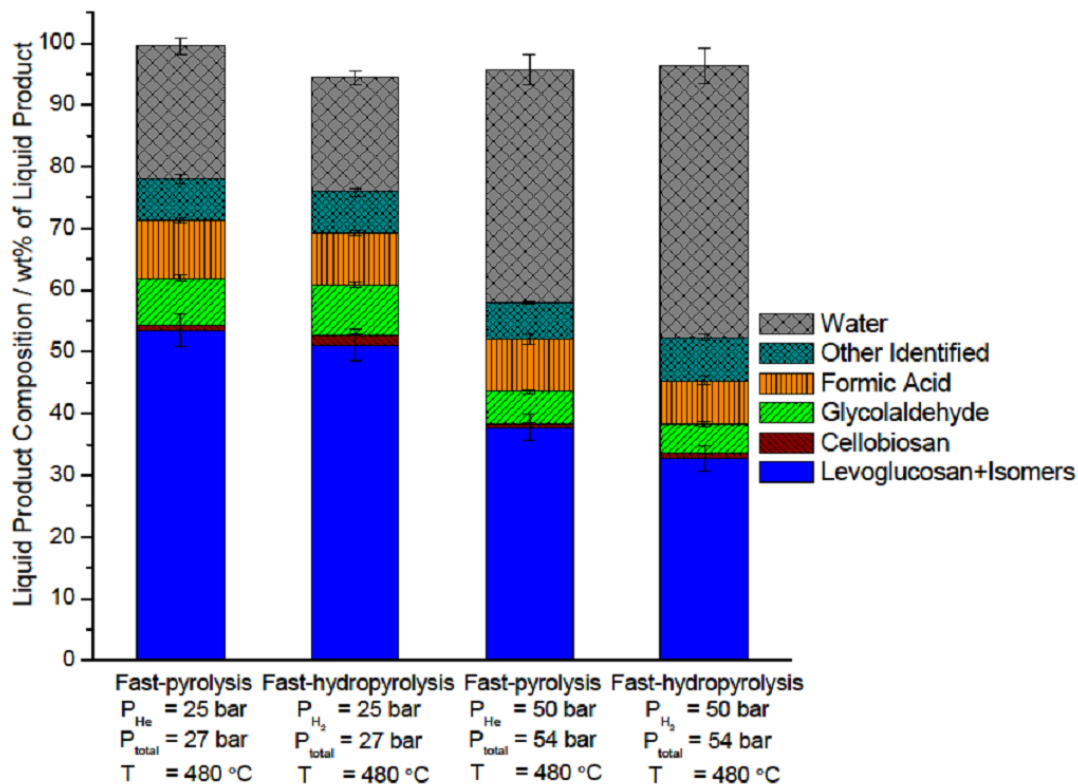


Figure 3.6. Bar graph showing differences in liquid product composition between fast-pyrolysis (25 bar He, 50 bar He) and fast-hydrolysis (25 bar H₂, 50 bar H₂) at 27 bar and 54 bar total pressure with 480°C pyrolysis temperature.

At 50 bar helium or hydrogen partial pressure and 480°C pyrolysis temperature, there were also no significant differences seen, within analytical error of the LC-MS method, in the compositions of the liquid products from fast-pyrolysis and fast-hydrolysis (Figure 3.6). In the 50 bar experiments there was higher char yield and corresponding water yield as compared to the 25 bar experiments in both fast-pyrolysis and fast-hydrolysis, but the permanent gas yields were comparable (Tables 3.1 and 3.2).

The lack of an effect of hydrogen shows that at these pyrolysis conditions hydrogen molecules are not sufficiently activated to enter the reaction mechanism. The liquid,

char and gas yields at 50 bar helium as compared to 50 bar hydrogen partial pressure were comparable, within experimental error. In the 50 bar experiments, however, in both the helium and hydrogen environments there was a significant increase in char formation as compared to the 25 bar experiments (Tables 3.1 and 3.2). Thermal conductivities of hydrogen and helium are nearly independent of pressure at 480°C. Since the char yields are similar between the experiments with hydrogen and helium at the same pressure, we conclude that the gas thermal conductivity is not the main reason for the char increase from 25 bar to 50 bar.

Hence, this difference in char yields in the 50 bar versus 25 bar experiments is attributed to the difference in the hydrodynamics of the entrained cellulose particles and feed gas at 25 bar versus 50 bar. At 50 bar total pressure the hydrodynamics are different than at 25 bar because the reactor inlet feed gas velocity (feed cellulose entraining velocity) at 50 bar was half of that at 25 bar since both were fed at the same standard condition total feed gas flow rate (~ 38 std. L \times min⁻¹). The cyclone radial velocity, as calculated based on reactor inlet feed gas velocity and fluid properties at operating conditions,[85] is lower in the 50 bar experiments as compared to the 25 bar experiments. Hence, the lower cyclone radial velocity leads to a decrease in the number of cellulose particles that impinge on the heated inner walls of this cyclone-type reactor. The particles that do not impinge the wall experience a lower heating rate since the gas-solid heating rate is lower than solid-solid heating rate, which leads to higher char formation. Higher char formation in the 50 bar experiments leads to higher water content and lower content of levoglucosan and its isomers in the liquid products as compared to 25 bar experiments.

3.4.4 Effect of hydrogen in cellulose fast-hydrolysis (25 bar H₂) at 580°C

While hydrogen had no significant effect at 25 bar partial pressure and 480°C, there were differences in the liquid product composition between fast-pyrolysis versus fast-hydrolysis at 580°C (Figure 3.7). At this higher temperature, yield of reactive light oxygenates like formic acid and glycolaldehyde decreased in the presence of

hydrogen. The reaction of hydrogen with these reactive oxygenates at these higher temperatures leads to a higher water content in the fast-hydrolysis liquid product as compared to the fast-pyrolysis case (Figure 3.7). However, we note that the movement of carbon, due to suppression of reactive light oxygenates, could not be conclusively tracked, with the 14 identified compounds on the LC-MS method, for the comparison at 580°C. The product yields of liquids, char and gases were comparable, within experimental error, for 25 bar helium versus 25 bar hydrogen partial pressure at 580°C (Tables 3.1 and 3.2).

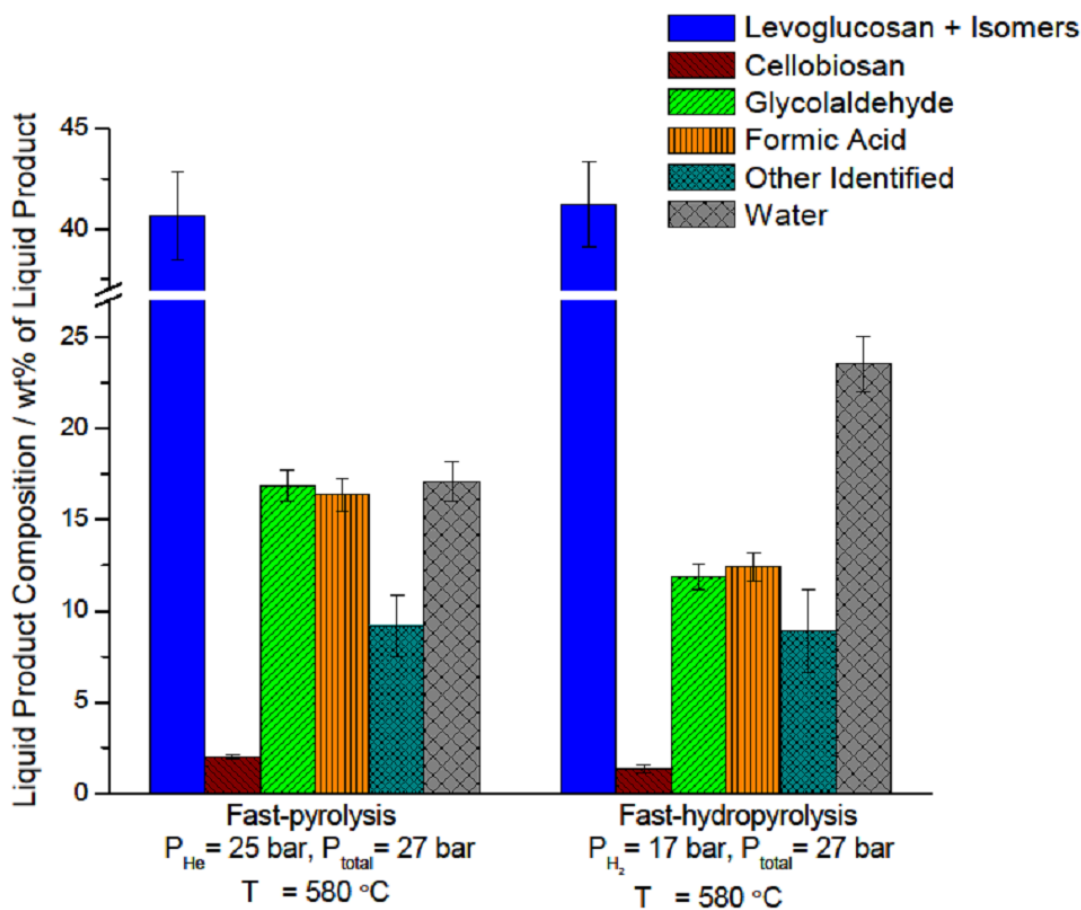


Figure 3.7. Graph showing differences in content of light oxygenate molecules, water, levoglucosan and its isomers in the liquid products from cellulose fast-pyrolysis and fast-hydrolysis at 580°C pyrolysis temperature.

3.4.5 Effect of candidate catalysts for HDO of cellulose fast-hydropyrolysis vapors

Table 3.3 shows the experimental conditions, while Figures 3.8 (a) and (b) show the product yields and gas phase compositions for base case fast-hydropyrolysis with no HDO catalyst and fast-hydropyrolysis runs with Al_2O_3 , 2% Ru/ Al_2O_3 and with 2% Pt/ Al_2O_3 in the downstream vapor-phase HDO reactor. Figure 3.9 shows the differences in the liquid product composition from these experiments and Figure 3.10 shows the conversions of levoglucosan and its isomers, glycolaldehyde and formic acid in the presence of the different candidate HDO catalysts as compared to the base case fast-hydropyrolysis with no HDO catalyst. We note that conversions on this basis show the ability of the HDO reactor to further deoxygenate the effluent from the fast-hydropyrolysis reactor.

Table 3.4 shows the elemental analysis (carbon, hydrogen and oxygen), O/C and H/C ratios on a dry basis, water content of the liquid product and calculated extent of deoxygenation on a dry basis for these experiments with different candidate HDO catalysts.

The water content in the liquid product progressively increased in the presence of Al_2O_3 , 2% Ru/ Al_2O_3 and 2% Pt/ Al_2O_3 as compared to the base case without catalyst. The oxygen content on dry basis in the liquid product progressively decreased in the same order of Al_2O_3 , 2% Ru/ Al_2O_3 and 2% Pt/ Al_2O_3 as compared to the base case without catalyst. The O/C ratio also decreased in the same order. The H/C ratio was the highest in the case of the Pt catalyst. The extent of deoxygenation on a dry basis, in the liquid product as compared to the feed, increased from $\sim 14\%$, in the base case, to $\sim 20\%$ in the presence of the Al_2O_3 catalyst, $\sim 22\%$ with the Ru catalyst and $\sim 27\%$ with the Pt catalyst (Table 3.4).

The liquid and permanent gas yields (Figure 3.8 (a)) in the presence of Al_2O_3 were similar to those in the base case experiment. The total solids (char and coke on the catalyst) yield was higher in presence of Al_2O_3 due to coking on the Al_2O_3 surface. The liquid yields in the experiments in the presence of the Ru and Pt catalysts were

Table 3.4.

Elemental analysis (carbon, hydrogen and oxygen), water content, H/C ratio, O/C ratio extent of deoxygenation (dry basis) from fast-hydropyrolysis experiments with candidate HDO catalysts and base case comparison with fast-hydropyrolysis experiment without HDO catalyst. Dry cellulose: (O/C) = 0.83, (H/C) = 1.67.

	Fast-Hydro- pyrolysis no catalyst	Fast-Hydro- pyrolysis Al ₂ O ₃	Fast-Hydro- pyrolysis 2% Ru/Al ₂ O ₃	Fast-Hydro- pyrolysis 2% Pt/Al ₂ O ₃
Carbon (dry basis) / wt % of liquid	47.8	49.8	50.5	50.9
Hydrogen (dry basis) / wt % of liquid	6.1	6	6	7.5
Oxygen (dry basis, by difference) / wt % of liquid	46.1	44.2	43.5	41.6
Water Content / wt % of liquid	23.5	31.1	45.7	47.8
H/C ratio (dry basis)	1.53	1.45	1.41	1.77
O/C ratio (dry basis)	0.72	0.67	0.65	0.61
Extent of deoxygenation (dry basis) / %	13.6	19.6	22	26.8

lower than for the base case due to loss of carbon to the gas phase in the form of methane and CO respectively. The yield of methane (Figure 3.8 (b)) in the gas phase increased from $\sim 1\text{wt}\%$ of feed cellulose in the base case to $\sim 9\text{wt}\%$ of feed cellulose in the presence of the 2% Ru/Al₂O₃ catalyst. The yield of CO in the gas phase increased from $\sim 10\text{wt}\%$ of feed cellulose in the base case to $\sim 25\text{wt}\%$ of feed cellulose in the presence of the 2% Pt/Al₂O₃ catalyst.

The comparison of liquid product compositions from these experiments (Figure 3.9) showed that the content of levoglucosan and its isomers, glycolaldehyde and formic acid progressively decreased in the presence of Al₂O₃, 2% Ru/Al₂O₃ and 2% Pt/Al₂O₃ as compared to the base case without catalyst. The conversion of levoglucosan and its isomers (Figure 3.10) increased from $\sim 26\%$ both in the presence of Al₂O₃ and 2% Ru/Al₂O₃ to $\sim 48\%$ in presence of 2% Pt/Al₂O₃. Similarly, the conversion of glycolaldehyde and formic acid also increased in the order of Al₂O₃ < 2% Ru/Al₂O₃ < 2%Pt/Al₂O₃. The total contents of other identified compounds (Figure 3.9) were similar between all the candidate HDO catalysts experiments and the base case.

In the downstream vapor-phase catalytic HDO experiments the predominant reaction pathways were dehydration on Al₂O₃, methanation on Ru and decarbonylation on Pt. Al₂O₃ is known to promote acid catalyzed dehydration reactions,[86, 87] which lead to higher water content in the liquid products and higher coking of the Al₂O₃ surface by the resulting olefins. Coking was avoided on the Al₂O₃ supported Pt and Ru catalysts because they favor hydrogenation on the metal site after the dehydration on the Al₂O₃. Both Pt and Ru favor C-C bond cleavage reactions that lead to loss of carbon to the gas phase, in the form of carbon monoxide in the case of Pt and methane in the case of Ru, at the expense of levoglucosan and its isomers and reactive light oxygenates, and hence lead to lower liquid yields with both the catalysts. The Pt catalyst showed the highest extent of deoxygenation ($\sim 27\%$) but also lead to the lowest carbon recovery in the liquid product. Among these experiments, the liquid product with the Pt catalyst had the highest H/C ratio due to the hydrogenation pro-

moted by Pt. The Pt catalyst also resulted in the highest conversion of levoglucosan and its isomers ($\sim 48\%$) and the reactive light oxygenates of glycolaldehyde ($\sim 94\%$) and formic acid ($\sim 91\%$) as compared to the base case fast-hydrolysis without a HDO catalyst.

None of these catalysts is an ideal choice for HDO catalysis in the H₂Bioil process, however, because they lower the carbon recovery in the liquid product as compared to fast-hydrolysis without a HDO catalyst. Ideal choices for catalysts for H₂Bioil process need to have a balance of acid and metal functionalities, where the acid sites promote dehydration of the OH groups to remove oxygen as water and the metal sites aid in hydrogenation with chemisorbed hydrogen. In addition, the ideal metal sites should favor C-O hydrogenolysis reactions rather than other pathways like C-C hydrogenolysis, decarbonylation and decarboxylation that lead to loss of precious carbon atoms to the permanent gas products. We are currently investigating and developing suitable catalysts for the HDO reaction.

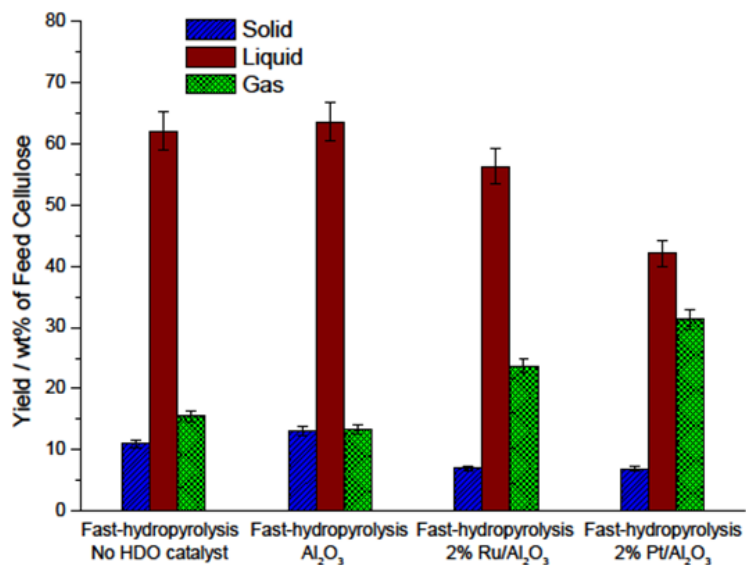
3.5 Conclusions

A high-pressure continuous-flow fast-hydrolysis and downstream vapor-phase catalytic hydrodeoxygenation (HDO) reactor was successfully designed, built, and used to convert cellulose as a model biomass feedstock. A liquid chromatography-mass spectrometry (LC-MS) based method was also developed for quantitative characterization of cellulose pyrolysis liquid products. Experiments show that the formation of permanent gases and light oxygenate species like glycolaldehyde and formic acid increased with increasing pyrolysis temperature in high-pressure fast-pyrolysis. In cellulose fast-hydrolysis, hydrogen was not active at a temperature of 480°C, even up to 50 bar of hydrogen partial pressure and thus gave no differentiation in performance relative to fast pyrolysis in inert atmosphere. At a higher temperature of 580°C, however, the presence of high-pressure hydrogen suppresses the formation of light oxygenate species like glycolaldehyde and formic acid. In our reactor system, increasing reaction pressure from 27 bar to 54 bar, at the same standard feed gas flow

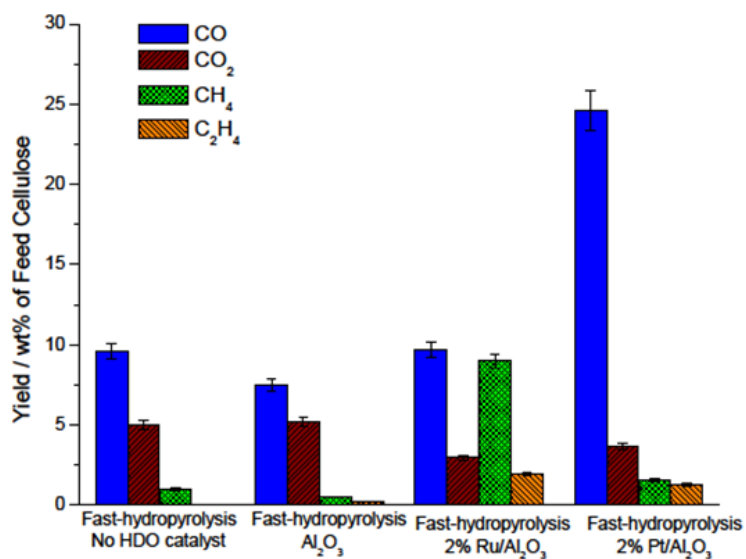
rate, led to higher char yields which was attributed to a lower overall rate of heat transfer. Candidate HDO catalysts Al_2O_3 , 2% Ru/ Al_2O_3 and 2% Pt/ Al_2O_3 improved the extents of deoxygenation of the cellulose fast-hydrolysis vapors, but these catalysts are not the ideal choices for the H_2 Bioil process, because they favor C-C bond cleavage and lower the carbon recovery in the liquid product. However, our reactor configuration provides a proven platform for testing further candidate vapor-phase HDO catalysts to improve the extent of deoxygenation with higher carbon recovery in the liquid product.

3.6 Acknowledgements

Reproduced from Ref. [8] with permission from The Royal Society of Chemistry



(a)



(b)

Figure 3.8. Comparison of (a) product yields and (b) gas phase compositions from fast-hydrolysis with no HDO catalyst and fast-hydrolysis with Al₂O₃, 2% Ru/Al₂O₃, 2% Pt/Al₂O₃ candidate HDO catalysts. Reaction conditions: Base case experiment with no HDO catalyst: P_{H₂} = 17 bar, P_{total} = 27 bar, fast-hydrolysis temperature = 580°C; Experiments with candidate HDO catalysts: P_{H₂} = 9 bar, P_{total} = 27 bar, catalyst bed temperature = 375°C, weight hourly space velocity (WHSV) = 9 hr⁻¹, fast-hydrolysis temperature = 550°C.

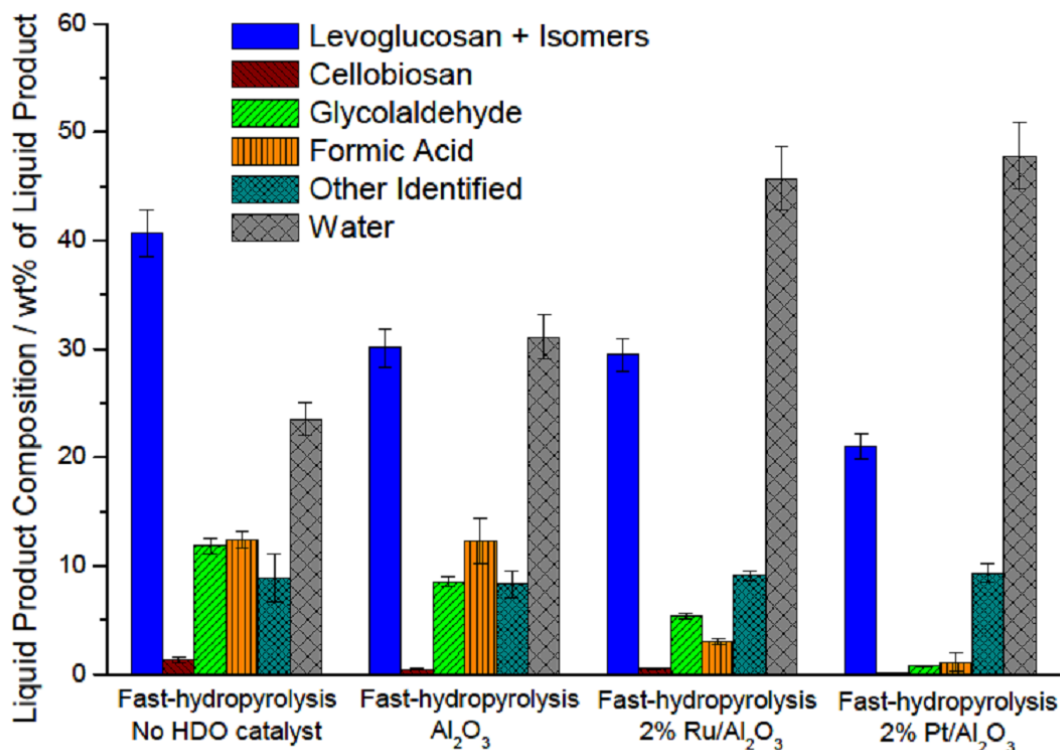


Figure 3.9. Comparison of liquid product compositions from fast-hydroxylation with no HDO catalyst and fast-hydroxylation with Al₂O₃, 2% Ru/Al₂O₃, 2% Pt/Al₂O₃ candidate HDO catalysts. Reaction conditions: Base case experiment with no HDO catalyst: P_{H₂} = 17 bar, P_{total} = 27 bar, fast-hydroxylation temperature = 580°C; Experiments with candidate HDO catalysts: P_{H₂} = 9 bar, P_{total} = 27 bar, catalyst bed temperature = 375°C, weight hourly space velocity (WHSV) = 9 hr⁻¹, fast-hydroxylation temperature = 550°C.

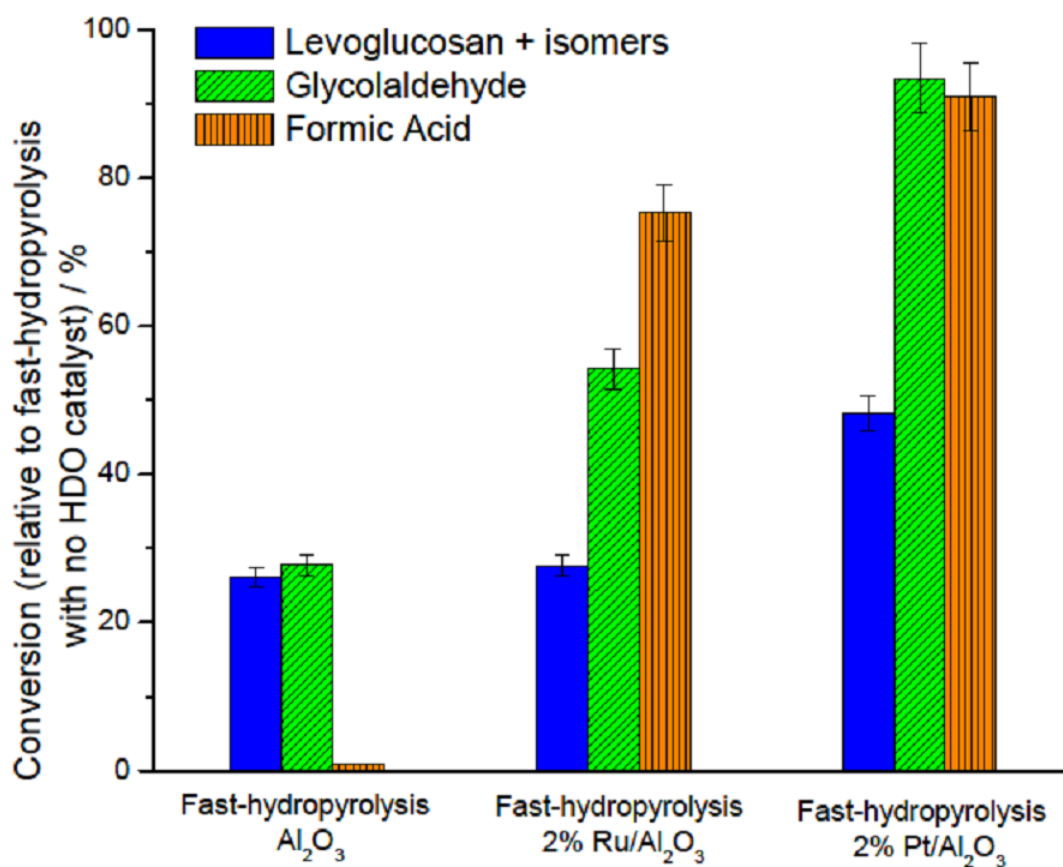


Figure 3.10. Comparison of conversions of levoglucosan and its isomers, glycolaldehyde and formic acid in fast-hydrolysis with Al₂O₃, 2% Ru/Al₂O₃ and 2% Pt/Al₂O₃ candidate HDO catalysts as compared to base case fast-hydrolysis with no HDO catalyst.

4. MASS SPECTROMETRIC STUDIES OF FAST PYROLYSIS OF CELLULOSE

4.1 Introduction

Fast pyrolysis (rapid heating in an inert atmosphere) is an attractive alternative for the conversion of biomass to fuels or valuable chemicals since it is a relatively simple and scalable process.[3, 4, 6, 19, 84, 88–90] Most studies thus far have focused on fast pyrolysis of cellulose since it is the simplest polymer in biomass.[3, 4, 6, 19, 84, 88–90] Unfortunately, even for cellulose, the final fast pyrolysis products (often referred to as biooil in the literature) are a complex unstable mixture of molecules having an oxygen content too high to be used (directly) as a fuel.[3, 4, 6, 19, 84, 88–90] Upgrading this mixture is hindered by its extreme complexity, which arises from numerous competing and consecutive reactions both during and after pyrolysis.[3, 4, 6, 19, 84, 88–90] Currently, no agreement exists in the literature on the mechanisms (e.g., radical, ionic, or neither) of fast pyrolysis reactions of cellulose, the sequence of these reactions, or the identity of the primary products of fast pyrolysis, although anhydro-oligomers in general have been proposed as intermediates several times.[3, 4, 6, 19, 40, 84, 88–91]

With the aim of gaining a deeper understanding of the fast pyrolysis of cellulose, which may allow better control over the final products, the primary products of fast pyrolysis of cellulose, cellobiose, cellotriose, cellotetraose, cellopentaose, and cellohexaose (Figure 4.1), as well as cellobiosan, cellotriosan and cellopentosan, were determined using a previously described mass spectrometry methodology.[9] Primary products, as considered here, are the very first products to evaporate from the hot surface (at 600°C) where pyrolysis occurs.

The reactor configuration utilized in this work was specifically designed to detect the primary products and not to allow them to undergo further reactions.[9] It has

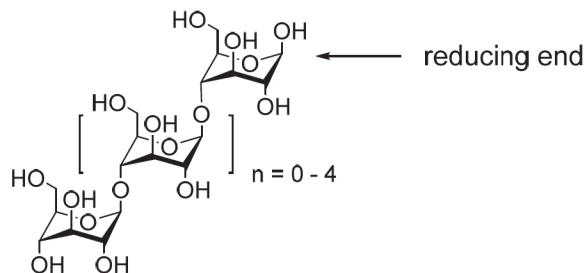


Figure 4.1. The carbohydrate molecules studied here contain two to six d-glucose units coupled to each other in a linear manner via $\beta(1-4)$ linkages, just as in cellulose.

been previously reported that pyrolysis reactor configuration is of critical importance to the product distribution produced from fast pyrolysis of cellulose.[4, 6, 19] Hence, the primary products detected here may not be the same detected in a reactor of a different design. The gaseous molecules were ion-ized via APCI using either chloroform in methanol (negative ion mode; Cl^- attachment) or ammonium hydroxide in water (positive ion mode; NH_4^+ or proton attachment) in order to ensure that all products were ionized and detected.[9] Based on previous model compound studies, both methods have been found to ionize all major pyrolysis products of cellobiose (some minor products were ionized by only one of the two methods).[9] Hence, only the positive ion mode results are discussed below. The structures of most of the ions formed from cellobiose and cellulose have been examined [9, 10] previously by using MS2 experiments (i.e., by isolating them and subjecting them to collision-activated dissociation (CAD)). When necessary, the structures of the fragment ions were examined by isolating them and subjecting them to CAD (MS3 experiment).[9] Where possible, structures were confirmed by analyzing authentic compounds. High resolution mass spectral data needed to determine elemental compositions of the ions were collected using a Thermo Scientific LQIT/Fourier-transform ion cyclotron resonance mass spectrometer.[9] Similar studies were carried out in this research for the fast py-

rolysis products of celotriose, cellotetraose, cellopentaose, and cellohexaose, as well as cellobiosan, cellotriosan and cellopentosan.

4.2 Experimental Methods

The pyrolysis method employed here is based on the coupling of a very fast-heating (up to $20,000^{\circ}\text{C} \times \text{s}^{-1}$) Pyroprobe 5200 (CDS Analytical, Oxford, PA) to a Thermo Scientific LTQ linear quadrupole ion trap (LQIT) mass spectrometer (Waltham, MA) through a custom-built adaptor.[9] The pyrolysis probe uses a resistively-heated platinum ribbon (2.1 mm x 35 mm x 0.1 mm). The pyrolysis probe was placed inside the atmospheric pressure chemical ionization (APCI) source of the linear quadrupole ion trap and the ribbon was heated up to 600°C at a rate of $1,000^{\circ}\text{C} \times \text{s}^{-1}$. The primary products of pyrolysis evaporated into a nitrogen atmosphere at 100°C in the ion source and were quenched. The gaseous molecules were ionized via APCI using ammonium hydroxide in water (positive ion mode; NH_4^+ or proton attachment). The structures of the ions were examined by CAD in MS2 and MS3 experiments and their elemental compositions were determined by high-resolution measurements by using a Thermo Scientific LQIT/Fourier-transform ion cyclotron resonance mass spectrometer. It should be noted here that we are currently unable to determine mass balance for this pyrolysis experiment. However, quantitation of the pyrolysis products was performed using pyrolysis-GC/MS set-up (see Supporting Information).

4.3 Results and Discussion

The primary products of fast pyrolysis of cellobiose, the simplest compound studied, are shown in Fig. 4.2 (top).[9, 10] The relative abundances of the ions reflect the relative abundances of the products that produced them, as verified earlier by using authentic compounds.[9] Only ten major products were observed (with an abundance of at least 10% compared to the most abundant product) and they are consistent with those recently reported in the literature.[9, 10] The unambiguously identified products

include hydroxymethylfurfural (protonated molecule; m/z 127), levoglucosan (NH_4^+ adduct; m/z 180), glucose (NH_4^+ adduct; m/z 198), glucosylpyrano- β -glycolaldehyde (NH_4^+ adduct; m/z 240; note that this product is formed [10] by loss of two glycolaldehyde units (or isomers) from cellobiose), and cellobiosan (NH_4^+ adduct; m/z 342).[9] Based on our preliminary computational studies, formation of cellobiosan has the lowest energy barrier of these reactions.[10] Two levoglucosan isomers were generated: one that forms an NH_4^+ adduct (m/z 180) like the authentic compound and one that does not (protonated molecule; m/z 163).[9, 10] This finding is in agreement with an earlier report wherein the a structure (anhydroglucofuranose) was proposed for the second isomer.[92] It is also noteworthy that levoglucosan is not the major primary product of fast pyrolysis although it is a major final product.[3, 19, 84, 88] In prior reports that utilized on-stream fast pyrolysis-GC/MS, the largest molecules that were observed for cellulose (and oligosaccharide) pyrolysis were levoglucosan and its isomers.[84, 88] This may be explained by the high final temperature of about 300°C typically used in GC analysis, which opens the possibility for secondary reactions of larger primary products. Further, the pyrolysis-MS reactor discussed here achieves both pyrolysis and downstream analysis in as little as 125 ± 57 ms (see Supplementary Information for details) whereas a pyrolysis-GC/MS reactor requires from 2 up to 30 minutes, depending on the elution times of the products.

All the major products observed upon fast pyrolysis of cellobiose were also observed for cellotriose, cellotetraose, cellopentaose, cellohexaose, and even cellulose, albeit with different relative abundances. Specifically, the abundances of glucosylpyrano- β -glycolaldehyde (m/z 240; dominant product for cellobiose formed via loss of two glycolaldehyde molecules (or isomers)), glucose (m/z 198), cellobiose that has lost a glycolaldehyde molecule (or isomer; m/z 300), and cellobiose that has lost both a glycolaldehyde molecule (or isomer) and a water molecule (m/z 282), decrease systematically proceeding from the dimer to trimer, tetramer, pentamer, hexamer and cellulose. For example, Figure 4.2 shows a comparison of the primary products of fast pyrolysis of cellobiose (top) and cellohexaose (bottom). It is obvious that the four

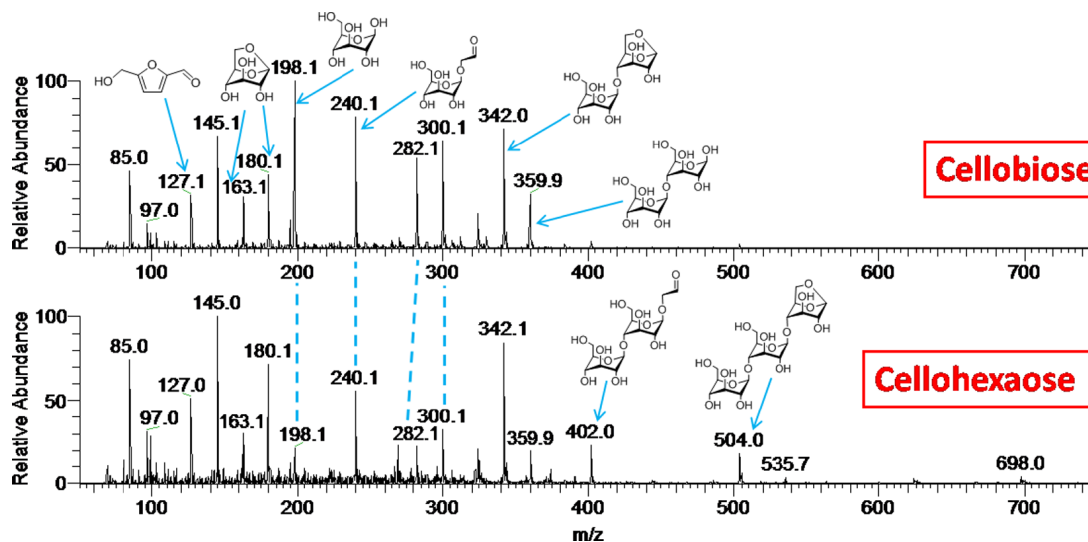


Figure 4.2. Positive ion mode mass spectra showing the primary products of the fast pyrolysis of cellobiose (top) and cellohexaose (bottom) ionized by APCI with ammonium hydroxide. The ions whose relative abundances differ the most are indicated with dotted lines. Two isomers of levoglucosan were observed, levoglucosan itself (ion of m/z 180) and another isomer (ion of m/z 163). All the structures shown for cellobiose have been identified [9] by CAD mass spectral comparison using authentic compounds.

products listed above (highlighted with dotted lines in Fig. 4.2) have substantially lower abundances for cellohexaose than for cellobiose. For cellulose, their abundances are even lower, as shown in Fig. 4.3 (bottom). These findings suggest that the four products described above are somehow associated with the terminal glucose units because the ratio of the terminal units to the total number of glucose units decreases as the size of the oligomer increases. Indeed, the end-group-to-monomer ratio has been reported to be a vital descriptor of cellulose pyrolysis chemistry.[89, 90]

In addition to the products observed for cellobiose, the oligomers studied generated two larger products: a molecule likely to be cellobiosylpyrano- β -glycolaldehyde (NH_4^+ adduct; m/z 402) and cellotriosan (NH_4^+ adduct; m/z 504; verified by comparison of its CAD mass spectrum to an authentic sample). Cellulose also produced a very small

amount of cellotetrosan (NH_4^+ adduct; m/z 666; verified by comparison of its CAD mass spectrum to an authentic sample; Fig. 4.3, bottom). Hence, cellotriosan appears to be the largest product with a significant abundance that is able to efficiently escape the hot pyrolysis surface for cellotriose and the larger oligosaccharides as well as cellulose during fast pyrolysis at 600°C .

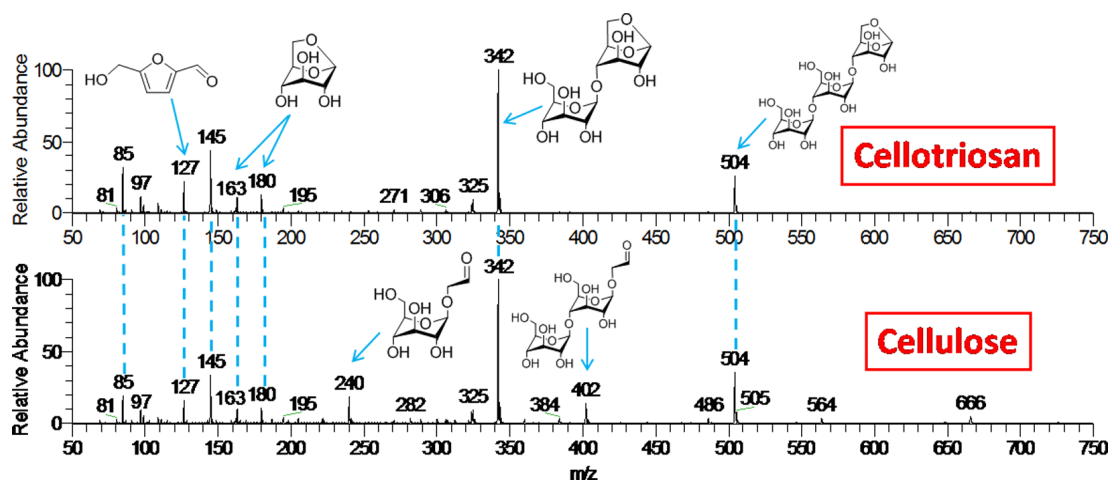


Figure 4.3. Positive ion mode mass spectra showing the primary products of the fast pyrolysis of cellotriosan (top) and cellulose (bottom) ionized by APCI with ammonium hydroxide. Some of the ions having the same m/z ratio are indicated with a dotted line.

Inspired by above observations, fast pyrolysis of cellotriosan was also performed. Cellobiosan dominates this product distribution. However, all major products observed for cellobiose and the oligomers were also observed, with the following exceptions: glucose (m/z 198), glucosylpyrano- β -glycolaldehyde (m/z 240), the product corresponding to cellobiose that has lost a glycolaldehyde molecule (or isomer; m/z 300) and the product corresponding to cellobi-ose that has lost both a glycolaldehyde (or isomer) and a water molecule (m/z 282). These are the four products mentioned above to be somehow associated with the terminal glucose units. Since the reducing end in cellotriosan has been modified compared to cellotriose, and cellotriose yields these four products but cellotriosan does not, the formation of these four products is

likely to depend on the presence of the reducing end in cellotriose. The same is true for cellobiosan (Fig. 4.4) except that no ions larger than m/z 342 (ionized cellobiosan) were observed. The mechanisms of these fragmentations are currently being investigated using quantum chemical calculations. The most surprising finding made in this study is that the fast pyrolysis product distribution of cellotriosan (and cellopentosan) is nearly identical to that of cellulose (Fig. 4.3). The most significant differences are the formation of glucosylpyrano- β -glycolaldehyde (m/z 240) and cellobiosylpyrano- β -glycolaldehyde (m/z 402) for cellulose but not for cellotriosan (or cellopentosan). These two products correspond to cellotriose that has lost two glycolaldehyde molecules (or isomers) (m/z 402) and cellobiose that has undergone the same losses (m/z 240). These findings suggest that the fast pyrolysis of cellulose may be initiated predominantly via two competing processes - formation of anhydro-oligosaccharides, such as cellobiosan, cellotriosan and cellopentosan (major route), and elimination of glycolaldehyde (or isomeric) units from the reducing end of oligosaccharides formed from cellulose during fast pyrolysis (minor route leading to products of m/z 240 and 402; Scheme 4.5).

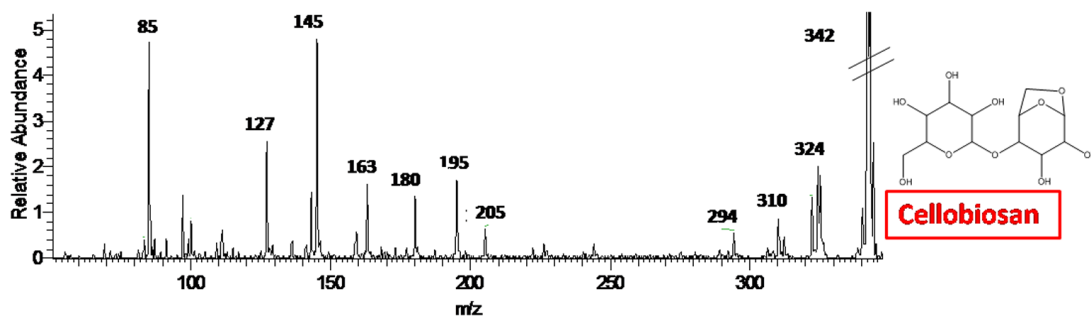


Figure 4.4. A positive ion mode mass spectrum showing the primary products of the fast pyrolysis of cellobiosan (m/z 342) ionized by APCI with ammonium hydroxide. The ions of m/z 85, 127, 145, 163, 180, and 195 are also formed for cellotriosan, cellopentosan and cellulose. The ion of m/z 324 results from the loss of H_2O from the ion of m/z 342.

4.4 Conclusions

The results suggest that molecules larger than cellotriosan are not able to efficiently leave the heated surface during fast pyrolysis of oligosaccharides at 600°C. Instead, they undergo further degradation on the hot surface. The observation of very similar primary product distributions for fast pyrolysis of cellotriosan and cellulose suggests that cellotriosan presents an excellent small-molecule surrogate for cellulose, and it should be a much better choice than glucose, which has been considered previously.[89, 90]

Based on the primary products observed for cellotriosan and cellulose, fast pyrolysis of cellulose under the conditions used here may be initiated predominantly via two competing pathways - formation of small anhydro-oligosaccharides (but not predominantly levoglucosan, as suggested in the literature [3, 19, 84, 88–90]) that either evaporate from the hot pyroprobe surface or degrade to yield most of the other primary products (major pathway), and elimination of glycolaldehyde (or isomeric) molecules from the reducing end of small oligosaccharides formed from cellulose during pyrolysis upon addition of water to yield volatile cellobiosylpyrano- β -glycolaldehyde and glucosylpyrano- β -glycolaldehyde molecules (ions of m/z 240 and 402; Scheme 4.5). Reactions of the primary products of fast pyrolysis are currently under investigation in order to understand better how the final fast pyrolysis products are formed. These reactions may explain why levoglucosan is a major final fast pyrolysis product but not a major primary product.

4.5 Acknowledgments

Reprinted with permission of IM Publications from J. Degenstein, M. Hurt, P. Murria, M. Easton, H. Choudhari, L. Yang, et al., Mass spectrometric studies of fast pyrolysis of cellulose, *European Journal of Mass Spectrometry*. 21 (2015) 321. doi:10.1255/ejms.1335.

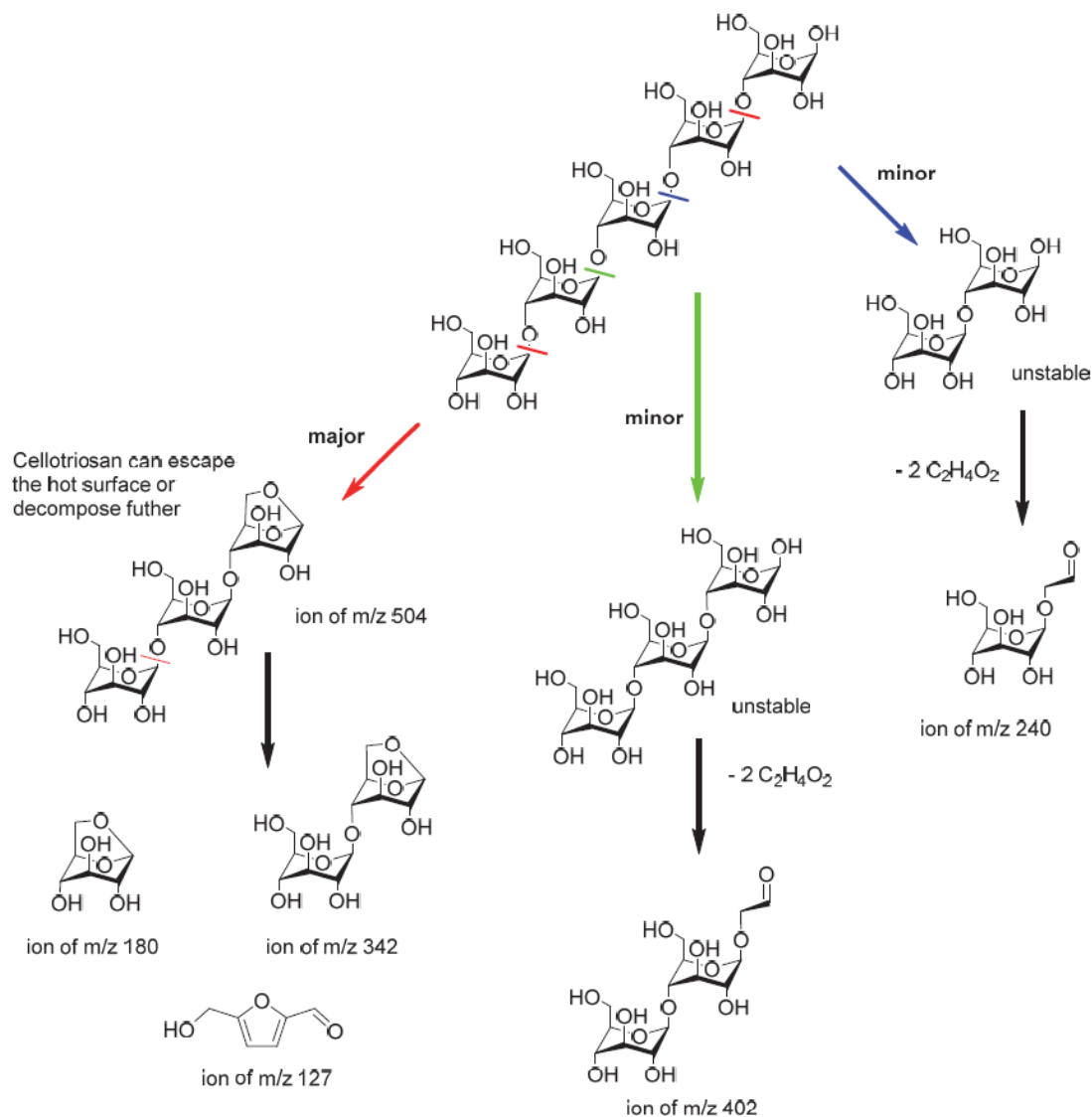


Figure 4.5. A simple schematic of the major fast pyrolysis pathways proposed for oligosaccharides formed from cellulose during fast pyrolysis upon addition of water. The cleavages indicated in red are thought to occur in the middle of a cellulose chain. The cleavages indicated in blue and green likely occur only at the reducing terminals, which for long chains of cellulose represent a small overall fraction of the total units. Hence, they are minor pathways.

5. FAST PYROLYSIS OF ^{13}C -LABELED CELLOBIOSES: GAINING INSIGHTS INTO THE MECHANISMS OF FAST PYROLYSIS OF CARBOHYDRATES

Fast pyrolysis is an efficient method for converting biomass to a low energy-density liquid (bio-oil) that can be further upgraded for use as fuel.[2] Optimization of fast pyrolysis to maximize the yields of compounds containing six or more carbons, which represent some of the most valuable potential end products, requires detailed knowledge of the dominant pyrolysis reactions.[93] However, the pathways and mechanisms (e.g., stepwise radical or ionic or concerted) of fast pyrolysis reactions are still largely unknown even for cellulose, the simplest component of biomass, as well as for analogous di- and oligosaccharides.[88, 93] The goal of this study was to explore these mechanisms by using selective ^{13}C isotope labeling since this has not been performed previously.

The inherent capability of mass spectrometers to separate ions that differ in their mass-to-charge ratios (such as those with and without a ^{13}C label) makes the combination of this technique with fast pyrolysis of selectively labeled carbohydrates a powerful approach for mechanistic studies. We report here the results obtained upon examination of the initial fast-pyrolysis products of unlabeled cellobiose (a glucose dimer with the same linkage as in cellulose; see Figure 5.1) and four selectively ^{13}C -labeled cellobioses by tandem mass spectrometry. It should be noted that “initial” products are defined here as the products that first leave the heated surface of the fast-pyrolysis probe. The experimental studies were complemented by extensive quantum chemical calculations.

The pyrolysis/tandem mass spectrometry technique utilized here has been described in detail in the literature.[9] It combines a pyrolysis probe that can be heated very fast (up to $20\,000^\circ\text{C} \times \text{s}^{-1}$) with a Thermo Scientific linear quadrupole ion

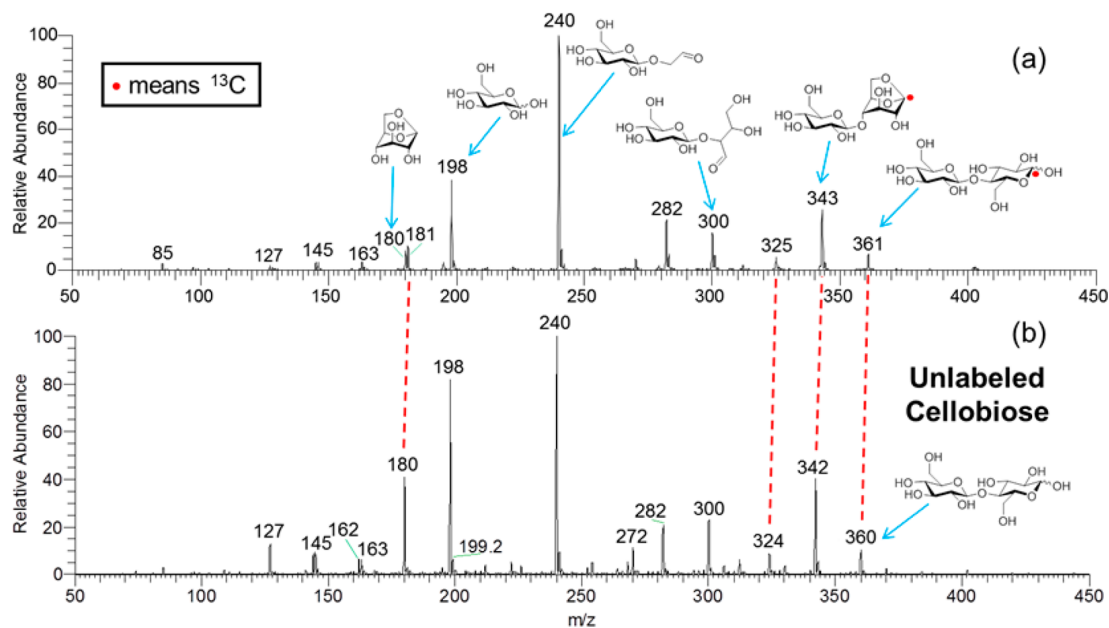


Figure 5.1. Positive ion-mode mass spectra showing the initial fast-pyrolysis products (either as ammonium adducts or protonated molecules) of (a) glucopyranosyl[1-¹³C]glucose and (b) unlabeled cellobiose ionized by APCI with ammonium hydroxide dopant. The structures of the intact molecules are shown at the far right in each spectrum. The products that are ¹³C-labeled in the top spectrum are connected with red dotted lines to the corresponding unlabeled products in the lower spectrum.

trap (LQIT) mass spectrometer. This technique was used to study the initial fast-pyrolysis products of cellobiose and four selectively ¹³C-labeled cellobioses: commercially available [1-¹³C]glucopyranosylglucose and glucopyranosyl[1-¹³C]glucose (Omicron Biochemicals, South Bend, IN) as well as glucopyranosyl[3-¹³C]glucose and glucopyranosyl[5-¹³C]glucose (synthesized according to literature procedures).[94, 95] The pyrolysis probe uses a resistively heated flat platinum ribbon (2.1 mm × 35 mm × 0.1 mm), which was placed inside the atmospheric-pressure chemical ionization (APCI) source of the LQIT. The ribbon was heated to 600°C at a rate of 1000°C × s⁻¹. The initial products of pyrolysis evaporated from the heated surface into a nitrogen atmosphere at 100°C (at atmospheric pressure) in the ion source and were quenched. It should be noted that this approach is very different from that used

in laboratory pyrolysis reactors, since laboratory pyrolysis reactors generally utilize heated surfaces in combination with heated gaseous environments. A soft ionization method, APCI with ammonium hydroxide dopant, was utilized to ionize the products since this method typically generates [9] only one ion (either the NH_4^+ adduct or the protonated molecule) without fragmentation for each product molecule of the type of interest here. The reactor and analysis suites were designed to prevent fragmentation of the pyrolysis products. Mass balances cannot be obtained using this new methodology; however, relative abundances of the products were determined, and much larger pyrolysis products were detected than reported previously.[4, 9, 90] Each reported mass spectrum is a result of a weighted average (based on total ion current) of the individual mass spectra measured during pyrolysis. No significant changes were detected in the product distribution during cellobiose pyrolysis; in other words, the relative abundances were constant during pyrolysis.

The structures of most of the ions were examined by using MS2 experiments (i.e., by isolating them and subjecting them to collision-activated dissociation (CAD)). When necessary, the structures of the fragment ions were examined by isolating them and subjecting them to further CAD (MS3 experiment). High-resolution data needed to determine the elemental compositions of the ions were collected using an LQIT/Fourier-transform ion cyclotron resonance mass spectrometer coupled with the pyrolysis probe as described above.

The initial fast pyrolysis products of unlabeled cellobiose are shown in Figure 5.1b, and they are in agreement with those reported previously.[9] The identified products include hydroxymethylfurfural (protonated molecule of m/z 127), levoglucosan (NH_4^+ adduct of m/z 180 and a protonated molecule of m/z 163), glucose (NH_4^+ adduct of m/z 198), and β -D-glucopyranosylglycolaldehyde (NH_4^+ adduct of m/z 240). β -D-Glucopyranosylglycolaldehyde is likely formed upon the loss of two glycolaldehyde (or isomeric) molecules from cellobiose upon fast pyrolysis. On the other hand, the pyrolysis product generating ions of m/z 300 (NH_4^+ adduct) is formed via the loss of a single glycolaldehyde (or isomeric) molecule from cellobiose, and the product

generating ions of m/z 282 (NH_4^+ adduct) is formed via the loss of glycolaldehyde (or isomeric) molecule and water from cellobiose. Evidence in support of these products being initial products instead of secondary products was obtained from the previously determined structure of the β -D-glucopyranosylglycolaldehyde product.[9] The glycosidic bond (i.e., the C-O bond at the oxygen atom on the carbon adjacent to the ring oxygen) in this pyrolysis product is still in the same position and has the same stereochemistry (β -1) as in cellobiose. If β -D-glucopyranosyl-glycolaldehyde were not an initial product but instead the result of recombination of smaller initial products, one would expect a mixture of linkage positions and stereochemistry. These larger products (>162 Da) are typically not seen with pyrolysis/GC-MS methodologies because of their thermal instability and low volatility, which may at least partially explain the incomplete mass balance of previous oligosaccharide pyrolysis studies.[4, 90] The results presented here are in agreement with recent mechanistic studies suggesting that glycolaldehyde may form directly from cellobiose (or a longer glucosaccharide) rather than through a glucose intermediate.[96–98]

The ionized initial fast-pyrolysis products of glucopyranosyl-[1- ^{13}C]glucose (with the label at the reducing end or the end containing a free hydroxyl group on the carbon adjacent to the ring oxygen) are shown in the mass spectrum in Figure 5.1a. Comparison of these products to those produced from unlabeled cellobiose (Figure 5.1b) revealed that only one product is partially ^{13}C -labeled (levoglucosan, NH_4^+ adducts of m/z 180 and 181), while all of the others are either completely labeled or do not contain the label at all. Specifically, cellobiosan (NH_4^+ adduct of m/z 343) and the product formed via loss of water from cellobiosan (NH_4^+ adduct of m/z 325) are completely ^{13}C -labeled, as expected, while all of the other products are unlabeled (Figure 5.1a). For example, glucose, β -D-glucopyranosylglycolaldehyde and β -D-glucopyranosylerythrose contain intact rings that originate exclusively from the nonreducing end since they have no label. The formation of glucose from the nonreducing end of cellobiose must occur via scission of the aglyconic bond (i.e., the other C-O bond of the oxygen atom involved in the glycosidic linkage) rather than the glyco-

sidic bond as previously proposed.[88, 99] In the literature, the only mechanisms that explain formation of glucose involve glycosidic bond cleavage and thermohydrolysis, which form glucose either from the reducing end only or from the reducing and nonreducing ends in equal amounts, respectively.[84, 88, 100] On the contrary, the present results indicate that the formation of glucose occurs exclusively from the nonreducing end of cellobiose (within the detection limits of our pyrolysis/MS experiment). This observation suggests that there is at least one additional glucose formation pathway that has not been proposed in the literature. Work is underway to explore alternate reaction pathways that explain formation of glucose from the nonreducing end.

The results also demonstrate that the first glycolaldehyde (or isomeric) molecule eliminated from cellobiose upon pyrolysis contains the ^{13}C label (NH_4^+ adduct of m/z 300); this process must involve the loss of ^{13}C -1 and most likely C-2 of the reducing end of cellobiose. Identification of the origin of the initially eliminated glycolaldehyde on the basis of carbon labeling indicates that certain mechanisms may be more feasible than others. For example, the retro-aldol mechanism considered here and elsewhere results in the elimination of glycolaldehyde from the C-1 and C-2 positions.[84, 100] On the other hand, 1,2-dehydration followed by retro-Diels-Alder reaction would result in elimination of glycolaldehyde from the C-5 and C-6 positions.

Levoglucosan must be formed via at least two pathways since two different ions (NH_4^+ adducts of m/z 180 and 181, corresponding to ammoniated molecules with and without the ^{13}C label) are produced. Hence, levoglucosan is likely formed from both the reducing and nonreducing ends of cellobiose. The ionized initial fast-pyrolysis products of another labeled cellobiose, $[1-^{13}\text{C}]\text{glucopyranosylglucose}$, with a ^{13}C label in the nonreducing end, are shown in the mass spectrum in Figure 5.2a. Comparison of these products to those obtained for unlabeled cellobiose revealed that all of the ionized products with m/z values greater than 180 contain the ^{13}C label. These results support the above conclusion that glucose is produced exclusively from the nonreducing end of cellobiose. Further, both labeled and unlabeled levoglucosan were observed, in agreement with the above proposal that more than one mechanism must

lead to levoglucosan and that it is likely to be formed from both the reducing and nonreducing ends. Finally, the results show that the first two glycolaldehyde (or isomeric) molecules eliminated from cellobiose come from the reducing end.

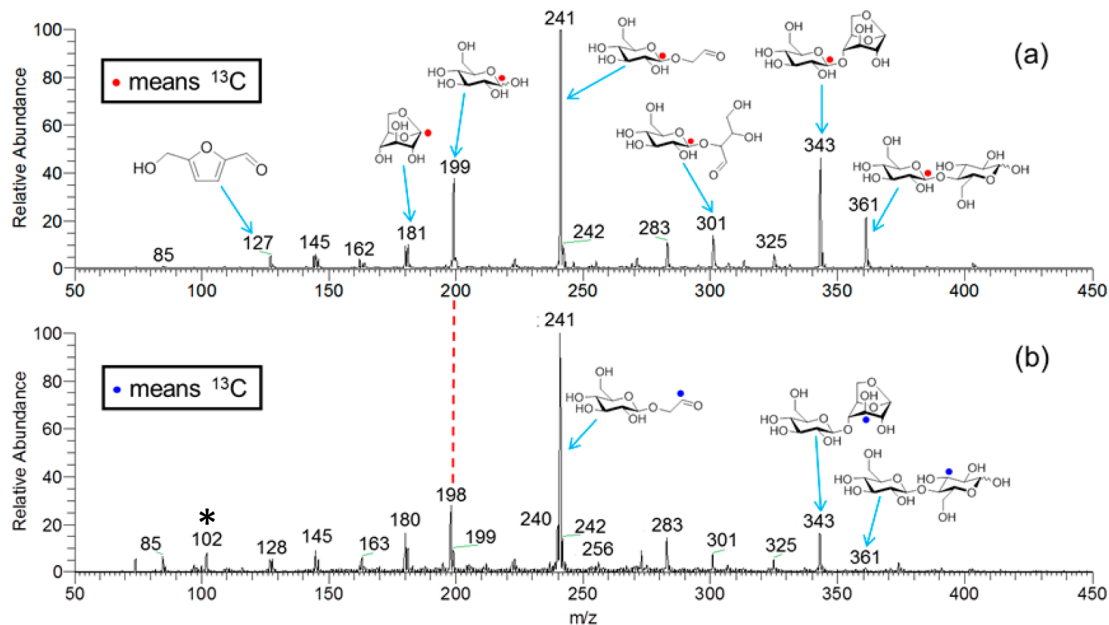


Figure 5.2. Positive ion-mode mass spectra showing the initial fast-pyrolysis products (either as ammonium adducts or protonated molecules) of (a) [1-¹³C]glucopyranosylglucose and (b) glucopyranosyl[3-¹³C]glucose ionized by APCI with ammonium hydroxide dopant. The structures of the intact molecules are shown at the far right in each spectrum. The only product that is labeled in the top spectrum but unlabeled in the bottom spectrum is glucose, as indicated by a red dotted line. The ion labeled with * corresponds to an unknown impurity.

In order to explore the mechanism for the elimination of the second glycolaldehyde (or isomeric) molecule from the reducing end of cellobiose (to yield the NH_4^+ adduct of m/z 240 for the unlabeled cellobiose), a third ¹³C-labeled cellobiose, glucopyranosyl[3-¹³C]glucose, was synthesized. The ionized initial fast-pyrolysis products of this compound are shown in the mass spectrum in Figure 5.2b. The presence of a major ion of m/z 301 (containing ¹³C) supports the above finding that the first glycolaldehyde (or isomeric) molecule eliminated from cellobiose upon pyrolysis contains

C-1 and C-2 of the reducing end (i.e., to form the ion of m/z 301). Furthermore, since elimination of the second glycolaldehyde (or isomeric) molecule yields an ion of m/z 241 (containing ^{13}C), this glycolaldehyde unit must contain C-5 and C-6 of the reducing end. Examination of a fourth ^{13}C -labeled compound, glucopyranosyl[5- ^{13}C]glucose, confirmed all of the above conclusions. In particular, the elimination of C-5 of the reducing end in the second eliminated glycolaldehyde (or isomeric) molecule was verified by the observation of β -D-glucopyranosylglycolaldehyde with no ^{13}C .

Quantum chemical calculations [101] at 600°C (see the Supporting Information for calculations performed at 25°C) at the M06-2X/6-311++G(d,p)//M06-2X/6-311++G(d,p) level of theory [102, 103] revealed a low-energy pathway for the consecutive elimination of one glycolaldehyde and two isomeric ethenediol molecules from cellobiose, eventually producing levoglucosan (Figure 5.3) (it is well-known that ethenediol converts readily into its tautomer glycolaldehyde; therefore, β -D-glucopyranosylethenediol was assumed to readily tautomerize to β -D-glucopyranosylglycolaldehyde). This pathway is consistent with the ^{13}C -labeling results described above. Work to identify additional pathways leading to levoglucosan and the other observed products is in progress.

In conclusion, identification of the initial fast-pyrolysis products of selectively ^{13}C -labeled cellobioses using a previously reported [9] experimental method has been demonstrated to be a powerful approach for exploring the details of the initial reactions in the fast pyrolysis of cellobiose. Several products that are likely to be produced by consecutive glycolaldehyde (or isomer) eliminations from the reducing end of cellobiose, including levoglucosan, were observed. Literature mechanisms proposed for the fast pyrolysis of cellobiose are not consistent with the results reported here. Quantum chemical calculations revealed a feasible low-energy pathway for some of the products observed.[88] Since many of the initial products have molecular weights greater than those of the final pyrolysis products reported for cellobiose in the literature,[4, 90] these initial products may be intermediates in the formation of the final products, which include light oxygenated hydrocarbons.

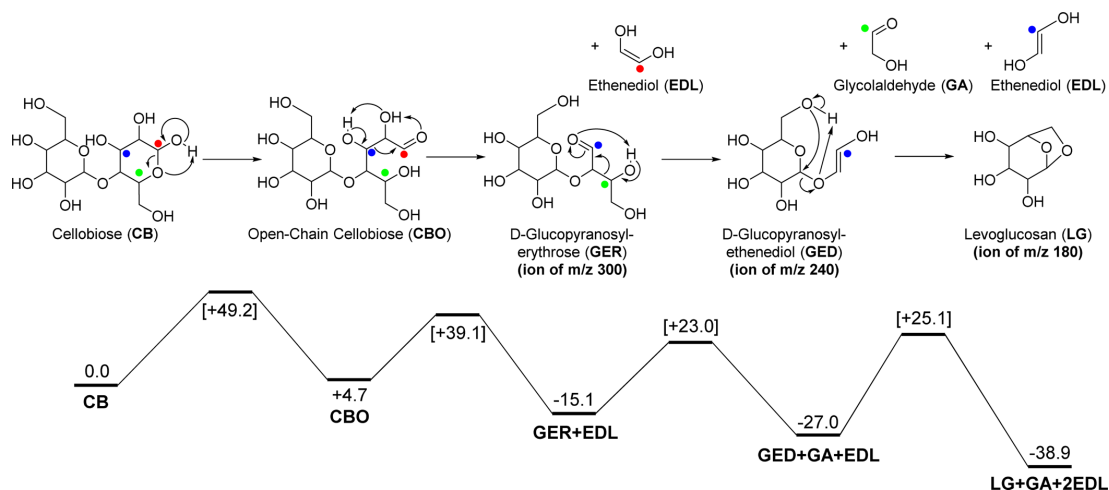


Figure 5.3. Calculated free energies (kcal mol^{-1}) of intermediates and transition states (square brackets) for the formation of levoglucosan from cellobiose via consecutive losses of one glycolaldehyde (GA) and two ethenediol (EDL) molecules (which are likely to eventually tautomerize to glycolaldehyde) at 600°C obtained at the M06-2X/6-311++G(d,p)//M06-2X/6-311++G(d,p) level of theory. The location of a ^{13}C label at C-1 in the reducing end is indicated by a red circle, at C-3 by a blue circle, and at C-5 by a green circle. The mass-to-charge (m/z) ratios are for unlabeled cellobiose.

Minimization of the production of low-molecular-weight oxygenated hydrocarbons is an important goal for fast pyrolysis of cellulose in order to maximize the production of fuel and high-value chemical products. Knowledge of the fragmentation pathways occurring during fast pyrolysis of smaller carbohydrates will contribute to the knowledge of fast pyrolysis of cellulose and ultimately fast pyrolysis of whole biomass, possibly enabling the tailoring of the product distribution obtained upon fast pyrolysis of whole biomass.

5.1 Acknowledgements

Reprinted with permission from J.C. Degenstein, P. Murria, M. Easton, H. Sheng, M. Hurt, A.R. Dow, et al., Fast Pyrolysis of ^{13}C -Labeled Cellobioses: Gaining Insights

into the Mechanisms of Fast Pyrolysis of Carbohydrates, *J. Org. Chem.* 80 (2015) 1909–1914. doi:10.1021/jo5025255. Copyright 2015 American Chemical Society.

6. DETERMINATION OF THE PRIMARY FAST PYROLYSIS PRODUCTS OF SYNTHETIC G-LIGNIN OLIGOMERS WITH β -O-4 LINKAGES VIA ON-LINE MASS SPECTROMETRY

6.1 Introduction

Fast pyrolysis holds a great potential for directly converting solid biomass into liquid biofuel when coupled with immediate downstream upgrading.[12, 19, 104–106] Lignocellulosic biomass is one of the most abundant renewable resources on earth. Lignin is the second most abundant component of this biomass (about 15% -30% by weight).[21, 107–110] Currently, lignin extracted from whole biomass by using methods such as organosolv and kraft is used as the starting material for pyrolysis. Several studies on pyrolysis of extracted lignins have been published over the past several decades.[111–114] However, due to the complex and often poorly characterized nature of these extracted lignins, the reaction mechanisms and primary products of fast pyrolysis of intact lignin, which are essential for understanding the fast pyrolysis process of biomass, are still poorly understood.

Since the examination of the fast pyrolysis processes of lignin is challenging, some studies have focused on the pyrolysis of monomeric lignin model compounds, such as guaiacol, syringol, isoeugenol, and vanillin. Free radical mechanisms have been proposed as the dominant pyrolysis mechanisms for these compounds.[115, 116] During the fast pyrolysis of guaiacol, methyl radical loss followed by two CO losses were observed as the primary radical products by using the gas chromatograph with a mass spectrometer (py-GC/MS). The imaging photoelectron photoion coincidence (iPEPICO) with VUV synchrotron radiation was also used to monitor the radical decomposition product during the fast pyrolysis.[117] The author proposed that these radicals could initiate reactions to produce recombination and rearrangement sec-

ondary products, such as 2-hydroxybenzaldehyde in the case of guaiacol.[117] However, in an early study, both free radical mechanisms and concerted mechanisms were proposed for the fast pyrolysis of guaiacol.[115] The fast pyrolysis behavior of dimers with β -O-4 linkages have been also studied.[118] Phenethyl phenyl ether, which is an analog of β -O-4 lignin dimer, is often used for pyrolysis studies. Fast pyrolysis of phenethyl phenyl ether at 500°C proceeded by C-O and C-C bond cleavages, in a 37:1 ratio, to produce styrene plus phenol as the dominant products.[118] Through examination of the deuterium isotope effect, it was shown that the C-O cleavage occurs by homolysis and by 1,2-elimination in a ratio of 1.4:1, respectively.[118] A comprehensive computational study on the fast pyrolysis of phenethyl phenyl ether derivatives with different functional groups was conducted. The homolytic oxygen-carbon bond dissociation enthalpy was calculated to be substantially lowered by oxygen substituents situated at the phenyl ring adjacent to the ether oxygen.[119] The reaction rates of hydrogen atom abstraction from methoxy phenethyl phenyl ethers by phenoxy and benzyl radicals were calculated.[120] The results showed that methoxy substituents decelerated the hydrogen atom abstraction by the phenoxy radical but not for benzyl radical.[120] Phenyl-shift reaction (Figure 6.1) for the β -radical of phenethyl phenyl ether during fast pyrolysis is an integral step in the fast pyrolysis of phenethyl phenyl ether. This reaction was calculated to proceed through an oxaspiro[2.5]octadienyl radical intermediate and substituents on the phenethyl ring were reported to have only little influence on the rate constants.[121] Both computational and experimental studies have been conducted on fast pyrolysis of phenethyl phenyl ether over a wide temperature range of 300°C - 1350°C.[13] The initial fast products were directly detected by photoionization time-of-flight mass spectrometry and by cryogenic matrix-isolated infrared spectroscopy.[13] Based on the results (Figure 6.2), It was suggested that concerted nonradical elimination reactions (retro-ene and Maccoll reactions) dominate over free radical reactions under typical fast pyrolytic conditions (<600°C).[13] Direct C-O bond homolysis was proposed to initiate radical chain mechanism during pyrolysis of a β -O-4 lignin dimer 1-(4-hydroxy-3-methoxyphenyl)-2-(2-

methoxyphenoxy)-1,3-propanediol.[122] It has been reported that the product distributions of fast pyrolysis of lignin dimers are more complex than those of monomers because more secondary reactions occur.[123] In a recent study, fast pyrolysis of a fully acetylated β -O-4 polymeric lignin model compound was studied. A free radical reaction pathway was proposed to explain the products.[123] However, compared to the fast pyrolysis of lignin monomers, the fast pyrolysis products of the lignin polymers were reported to undergo more secondary and tertiary reactions, which complicates the interpretation of the results.[123]

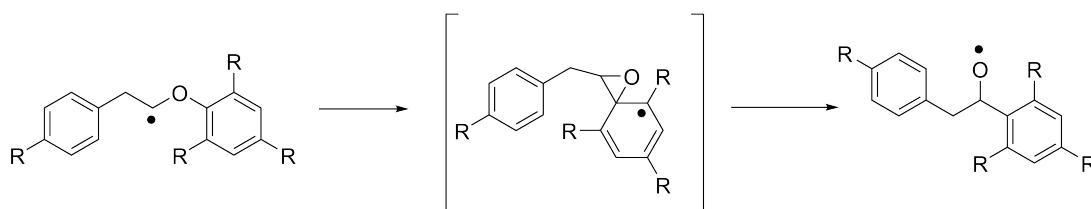


Figure 6.1. The proposed phenyl-shift reaction for the β -radical of phenethyl phenyl ether during fast pyrolysis.[121]

Since very few studies [13, 117] are available on the determination of the fast pyrolysis primary products of lignin monomers and dimers, it is obvious that more studies on the primary products and mechanisms of fast pyrolysis reactions of lignin model compounds are needed to further unravel the complicated processes involved. Previously, fast pyrolysis experiments have been coupled with gas chromatography/mass spectrometry (py-GC/MS) to carry out on-line studies of the primary and later pyrolysis products [14] of organosolv lignin. The primary products were proposed to be monomers that form oligomeric products through radical repolymerization.[14] In a recent study, organosolv lignin was pyrolyzed in a micropyrolyzer and the vapor was directly analyzed using online GC/MS, or recovered in a cold solvent and then analyzed using gel permeation chromatography and high-resolution FT-ICR mass spectrometry.[124] A total of 569 phenolic compounds with molecular weight less than 504 Da were found using py-GC/MS. The molecular weight of the pyrolysis

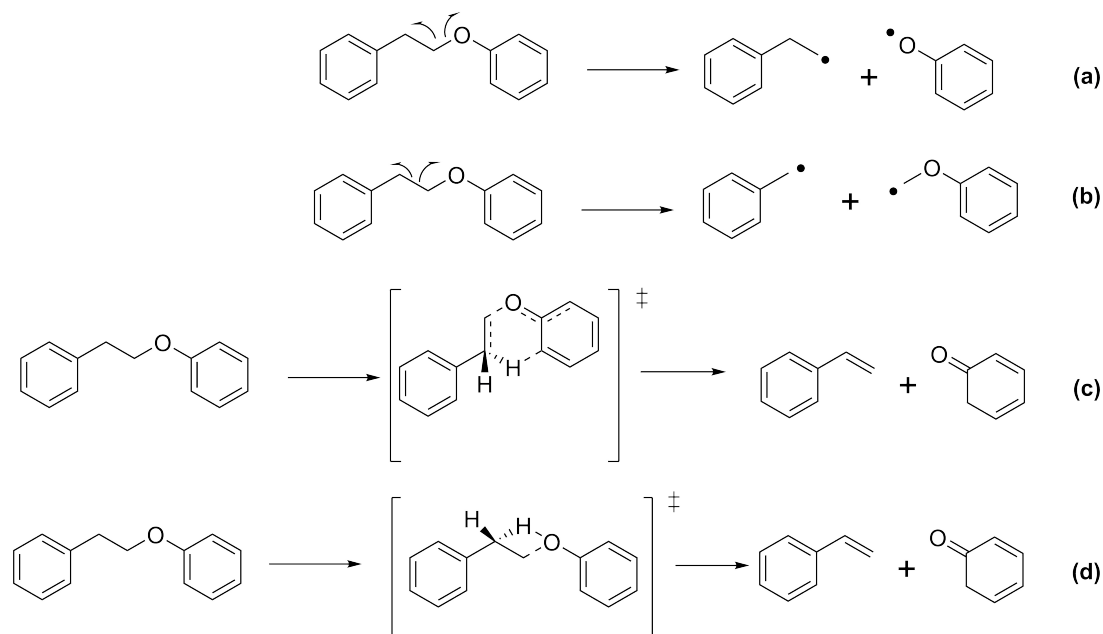


Figure 6.2. Four proposed routes for the initial decomposition of phenethyl phenyl ether during fast pyrolysis. Routes a and b involve free radical mechanisms. Routes c and d involve retroene and MacColl reactions, respectively.[13]

products measured by GC/MS were found to be smaller than phenolic oligomers in condensed bio-oil recovered from fast pyrolysis reactors. The most abundant phenolic compounds among these smaller molecules were monomers followed by dimers, trimers and tetramers according to gel permeation chromatogram. It was proposed that reactive phenolic monomers could reoligomerize during fast pyrolysis.[124] A limitation of the GC/MS approach is that it only allows relatively volatile and thermally stable compounds to be observed and it may not allow detection of primary products with high molecular weight. Thus, only certain lignin dimer and monomer products can be detected (MW < 300Da).[9, 14, 124]

In order to overcome the above limitations of pyrolysis/GC/MS, an on-line mass spectrometric analysis method published recently[28] was employed to detect the primary products of fast pyrolysis of lignin model compounds ranging from trimers

to a polymer. The primary products are defined here as the products that first leave the hot pyrolysis surface. This is likely to be the first time that pure lignin oligomers (larger than dimer) are studied in fast pyrolysis. All the lignin model compounds were synthesized and the synthetic procedures were described in a separate paper. All model compounds contain the β -O-4 linkage as this is the most abundant type of a lignin linkage in nature, constituting about 50% of the linkages in total lignin in softwood.[12]

6.2 Results and Discussion

Four β -O-4 lignin model compounds 1-4 (Figure 6.3) were used in this study, i.e., two trimers (1 and 2), one tetramer (3) and one polymer (4). The degree of polymerization (n) of polymer 4 is about 20.[125] The synthesis procedures used for 1-4 have been described previously.[125] All phenyl rings in compounds 1-3 are named starting from the phenolic 4-end on the left to 1-end on the right as A, B, and C rings for trimers 1 and 2 and A, B, C, and D rings for tetramer 3 (Figure 6.3). The A ring is named as the 4-end unit. The B ring in 1 and 2 and the B and C rings in 3 are named as middle units. The C ring in 1 and 2 and D ring in 3 are named as 1-end unit. Compounds 1 and 3 share the same 4-end, middle and 1-end units, which is also true for compounds 2 and 4. However, the 1-end unit (guaiacol) of 1 and 3 is different from the 1-end unit (guaiacol with a 1,3-propanediol moiety) of 2 and 4. The difference in the 1-end units among these compounds could allow the facile identification of 1-end unit related pyrolysis products.

For fast pyrolysis experiments, the lignin model compounds 1-4 (1mg) were loaded onto the ribbon of the pyrolysis probe, which was then heated at a rate of 1000°C/s up to a final temperature of 600°C and held there for one second. During pyrolysis, the primary products evaporated off the ribbon and were quenched by nitrogen gas in the ion source, instantly ionized by (-)APCI with ammonia hydroxide dopant, [16, 126, 127] and then detected by a linear quadrupole ion trap (LQIT) mass spectrometer. Because (-)APCI with ammonium hydroxide as dopant facilitates the ionization

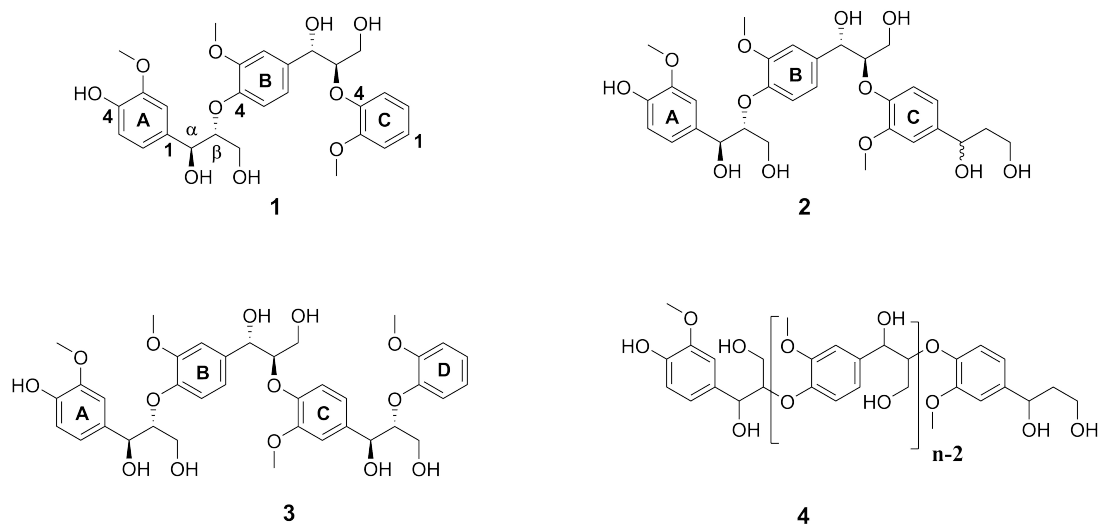


Figure 6.3. The lignin model compounds (1-4) used in this study. The β -O-4 linkages in compounds 1-3 are in trans relative configuration. Polymer 4 has a ratio of 1:1 for cis/trans β -O-4 linkages. The number n is about 20 for 4.

of phenolic moieties, all the lignin pyrolysis products with a free phenol group are expected to be ionized and detected at nearly equal efficiency. The total residence plus analysis time (the time between when the pyrolysis probe starts heating and the detection of the first pyrolysis products by the mass spectrometer) was 125 ± 57 ms.[34] The short residence time minimizes secondary reactions. Under the above fast pyrolysis conditions, the β -O-4 lignin dimer undergoes thermal evaporation rather than complete pyrolysis since the β -O-4 lignin dimer molecule is the only product observed during fast pyrolysis. Hence, the lignin trimers and tetramer 1-3 are the smallest model compounds studied.

In this section, a detailed comparison of the primary fast pyrolysis products of 1-4 will be presented. Then the possible mechanisms for fast pyrolysis of β -O-4 lignin are discussed using tetramer 3 as an example.

6.2.1 Comparison of the primary fast pyrolysis products of 1-4

The negative-mode APCI mass spectra (MS^1) measured for the primary fast pyrolysis products of compounds 1-3 are shown in Figure 6.4. The ionized pyrolysis products are distributed in monomeric (m/z 100-250), dimeric (m/z 250-450), trimeric (m/z 450-600) and tetrameric (m/z 600-750) mass regions according to their mass-to-charge ratio (m/z). The deprotonated 1-3 (m/z 515, 589 and 711) are observed in the mass spectra, indicating that some intact 1-3 molecules were able to evaporate off the ribbon without being fragmented. The ionized pyrolysis products that came directly from the molecules without any H_2O and CH_2O losses during pyrolysis are called key pyrolysis products, such as AB (m/z 391 of deprotonated form) and BC (m/z 319) of 1. The structures of these deprotonated key pyrolysis products were confirmed through CAD via comparison to CAD measured for deprotonated authentic compounds in a previous study (e.g., ions of m/z 319, 271 and 515 for 3, Figures E.1, E.2, E.3 in supporting information). For example, as shown in Figure E.1, the MS^2 spectrum of the deprotonated β -O-4 dimer (m/z 319) obtained through direct injection of a synthesized dimer into the ion source followed by ionization is similar to that measured for an ion of m/z 319 isolated from the MS^1 pyrolysis/ionization mass spectrum of 3 (Figure 6.5). This means that the structures of these two m/z 319 ions are the same. This is also true for dimer ion m/z 271 (Figure E.2) and trimer ion m/z 515 (Figure E.3). This observation demonstrated that these primary lignin pyrolysis products came directly from the fragmentation of the parent molecules 1-3 and not via repolymerization of monomeric products, which is in disagreement with a previous report that the primary fast pyrolysis products of lignin are monomers and the lignin oligomers observed after pyrolysis came from repolymerization of the monomers.[14]

The dimeric and monomeric pyrolysis products were the most abundant products for 1-3. In the monomer mass region (Figure 6.4), the ionized 4-end A unit, a the key ionized pyrolysis product (m/z 195), can be easily identified for 1-3 that share the same 4-end A unit. 1 and 3 share the same 1-end C or D unit. Indeed, a key ionized

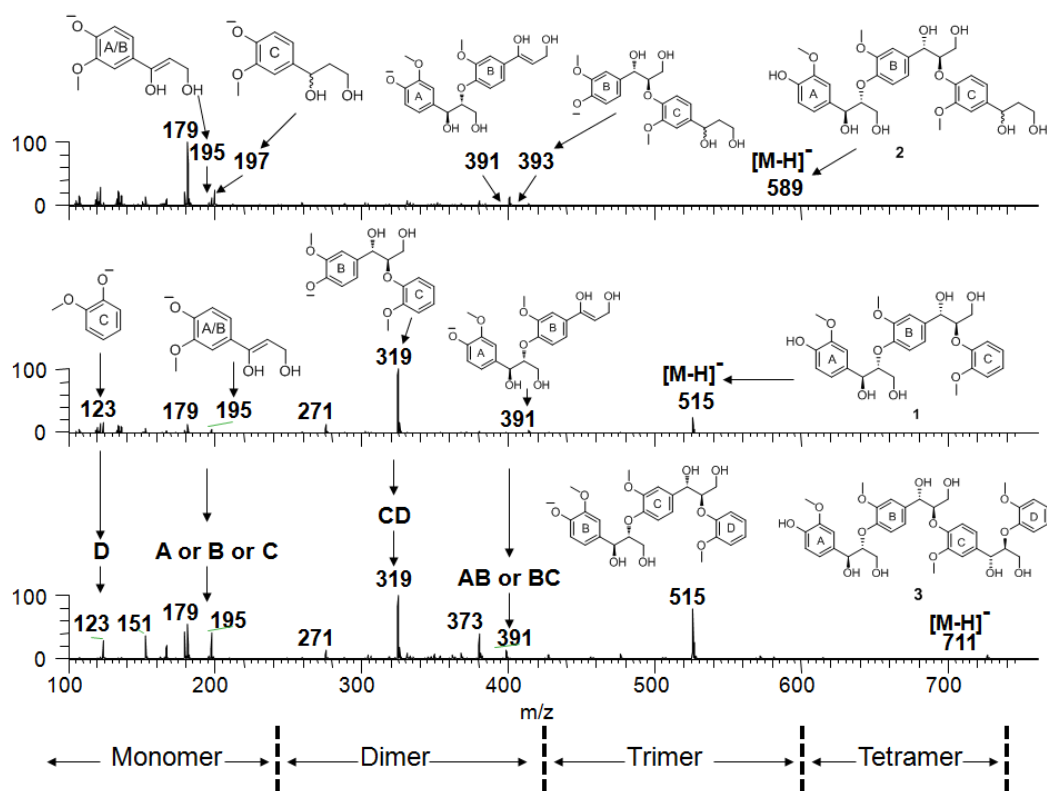


Figure 6.4. The negative-mode APCI mass spectra (MS^1) measured for compounds 1-3 after fast pyrolysis.

pyrolysis product (m/z 123) of the 1-end C or D unit of 1 and 3 can be identified. The ionized 1-end C unit of 2 (m/z 197) can also be detected. In the monomer region, all three compounds show similar pyrolysis products.

The proposed structures of monomer pyrolysis products of 3 in the mass range of m/z 100-200 are shown in Figure 6.6. These structures were deduced based on their elemental compositions and CAD patterns (Table E.1). Some monomeric pyrolysis products observed in this study are consistent with those published in previous reports of pyrolysis/GC/MS of organosolv lignin,[15] such as 2-methoxyphenol and coniferyl alcohol.

In the dimer mass region (Figure 6.4), three key ionized pyrolysis products are identified: ions with m/z 319 (BC or CD unit for 1 and 3), m/z 391 (AB unit for 1-3

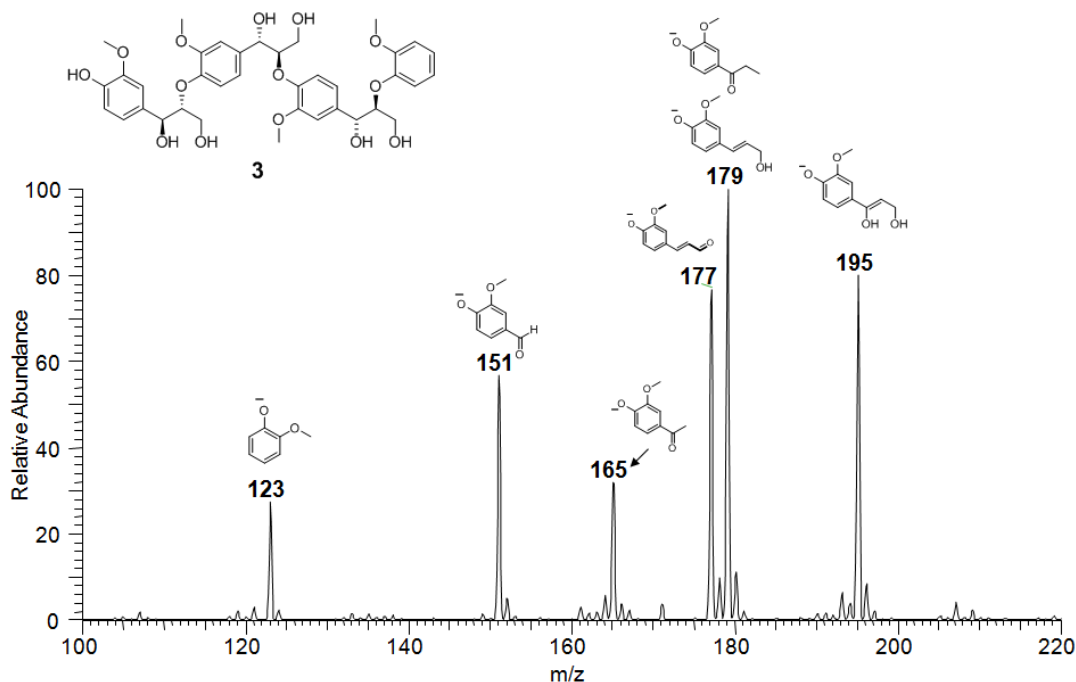


Figure 6.5. Proposed structures for several monomeric fast pyrolysis products (detected as deprotonated molecules) of **3**. Ion m/z 164 in the box is radical anion.

and BC unit for **3**) and m/z 393 (BC unit for **2**). Most other ionized dimer pyrolysis products are formed through different degrees of H_2O and CH_2O losses from these three dimer key pyrolysis product (Table E.1). For example, the dimeric pyrolysis products of **3** are shown in Figure 6.6. Three ionized key pyrolysis products (a with m/z 515, b with m/z 391 and c with m/z 319) are identified. Other dimeric pyrolysis products are formed through H_2O and CH_2O losses from these three products. In the trimer mass region, a key ionized pyrolysis product of m/z 515 is visible for tetramer **3**. The observed tetrameric, trimeric, dimeric and monomeric pyrolysis products of 1-3 are summarized in Table E.1 in supporting information.

As for fast pyrolysis of the polymer **4** (Figure 6.7), the dimers and monomers are the major products, as for 1-3. Small amounts of trimers and tetramers could be also detected. However, no oligomers (deprotonated molecules with m/z values

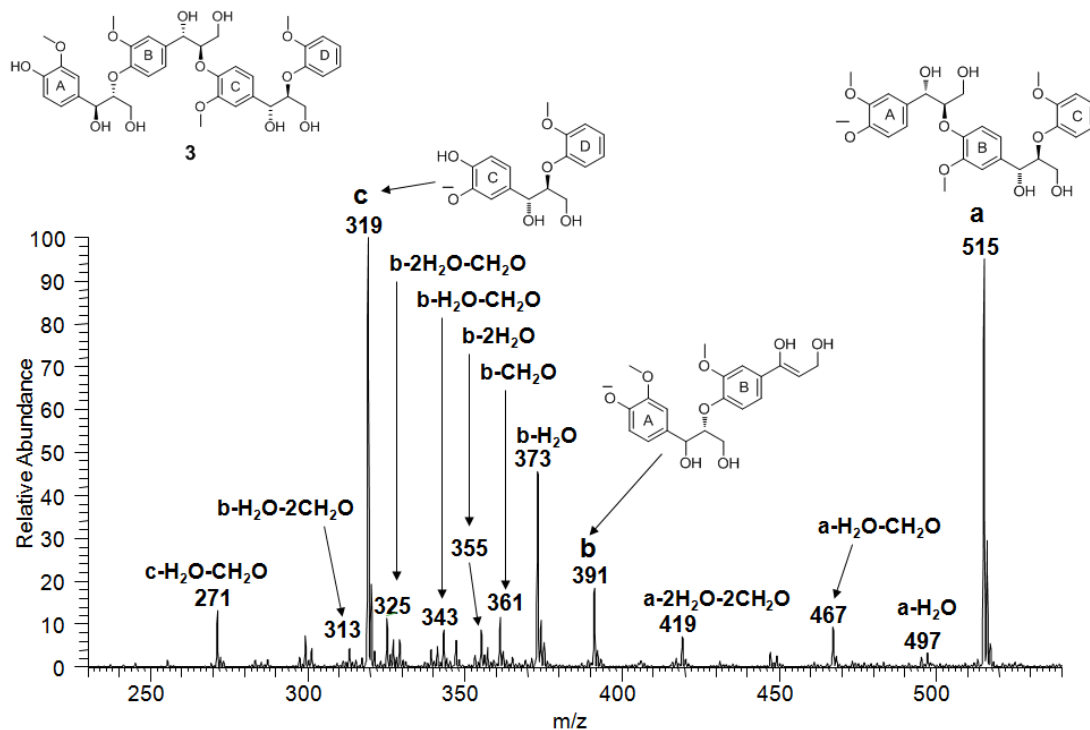


Figure 6.6. Dimeric fast pyrolysis products (detected as deprotonated molecules) of 3. Three key pyrolysis product with m/z 515 (a), m/z 391(b) and m/z 319 (c) as well as other pyrolysis products with different degrees of H_2O and CH_2O losses from the key products can be identified.

>800) larger than the tetramer could be detected, which indicates that the largest oligomer that is volatile enough to leave the ribbon surface intact is a tetramer. Hence, oligomers larger than tetramers break down into tetramers or smaller molecules before evaporating from the heated ribbon surface during fast pyrolysis. 3 and 4 yield similar pyrolysis products in the dimer and monomer regions (Figure 6.4). Three key pyrolysis products ions of 4 (m/z 195, 391 and 393) can be observed. The deprotonated pyrolysis products of m/z 319 and m/z 271 (formed by H_2O and CH_2O losses from ion of m/z 319) represent the CD dimer 1-end unit of 3 whereas polymer 4 does not contain this 1-end dimer unit. The 1-end dimer unit of 4 is detected as ion of m/z 393. The ion of m/z 393 is the same as the 1-end dimer BC unit of 2. Since both 3 and 4 share the same 4-end and middle units, they form the same key pyrolysis

dimer product (ion of m/z 391) as well as all the other pyrolysis products arising via H_2O and CH_2O losses from this key pyrolysis product. This finding confirms that the ionized 1-end monomer unit, middle dimer units and 4-end dimer unit of polymer 4 can be detected. The observation of similar pyrolysis products for polymer 4 and tetramer 3 implies that they share similar pyrolysis mechanisms, which will be discussed in the next section. Moreover, this finding demonstrates that tetramer 3 is a good surrogate to study pyrolysis of β -O-4 lignin polymers.

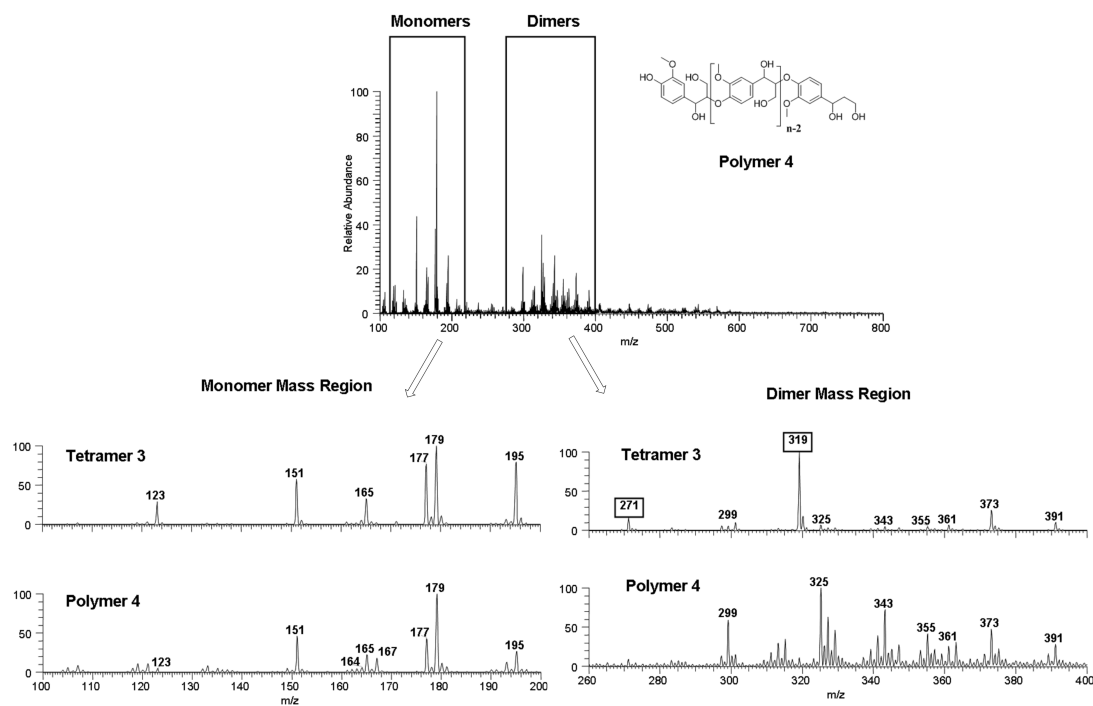


Figure 6.7. The negative-mode APCI mass spectrum (MS¹) measured for polymer 4 after fast pyrolysis and the comparison of the monomer and dimer regions for polymer 4 and tetramer 3. The ions of m/z 319 and 271 are not found in the mass spectrum of polymer 4 since 4 does not have the same end units as tetramer 3.

6.2.2 Insights into the mechanisms of fast pyrolysis of β -O-4 lignin tetramer 3: concerted nonradical elimination mechanisms vs radical mechanisms

It is essential to understand the mechanism(s) for the cleavage of the β -O-4 linkage during fast pyrolysis since this mechanism is directly related to primary product formation. As described as above, both radical and non-radical mechanisms were proposed for fast pyrolysis.[13–15, 117–123] In this section, lignin tetramer 3 is used to illustrate the possible mechanisms leading to the formation of the primary pyrolysis products. As shown in the previous section, the major dimeric, trimeric and tetrameric pyrolysis products are nonradical products for compounds 1-4, indicating that nonradical mechanisms are involved in the cleavage of β -O-4 linkages during pyrolysis. Evidence in support for concerted nonradical elimination mechanisms comes from the key pyrolysis product ions (m/z 195, 319, 391 and 393). First, the observation of all these products for 1-4 during fast pyrolysis implies that the mechanism leading to these products is energetically favored. As shown in Figure 6.8, the barrier for concerted Maccoll elimination of β -O-4 linkage is calculated to be only 44.8 kcal/mol. The previous study [123] demonstrated that the homolytic bond dissociation energies for the C-O and C-C bonds (radical mechanism) in the β -O-4 linkage are 69 kcal/mol and 76 kcal/mol, respectively, which is much more than the barrier for Maccoll elimination. Moreover, the barrier for concerted H₂O and CH₂O losses was calculated to be only 44 kcal/mol (Figure 6.8), which is similar to the barrier of Maccoll elimination (45 kcal/mol, Figure 6.8), The similar barriers for Maccoll elimination and concerted H₂O and CH₂O losses indicates that both processes can occur simultaneously during fast pyrolysis, which is also confirmed by experimental data. Second, if the mechanism of cleavage of the β -O-4 linkage proceeds through radical mechanism to form these key pyrolysis products, more radical related products, such as H abstraction products and polymerized products, can be expected. However, none of these radical related products were observed as major product.

The third piece of evidence comes from the comparison of the mass spectrum measured for the pyrolysis products of 3 (MS¹) and the collision-activated dissociation

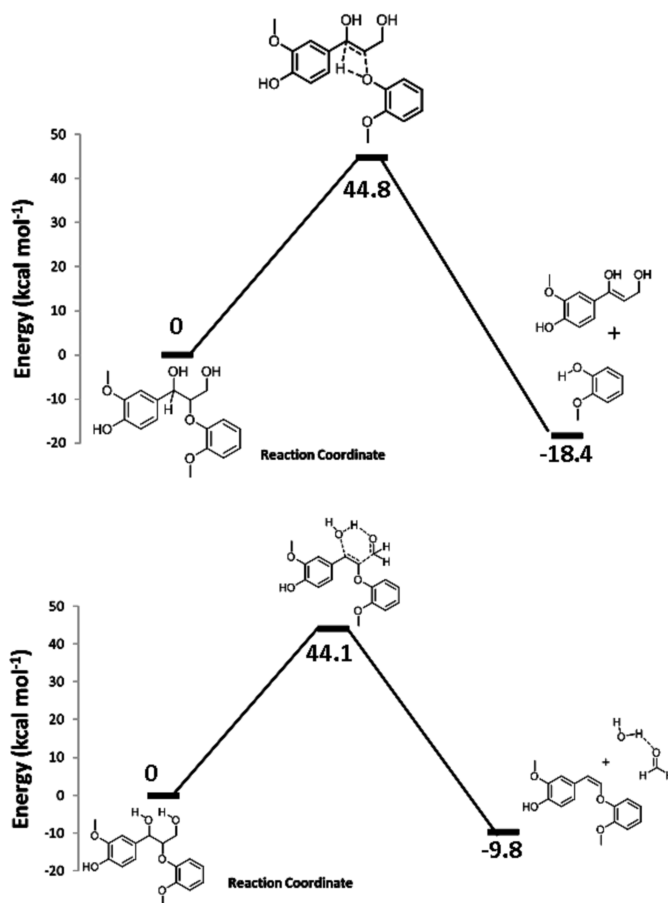
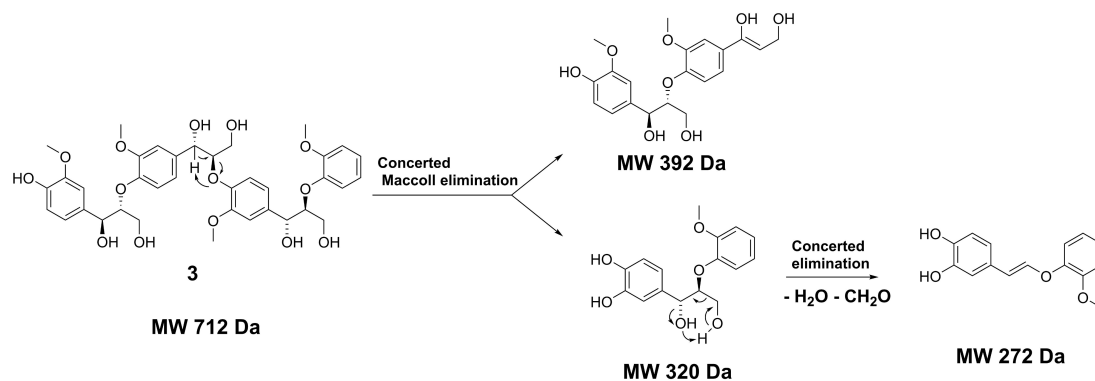


Figure 6.8. Proposed fast pyrolysis mechanisms for the cleavage of β -O-4 linkages and the elimination of water and formaldehyde. The energy barriers for these processes were calculated at the B3LYP/6-31G(d,p) level of theory.[30]

(CAD) products of deprotonated 3 (MS^2) (Figure 6.9). CAD is achieved through the collision of the ionized molecule with helium buffer gas in the ion trap of the mass spectrometer. Obviously, CAD is a lower energy fragmentation process compared with fast pyrolysis. In previous studies, the gas-phase fragmentation mechanisms of deprotonated lignin oligomers 1-3 were examined.[16, 126, 127] Both charge-driven and charge-remote (concerted) mechanisms were proposed for the cleavage of β -O-4 linkages during CAD.[16, 126, 127] As shown in Figure 6.9, key product ions such as ions of m/z 587, 515, 391, 319 and 195, are observed in both the pyrolysis mass spectrum and the CAD spectrum, which implies that these two completely different process may share similar mechanisms. Moreover, these products were to be formed through concerted elimination during CAD. This finding indicates that concerted Maccoll elimination is the favored low energy fragmentation pathway. There are also some clear differences between the pyrolysis mass spectrum and the CAD mass spectrum of 3. First, the ions of m/z 693 and m/z 663 in the CAD mass spectrum is formed through charge-driven H_2O and CH_2O losses during CAD. The H_2O loss has a barrier of only 10 kcal/mol. However, in the pyrolysis mass spectrum, only small amounts of deprotonated pyrolysis products of m/z 663 are observed, which are likely formed through concerted elimination of H_2O and CH_2O with a barrier of 44 kcal/mol. Second, the pyrolysis mass spectrum shows more than twenty ionized products (Table E.1) with different degrees of H_2O and CH_2O losses from the key pyrolysis products whereas only six similar products (m/z 693, 663, 539, 467, 343, 271) are found in the CAD mass spectrum. These two differences clearly indicate that fast pyrolysis is a higher energy fragmentation process. In conclusion, as shown in Figure 6.10, concerted Maccoll elimination is proposed to be the dominant mechanism leading to the cleavage of β -O-4 linkages and the formation of the key pyrolysis products. Simultaneous concerted H_2O and CH_2O losses occur from these key pyrolysis products, leading to the formation of the primary monomer, dimer, trimer and tetramer pyrolysis products during the first 125 ± 57 ms of fast pyrolysis.

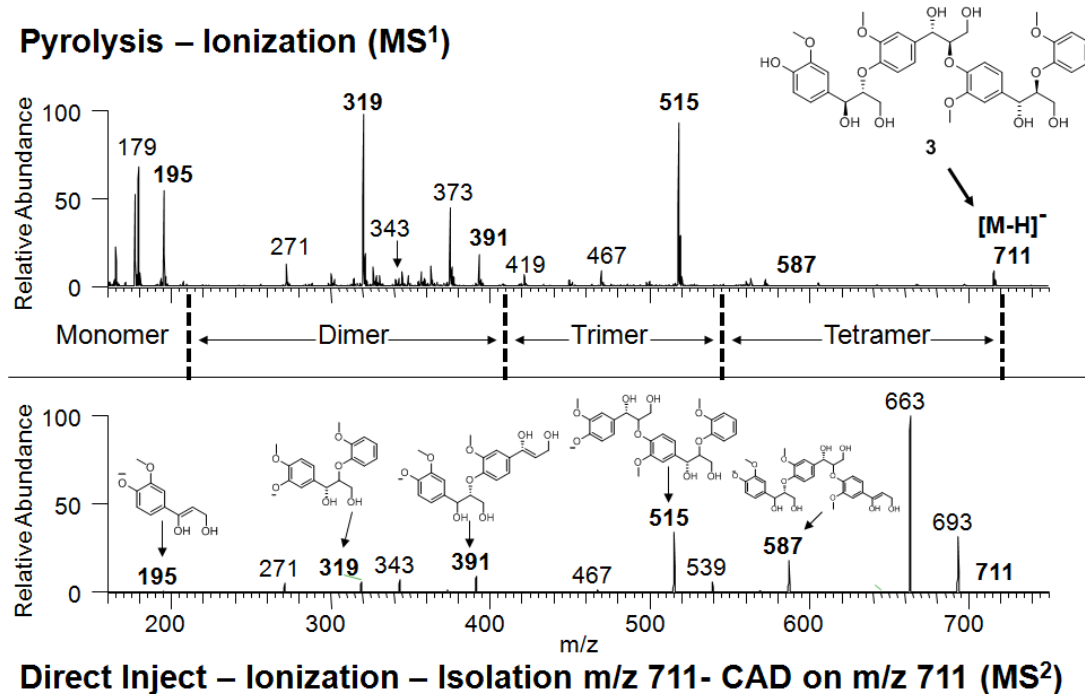


Figure 6.9. The top mass spectrum (MS¹) shows all the major primary fast pyrolysis products of compound 3 that were ionized under APCI negative mode. The bottom negative-mode APCI mass spectrum (MS²) shows the CAD fragment ions of deprotonated 3 introduced into the mass spectrometer using direct injection. Ions marked in bold (m/z 587, 515, 391, 319 and 195) are key pyrolysis products formed through Maccoll elimination from deprotonated 3 without H₂O and CH₂O losses.

6.3 Conclusions

The primary fast pyrolysis products of four β -O-4 lignin model compounds were determined using a linear quadrupole ion trap mass spectrometer coupled with a fast heating pyrolysis probe. Both calculations and experimental data suggest that cleavages of the β -O-4 linkages likely occur via concerted Maccoll elimination rather than radical mechanisms. Based on the results presented here, the first steps of fast pyrolysis of lignin oligomers mainly involve concerted Maccoll eliminations as well

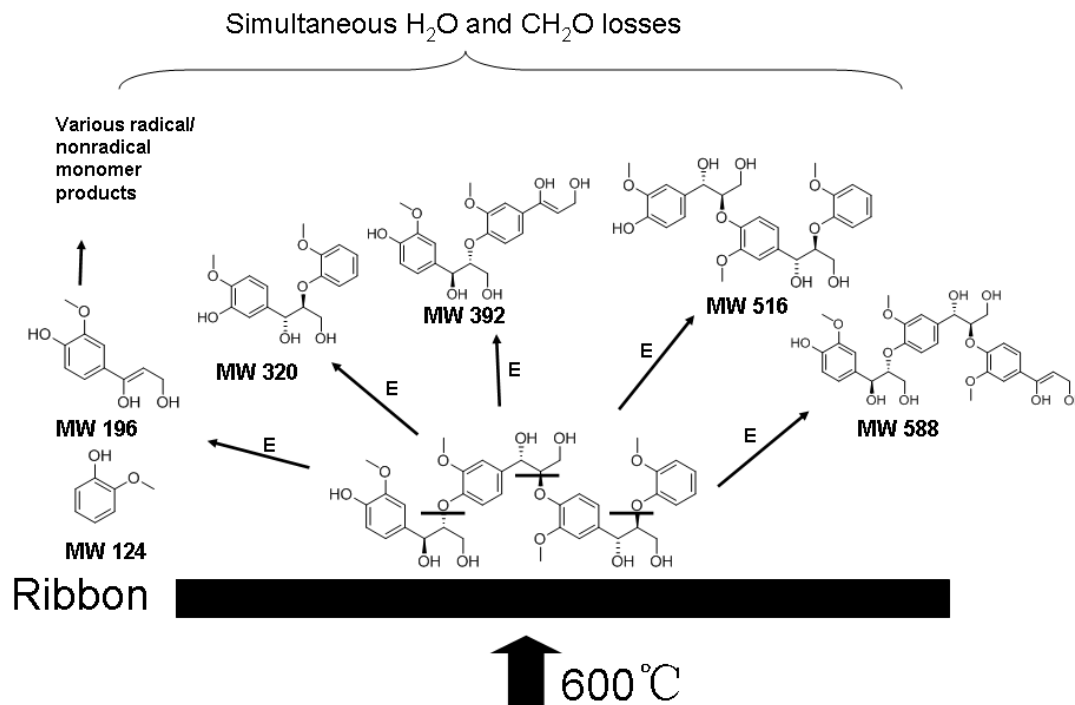


Figure 6.10. The proposed primary products for fast pyrolysis of 3. Compound 3 yields trimer, dimer and monomer fragments via concerted Maccoll elimination (E) upon rapid heating. Simultaneous water and formaldehyde losses also occur during this process. The resulting products are evaporated off the ribbon surface, ionized and detected by the mass spectrometer.

as concerted H₂O and CH₂O losses to give primary pyrolysis products ranging from monomers to tetramers. The lignin tetramer was found to be the largest oligomer that could evaporate intact off the ribbon surface during pyrolysis. Finally, lignin tetramer 3 was discovered to be a good surrogate to study the details of pyrolysis of β -O-4 lignin polymers.

6.4 Experimental Methods

6.4.1 Materials

The synthesis of the lignin model compounds 1-4 is described.[30] Methanol (Optima LC/MS $\geq 99.9\%$, CAS 67-56-1) was purchased from Fisher Scientific, ammonium hydroxide (28-30% as NH_3 , CAS 1336-21-6) was purchased from Mallinckrodt Chemicals, and compressed nitrogen gas ($\geq 99.9\%$, CAS 7727-37-9) was purchased from Indiana Oxygen. All purchased chemicals were used without further purification.

6.4.2 Mass Spectrometry

Detection and characterization of lignin fast pyrolysis products was performed using a Thermo Scientific (Waltham, MA) LTQ linear quadrupole ion trap (LQIT) mass spectrometer, as described previously.[9, 10] High resolution data to determine elemental compositions were collected using a 7 Tesla Thermo Scientific LTQ-FT-ICR. Solutions for direct injection experiments of model compounds were made at a concentration of 10^{-5} M in 3 mL methanol : water (50 : 50 v/v) with 200 μL ammonium hydroxide dopant for negative ion mode mass spectrometry. The solutions were pumped into an APCI source via the APCI probe at a rate of 3 $\mu\text{L}/\text{min}$ with a solution of methanol : water (50 : 50 v/v) tee-infused from the LC at a rate of 100 $\mu\text{L}/\text{min}$. During pyrolysis experiments, ammonium hydroxide: water (75 : 25 v/v) dopant solution was pumped into the APCI source via the APCI probe at a rate of 1 $\mu\text{L}/\text{min}$ with a solution of methanol : water (50 : 50 v/v) tee-infused from the LC at a rate of 300 $\mu\text{L}/\text{min}$. The variables of the LQIT were set to the following values for all experiments: discharge current 5.0 μA , vaporizer temperature 300°C, sheath gas (N_2) flow 40 arbitrary units, auxiliary gas flow (N_2) 10 arbitrary units, sweep gas flow (N_2) 0 arbitrary units, capillary temperature 250°C, capillary voltage -1 V, and tube lens voltage -105 V. Collisionally activated dissociation (CAD) experiments used an ion isolation window of ± 2 Daltons (Da), with the normalized collision energy ranging

from 5 up to 30 arbitrary units and activation time being 30 ms. Data collection and processing was carried out using Xcalibur 2.1 software.

6.4.3 Pyrolysis

All pyrolysis experiments were performed using an experimental set-up published earlier.[9, 10] The pyrolysis probe is based on a Pyroprobe 5200HP purchased from CDS Analytical (Oxford, PA). The pyrolysis probe uses a resistively heated platinum ribbon ($2.1 \text{ mm} \times 35 \text{ mm} \times 0.1 \text{ mm}$) with the ability to heat at rates up to $20,000^\circ\text{C} \times \text{s}^{-1}$. Based on previous work in other laboratories, platinum does not act as a catalyst during the pyrolysis experiments.[42, 43] Roughly tens to hundreds of micrograms of sample were loaded onto the platinum ribbon and held onto the surface via electrostatic attraction. This method of loading of the ribbon resulted in a submonolayer of sample on its surface. This was done to ensure rapid and uniform heat transfer to all particles. The ribbon was heated up to 600°C at a rate of $1,000^\circ\text{C} \times \text{s}^{-1}$ resulting in a heating time of 0.6 s. The pyroprobe was maintained at 600°C for 1 s.

6.4.4 Determination of the primary products of fast pyrolysis of lignin model compounds

The tip of the probe described above was inserted into the ionization chamber of the LQIT through a home-built adaptor that was placed into the unused atmospheric pressure photoionization (APPI) port. This adaptor positioned the platinum ribbon approximately 5 mm in front of and 5 mm below the skimmer cone/inlet of the LQIT. A diagram of this setup has been published previously.[9] Once pyrolysis occurred, the evaporated products were immediately diluted via diffusion into the 2 L ionization chamber and subsequently quenched via collisions with nitrogen gas (at about 100°C), which prevented secondary reactions. The products were ionized and characterized by multi-stage tandem mass spectrometry experiments.

7. FAST PYROLYSIS OF GUAIACYL LIGNIN MODEL COMPOUNDS WITH β -O-4 LINKAGES

7.1 Introduction

Biomass is a major source of renewable carbon which can be converted to hydrocarbon fuel with the aim of reducing the dependence on fossil based sources. The CO₂ emissions from biomass-based renewable fuels can be considered to be part of a renewable cycle of carbon emissions. Fast pyrolysis followed by catalytic hydrodeoxygenation is considered a promising biomass conversion route to produce drop in hydrocarbon fuels.[26] Fast pyrolysis is the process of heating biomass to a high temperature (400-600°C), with high heating rates in the presence of inert with a low vapor residence time before condensation of the bio-oil.[128] Typical crude bio-oil derived from fast pyrolysis of wood possesses a low energy density (17 MJ/kg) while that of petroleum is ~40 MJ/kg.[26, 128] This low energy density is primarily due to high oxygen content (35-40 wt%), and hence it is necessary to remove oxygen to <1% for utilizing it as a fuel. However, upgrading condensed bio-oil (hydrotreating) has several drawbacks like secondary reactions during revaporisation of bio-oil leading to an overall reduced yield of products as well as due to reactor plugging as well as catalyst coking.[129] To overcome these obstacles, the H₂Bioil process was proposed as an integrated high pressure fast hydrolysis and catalytic vapor phase hydrodeoxygenation (HDO) pathway for conversion of biomass to produce high energy density fuel.[58, 60, 61, 63, 130] In order to develop a suitable catalyst for hydrodeoxygenation, it is very important to understand the vapor phase composition of the fast pyrolysis products of biomass. As such the vapor phase residence time between pyrolysis and catalytic hydrodeoxygenation becomes a critical parameter for tailoring the pyrolysis product distribution by promoting/mitigating the secondary reactions occurring in the vapor

phase. Neumann et al. have shown that presence of lignin dimeric species results in higher degree of coking over zeolites as compared to monomeric counterparts.[131] In this study we have investigated the effect of vapor phase residence time on the product distribution from pyrolysis of model lignin oligomers.

Biomass is primarily composed of three types of polymers; cellulose, hemicellulose, and lignin, which are intertwined to make the structural framework of the plants. Although, lignin only constitutes 10-30% of lignocellulosic biomass it accounts for 25-40% of the energy content of biomass, this is in part due to the higher C/O ratio than cellulose and hemicellulose.[132] Additionally, the presence of aromatic rings in the structural framework of the lignin polymer makes it a highly attractive source of a high-octane hydrocarbon fuel . Typically lignin is extracted from biomass by different types of processes, such as the organosolv process.[12, 133, 134] Numerous lignin pyrolysis studies have been performed with extracted lignin to study the effect of pyrolysis parameters on the product distribution. An increase in temperature was shown to decrease the amount of char left behind while increasing the yield of bio-oil.[135] The char yield from lignin pyrolysis was found to vary between 10-60% depending on the temperature and heating rate, while the yield for bio-oil was in the range of 20-60%.[15, 114, 133, 135–138] The products identified in the lignin pyrolysis bio-oils have a distribution of monomeric and oligomeric molecules. The formation of oligomers is a debated topic in literature with significant evidence for their formation by oligomerization of monomeric species in the condensed bio-oil.[14] However, in another study oligomeric molecules have been shown to be directly formed during pyrolysis of lignin and are proposed to be precursors to monomeric molecules.[139] The contribution of the oligomeric species to the initial vapor phase product distribution is unclear due to an absence of quantitative analytical tools for online analysis of oligomer-containing vapors. One of the objectives of this study is to understand the contribution of dimeric species to the initial product distribution via online GC/MS studies of pyrolysis of lignin model compounds.

In the literature, several studies have been published on pyrolysis of lignin where multiple analytical techniques were utilized due to the wide molecular weight range (50-2000 Da) of the detected products.[14, 137, 139, 140] It is clear that a single analytical technique is not capable of providing qualitative and quantitative results for condensed bio-oil. Common techniques used for identification of lignin pyrolysis products are GC/MS, MBMS (molecular beam mass spectrometry), FTIR, and mass spectrometry with an arsenal of different ionization methods.[124, 141–145] Amongst these, GC/MS is the most widely used tool for identification and quantification of monomeric products from lignin pyrolysis. Whereas HPLC and GPC (liquid chromatography techniques), have been frequently used for analysis of oligomeric products in the bio-oil.[14, 124, 139, 146] Depending on the type of lignin pyrolyzed and the pyrolysis conditions, monomeric products may account for anywhere between 15 and 60% of the product distribution.[113, 147] In a scenario where the amount of oligomers is >10%, GC/MS is not entirely sufficient for quantitative analysis due to low volatility of oligomer molecules. Previously, Guillen and Ibargoitia [148] have shown that lignin derived dimers can be qualitatively observed with GC-MS. However, there is a need to develop quantitative gas chromatography for lignin derived dimers as it would enable the analysis of a significant proportion of the vapor phase product distribution. In this manuscript we have developed a quantitative analytical technique using a GC/MS for the monomer and dimer fractions of the lignin pyrolysis products.

It is known that extracted lignin may undergo structural changes depending on the severity of the extraction process.[16, 134] Another shortcoming of extracted lignin is that it may have a higher proportion of impurities and mineral content, which has been shown to affect the product distribution and bio-oil yield.[149] As a result, synthetic model polymers have been previously employed for studying the pathways and mechanisms of lignin pyrolysis.[13, 147, 150–154] Lignin is a heteropolymer with three major types of building blocks (coniferyl, syringyl and coumaryl) and at least 8 different types of linkages connecting the monomer units to form a cross linked polymer.[12] The β -O-4 linkage is the most abundant type of linkage and accounts for

up to 50% of the linkages in softwood lignin. Therefore synthetic model dimers and polymers with β -O ether linkages have been studied widely to understand the bond cleavage pathways as well as mechanism. From previous studies it can be concluded that the mechanism of β -O ether bond cleavage is majorly dependent on two factors 1) Substituents on the α and γ carbon atoms of the model compound 2) Temperature of pyrolysis. Jarvis et al [13] have observed that below 1000°C the dominant reactions in cleavage of β -O ether bond are retro-ene and Maccoll reactions, while above 1000°C homolytic bond scission plays a prominent role as well.[122] Huaming et. al. (Chapter 6) have provided evidence based on theory and experiments for a dominant non-radical based mechanism for β -O-4 cleavage during pyrolysis at 600°C. In another study with a model dimer, it was shown that the presence of an -OH substituent on the γ carbon, modifies the β -O ether bond cleavage mechanism when compared with other substituents like -H.[122, 155] This indicates that choice of model compound also plays an important role in the governing mechanism for β -O ether bond scission, and the model compound should be an accurate structural representation of the natural lignin polymer. Therefore, in this study we have chosen synthetic model compounds with -OH substituent on the α and γ carbon atoms.

7.2 Experimental Methods

7.2.1 Reactor Description

Lignin pyrolysis experiments were carried out using a Pyroprobe 5200 HP (CDS Analytical Inc.) connected to an online Gas Chromatograph (7890A) equipped with a Flame ionization detector and a Mass Spectrometer (5975C). A resistively heated Pt coil was used as a heating source for pyrolysis of the lignin model compounds. A known weight of the reactant sample was loaded in a quartz tube (0.15cm ID X 2.5cm length) which was subsequently placed in the opening of the Pt coil. A heating rate of $1000^{\circ}\text{C} \times \text{s}^{-1}$ was used to attain a final temperature of 500°C during pyrolysis of the sample. The pyrolysis vapors were flushed out from the quartz tube by the

carrier gas (He) and carried into the GC/MS. The GC was equipped with an HP-5ms column (solid phase - 5% diphenyl and 95% dimethylpolysiloaxane (5PMPS)) connected to a three way splitter with auxiliary gas input. The flow from the column was split to the FID and MS with synchronized peaks for quantification and identification, respectively. Multiple columns with different dimensions (as shown in Table 7.1) were tested to obtain a suitable configuration for quantitative analysis of lignin derived dimeric molecules. The details about the column selection procedure have been provided in the results section.

7.2.2 Loading and Reactor Operation

The sample was coated on the inner surface of the quartz tube and the amount of sample was measured by weighing the quartz tube before and after the sample loading. The sample (0.2-1 mg) was coated on the inner walls of the quartz tube by mechanical force. No quartz wool was loaded in the quartz tube so that the carrier gas would flow through the tube and carry out the vapors efficiently. This was critical for accurate control of the vapor phase residence time after pyrolysis. The sample loading procedure was tested via carrier gas flow experiments to ensure that the sample was firmly coated to the wall and was not dislodged by the flowing gas before pyrolysis.

After loading the sample, the quartz tube was placed inside the Pt coil, which is mounted on a probe. The probe was then placed inside the pyrolysis chamber (refer to Figure F.2) and the air was flushed out using nitrogen. The valves were switched to introduce the carrier gas (He) and flush out the nitrogen. The pyrolysis chamber was then heated by an external heater to a temperature of 300°C in ~ 10 s followed by the Pt coil being heated to a final temperature of 500°C at a heating rate of $1000^{\circ}\text{C} \times \text{s}^{-1}$. The pyrolysis vapors were carried out from the quartz tube, through the heat traced transfer tubing into the online GC-MS. The split/splitless inlet of the GC was maintained at a temperature of 300°C and a split ratio of 100:1 was used for the standard runs. For column 4, the oven was initially maintained at 33°C for 10 min, followed by a $10^{\circ}\text{C} \times \text{s}^{-1}$ ramp to 320°C. The final temperature was held for 10 min.

Table 7.1.
List of the GC columns tested with the relevant parameters.

Column #	Column Name	Solid phase composition	Solid phase thickness / μm	Column Length / m	Column id / μm	Internal Surface area / mm^2	Solid phase volume / mm^3
Column 1	HP5	5PMPS	1.5	30	530	24892	37.4
Column 2	HP5-ms	5PMPS	0.25	30	320	15060	3.8
Column 3	Blank capillary	none	n/a	25	320	n/a	n/a
Column 4	HP5-ms	5PMPS	0.25	2.6	320	1285	0.3

7.2.3 Product Identification and Quantification

The peaks observed in the gas chromatogram (FID) were quantified on the basis of calibrations made by using standard compounds. The identification of the observed products was performed by comparing the EI spectrum from the mass spectrometer to those in the MS NIST (National Institute of Standards and Technology) database. Some of the compounds which were not available in the database were identified by comparison with those from similar experiments performed with pyrolysis-MS analytical technique (Chapter 6). The char analysis was obtained by weighing the quartz tube after pyrolysis and obtaining the difference with the weight of the empty quartz tube.

7.2.4 Model Compound Synthesis

The lignin model compounds (Figure 7.1) used for pyrolysis in this study (with the exception of Dimer 1) were synthesized at Purdue University. Dimer 1 (Guaiacyl-glycerol- β -guaiacyl ether, >97% purity) was obtained from TCI America. Trimer 2, tetramer 3, trimer 4 were synthesized using the procedure outlined in Huaming et al. Polymer 5 was synthesized by the procedure outlined by Kishimoto et al. and its structure was verified by using NMR.[156] For the synthesized molecules the structural conformity was tested by using HNMR and CNMR studies.

7.3 Results

7.3.1 Quantitative analysis of dimeric molecules using a GC/MS

Fast pyrolysis of the lignin component of the biomass is known to produce a distribution of molecules composed of monomeric, dimeric, and oligomeric depolymerization products. However quantitative analysis of oligomers derived from lignin via GC-MS is considered to be a challenge due to their low volatility. Typically, liquid chromatography techniques (gel permeation chromatography, HPLC) have been used to identify and quantify the aforementioned oligomeric fraction of bio-oil.[146] How-

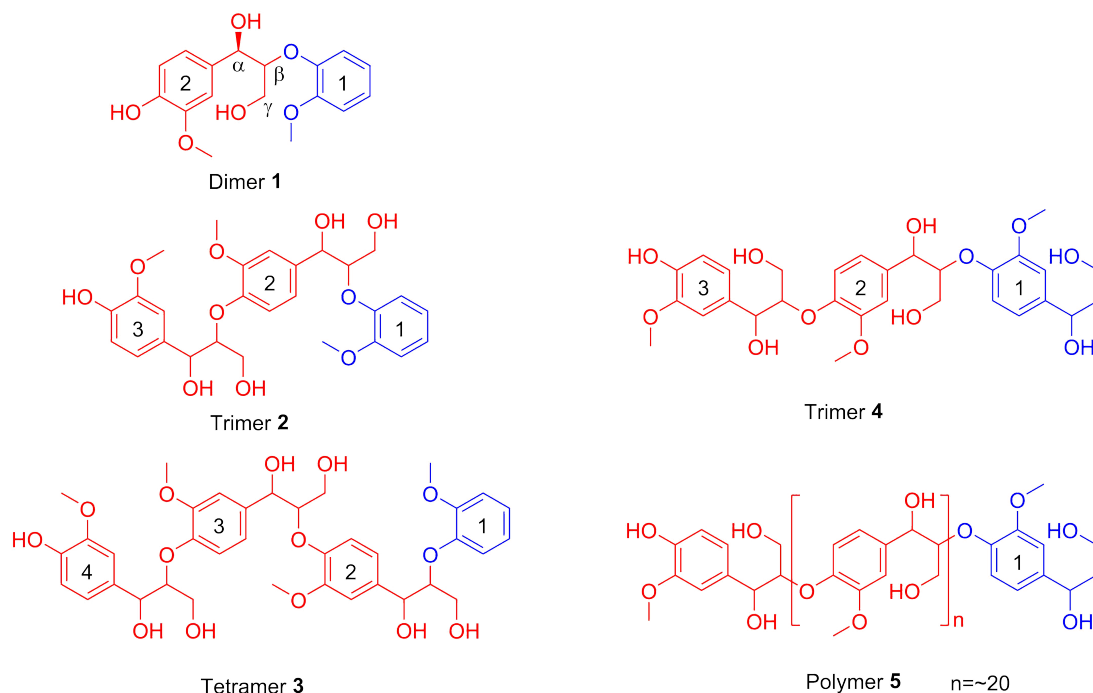


Figure 7.1. Lignin model compounds (1-5) used in this study. Numbers inside the rings are for notation purposes only, relevant end groups are highlighted in blue.

ever, liquid chromatography techniques are unsuitable for determining the accurate vapor phase product distribution due to secondary reactions accompanying condensation of the pyrolysis vapors.[14] Therefore, online analysis of vapor phase pyrolysis products is essential for understanding 1) The pathways governing depolymerisation of lignin during pyrolysis and 2) Designing a downstream catalyst for direct vapor phase hydrodeoxygenation of the pyrolysis products.

In our efforts to develop a quantitative method of analysis of lignin derived dimeric species, we tested four different columns on the GC/MS (Table 7.1). Dimer 1 was chosen as a model dimer, and each column configuration was tested with online vapor phase analysis of pyrolysis products from dimer 1. The observed product distribution has been divided into two major groups, namely monomeric products and dimer 1. The overall mass balance for column 1 was $\sim 40\%$ with $\sim 27\%$ yield of monomeric

products. For column 2, which has a lower solid phase thickness ($0.25 \mu\text{m}$), the overall mass balance increased to $\sim 72\%$ with $\sim 26\%$ yield of monomeric products. Decreasing the solid phase thickness possibly reduced the interactions of the dimeric molecules resulting in more molecules being able to elute out from the column. Column 3 did not have any solid phase and was unable to provide an adequate degree of resolution for the observed products, making identification and quantification very difficult. Column 4 was fabricated by using a fraction of the length from column 2 to reduce the total interactions with the solid phase while still retaining an adequate degree of resolution to delineate the observed peaks. The overall mass balance with column 4 was $\sim 98\%$ with 27% yield to monomeric products. From column 1, 2 and 4 we observed an increase in the quantified amount of dimer 1 and other dimeric molecules, while the total amount of monomers remained constant. Increasing interactions with the solid phase can cause the dimeric species to get trapped in the column and hence cannot be detected. Table 7.2 shows the increase in the dimeric species observed when the total solid phase volume was decreased by two orders of magnitude from column 1-4. It should also be noted that the dimeric species do not breakdown or degrade to form monomers, since the total amount of monomers observed over different columns (each column having different elution times for dimer 1 - Table F.3) remains constant. Similar results were also obtained for the tetramer 3, with an increase in the quantified dimeric species from column 1 to column 4 (Table 7.3). These results indicate that column 4 is suitable for quantitative analysis of lignin derived pyrolysis products comprising of monomers and dimers. This study has also demonstrated that one frequently used, commercially available configuration of GC column (Column 3) is not suitable for quantitative analysis of lignin derived dimeric species, since only a small proportion may be observed.

7.3.2 Pyrolysis of Dimer 1

As shown in Table 7.2, the overall mass balance achieved during pyrolysis of dimer 1 was $>97\%$, when the column 4 was used for analysis of the products. The monomeric

Table 7.2.
Lumped pyrolysis products of dimer 1 as a function of the columns tested.

Column #	Solid phase volume / mm ³	Dimer 1 / % wt of feed	Monomeric species / % wt of feed	Total mass balance / % wt of feed
Column 1	37.4	5.6	26.4	40.2
Column 2	3.8	39.4	26.3	72
Column 4	0.3	63.4	25.3	97.9

Table 7.3.
Lumped pyrolysis products of tetramer 3 as a function of the columns tested.

Column #	Solid phase volume / mm ³	Dimeric species / % wt of feed	Monomeric species / % wt of feed	Total mass balance / % wt of feed
Column 1	37.4	3.6	42.8	68.7
Column 2	3.8	18.1	40.6	77.6
Column 4	0.3	30.9	41.5	94.4

products accounted for 25.3 wt% of dimer 1 pyrolyzed, the detailed product distribution of major identified molecules is provided in Table 7.4. The major monomeric products observed as a result of β -O-4 bond cleavage were guaiacol and coniferyl alcohol. Guaiacol was formed from the end group aromatic ring (blue aromatic ring in Figure 7.1), which does not have an alkyl substituent, with the expected \sim 12 wt% theoretical abundance (moles of dimer 1 converted via β -O-4 bond scission = total moles of guaiacol formed). However since such end groups are not a significant part of the natural lignin polymer, guaiacol is not expected to be a major product from lignin pyrolysis. As a consequence, the high abundance of guaiacol can be considered as an artifact of the model compound. Therefore, the major product from β -O-4 bond cleavage of dimer 1 was coniferyl alcohol. The dimeric products account for \sim 70% of the pyrolysis products of the dimer 1 model compound pyrolyzed. It is also interesting to note that \sim 64 wt% of dimer 1 evaporated cleanly during pyrolysis, and was detected unaltered in the GC/MS.

7.3.3 Pyrolysis of Trimer 2, Tetramer 3, Trimer 4 and Polymer 5

From the results in Table 7.4, it can be seen that similar monomeric products were observed for dimer 1, trimer 2, and tetramer 3, with varying abundances. The varying proportions of the monomeric species can be attributed to, a) varying proportion of guaiacyl end group (blue aromatic rings in Figure 7.1, b) varying degree of evaporation versus pyrolysis. It should be noted that for all the model compounds the major monomeric product observed was coniferyl alcohol. Amongst the dimeric products, only two molecules were identified (dimer 1 and 2-methoxy-4-(2-(2-methoxyphenoxy)-vinyl)phenol), due to lack of suitable matches in the NIST identification database for the other products. However, Huaming et al. (6) have been able to identify dimeric molecular species using MS_n experiments which would also be expected to be a part of the pyrolysis product distribution here. Dimer 1 was not detected from pyrolysis of trimer 4 and polymer 5 due to absence of the guaiacyl end group. However for all the model compounds, the abundance of the dimeric species was greater than or equal

Table 7.4.
Quantified pyrolysis product distribution (wt% of starting model compound) of various lignin model compounds.

Compound	Dimer	Trimer	Tetramer	Trimer	Polymer
	1	2	3	4	5
Light Oxygenated					
Hydrocarbons (C₁-C₃)^(a)	1.8	8.9	7	7.3	7.4
Monomeric species^(b)					
Guaiacol (2-methoxy-phenol)	12.1	12.7	7.8	1.8	1.7
4-methoxy-4-methylphenol	n.d.	n.d.	0.1	0.2	0.5
3-methoxy-benzaldehyde	0.4	0.4	0.4	n.d.	n.d.
2-methoxy-4-vinylphenol	0.1	0.3	0.5	1.5	1.5
4-hydroxy-3-methoxybenzaldehyde	0.5	1.7	2	1.5	2.9
1-(4-hydroxy-3-methoxyphenyl)-ethan-1-one	0.6	1.9	2.1	1.8	1.7
1-(4-hydroxy-3-methoxyphenyl)-prop-2-en-1-one	1.5	3.5	3.8	3.2	2.5
4-(3-hydroxyprop-1-en-1-yl)-2-methoxyphenol	0.6	1.8	2.2	2.4	1.8
3-(4-hydroxy-3-methoxyphenyl)-acrylaldehyde	0.3	0.9	0.9	1.6	1.1
Coniferyl alcohol (4-(3-hydroxyprop-1-en-1-yl)-2-methoxyphenol)	5.9	14.9	16.6	19.9	14.4
3-hydroxy-1-(4-hydroxy-3-methoxyphenyl)propan-1-one	1.8	1.6	1.3	0.7	0.4
Other monomeric species	1.7	2	3.8	9.9	10.4
Dimeric species^(a)					
Dimer 1	63.4	18.4	16	n.d.	n.d.
2-methoxy-4-(2-(2-methoxyphenoxy)vinyl)phenol	1.2	1.8	1.5	n.d.	n.d.
Other dimeric species	6	9.6	13.4	22.6	19
Char	n.d.	12.5	15	22.2	27
Total	97.9	92.9	94.4	96.7	92.3

(a) Formaldehyde and residual solvents were used during model compound synthesis

(b) Structures for the monomeric and dimeric species are shown in Figure 2

to 19%, indicating that they made up a significant proportion of the vapor phase product distribution.

7.4 Discussion

7.4.1 Product distribution from lignin model compounds

As discussed previously, a significant proportion (>60%) of the dimer 1 was detected intact after pyrolysis. A similar result was reported in literature by Kawamoto et al. with ~50% of dimer 1 evaporating under pyrolysis conditions.[155] This result is a consequence of two competing phenomenon occurring while the model compound is being heated to the pyrolysis temperature, evaporation and structural change due to pyrolysis. The relative proportion of products obtained from evaporation and pyrolysis are primarily governed by the volatility of the reactant molecule and the temperature of pyrolysis. As such, dimer 1 is not an ideal molecule to study the effect of pyrolysis parameters on the product distribution from lignin pyrolysis due to significant evaporation under fast pyrolysis conditions. However, studying pyrolysis of dimer 1 provided valuable information not only about the types of products that would be expected from pyrolysis of lignin, but also the reaction pathways. Two major reaction pathways were observed, a) cleavage of the β -O-4 linkage to form guaiacol and coniferyl alcohol, b) formaldehyde (γ elimination) and water loss. Studies by Kawamoto et al. have previously reported these two pathways during pyrolysis of dimer 1.[155] Pathway 1, which is the cleavage of the β -O-4 linkage was the major pathway for formation of monomeric species, while Pathway 2 was a minor pathway which resulted in formation of the dimeric species, 2-methoxy-4-(2-(2-methoxyphenoxy)vinyl)phenol), as shown in Figure 7.2. In addition to these two pathways, we observed significant amounts of other monomeric products. The other monomeric products may be formed by alternate pathways as well as by secondary transformations from coniferyl alcohol.[157] All the major identified monomeric species have the characteristic phenolic and methoxy groups re-

spectively at para and meta positions relative to the substituted alkyl chain as shown in Figure 7.3. Also, a major fraction (>85%) of the observed monomeric products (excluding guaiacol, from the end group) were composed of 10 carbon atoms indicating a low degree of C-C bond scission during pyrolysis (Table F.2). Monomeric products with 8 or 9 carbon atoms per molecule were observed due to carbon losses occurring from the substituted alkyl side chain.

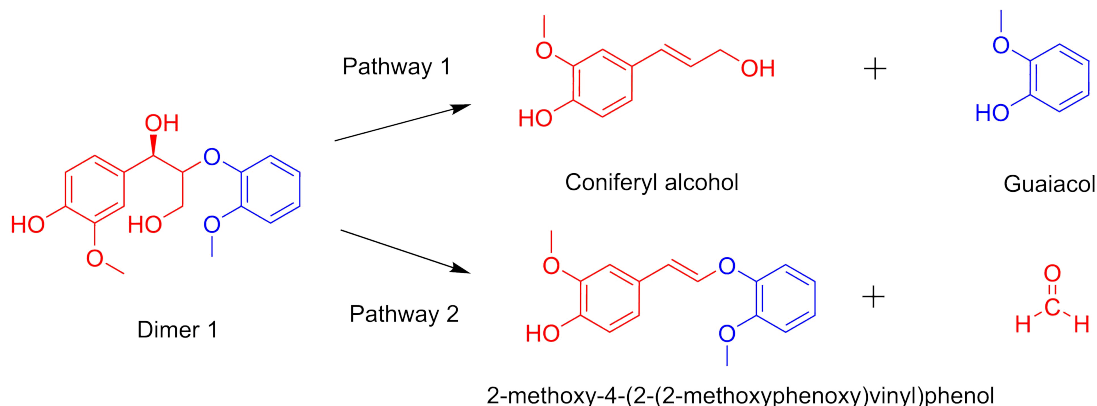


Figure 7.2. Two pathways observed during pyrolysis of dimer 1.

As stated earlier, the major monomeric product observed was coniferyl alcohol and had the highest absolute abundance for all the model compounds 1-5. However, the absolute abundance varied for each of the model compounds 1-5, primarily due to a change in the degree of polymerization which resulted in a prominent guaiacyl end group effect (different relative proportion of guaiacol to monomeric fragments after β -O-4 bond scission). Additional causes include the extent of β -O-4 bond scission which was different for each of the model compounds. One can hypothesize that the extent of β -O-4 bond scission is not only dependent on the volatility of the parent molecule but also the volatility of the molecular fragments formed during pyrolysis. For instance, if the β -O-4 linkage # 1 in trimer 2 cleaves via pathway 1, it will produce a dimeric species dimer 6 and guaiacol (as shown in Figure 7.4). While with cleavage of β -O-4 linkage # 2 it will produce dimer 1 and a monomeric product, coniferyl alcohol

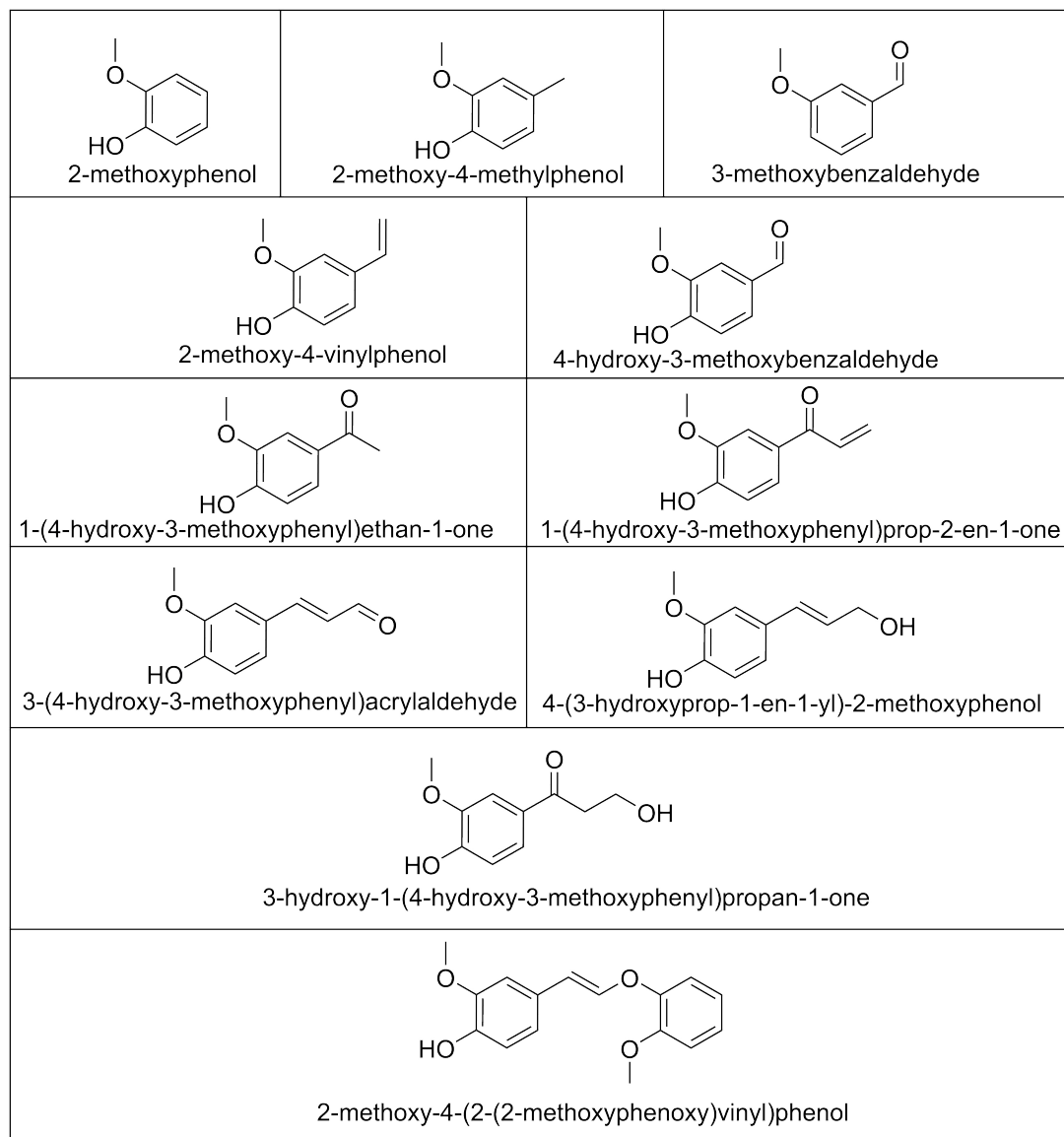


Figure 7.3. Structures of the major products from pyrolysis of lignin model compounds.

(Figure 7.4). The dimeric species comprising of the guaiacyl end group (dimer 1) will have a higher volatility as compared to its counterpart (dimer 6), in part due to its lower molecular weight (see Table F.1 for estimated boiling points). As such there is a higher propensity for dimer 6 to undergo secondary reactions before being

vaporized. This is evident in Table 7.4 since the total amount of dimer 1 observed is ~ 2 times that of the total amount of other dimeric species (the majority of which can be assumed to originate from cleavage of β -O-4 linkage # 1). Furthermore model compounds trimer 4 and polymer 5 are devoid of the guaiacyl end group, which is reflected in a drastic decrease in the amount of guaiacol observed when compared with that for model compounds 1-3. These differences make it difficult to directly compare the monomeric product distribution amongst the five model compounds. Therefore, to compare the monomeric product distribution, all the products were normalized by the absolute abundance (wt% of feed) of the major monomeric product, coniferyl alcohol. The results have been shown in Table 7.5. It is evident that the relative normalized proportion of all the major identified products (with the exception of 3-hydroxy-1-(4-hydroxy-3-methoxyphenyl)propan-1-one) is similar irrespective of the model compound 1-5 pyrolyzed. Guaiacol was formed in different proportions depending on the end group ratio (the ratio of blue to red rings from Figure 7.1) for model compounds 1-3 and hence not included in Table 7.5. These results suggest that reactions occurring during β -O-4 bond scission are probably independent of the degree of polymerization, and the nature of the end group (presence or absence of alkyl substituent on the guaiacyl end group) does not play a dominant role. Although the nature of the end group may influence the monomeric products formed as a result of secondary reactions of products formed via pathway 2, it can be considered a minor effect and would contribute to the variation in the relative proportion.

7.4.2 Char Formation

Char is the residue that is left behind during pyrolysis of biomass, and numerous studies have been carried out on char formation during pyrolysis of extracted lignin. Lignin is considered a significant contributor to char during biomass pyrolysis therefore it is necessary to understand the factors which influence char formation with the goal to increase the carbon yield. Here, we have systematically studied the amount of char formed as a function of the degree of polymerization by keeping all

Table 7.5.

Relative abundances of identified monomeric pyrolysis products normalized with respect to coniferyl alcohol (4-(3-hydroxyprop-1-en-1-yl)-2-methoxyphenol).

Compound	Dimer	Trimer	Tetramer	Trimer	Polymer
	1	2	3	4	5
Monomeric species					
2-methoxy-4-vinylphenol	1.4	1.8	2.7	7.8	10.7
4-hydroxy-3-methoxybenzaldehyde	8.2	11.6	12.3	7.3	20.1
1-(4-hydroxy-3-methoxyphenyl)-ethan-1-one	10.1	12.8	12.7	8.9	11.9
1-(4-hydroxy-3-methoxyphenyl)-prop-2-en-1-one	25.9	23.4	22.7	16.3	17
4-(3-hydroxyprop-1-en-1-yl)-2-methoxyphenol	9.4	11.9	13.2	12.2	12.3
3-(4-hydroxy-3-methoxyphenyl)-acrylaldehyde	5.9	5.8	5.4	8	7.7
4-(3-hydroxyprop-1-en-1-yl)-2-methoxyphenol	100	100	100	100	100
3-hydroxy-1-(4-hydroxy-3-methoxyphenyl)propan-1-one	31.2	10.9	8.1	3.6	2.8

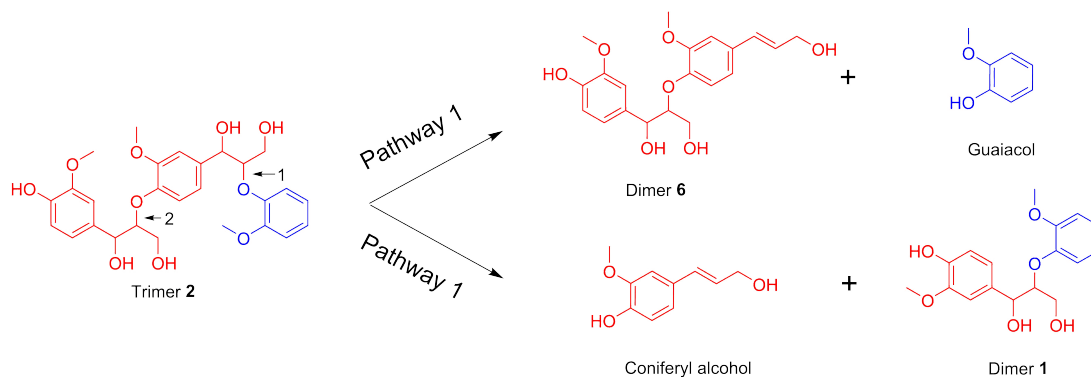


Figure 7.4. Transformation of trimer 2 to potential products via pathway 1.

the other influencing parameters constant. Additionally there was no influence of inorganic impurities on char formation since pure synthetic lignin oligomers have been used in this study. It was observed that the quantity of char formed increased with an increase in the degree of polymerization for model compounds 1,2,3,5 as shown in Figure 7.5. The degree of polymerization is indirectly linked to the volatility of the parent molecule as well as the number of bonds that need to be broken to form fragments which have a rate of vaporization that is high relative to the rates of subsequent reactions. Therefore it seems logical that char formation is proportional to the degree of polymerization of the lignin model compounds. Kotake et al. have predicted a "polymer effect" which states that, the pyrolysis fragments tend to spend more time on the heated surface when more bonds are required to be broken, resulting in greater extent of char formation.[158] A comparison of the char yields between trimer 2 (12.5%) and trimer 4 (22.2%) showed a notable increase in the amount of char formed for trimer 4. In the case of trimer 4, the end group has an alkyl substituent which results in an increase in the molecular weight and as well as the predicted boiling point of the compound when compared to trimer 2 (Table F.1). Additionally, the monomers/dimers formed from the substituted end group as a result of β -O-4 bond cleavage have a lower volatility, as compared to those from trimer 2. These

factors could explain an increase in the amount of char formation which progressively increases up to that produced by polymer 5 ($D_p = 20$).

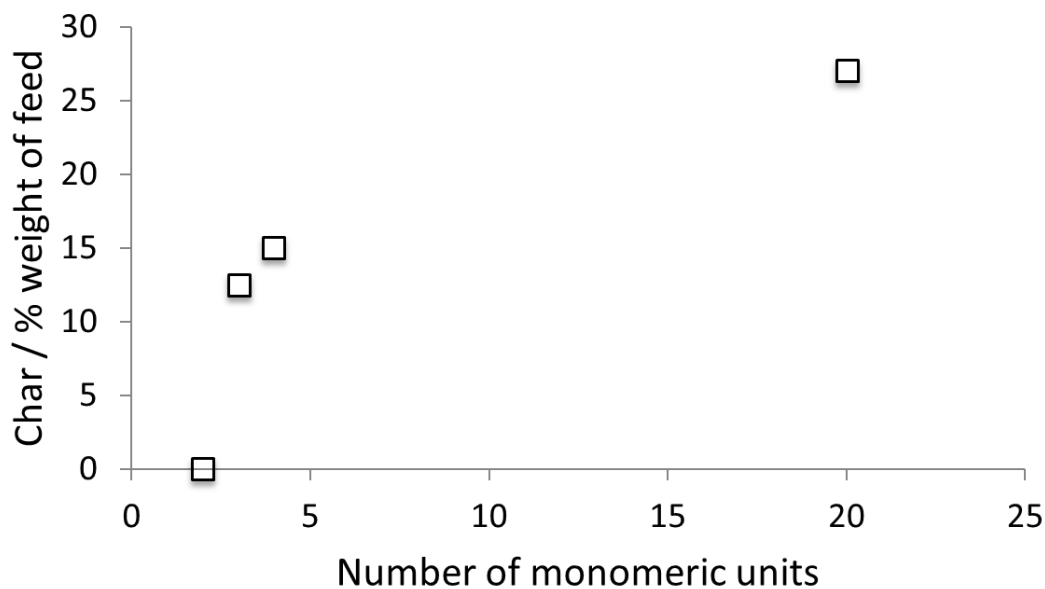


Figure 7.5. Char yield as a function of the degree of polymerization of the lignin model compounds.

An additional factor for char formation could be the concentration of coniferyl alcohol species at the pyrolysis surface. Studies have shown that when heated to temperature greater than 250°C, coniferyl alcohol undergoes polymerization reactions in addition to char formation, evaporation and secondary reactions to form other monomeric species.[157–160] On further investigation under pyrolysis conditions of 500°C, formation of dimeric molecules from coniferyl alcohol was observed along with formation of char, ~10% (Table F.4). Only ~35% of it evaporated intact, proving that it is an extremely reactive species and could be responsible for formation of char during pyrolysis of the model polymers. Condensation reactions have also been observed with lignin monomers having a $C\alpha=C\beta$ which could be precursors for polymerization and eventual formation of char.[159] The expected concentration of coniferyl alcohol species and its oligomeric counterparts at the pyrolysis surface is also proportional

to the degree of polymerization (Figure F.2). Therefore polymerization of pyrolysis fragments (monomeric and oligomeric) with $C\alpha=C\beta$ could also result in formation of char which has been shown to possess a polyaromatic structure.[135]

7.4.3 Effect of Vapor Phase Residence Time

Vapor phase residence time is considered to be a critical parameter in controlling the product distribution from fast pyrolysis of biomass. Previous studies have suggested that the primary products of lignin pyrolysis are monomeric compounds which subsequently undergo secondary reactions that lead to the formation of oligomers.[14, 124] There is evidence that these reactions occur during/after condensation of the pyrolysis vapors and are aided by presence of acidic species in the bio-oil. However, it is unclear whether the oligomerization reactions also occur in the vapor phase. Hoekstra et al. performed vapor phase residence time studies on pyrolysis vapors from pine wood and observed a decrease in the yield of pyrolytic lignin (from bio-oil) with an increase in the residence time.[149] This result points towards a decrease in the average molecular weight of the product distribution from biomass, however there is little information on the composition of the pyrolytic lignin and the condensed bio-oil. In order to understand the nature of these secondary reactions, we performed lignin pyrolysis experiments at different vapor phase residence times by varying the gas flow rate through the pyrolysis zone. It should be noted that condensation was entirely avoided by having online analysis GC/MS capability and fully heat-traced transfer lines. The residence times were calculated based on the gas flow rate and the estimated volume between the sample quartz tube and the GC column. The pyrolysis and analysis conditions were identical for these experiments and any change in the product distribution was attributed to a change in the vapor phase residence time.

These experiments were limited to the two model compounds, dimer 1 and polymer 5, and the residence time was varied from 0.5 s to 3 s while maintaining the temperature of the entire post pyrolysis zone at 300°C. At the lowest residence time (0.5 s), the pyrolysis product distribution from dimer 1 comprised of ~63% of the

dimer 1, and as the residence time was increased to 3 s the amount of dimer 1 observed went down to $\sim 24\%$ (Figure 7.6). This was indicative of the dimer 1 undergoing secondary transformation to form other products in the vapor phase. The decrease in the dimer 1 abundance was simultaneously accompanied by an increase in the total monomeric products observed, thereby providing evidence for β -O-4 bond scission in the vapor phase. The most abundant monomeric product observed was coniferyl alcohol and its yield increased with an increase in the residence time. 2-methoxy-4-(2-(2-methoxyphenoxy)vinyl)phenol (MW 272 Da) also showed an increasing trend lending credence to the existence of a parallel pathway 2 for formation a dimeric species with a lower molecular weight than the parent species (MW 320 Da). The detailed product distribution from dimer 1 as a function of the residence time has been tabulated in Table F.7. These results illustrate that the average molecular weight of the pyrolysis product distribution decreases with an increase in the vapor phase residence time and is attributed primarily to the β -O-4 bond scission.

Polymer 5 was also pyrolyzed under identical conditions to verify the observations from the residence time studies with dimer 1. As stated previously, we were unable to identify the structures of dimeric species that were produced during pyrolysis of the polymer 5. As a consequence, the entire product distribution in the dimer range has been lumped together. The total quantified dimeric products account for $\sim 19\%$ at the low residence time of 0.5 s and decrease to $\sim 13.5\%$ at a residence time of 1.6 s. The overall yield to the dimeric products is low compared to that from dimer 1 in part due to low volatility of the dimeric products formed from the polymer as they are expected have a substituted alkyl side chain on both the aromatic rings (i.e. dimer 6, Figure F.1) . These results indicate that the initial vapor phase products from pyrolysis are formed by thermal depolymerisation of the lignin oligomers and are volatile enough to vaporize. These initial vapor phase products include monomers and dimers and possibly a minor fraction of trimers. The estimated boiling point for trimers is in excess of 690°C (Table F.1) and hence trimers are expected to constitute only a minor fraction of the vapor phase under our standard pyrolysis conditions

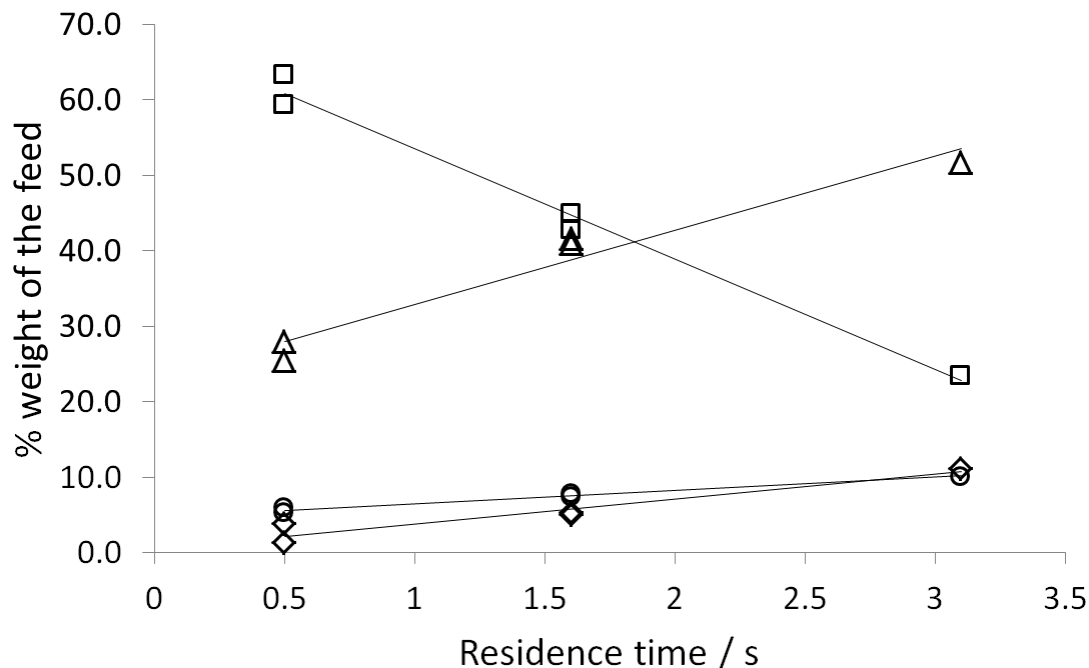


Figure 7.6. Yield of products from pyrolysis of dimer 1 as a function of vapor phase residence time. Dimer 1 (squares), Monomeric species (triangles), Coniferyl alcohol (circles), 2-methoxy-4-(2-(2-methoxyphenoxy)-vinyl)phenol (diamonds).

(500°C). These products are then subjected to secondary reactions as they traverse through the heat traced tubing at 300°C before being quenched at the inlet of the online GC-MS. As a consequence of these secondary reactions, the dimers and trimers breakdown to form monomers.

7.4.4 Primary Products of Lignin Pyrolysis

There is no general consensus in literature about the primary products of pyrolysis, which are generally regarded as either the first products to enter the vapor phase, or in a somewhat different interpretation, the major quantifiable products of pyrolysis. Analysis of these primary vapor phase products hold the key to understanding the pyrolysis pathways. In this study we have observed both monomeric and dimeric

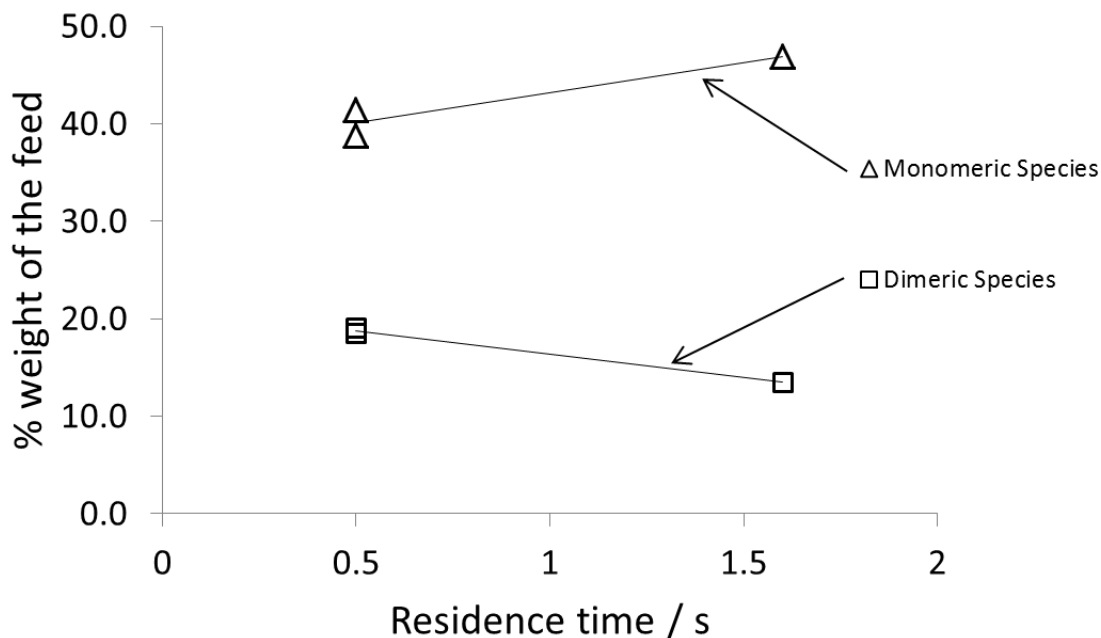


Figure 7.7. Yield of products from pyrolysis of polymer 5 as a function of vapor phase residence time. Dimeric species (squares), Monomeric species (triangles).

species at the lowest residence time of 0.5 s for lignin model compounds. These dimeric species undergo secondary reactions with an increase in the residence time. If one were to extrapolate this backwards, it would be prudent to say that the primary products of pyrolysis comprise of monomers, dimers and possibly trimers. This is in agreement with results in literature from Zhou et al., [139] who observed oligomers as primary products in their wire mesh reactor with instant quenching of the vapors. These experiments were carried out under vacuum conditions, which resulted in higher volatility for the oligomeric species when compared with other studies which were conducted at ambient pressure. Therefore when addressing the issue of primary products it is important to acknowledge the role of pyrolysis conditions under which these products are detected. While oligomeric fragments are formed by depolymerization of lignin, their abundance in the vapor phase as primary products will depend on their volatility under the local temperature and pressure conditions during pyrol-

ysis. From this study, it can be concluded that primary vapor phase products from lignin pyrolysis are a mixture of monomers and oligomers whose relative proportion is dependent on their structure and pyrolysis conditions.

7.5 Conclusions

In this study we have developed a new approach for analysis of lignin derived dimeric species via an online GC/MS. Pyrolysis experiments were carried out with model lignin polymers with this approach to attain greater than 90% mass closure. This study provides quantitative results on pyrolysis of pure lignin model compounds with β -O-4 linkages to understand the underlying factors that govern the product distribution without the unwanted effects from impurities (inorganic, sugars and multiple poorly characterized reactants) which are generally present in extracted lignins. The major monomeric product observed from β -O-4 bond scission was coniferyl alcohol. A significant proportion of the pyrolysis products from the all of the model compounds tested comprised of dimeric species with greater than 19% abundance. The relative ratios of major monomeric compounds were similar for all the model compounds indicating that the nature of β -O-4 bond scission was independent of the degree of polymerization. The amount of char formed increased with the degree of polymerization providing insight into the factors which govern char formation like the volatility and reactivity of the fragments formed during pyrolysis. Additionally, vapor phase residence time was shown to have an important effect on the product distribution due to secondary reactions. An increase in the vapor phase residence time resulted in the dimeric species breaking down to form monomeric products thereby decreasing the average molecular weight of the product distribution. Vapor phase primary products from lignin pyrolysis comprised of both monomeric and dimeric species (and possibly trimeric species) which underwent secondary (cracking/depolymerization) reactions in the vapor phase. This has important implications on the ability to tailor the vapor phase product distribution from lignin before it is passed over a catalyst for hydrodeoxygenation.

8. A SYNERGISTIC BIOREFINERY BASED ON CATALYTIC CONVERSION OF LIGNIN PRIOR TO CELLULOSE STARTING FROM LIGNOCELLULOSIC BIOMASS

8.1 Introduction

Production of liquid fuels and chemicals from lignocellulosic biomass is an integral part of the solution to the energy grand challenge.[161] Biorefinery concepts for the production of liquid fuels and chemicals from biomass have been developed and some commercially implemented.[162–164] However, any renewable platform must provide both liquid fuels and commodity chemicals on a large scale. For example, in 2012 the U.S. consumed ~ 4.6 billion barrels of liquid fuels and produced greater than 90 Mton of organic commodity chemicals, respectively (including ~ 8 Mton of benzene).[165–167] Cellulosic conversion methods to ethanol and other liquid fuels make use of only the carbohydrate components of biomass ($\sim 50\text{--}60\%$ by weight).[168–170] In comparison, the lignin component (20–30% by weight but accounting for $\sim 37\%$ of the carbon in biomass) inhibits the conversion of cellulose and constitutes a major waste stream that is burned for its heat value in most applications.[12] Therefore, lignin represents an opportunity for meeting the demand for a renewable platform of aromatic fuels and commodity chemicals (e.g. benzene, toluene, xylene (BTX), styrene, and cumene). As a result, methods for the selective conversion of lignin are important.[12]

The concept of lignin utilization to produce high-value products is not new.[171, 172] However, actual reaction schemes to effectively convert lignin with high yield to useful end-products remains a significant challenge. There are processes that produce organosolv lignin separating it from hemicellulose and cellulose, but the resulting organosolv lignin fraction is an extremely complex mixture, which upgrading to a reasonable number of products in any significant yields is yet to be demonstrated.[16]

Currently one of the few notable commercial processes utilizes lingo-sulfonate lignin derived from sulfite pulping to produce vanillin at a maximum yield of only 7.5% by mass.[173] Even though new catalysts have been reported for the cleavage of ether C-O bonds and hydrodeoxygenation (HDO) of lignin model compounds, only limited successes have been reported with lignin or biomass.[174–181] Heterogeneous Ni catalysts have been used recently with liginosulfonate to give a mixture of phenolic compounds and dimeric lignin fragments with removal of the sulfur as H₂S.[180] Ford and co-workers have reported a catalytic method in supercritical methanol at 300–320°C and 160–220 bar of H₂ that converts the lignified components of biomass to hydrogenated cyclic alcohols.[181] A recent report has appeared on the conversion of birch sawdust to phenolic compounds utilizing a Ni/C catalyst.[182, 183] Previously we reported on a catalytic system that could cleave the β -O-4 linkages found in lignin dimeric and polymeric model compounds with high selectivity and yields.[184]

Here we present the use of a bimetallic catalyst based on Zn and nanoparticulate Pd in a selective conversion process compatible with diverse species of intact woody biomass. The catalyst produces a single lignin-derived product stream in high yields, leaving essentially all polysaccharide components of the biomass as a solid residue, which we have demonstrated undergoes enzymatic hydrolysis, resulting in high yields of glucose (Figure 8.1). In addition to several wild type species of poplar, conversion of genetically modified poplar that contain high S type lignin is described.[185] This type of bioengineering offers a method to control the potential products from reactions involving biomass. Furthermore, methoxypropylphenols similar to those produced during this catalytic reduction of lignin can be converted quantitatively in a second step using a bifunctional Pt-Mo catalyst to hydrocarbon fuel or propylbenzene. The latter serves as platform for production of aromatic chemicals.

8.2 Selective Catalytic Conversion of Lignin

Our biomass conversion process is accomplished via a bimetallic catalytic system composed of ZnII sites and metallic Pd nanoparticles (3–4 nm) dispersed on a car-

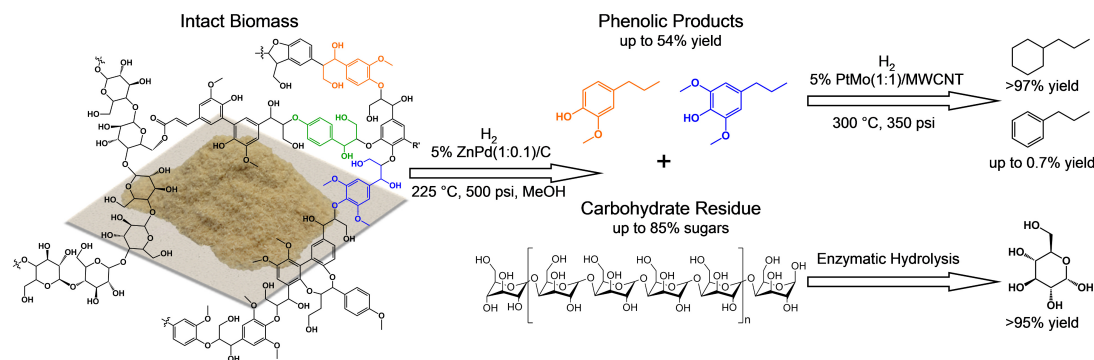


Figure 8.1. Selective depolymerization and hydrodeoxygenation (HDO) of lignin first from wood biomass to give a lignin-derived hydrocarbon platform and glucose from the carbohydrate residue.

bon support. This bimetallic system has been shown previously to have a synergistic effect that cleaves β -O-4 linkages found in model compounds more effectively than either component alone.[184] For this catalytic process the biomass was first milled to pass through a 40 mesh screen then washed consecutively with water and ethanol via soxhlet extraction. Three different types of pretreated wild-type (WT) poplar (species within the genus *Populus*) wood were reacted with the Zn/Pd/C catalyst in methanol (MeOH) at 225°C and 500 psig of H₂ which resulted in 40-54% of the available lignin being converted to two products: 2-methoxy-4-propylphenol (dihydroeugenol) and 2,6-dimethoxy-4-propylphenol (Table 8.1, entries 1, 3, and 4, and Figure 8.2A). Based on our experimental results, Zn, Pd, and H₂ are all required for catalysis. Control reactions with poplar biomass using Zn alone gave minimal conversion to multiple oxygenated products and no products were generated in the absence of H₂. Reactions of poplar wood with Pd/C alone gave low yields of more highly oxygenated methoxypropylphenol products. To facilitate separation and recycling (shown in Table G.1) of the Zn/Pd/C catalyst, we ran the reaction employing a microporous cage (325 mesh) to separate the Pd/C from the biomass. Such a cage allows the solvent and solute to access the catalyst and leaves behind a cellulosic biomass residue that is Pd/C free. This result is also consistent with the mechanism

proposed in our previous study with model compounds where the Zn can be desorbed from the carbon surface and is free to pass in and out of the microporous cage.[184]

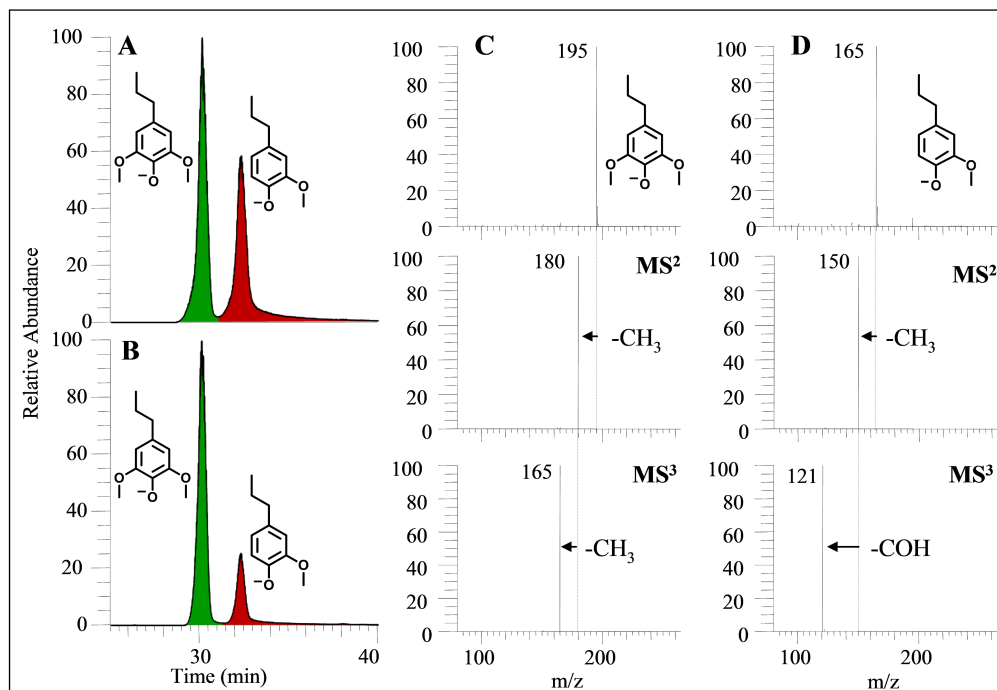
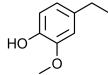
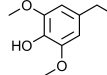


Figure 8.2. Single ion monitoring ESI(-)/HPLC/MS of lignin products (m/z 165 and m/z 195) from (a) WT-717 poplar and (b) 717-F5H, a high-S transgenic line. CAD MS/MS of (c) deprotonated 2,6-dimethoxy-4-propylphenol and (d) deprotonated dihydroeugenol derived from WT-717 poplar.

The described preparation/pretreatment of biomass is minimal and all the steps are scalable, an important prerequisite of any process for large-scale application in a biorefinery. The two products reflect guaiacyl (G) and syringyl (S) lignin components present in WT poplar and illustrate the applicability of our catalysis to variants within the genus *Populus*. Following our single-step catalytic conversion, the starting biomass is fractionated into two forms, the first is a solid residue that is easily filtered and the second consists of products that are soluble in MeOH. The MeOH liquid-phase contains the methoxypropylphenol products shown in Table 8.1 and a small

Table 8.1.
Conversion of lignin starting with intact lignocellulosic biomass over Zn/Pd/C catalyst.

Biomass Type	%G Lignin ^a	%S Lignin ^a	% Lignin Content ^b	Selectivity		Yield (wt%) ^c
						
Poplar WT-717	44	51	19	31	69	40
Poplar 717-F5H (High S Poplar)	20	73	20	17	83	36
Poplar WT-NM-6	40	55	18	28	72	44
Poplar WT-LORRE	49	47	19	45	55	54
WT-White Birch	44	49	16	31	69	52
WT-Eucalyptus	34	65	24	30	70	49
WT-Lodgepole Pine	100	0	31	100	NA	19

amount of soluble sugars that mostly originate from hemicellulose (Table G.2 and Table G.5). An additional phenolic product of methylparaben was detected and quantified from the reaction with the poplar species (Table G.1). This product is extracted in various quantities from all reactions using poplar, even those without catalyst present, and its exact origin is unknown as the amounts of H lignin found in the poplar species is very low (Table G.3). There is no evidence that the solvent, MeOH, is consumed during this reaction and its volatility makes it easy to separate from both the phenolic products and sugar residue. Upon removal of methanol, dihydroeugenol and 2,6-dimethoxypropylphenol can be extracted from the remaining residue using diethylether. NMR spectra of this extract confirm it consists of mainly two products with small amounts of unidentified impurities (see Supp. Inf. of Parsell et. al [186]). The non-ether soluble fraction was also analyzed via NMR and gave spectra with features consistent with sugars and aromatic lignin fragments suggesting that a portion of our unaccounted for lignin is present in the methanol solution.[186] This fraction was then subjected to analysis for carbohydrates and found to contain a majority of xylans with smaller amounts of glucans and arabinans (Table G.5).

In comparison to the Pd-Zn catalytic process described above for intact wood biomass, organosolv lignin contains hundreds of compounds,[173] rendering its conversion to a reasonable number of products extremely difficult (Figure G.1c).

8.3 Carbohydrate Residue Retains its Value

To determine the composition of the leftover carbohydrate residue it was digested by acid hydrolysis, which produced mainly glucose (Table G.6). This leftover carbohydrate residue was subjected to cellulase enzyme digestion, giving 95% of the theoretical glucose yield.[187] In comparison, intact poplar wood released only 11% of theoretical glucose from cellulase enzyme digestion over the same time period. These results are consistent with those reported in the literature showing that cellulose can be hydrolyzed by enzymes once lignin is removed, as lignin and deactivates cellulase enzymes.[188] The sugars from hydrolysis as well as the sugars present in

the MeOH phase were analyzed allowing mass balance closure of 74% of the starting biomass weight in quantified products (Figure 8.3). Our results illustrate the positive impact of lignin conversion by the Zn/Pd/C catalyst on enhancing sugar yields from poplar. Furthermore, the released sugar can be upgraded by known biological and chemical catalytic conversion processes that have been developed independently for pure carbohydrates.[189, 190]

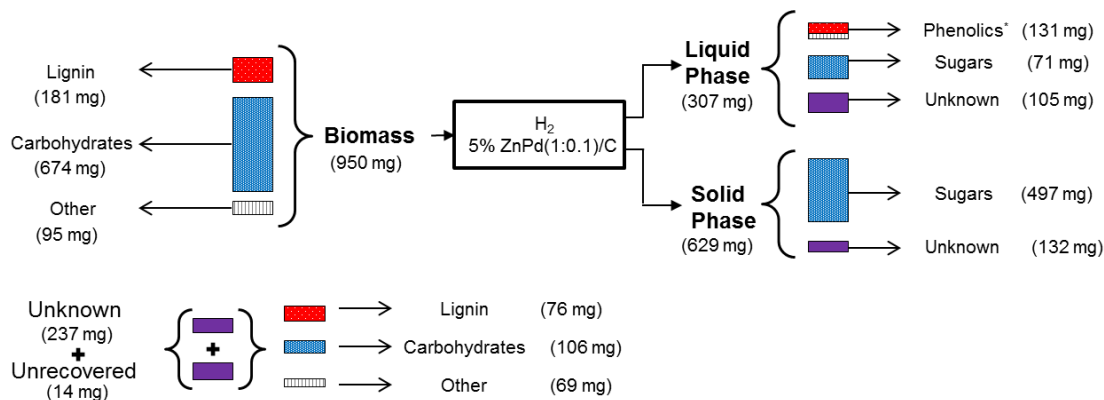


Figure 8.3. Mass balance after catalytic cleavage and HDO of WT poplar lignin over Zn/Pd/C catalyst. *Mass of phenolic products includes all quantified phenolics and also accounts for the loss of O into H₂O during HDO. Liquid Phase sugars were quantified by HPLC analysis. The solid phase residue was hydrolyzed with acid. Then glucose, arabinose, and xylose were quantified by HPLC analysis.

The availability of the leftover carbohydrate residue for direct conversion was demonstrated by subjecting the sample to analytical fast pyrolysis in a pyroprobe / mass spectrometer developed previously for the determination of primary pyrolysis products.[9] The results obtained for pure cellulose and the leftover carbohydrate residue derived from woody biomass are compared in Figure 8.4, together with fast-pyrolysis products of raw woody biomass. The solid residue behaved similarly to pure cellulose, yielding a similar product distribution, the main product of which was cellobiosan. This result is in sharp contrast to the highly complex mixture obtained upon fast pyrolysis of the lignified raw biomass (Figure 8.4A).

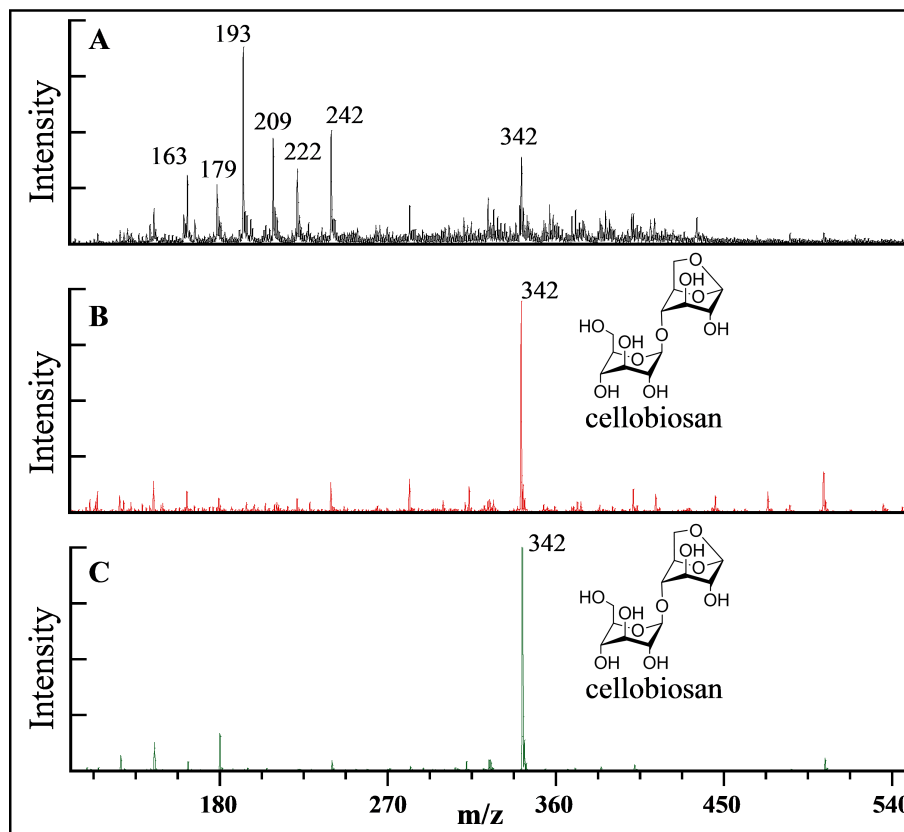


Figure 8.4. Positive mode ammonium attachment Atmospheric Pressure Chemical Ionization mass spectra measured for fast pyrolysis [9] products of (a) WT-LORRE poplar, (b) carbohydrate residue from WT poplar after our one-step catalytic conversion of lignin over Zn/Pd/C, and (c) pure crystalline cellulose.

8.4 Genetic Variants Control Products

Lignin is made by radical polymerization of p-hydroxyphenyl (H), G, and S monomeric units to give various linkage types (Figure 8.1). The most ubiquitous linkage is the β -O-4. H, G, and S subunit abundance in lignin varies depending on the plant species, and the availability of different monomers can be manipulated genetically.[191, 192] To evaluate whether such engineered lignins can be successfully converted using our process, we employed a genetically engineered line (717-F5H)

with high-S lignin (Table 8.1, entry 2).[185, 193] Unmodified WT-717 poplar gives a \sim 1:2 ratio of dihydroeugenol to 2,6-dimethoxy-4-propylphenol. In comparison the high-S line gives a greater yield of 2,6-dimethoxy-4-propylphenol with a final product distribution of 1:6 (Figure 8.2B). The results from this experiment demonstrate how tailoring biomass through genetic control can affect the product distribution.

Wood from other tree species, such as pine, white birch, and eucalyptus, can also be broken down by our catalyst (Table 8.1, entries 5-7). Pine contains exclusively G lignin and has very high lignin content (30% by weight). Pine gave exclusively dihydroeugenol as the phenolic product but with lower yield compared to poplar and birch, presumably due to the high degree of cross-linking in G lignins. Although the lignin content of white birch is only 16% by weight, it gave an impressive yield (52%) (Table 8.1, entry 6); whereas, the combination of high lignin content (24% by weight) and high yield 49% from eucalyptus produced the greatest overall yield of products from a mass standpoint (\sim 12% of the total biomass converted to the two phenolic products).

8.5 Lignin-Derived Fuel and Chemical Platform

While the methoxypropylphenol products have value as chemicals, we have also developed novel catalysis for their conversion to the high-octane liquid fuel propylbenzene (Figure 8.1). When dihydroeugenol; 2,6-dimethoxy-4-propylphenol; or a mixture of the two was reacted with H_2 over a Pt-Mo bimetallic catalyst at 300°C and 342 psig H_2 , propylcyclohexane and propylbenzene were obtained in $>97\%$ and $\sim 0.7\%$ yield, respectively (Table G.8a). This is the highest reported yield of hydrocarbons from the continuous, vapor-phase reaction of lignin-derived methoxypropylphenols to date. The propylcyclohexane can be aromatized via a dehydrogenation reaction to give additional propylbenzene and return 3 equivalents of the H_2 used in the hydrogenation of methoxypropylphenols over the Pt-Mo catalyst.[194, 195] Current work is aimed at the direct production of propylbenzene from methoxypropylphenols.

The effective lignin processing demonstrated here opens a new direction for biorefinery configurations and synergies. The catalytic depolymerization of lignin into methoxypropylphenols employs the lignin portion of biomass first, while simultaneously leaving behind an essentially intact solid-carbohydrate fraction that can be further processed via traditional biorefinery methods. Utilization of all components of lignocellulosic biomass feedstock (lignin, cellulose, and hemicellulose) is critical for maximizing fuel and chemical yield per acre. The selective production of two methoxypropylphenols and their further conversion to the hydrocarbon propylcyclohexane/propylbenzene platform reported here enables many options for the conversion of the natural aromatic structure of lignin into currently used aromatic chemicals that were previously not viable. In addition, we envision a biorefinery that encompasses multiple synergies (as opposed to conventional biorefineries involving only one processing method) designed to minimize chemical bond breaking by making products that exploit the natural structure of biomass.

The lignin-derived methoxypropylphenols can be used in the fragrance industry (i.e. dihydroeugenol), as well as be catalytically upgraded to a variety of fuels (e.g. propylbenzene, toluene, etc.) and chemicals (e.g. propane, methanol, benzene, cumene, para-xylene, ethylbenzene, styrene, phenol, and acetone) as shown in Figure 8.5. We have demonstrated high-yield production of the hydrocarbon propylcyclohexane from lignin. Propylcyclohexane can be converted via dehydrogenation to propylbenzene, which can be hydrocracked subsequently to benzene and propane.[196] Benzene can be used as a chemical building block for production of fuels and chemicals via a variety of known and practiced conversions, such as: alkylation of benzene with co-produced propane (propylene after dehydrogenation) to form cumene, alkylation with co-produced MeOH to form toluene or xylenes, or alkylation with ethanol or ethylene to form ethylbenzene and styrene.[197, 198] The propane produced can be dehydrogenated and employed for polymer production or converted further to acetone; which when reacted with phenol forms the polycarbonate monomer, bisphenol-A.[199]

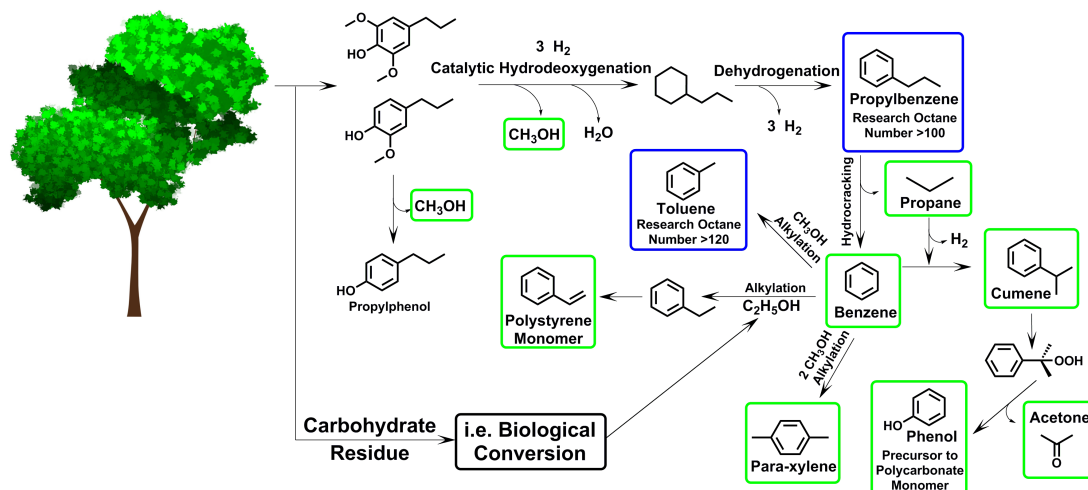


Figure 8.5. Pathways for the production of renewable fuels (in blue) and chemicals (in green) from the lignin portion of biomass. Methoxypropylphenols can be used as is for the fragrance industry (dihydroeugenol), or can be catalytically tailored to fuels (such as propylbenzene and toluene) or used for the production of chemicals (such as propane, methanol, benzene, cumene, para-xylene, ethylbenzene, styrene, phenol, and acetone).

The solid carbohydrate fraction can be further processed to fuels and chemicals by currently employed chemistries such as liquid-phase (catalytic) processing and biological conversion such as fermentation, or thermochemical processes such as fast hydrolysis or gasification followed by further catalytic upgrading.[2] Additionally, the waste from some steps, such as carbonaceous residue or char, can be utilized by feeding to a thermo-chemical unit (fast-pyrolysis or gasification) for conversion into a variety of intermediate products that can be upgraded.

New synergies emerge from integration of lignin and carbohydrate chemistries. For example, in Figure 8.5, we show alkylation of benzene with methanol to form para-xylene (an important chemical) or alkylbenzene molecules as fuels. The methanol can be sourced from cleavage of the methoxy groups of methoxypropylphenols or produced from the breakdown of the carbohydrate fraction. Additionally, methanol derived from the biomass itself can be used as the solvent for the lignin depolymerization

step with the aforementioned Zn/Pd/C catalyst. Styrene can be produced through an integrated pathway involving alkylation of benzene using ethylene or renewable ethanol produced from sugar fermentation.

In addition to the pathways discussed above, the development of new and more-direct pathways are immediately recognizable, utilizing the natural aromatic lignin structure (aromatic ring, alkyl and oxygen substituents) and minimizing the number of conversion steps to generate renewable commodities. For example, cumene could be synthesized directly from propylbenzene via isomerization of the propyl substituent, and hydrocracking of propylphenol could afford a direct route to phenol and propane. Some of these transformations present the need to develop new chemistries starting from a variety of different intermediate chemicals that go beyond “traditional” chemistry used in the petrochemical industry.

8.6 Conclusion

Catalytic conversion of lignin to discrete phenolic molecules was achieved with good yields utilizing a process that produces a clean carbohydrate residue. This was accomplished under reasonable conditions (225°C, 500 psi H₂) using a synergistic Pd/C and Zn system that cleaves and deoxygenates the β -O-4 linkages in native lignin. These lignin-derived methoxypropylphenols can be further converted to a variety of valuable aromatic fuels and chemicals. This new approach to utilization of lignin enables the future biorefinery to obtain higher yields of fuels and chemicals. The newfound ability to utilize lignin-first for fuels and chemicals presents a new paradigm for biofuel production in which lignin is potentially more valuable than cellulose and provides opportunity for plant biologists to tailor biomass that contains more lignin. Mapping of products based on the natural structure of lignin identifies new chemical transformations and catalysis that will stimulate target driven fundamental research.

8.7 Materials and Methods

Pd/C (5 wt%) was purchased from Strem Chemicals (Newburyport, MA). 4-Allyl-2,6-dimethoxyphenol (98% purity) was purchased from Alfa Aesar (Ward Hill, MA). Isoeugenol, eugenol, 2-methoxy-4-propylphenol (all >98% purity) and ammonium formate (>99% purity) were purchased from Sigma-Aldrich (St. Louis, MO). 2-Methoxy-4-methylphenol (98% purity) and methylparaben (>99% purity) were obtained from TCI America (Portland, OR). High-performance liquid chromatography-mass spectrometry (HPLC-MS) grade water and acetonitrile were purchased from Fisher Scientific (Pittsburgh, PA). All chemicals were used without further purification. A Zorbax SB-C18 column (4.6 × 250 mm, 5 μm particle size) was purchased from Agilent Technologies (Santa Clara, CA). 2,6-Dimethoxy-4-propylphenol was synthesized as outlined below.

Poplar genotype NM-6 (*Populus nigra* × *P. maximowiczii*, WT-LORRE) was provided by Adam Wiese of the USDA Northern Research Station in Rhinelander, Wisconsin.[200] Hybrid aspen INRA 717-1B4 (*P. tremula* × *P. alba*, WT-717), Poplar (*P. nigra* × *P. maximowiczii*) WT-NM-6, the genetically engineered line 717-F5H and WT-White Birch (*Betula papyrifera*) were provided by Purdue University's Department of Forestry and Natural Resources Department. The WT lodgepole pine (*Pinus contorta*) was provided by Mr. Jerry Warner (COL, U.S. Army Ret.), Managing Director of Defense LifeSciences, LLC (Alexandria, VA). The WT-Eucalyptus (*Eucalyptus grandis* × *E. urophylla*) was provided by William H. Rottman, ArborGen, Inc. (Ridgeville, SC).

2,6-Dimethoxy-4-propylphenol was synthesized through the hydrogenation of the side chain of 4-allyl-2,6-dimethoxyphenol. 4-Allyl-2,6-dimethoxyphenol was dissolved in a suspension of Pd/C (5 wt%, 105 mg) in 15 mL MeOH (1.945 g, 10.1 mmol). The reaction mixture was placed in a stainless steel Parr reactor, pressurized with 500 psig bar H₂ and heated at 60°C for 3 hours. Pd/C was removed by filtration and methanol was removed in vacuo to yield 2,6-dimethoxy-4-propylphenol as a colorless

oil. The reaction product was further purified on a silica-gel column with a mobile phase of 17% ethyl acetate and 83% hexanes. ^1H NMR (CDCl_3) δ 0.93 (t, 3H, CH_3), 1.61 (s, 2H, CH_2), 2.50 (t, 2H, CH_2), 3.85 (s, 6H, OCH_3), 5.42 (s, 1H, OH), 6.39 (s, 2H, ArH).

Biomass was first milled to pass through a 40 mesh screen using a Mini Wiley Mill (Thomas Scientific, Swedesboro, NJ). Biomass was washed consecutively with water and ethanol soxhlet using the LAP Determination of Extractives in Biomass procedure.[201] Following soxhlet extraction, the biomass was dried and evaluated using a moisture analyzer (Halogen model HB43-S, Mettler-Toledo LLC, Columbus, OH).

In a typical experiment, 1.0 g of biomass, Pd/C (5 wt%), ZnCl_2 (5-10 wt%), methanol (30 mL), and glass stir bar were added to a stainless steel Parr reactor, which was subsequently sealed. While stirring the mixture was purged with UHP grade H_2 for ~ 1 min, then pressurized with H_2 (500 psig, 34 bar). The mixture was heated to 225°C . This temperature was maintained for ca. 12 hours. The reaction was terminated by removing the heat and cooling the reactor to room temperature (WARNING! Use caution when handling and venting the reactor; reduced Pd/C with methanol is flammable). The reaction mixture was filtered to remove Pd/C and remaining solid biomass residue. This Pd/C/biomass mixture was washed with additional MeOH and the filtrate was collected and diluted in a volumetric flask. This solution was analyzed by GC-FID and HPLC/MS as described below to determine amounts of methoxypropylphenols.

8.8 Acknowledgements

Reproduced from Ref. [186] with permission from The Royal Society of Chemistry

9. A NOVEL THEORY OF THE PHYSICAL AND CHEMICAL PROCESSES OF PYROLYSIS

There have been many attempts to create kinetic models that describe the behavior of pyrolysis of biomass-related materials, with the main focus being on cellulose and related glucosaccharides. The initial cellulose pyrolysis model from Broido et. al. [202] was a lumped parameter model that utilized experimental kinetic parameters with an intermediate “active cellulose”. This approach produced very close agreement in the rate of pyrolysis between the model and experimental results. The disadvantage of the lumped approach is that knowledge of the important steps to the overall product yields is not captured by such a simplistic model. The issue with developing a more complicated individual-component/individual-reaction model, is that it requires measurement of individual kinetic parameters, something which is almost always not possible during pyrolysis of cellulose, which involves hundreds of separate reactions that happen simultaneously.

Much more recently, Vinu et. al. [84] published a detailed model based upon individual components with individual kinetic parameters which were sourced primarily from Density Functional Theory (DFT) calculations with a few parameters used from experimental kinetic studies. Despite the huge increase in complexity of their approach, they were able to show good agreement in the model yields and experimental yields. This success was due in part to fitting some of the pre-exponential factors to improve the model/experimental agreement. Another major factor in the excellent agreement, however, was the use of one critical kinetic parameter, E_a , for hydrolysis of cellobiose which was taken from an experimental kinetic study despite the fact this is readily calculatable using DFT.[84, 203] One major issue with this activation energy was that it was measured at conditions far away from the conditions

at which the experimental pyrolysis data were generated. The experimental pyrolysis data were gathered between 400 and 650°C whereas this hydrolysis parameter was estimated in liquid water with sulfuric acid at between 100 and 140°C. Furthermore, this barrier is one of the lowest barriers used in their kinetic model with a value of approximately 34 kcal/mol.[84, 203] Also, it is well known that Brønsted acids catalyze hydrolysis reactions and thus for these reasons this parameter should not have been used in their model.

The other major issue, which is also related to hydrolysis, is the overall formulation of the Vinu et. al. model.[84] What occurs physically during pyrolysis of cellulose is a transition to a short lived reacting liquid intermediate which is accompanied by evaporation into the gas-phase environment where reactions can continue to happen depending on the conditions.[204, 205] In the model from Vinu et. al. [84] the authors formulated a reaction network which is heavily reliant on a glucose intermediate, from which many of the observed small molecules are produced. This is problematic because glucose can only be formed in their reaction network from the hydrolysis of the β -1,4 bonds present in the cellulose or glucosaccharides, and yet the experimental data were gathered at temperatures in excess of 400°C, far above the boiling point of water at the atmospheric pressure used in the experiments. Thus the use of a batch reactor model in Vinu et. al. presents a physically unrealistic situation in which large concentrations of water are able to accumulate and participate in the reaction network via hydrolysis.[84]

Thus, it is the opinion of this author that the aforementioned agreement of the Vinu et. al. model [84] with the experimental data are fortuitous and/or a result of fitted parameters rather than illustrative of the accuracy of the approach. For this reason, it is worthwhile to formulate a new kinetic model of cellulose / glucosaccharide pyrolysis which captures the phase change observed experimentally by Teixeira et. al.[204] In Figure 9.1 a schematic of this proposed model is shown.

The proposed model in Figure 9.1 is attractive for a number of important reasons. The first of which is that it is capable of more accurately capturing the concentrations

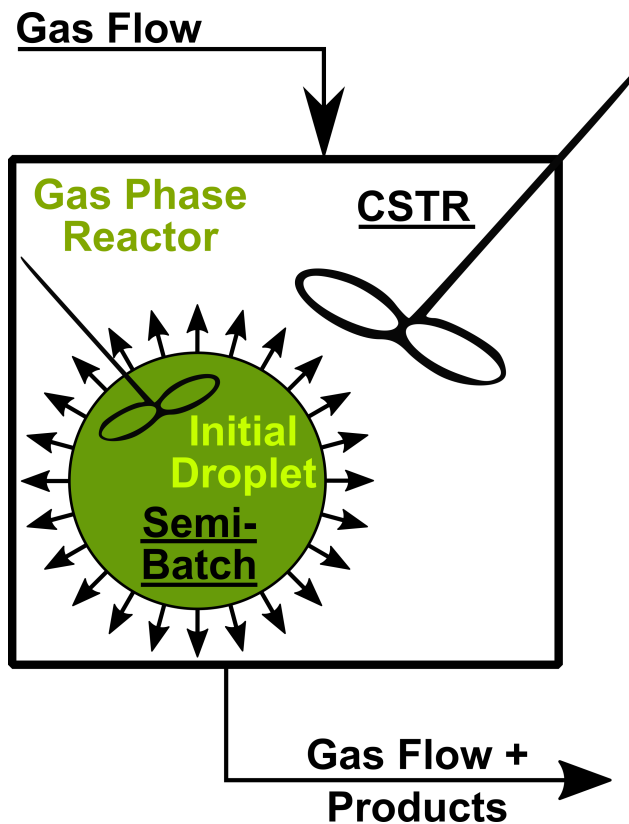


Figure 9.1. A new model for pyrolysis that utilizes reactions in both the intermediate liquid and gas phases. The liquid droplet is assumed to be at a uniform temperature and composition and shrinks from an initial size due to evaporation and reaction, which is modeled by a semi-batch reactor. The gas-phase is also assumed to be at a uniform temperature and composition, but conforms more closely to a CSTR model due to the continuous gas flow. (Note: not drawn to scale)

of the species in each individual phase. In other words, something which is extremely volatile (e.g. water) will rapidly enter the gas phase where it may still participate in reactions. Secondly, the model is capable of using different temperatures for the liquid and gas-phases. This advantage is of particular importance to this thesis due to our experimental observations of extremely large products, which is in direct conflict with previous experimental studies (see Chapters 2, 4, 5, 6 and 8 for further detailed discussion of this issue). The preliminary results from this model have shown that

if a low temperature of 150°C is chosen for the gas phase versus a liquid phase temperature of 600°C the products produced by the model are similar in average molecular weight to what is observed experimentally. Conversely, if 600°C is used for both phases, then the results better approximate the results reported in the literature by other researchers as well as the data shown in Chapter 3 (collected using a different reactor).

Parameterization of this model is particularly important to generate meaningful results. As done by Vinu et. al. use of a combination of kinetic parameters primarily from DFT with a few experimentally measured kinetic parameters (such as for Char formation) is the preferred approach. The primary difficulty arises from estimating the needed liquid vapor pressure information to correctly predict the rate at which the droplet evaporates. This is especially challenging because experimental vapor pressures for many of the reactants, intermediates and products are not available. Thus, a method for predicting pure component vapor pressures is needed. Also, the saccharide and saccharide-derived molecules in question are both extremely polar and often extremely large. Group contribution methods were not designed to predict the vapor pressures of many of these species, and indeed do not accurately predict the vapor pressure of the most non-ideal components when compared to the sparse amount of available experimental vapor pressure data.[206, 207] Our preliminary results show that using molecular dynamics can accurately predict vapor pressures of the species in the model.

10. SUMMARY

The main goal of this section is to provide recommendations for future work, since there is a conclusion section in each dissertation chapter. The major remaining issues concerning pyrolysis of cellulose and related models is twofold; the need to elucidate the mechanism for production of glucose from the non-reducing end of cellobiose, and secondly to test our hypothesis of end-chain-initiation via pyrolysis of a carbon-13 labeled cellotriose.

Lignin model compound linkage type on the other hand could open up completely new mechanisms, and the results presented here with only β -O-4 linkages is only one of the roughly eight important lignin linkages found in native lignin.[12] Thus, the best research direction is towards new linkage lignin models. Eventually connections must be drawn with native lignin, but how to perform this study in a controlled fashion is still somewhat elusive. One option is to pyrolyze genetically modified *Arabidopsis Thaliana* of which the S-lignin component likely possesses a greater percentage of β -O-4 linkages than the wild plants. Hemicellulose pyrolysis is another area in which there are many opportunities for study of pyrolysis due to the branched nature of the structure of this component *in planta*.

Study into the mechanisms that govern char formation is another critical research direction since approximately $\sim 30\%$ of the carbon may end up in char during pyrolysis of whole biomass. Any reduction of char formation would be of great interest to the biofuels community since it would increase fuel yield per acre. The primary issue concerns how to obtain useful information about the pathways and mechanisms for char formation, since presumably molecules that form char are never able to leave the reactor wall. Thus, analyzing the vapor phase product distribution may not yield much information about how the char is formed.

During my Ph.D. there was always one point of frustration which was the only semi-quantitative nature of the pyrolysis - mass spectrometry setup described in detail in Chapter 2. We made several attempts to improve the value of our results by performing various types of calibrations to achieve truly quantitative datum, but were ultimately not successful in achieving this. One of the reasons for not being able to perform these calibrations centered a on quirk of the mass spectrometers used in this study, known as the tube lens. This lens attempts to prevent neutral molecules from entering the high vacuum region of the instrument by forcing the ions through a sharp bend. The problem with this approach is that adjusting the value of the tube lens can completely alter the relative abundances of ions measured by the instrument. In Chapter 2 we detailed an attempt to calibrate these relative abundances, but the validity of this approach depends on being able to directly compare direct injection through the Atmospheric Pressure Chemical Ionization (APCI) source versus pyrolysis in which products are directly introduced into the vapor phase. In the future, it would be extremely valuable to repeat some of the experiments detailed in this dissertation on several different types of mass spectrometers and compare the relative abundances of the ions observed by each instrument. Furthermore, faster scanning rates that are provided by time-of-flight mass spectrometers may yield additional information about the time dependence of the pyrolysis product distributions.

BIBLIOGRAPHY

- [1] V. K. Venkatakrishnan et al. “Oxygen removal from intact biomass to produce liquid fuel range hydrocarbons via fast-hydrolysis and vapor-phase catalytic hydrodeoxygenation”. en. In: *Green Chemistry* (Oct. 2014). DOI: 10.1039/C4GC01746C.
- [2] D. Mohan, C. U. Pittman, and P. H. Steele. “Pyrolysis of Wood/Biomass for Bio-oil: A Critical Review”. In: *Energy & Fuels* 20.3 (May 2006), pp. 848–889. DOI: 10.1021/ef0502397.
- [3] D. Shen et al. “The pyrolytic behavior of cellulose in lignocellulosic biomass: a review”. In: *RSC Advances* 1.9 (Nov. 28, 2011), pp. 1641–1660. DOI: 10.1039/C1RA00534K.
- [4] P. R. Patwardhan et al. “Product distribution from fast pyrolysis of glucose-based carbohydrates”. In: *Journal of Analytical and Applied Pyrolysis* 86.2 (Nov. 2009), pp. 323–330. DOI: 10.1016/j.jaap.2009.08.007.
- [5] P. R. Patwardhan et al. “Influence of inorganic salts on the primary pyrolysis products of cellulose”. In: *Bioresource Technology* 101.12 (June 2010), pp. 4646–4655. DOI: 10.1016/j.biortech.2010.01.112.
- [6] P. R. Patwardhan et al. “Distinguishing primary and secondary reactions of cellulose pyrolysis”. In: *Bioresource Technology* 102.8 (Apr. 2011), pp. 5265–5269. DOI: 10.1016/j.biortech.2011.02.018.
- [7] M. S. Mettler et al. “The chain length effect in pyrolysis: bridging the gap between glucose and cellulose”. In: *Green Chemistry* 14.5 (May 1, 2012), pp. 1284–1288. DOI: 10.1039/C2GC35184F.

- [8] V. K. Venkatakrishnan et al. “High-pressure fast-pyrolysis, fast-hydropyrolysis and catalytic hydrodeoxygenation of cellulose: production of liquid fuel from biomass”. In: *Green Chemistry* 16.2 (2014), pp. 792–802.
- [9] M. R. Hurt et al. “On-Line Mass Spectrometric Methods for the Determination of the Primary Products of Fast Pyrolysis of Carbohydrates and for Their Gas-Phase Manipulation”. In: *Analytical Chemistry* 85.22 (Nov. 2013), pp. 10927–10934. DOI: 10.1021/ac402380h.
- [10] J. C. Degenstein et al. “Fast Pyrolysis of ^{13}C -Labeled Cellobioses: Gaining Insights into the Mechanisms of Fast Pyrolysis of Carbohydrates”. In: *Journal of Organic Chemistry* 80.3 (2015), pp. 1909–1914.
- [11] J. C. Degenstein et al. “Mass spectrometric studies of fast pyrolysis of cellulose”. In: *European Journal of Mass Spectrometry* 21.3 (2015), pp. 321–326.
- [12] J. Zakzeski et al. “The Catalytic Valorization of Lignin for the Production of Renewable Chemicals”. In: *Chemical Reviews* 110.6 (June 2010), pp. 3552–3599. DOI: 10.1021/cr900354u.
- [13] M. W. Jarvis et al. “Direct Detection of Products from the Pyrolysis of 2-Phenethyl Phenyl Ether”. In: *J. Phys. Chem. A* 115.4 (Feb. 2011), pp. 428–438. DOI: 10.1021/jp1076356.
- [14] P. R. Patwardhan, R. C. Brown, and B. H. Shanks. “Understanding the fast pyrolysis of lignin”. In: *ChemSusChem* 4.11 (2011), pp. 1629–1636.
- [15] S. Chu, A. V. Subrahmanyam, and G. W. Huber. “The pyrolysis chemistry of a β -O-4 type oligomeric lignin model compound”. In: *Green Chemistry* 15.1 (2013), pp. 125–136.
- [16] T. M. Jarrell et al. “Characterization of organosolv switchgrass lignin by using high performance liquid chromatography/high resolution tandem mass spectrometry using hydroxide-doped negative-ion mode electrospray ionization”. In: *Green Chemistry* 16.5 (2014), pp. 2713–2727.

- [17] W. D. Bauer et al. “The structure of plant cell walls II. The hemicellulose of the walls of suspension-cultured sycamore cells”. In: *Plant Physiology* 51.1 (1973), pp. 174–187.
- [18] P. R. Patwardhan, R. C. Brown, and B. H. Shanks. “Product Distribution from the Fast Pyrolysis of Hemicellulose”. en. In: *ChemSusChem* 4.5 (May 2011), pp. 636–643. DOI: 10.1002/cssc.201000425.
- [19] G. W. Huber, S. Iborra, and A. Corma. “Synthesis of Transportation Fuels from Biomass: Chemistry, Catalysts, and Engineering”. In: *Chem. Rev.* 106.9 (Sept. 2006), pp. 4044–4098. DOI: 10.1021/cr068360d.
- [20] A. V. Bridgwater. “Biomass Fast Pyrolysis”. In: *Thermal Science* 8.2 (2004), pp. 21–49.
- [21] T. P. Vispute et al. “Renewable Chemical Commodity Feedstocks from Integrated Catalytic Processing of Pyrolysis Oils”. In: *Science* 330.6008 (Nov. 26, 2010), pp. 1222–1227. DOI: 10.1126/science.1194218.
- [22] A. J. Ragauskas et al. “The path forward for biofuels and biomaterials”. In: *science* 311.5760 (2006), pp. 484–489.
- [23] R. Lanza, D. Dalle Nogare, and P. Canu. “Gas phase chemistry in cellulose fast pyrolysis”. In: *Industrial & Engineering Chemistry Research* 48.3 (2008), pp. 1391–1399.
- [24] R. Agrawal and N. R. Singh. “Solar energy to biofuels”. In: *Annu Rev Chem Biomol Eng* 1 (2010), pp. 343–364. DOI: 10.1146/annurev-chembioeng-073009-100955.
- [25] A. G. Bradbury, Y. Sakai, and F. Shafizadeh. “A kinetic model for pyrolysis of cellulose”. In: *Journal of Applied Polymer Science* 23.11 (1979), pp. 3271–3280.
- [26] S. Czernik and A. Bridgwater. “Overview of applications of biomass fast pyrolysis oil”. In: *Energy & Fuels* 18.2 (2004), pp. 590–598.

- [27] A. Oasmaa et al. “Application of standard fuel oil analyses”. In: *VTT Publication* 306 (1997).
- [28] D. C. Elliott. “Historical developments in hydroprocessing bio-oils”. In: *Energy & Fuels* 21.3 (2007), pp. 1792–1815.
- [29] E. Furimsky. “Catalytic hydrodeoxygenation”. In: *Applied Catalysis A: General* 199.2 (June 12, 2000), pp. 147–190. DOI: 10.1016/S0926-860X(99)00555-4.
- [30] R. J. Evans and T. A. Milne. “Molecular characterization of the pyrolysis of biomass. 2. Applications”. In: *Energy & Fuels* 1.4 (1987), pp. 311–319.
- [31] R. Overend, T. Milne, and L. Mudge. *Fundamentals of thermochemical biomass conversion*. Elsevier Applied Science Publishers Ltd., 1985.
- [32] D. S. Radlein et al. “On the presence of anhydro-oligosaccharides in the sirups from the fast pyrolysis of cellulose”. In: *Journal of Analytical and Applied Pyrolysis* 12.1 (June 1987), pp. 39–49. DOI: 10.1016/0165-2370(87)80013-X.
- [33] D. S. Scott, J. Piskorz, and D. Radlein. “Liquid products from the continuous flash pyrolysis of biomass”. In: *Industrial & Engineering Chemistry Process Design and Development* 24.3 (1985), pp. 581–588.
- [34] G. Peacocke and A. Bridgwater. “Ablative plate pyrolysis of biomass for liquids”. In: *Biomass and Bioenergy* 7.1 (1994), pp. 147–154.
- [35] M. J. Antal et al. “Design and operation of a solar fired biomass flash pyrolysis reactor”. In: *Solar Energy* 30.4 (1983), pp. 299–312.
- [36] C. Torri et al. “Investigation on catalytic pyrolysis of pine sawdust: Catalyst screening by Py-GC-MIP-AED”. In: *Journal of Analytical and Applied Pyrolysis* 88.1 (2010), pp. 7–13.
- [37] Q. Lu et al. “Selective fast pyrolysis of biomass impregnated with ZnCl₂ to produce furfural: analytical Py-GC/MS study”. In: *Journal of Analytical and Applied Pyrolysis* 90.2 (2011), pp. 204–212.

- [38] Y.-C. Lin et al. “Kinetics and Mechanism of Cellulose Pyrolysis”. In: *The Journal of Physical Chemistry C* 113.46 (Nov. 19, 2009), pp. 20097–20107. DOI: 10.1021/jp906702p.
- [39] X. Zhang et al. “Formation mechanism of levoglucosan and formaldehyde during cellulose pyrolysis”. In: *Energy & Fuels* 25.8 (2011), pp. 3739–3746.
- [40] J. Piskorz et al. “Flash pyrolysis of cellulose for production of anhydrooligomers”. In: *Journal of Analytical and Applied Pyrolysis* 56.2 (Nov. 2000), pp. 145–166. DOI: 10.1016/S0165-2370(00)00089-9.
- [41] S. E. Anderson et al. “Evaluation of the contact and respiratory sensitization potential of volatile organic compounds generated by simulated indoor air chemistry”. In: *Toxicological Sciences* 97.2 (2007), pp. 355–363.
- [42] E. M. Andersson and I. Ericsson. “Determination of the temperature-time profile of the sample in pyrolysis-gas chromatography”. In: *Journal of Analytical and Applied Pyrolysis* 1.1 (1979), pp. 27–38.
- [43] E. M. Anderson and I. Ericsson. “Thermal degradation of organic polymers using different metals as the pyrolysis filament”. In: *Journal of Analytical and Applied Pyrolysis* 3.1 (1981), pp. 35–47.
- [44] J. Lédé. “Cellulose pyrolysis kinetics: An historical review on the existence and role of intermediate active cellulose”. In: *Journal of Analytical and Applied Pyrolysis* 94 (2012), pp. 17–32.
- [45] R. Čmelík and J. Chmelík. “Structural analysis and differentiation of reducing and nonreducing neutral model starch oligosaccharides by negative-ion electrospray ionization ion-trap mass spectrometry”. In: *International Journal of Mass Spectrometry* 291.1 (2010), pp. 33–40.
- [46] N. R. Vinueza et al. “Analysis of carbohydrates by atmospheric pressure chloride anion attachment tandem mass spectrometry”. In: *Fuel* 105 (2013), pp. 235–246.

- [47] J. Zhu and R. B. Cole. “Ranking of gas-phase acidities and chloride affinities of monosaccharides and linkage specificity in collision-induced decompositions of negative ion electrospray-generated chloride adducts of oligosaccharides”. In: *Journal of the American Society for Mass Spectrometry* 12.11 (2001), pp. 1193–1204.
- [48] J. A. Lomax, J. J. Boon, and R. A. Hoffmann. “Characterisation of polysaccharides by in-source pyrolysis positive-and negative-ion direct chemical ionisation-mass spectrometry”. In: *Carbohydrate research* 221.1 (1991), pp. 219–233.
- [49] K. Madhusudanan. “Tandem mass spectra of ammonium adducts of monosaccharides: differentiation of diastereomers”. In: *Journal of mass spectrometry* 41.8 (2006), pp. 1096–1104.
- [50] R. Helleur and R. Guevremont. “Initial application of desorption chemical ionization-pyrolysis-tandem mass spectrometry to structural analysis of carbohydrates”. In: *Journal of Analytical and Applied Pyrolysis* 15 (1989), pp. 85–95.
- [51] T. T. Fang and B. Bendiak. “The stereochemical dependence of unimolecular dissociation of monosaccharide-glycolaldehyde anions in the gas phase: a basis for assignment of the stereochemistry and anomeric configuration of monosaccharides in oligosaccharides by mass spectrometry via a key discriminatory product ion of disaccharide fragmentation, m/z 221”. In: *Journal of the American Chemical Society* 129.31 (2007), pp. 9721–9736.
- [52] H. Kawamoto, M. Murayama, and S. Saka. “Pyrolysis behavior of levoglucosan as an intermediate in cellulose pyrolysis: polymerization into polysaccharide as a key reaction to carbonized product formation”. In: *Journal of Wood Science* 49.5 (2003), pp. 469–473.
- [53] M. Wolfrom, A. Thompson, and R. Ward. “The composition of pyrodextrins. II. Thermal polymerization of levoglucosan¹”. In: *Journal of the American Chemical Society* 81.17 (1959), pp. 4623–4625.

- [54] A. Pictet and J. Sarasin. “Sur la distillation de la cellulose et de l’amidon sous pression reduite”. In: *Helvetica Chimica Acta* 1.1 (1918), pp. 87–96.
- [55] J. da Silva Carvalho, W. Prins, and C. Schuerch. “Addition Polymerization of Anhydrosugar Derivatives. I. A Polyanhydroglucose¹”. In: *Journal of the American Chemical Society* 81.15 (1959), pp. 4054–4058.
- [56] G. R. Ponder and G. N. Richards. “Polysaccharides from thermal polymerization of glucosides”. In: *Carbohydrate research* 208 (1990), pp. 93–104.
- [57] M. Ramage and J. Katzer. “Liquid Transportation Fuels from Coal and Biomass: Technological Status, Costs, and Environmental Impacts”. In: *America’s Energy Future Panel on Alternative Liquid Transportation Fuels, National Research Council* (May 20, 2009).
- [58] R. Agrawal and N. R. Singh. “Synergistic routes to liquid fuel for a petroleum-deprived future”. In: *AIChE Journal* 55.7 (2009), pp. 1898–1905.
- [59] “Integrated gasification–pyrolysis process”. US 8217210 (US). R. Agrawal and N. R. Singh. 2012.
- [60] “Process for producing liquid hydrocarbon by pyrolysis of biomass in presence of hydrogen from a carbon-free energy source”. US 8217211 (US). R. Agrawal, M. Agrawal, and N. R. Singh. 2012.
- [61] N. R. Singh et al. “Economic analysis of novel synergistic biofuel (H₂Bioil) processes”. In: *Biomass Conversion and Biorefinery* 2.2 (2012), pp. 141–148.
- [62] A. Bridgwater and G. Peacocke. “Fast pyrolysis processes for biomass”. In: *Renewable and Sustainable Energy Reviews* 4.1 (Mar. 2000), pp. 1–73. DOI: 10.1016/S1364-0321(99)00007-6.
- [63] N. R. Singh et al. “Estimation of liquid fuel yields from biomass”. In: *Environmental science & technology* 44.13 (2010), pp. 5298–5305.

- [64] H. F. Gerçel, A. E. Pütün, and E. Pütün. “Hydropyrolysis of extracted *Euphorbia rigida* in a well-swept fixed-bed tubular reactor”. In: *Energy Sources* 24.5 (2002), pp. 423–430.
- [65] D. Meier et al. “Analytical pyrolysis and semicontinuous catalytic hydrolysis of Organocell lignin”. In: *Journal of Analytical and Applied Pyrolysis* 25 (1993), pp. 335–347.
- [66] R. V. Pindoria et al. “Structural characterization of biomass pyrolysis tars/oils from eucalyptus wood waste: effect of H₂ pressure and sample configuration”. In: *Fuel* 76.11 (1997), pp. 1013–1023.
- [67] A. Pütün et al. “Fixed-bed pyrolysis and hydrolysis of sunflower bagasse: product yields and compositions”. In: *Fuel Processing Technology* 46.1 (1996), pp. 49–62.
- [68] J. Rocha et al. “Hydrolysis: a versatile technique for solid fuel liquefaction, sulphur speciation and biomarker release”. In: *Journal of Analytical and Applied Pyrolysis* 40 (1997), pp. 91–103.
- [69] F. Melligan et al. “Pressurised pyrolysis of *Miscanthus* using a fixed bed reactor”. In: *Bioresource Technology* 102.3 (2011), pp. 3466–3470.
- [70] N. Mahinpey et al. “Analysis of bio-oil, biogas, and biochar from pressurized pyrolysis of wheat straw using a tubular reactor”. In: *Energy & Fuels* 23.5 (2009), pp. 2736–2742.
- [71] M. J. Antal et al. “High-yield biomass charcoal”. In: *Energy & Fuels* 10.3 (1996), pp. 652–658.
- [72] W. S.-L. Mok and M. J. Antal. “Effects of pressure on biomass pyrolysis. I. Cellulose pyrolysis products”. In: *Thermochimica Acta* 68.2 (1983), pp. 155–164.

- [73] R. Pindoria et al. “A two-stage fixed-bed reactor for direct hydrotreatment of volatiles from the hydrolysis of biomass: effect of catalyst temperature, pressure and catalyst ageing time on product characteristics”. In: *Fuel* 77.15 (1998), pp. 1715–1726.
- [74] J. D. Rocha, C. A. Luengo, and C. E. Snape. “The scope for generating bio-oils with relatively low oxygen contents via hydrolysis”. In: *Organic Geochemistry* 30.12 (1999), pp. 1527–1534.
- [75] H. Zhang et al. “Biomass fast pyrolysis in a fluidized bed reactor under N₂, CO₂, CO, CH₄ and H₂ atmospheres”. In: *Bioresource Technology* 102.5 (2011), pp. 4258–4264.
- [76] S. Meesuk et al. “Study of catalytic hydrolysis of rice husk under nickel-loaded brown coal char”. In: *Energy & Fuels* 25.11 (2011), pp. 5438–5443.
- [77] F. Melligan et al. “Hydro-pyrolysis of biomass and online catalytic vapor upgrading with Ni-ZSM-5 and Ni-MCM-41”. In: *Energy & Fuels* 26.10 (2012), pp. 6080–6090.
- [78] A. A. Lappas et al. “Catalytic pyrolysis of biomass for transportation fuels”. In: *Wiley Interdisciplinary Reviews: Energy and Environment* 1.3 (2012), pp. 285–297.
- [79] H. Zhang et al. “Catalytic fast pyrolysis of wood and alcohol mixtures in a fluidized bed reactor”. In: *Green Chemistry* 14.1 (2012), pp. 98–110.
- [80] T. L. Marker et al. “Integrated hydrolysis and hydroconversion (IH₂) for the direct production of gasoline and diesel fuels or blending components from biomass, part 1: Proof of principle testing”. In: *Environmental Progress & Sustainable Energy* 31.2 (2012), pp. 191–199.
- [81] D. C. Dayton et al. “Biomass hydrolysis in a pressurized fluidized bed reactor”. In: *Energy & Fuels* 27.7 (2013), pp. 3778–3785.

- [82] J. Lédé. “The cyclone: a multifunctional reactor for the fast pyrolysis of biomass”. In: *Industrial & Engineering Chemistry Research* 39.4 (2000), pp. 893–903.
- [83] M. S. Mettler et al. “Revealing pyrolysis chemistry for biofuels production: Conversion of cellulose to furans and small oxygenates”. In: *Energy & Environmental Science* 5.1 (Jan. 1, 2012), pp. 5414–5424. DOI: 10.1039/C1EE02743C.
- [84] R. Vinu and L. J. Broadbelt. “A mechanistic model of fast pyrolysis of glucose-based carbohydrates to predict bio-oil composition”. In: *Energy & Environmental Science* 5.12 (2012), pp. 9808–9826.
- [85] M. J. Rhodes. *Introduction to particle technology*. John Wiley & Sons, 2008.
- [86] D. M. Alonso, J. Q. Bond, and J. A. Dumesic. “Catalytic conversion of biomass to biofuels”. In: *Green Chemistry* 12.9 (2010), pp. 1493–1513.
- [87] C. Zhao, T. Brück, and J. A. Lercher. “Catalytic deoxygenation of microalgae oil to green hydrocarbons”. In: *Green Chemistry* 15.7 (2013), pp. 1720–1739.
- [88] H. B. Mayes and L. J. Broadbelt. “Unraveling the Reactions that Unravel Cellulose”. In: *J. Phys. Chem. A* 116.26 (July 2012), pp. 7098–7106. DOI: 10.1021/jp300405x.
- [89] M. S. Mettler et al. “Revealing pyrolysis chemistry for biofuels production: Conversion of cellulose to furans and small oxygenates”. en. In: *Energy Environ. Sci.* 5.1 (Jan. 2012), pp. 5414–5424. DOI: 10.1039/C1EE02743C.
- [90] M. S. Mettler et al. “The chain length effect in pyrolysis: bridging the gap between glucose and cellulose”. en. In: *Green Chem.* 14.5 (May 2012), pp. 1284–1288. DOI: 10.1039/C2GC35184F.
- [91] V. Agarwal et al. “Ab Initio Dynamics of Cellulose Pyrolysis: Nascent Decomposition Pathways at 327 and 600°C”. In: *J. Am. Chem. Soc.* 134.36 (Sept. 2012), pp. 14958–14972. DOI: 10.1021/ja305135u.

- [92] Q. Lu et al. "Influence of pyrolysis temperature and time on the cellulose fast pyrolysis products: Analytical Py-GC/MS study". In: *Journal of Analytical and Applied Pyrolysis* 92.2 (2011), pp. 430–438.
- [93] M. S. Mettler, D. G. Vlachos, and P. J. Dauenhauer. "Top ten fundamental challenges of biomass pyrolysis for biofuels". en. In: *Energy Environ. Sci.* 5.7 (June 2012), pp. 7797–7809. DOI: 10.1039/C2EE21679E.
- [94] Y. Yoneda et al. "Synthesis of methyl 4'-O-methyl-13C 12- β -d-cellobioside from 13C 6-d-glucose. Part 1: Reaction optimization and synthesis". In: *Carbohydrate Research* 340.15 (2005), pp. 2428–2435.
- [95] S. Zheng et al. "Synthesis and biological profiling of tellimagrandin I and analogues reveals that the medium ring can significantly modulate biological activity". In: *Organic & Biomolecular Chemistry* 10.13 (2012), pp. 2590–2593.
- [96] H. B. Mayes et al. "The Alpha-Bet(a) of Glucose Pyrolysis: Computational and Experimental Investigations of 5-Hydroxymethylfurfural and Levoglucosan Formation Reveal Implications for Cellulose Pyrolysis". In: *ACS Sustainable Chem. Eng.* 2.6 (June 2014), pp. 1461–1473. DOI: 10.1021/sc500113m.
- [97] V. Seshadri and P. R. Westmoreland. "Concerted Reactions and Mechanism of Glucose Pyrolysis and Implications for Cellulose Kinetics". In: *J. Phys. Chem. A* 116.49 (Dec. 2012), pp. 11997–12013. DOI: 10.1021/jp3085099.
- [98] J. B. Paine III, Y. B. Pithawalla, and J. D. Naworal. "Carbohydrate pyrolysis mechanisms from isotopic labeling: Part 2. The pyrolysis of d-glucose: General disconnective analysis and the formation of C1 and C2 carbonyl compounds by electrocyclic fragmentation mechanisms". In: *Journal of Analytical and Applied Pyrolysis* 82.1 (May 2008), pp. 10–41. DOI: 10.1016/j.jaap.2008.01.002.
- [99] T. Hosoya et al. "Thermal Degradation of Methyl β -d-Glucoside. A Theoretical Study of Plausible Reaction Mechanisms". In: *J. Org. Chem.* 74.17 (Sept. 2009), pp. 6891–6894. DOI: 10.1021/jo900457k.

- [100] X. Zhou et al. “Experimental and mechanistic modeling of fast pyrolysis of neat glucose-based carbohydrates. 1. Experiments and development of a detailed mechanistic model”. In: *Industrial & Engineering Chemistry Research* 53.34 (2014), pp. 13274–13289.
- [101] M. Frisch et al. “Gaussian 09, Revision D. 01; Gaussian: Wallingford, CT, USA, 2009”. In: ().
- [102] R. Krishnan et al. “Self consistent molecular orbital methods. XX. A basis set for correlated wave functions”. In: *The Journal of Chemical Physics* 72.1 (Jan. 1980), pp. 650–654. DOI: 10.1063/1.438955.
- [103] Y. Zhao and D. G. Truhlar. “The M06 suite of density functionals for main group thermochemistry, thermochemical kinetics, noncovalent interactions, excited states, and transition elements: two new functionals and systematic testing of four M06-class functionals and 12 other functionals”. en. In: *Theor Chem Account* 120.1-3 (May 2008), pp. 215–241. DOI: 10.1007/s00214-007-0310-x.
- [104] T. R. Carlson, T. P. Vispute, and G. W. Huber. “Green gasoline by catalytic fast pyrolysis of solid biomass derived compounds”. In: *ChemSusChem* 1.5 (2008), pp. 397–400.
- [105] D. Vamvuka. “Bio-oil, solid and gaseous biofuels from biomass pyrolysis processes An overview”. In: *International Journal of Energy Research* 35.10 (2011), pp. 835–862.
- [106] M. H. El-barbary, P. H. Steele, and L. Ingram. “Characterization of fast pyrolysis bio-oils produced from pretreated pine wood”. In: *Applied Biochemistry and Biotechnology* 154.1-3 (2009), pp. 3–13.
- [107] D. A. Laird et al. “Review of the pyrolysis platform for coproducing bio-oil and biochar”. In: *Biofuels, Bioproducts and Biorefining* 3.5 (2009), pp. 547–562.
- [108] P. Badger et al. “Techno-economic analysis: Preliminary assessment of pyrolysis oil production costs and material energy balance associated with a transportable fast pyrolysis system”. In: *BioResources* 6.1 (2010), pp. 34–47.

- [109] P. Bhattacharya et al. “Wood/plastic copyrolysis in an auger reactor: Chemical and physical analysis of the products”. In: *Fuel* 88.7 (2009), pp. 1251–1260.
- [110] K. Papadikis, S. Gu, and A. V. Bridgwater. “CFD modelling of the fast pyrolysis of biomass in fluidised bed reactors: modelling the impact of biomass shrinkage”. In: *Chemical Engineering Journal* 149.1 (2009), pp. 417–427.
- [111] E. Dorrestijn et al. “The occurrence and reactivity of phenoxy linkages in lignin and low rank coal”. In: *Journal of Analytical and Applied Pyrolysis* 54.1 (2000), pp. 153–192.
- [112] B. Iatridis and G. R. Gavalas. “Pyrolysis of a precipitated kraft lignin”. In: *Industrial & Engineering Chemistry Product Research and Development* 18.2 (1979), pp. 127–130.
- [113] G. Jiang, D. J. Nowakowski, and A. V. Bridgwater. “Effect of the temperature on the composition of lignin pyrolysis products”. In: *Energy & Fuels* 24.8 (2010), pp. 4470–4475.
- [114] D. J. Nowakowski et al. “Lignin fast pyrolysis: results from an international collaboration”. In: *Journal of Analytical and Applied Pyrolysis* 88.1 (2010), pp. 53–72.
- [115] A. I. Vuori and J. B.-s. Bredenberg. “Thermal chemistry pathways of substituted anisoles”. In: *Industrial & Engineering Chemistry Research* 26.2 (1987), pp. 359–365.
- [116] R. H. Schlosberg et al. “Pyrolysis studies of organic oxygenates: 3. High temperature rearrangement of aryl alkyl ethers”. In: *Fuel* 62.6 (1983), pp. 690–694.
- [117] V. B. Custodis et al. “Mechanism of fast pyrolysis of lignin: studying model compounds”. In: *The Journal of Physical Chemistry B* 118.29 (2014), pp. 8524–8531.

- [118] P. F. Britt et al. “Flash vacuum pyrolysis of methoxy-substituted lignin model compounds”. In: *Journal of Organic Chemistry* 65.5 (2000), pp. 1376–1389.
- [119] A. Beste and A. Buchanan III. “Computational study of bond dissociation enthalpies for lignin model compounds. Substituent effects in phenethyl phenyl ethers”. In: *Journal of Organic Chemistry* 74.7 (2009), pp. 2837–2841.
- [120] A. Beste and A. Buchanan III. “Substituent effects on the reaction rates of hydrogen abstraction in the pyrolysis of phenethyl phenyl ethers”. In: *Energy & Fuels* 24.5 (2010), pp. 2857–2867.
- [121] A. Beste and A. Buchanan III. “Kinetic analysis of the phenyl-shift reaction in β -O-4 lignin model compounds: A computational study”. In: *Journal of Organic Chemistry* 76.7 (2011), pp. 2195–2203.
- [122] H. Kawamoto, M. Ryoritani, and S. Saka. “Different pyrolytic cleavage mechanisms of β -ether bond depending on the side-chain structure of lignin dimers”. In: *Journal of Analytical and Applied Pyrolysis* 81.1 (Jan. 2008), pp. 88–94. DOI: 10.1016/j.jaap.2007.09.006.
- [123] T. Hosoya, H. Kawamoto, and S. Saka. “Secondary reactions of lignin-derived primary tar components”. In: *Journal of Analytical and Applied Pyrolysis* 83.1 (Sept. 2008), pp. 78–87. DOI: 10.1016/j.jaap.2008.06.003.
- [124] X. Bai et al. “Formation of phenolic oligomers during fast pyrolysis of lignin”. In: *Fuel* 128 (2014), pp. 170–179.
- [125] T. Kishimoto, Y. Uraki, and M. Ubukata. “Synthesis of β -O-4-type artificial lignin polymers and their analysis by NMR spectroscopy”. In: *Organic & Biomolecular Chemistry* 6.16 (2008), pp. 2982–2987.
- [126] L. J. Hauptert et al. “Characterization of model compounds of processed lignin and the lignome by using atmospheric pressure ionization tandem mass spectrometry”. In: *Fuel* 95 (2012), pp. 634–641.

- [127] B. C. Owen et al. “High-performance liquid chromatography/high-resolution multiple stage tandem mass spectrometry using negative-ion-mode hydroxide-doped electrospray ionization for the characterization of lignin degradation products”. In: *Analytical chemistry* 84.14 (2012), pp. 6000–6007.
- [128] A. V. Bridgwater. “Review of fast pyrolysis of biomass and product upgrading”. In: *Biomass and bioenergy* 38 (2012), pp. 68–94.
- [129] A. H. Zacher et al. “A review and perspective of recent bio-oil hydrotreating research”. In: *Green Chemistry* 16.2 (2014), pp. 491–515.
- [130] R. Agrawal and N. R. Singh. “Producing liquid hydrocarbons from biomass via hydropyrolysis of biomass with a gaseous exhaust stream comprising CO₂, CO, H₂, and water formed from one of gasification and reforming of carbon containing moiety (CCM) such as natural gas; biofuels”. In: (July 10, 2012).
- [131] G. T. Neumann et al. “Correlating lignin structure to aromatic products in the catalytic fast pyrolysis of lignin model compounds containing β -O-4 linkages”. In: *Catalysis Science & Technology* 4.11 (2014), pp. 3953–3963.
- [132] W. Glasser et al. “Fundamentals of Thermochemical Biomass Conversion”. In: (1985).
- [133] P. De Wild, W. Huijgen, and H. Heeres. “Pyrolysis of wheat straw-derived organosolv lignin”. In: *Journal of Analytical and Applied Pyrolysis* 93 (2012), pp. 95–103.
- [134] G. Jiang, D. J. Nowakowski, and A. V. Bridgwater. “A systematic study of the kinetics of lignin pyrolysis”. In: *Thermochimica Acta* 498.1 (2010), pp. 61–66.
- [135] R. K. Sharma et al. “Characterization of chars from pyrolysis of lignin”. In: *Fuel* 83.11 (2004), pp. 1469–1482.
- [136] S. Beis et al. “Fast pyrolysis of lignins”. In: *BioResources* 5.3 (2010), pp. 1408–1424.

- [137] T. N. Trinh et al. “Fast pyrolysis of lignin using a pyrolysis centrifuge reactor”. In: *Energy & Fuels* 27.7 (2013), pp. 3802–3810.
- [138] T. R. Nunn et al. “Product compositions and kinetics in the rapid pyrolysis of milled wood lignin”. In: *Industrial & engineering chemistry process design and development* 24.3 (1985), pp. 844–852.
- [139] S. Zhou et al. “Effect of the fast pyrolysis temperature on the primary and secondary products of lignin”. In: *Energy & fuels* 27.10 (2013), pp. 5867–5877.
- [140] B. Scholze, C. Hanser, and D. Meier. “Characterization of the water-insoluble fraction from fast pyrolysis liquids (pyrolytic lignin): Part II. GPC, carbonyl groups, and ^{13}C -NMR”. In: *Journal of Analytical and Applied Pyrolysis* 58 (2001), pp. 387–400.
- [141] R. Bayerbach et al. “Characterization of the water-insoluble fraction from fast pyrolysis liquids (pyrolytic lignin): Part III. Molar mass characteristics by SEC, MALDI-TOF-MS, LDI-TOF-MS, and Py-FIMS”. In: *Journal of Analytical and Applied Pyrolysis* 77.2 (2006), pp. 95–101.
- [142] B. Scholze and D. Meier. “Characterization of the water-insoluble fraction from pyrolysis oil (pyrolytic lignin). Part I. PY-GC/MS, FTIR, and functional groups”. In: *Journal of Analytical and Applied Pyrolysis* 60.1 (2001), pp. 41–54.
- [143] R. J. Evans, T. A. Milne, and M. N. Soltys. “Direct mass-spectrometric studies of the pyrolysis of carbonaceous fuels: III. Primary pyrolysis of lignin”. In: *Journal of Analytical and Applied Pyrolysis* 9.3 (1986), pp. 207–236.
- [144] W. Mu et al. “Lignin pyrolysis components and upgrading-technology review”. In: *Bioenergy Research* 6.4 (2013), pp. 1183–1204.
- [145] E. R. van der Hage, M. M. Mulder, and J. J. Boon. “Structural characterization of lignin polymers by temperature-resolved in-source pyrolysis-mass spectrometry and Curie-point pyrolysis-gas chromatography/mass spectrometry”. In: *Journal of Analytical and Applied Pyrolysis* 25 (1993), pp. 149–183.

- [146] M. Kinne et al. “Oxidative cleavage of non-phenolic β -O-4 lignin model dimers by an extracellular aromatic peroxygenase”. In: *Holzforschung* 65.5 (2011), pp. 673–679.
- [147] J.-Y. Liu, S.-B. Wu, and R. Lou. “Chemical structure and pyrolysis response of beta-O-4 lignin model polymer”. In: *BioResources* 6.2 (2011), pp. 1079–1093.
- [148] M. D. Guilln and M. L. Ibargoitia. “GC/MS analysis of lignin monomers, dimers and trimers in liquid smoke flavourings”. In: *Journal of the Science of Food and Agriculture* 79.13 (1999), pp. 1889–1903.
- [149] E. Hoekstra et al. “Heterogeneous and homogeneous reactions of pyrolysis vapors from pine wood”. In: *AIChE journal* 58.9 (2012), pp. 2830–2842.
- [150] T. Nakamura, H. Kawamoto, and S. Saka. “Pyrolysis behavior of Japanese cedar wood lignin studied with various model dimers”. In: *Journal of Analytical and Applied Pyrolysis* 81.2 (2008), pp. 173–182.
- [151] P. F. Britt et al. “Pyrolysis mechanisms of lignin: surface-immobilized model compound investigation of acid-catalyzed and free-radical reaction pathways”. In: *Journal of Analytical and Applied Pyrolysis* 33 (1995), pp. 1–19.
- [152] K. H. Kim, X. Bai, and R. C. Brown. “Pyrolysis mechanisms of methoxy substituted α -O-4 lignin dimeric model compounds and detection of free radicals using electron paramagnetic resonance analysis”. In: *Journal of Analytical and Applied Pyrolysis* 110 (2014), pp. 254–263.
- [153] H. Kawamoto, S. Horigoshi, and S. Saka. “Pyrolysis reactions of various lignin model dimers”. In: *Journal of Wood Science* 53.2 (2007), pp. 168–174.
- [154] C. Amen-Chen, H. Pakdel, and C. Roy. “Production of monomeric phenols by thermochemical conversion of biomass: a review”. In: *Bioresource Technology* 79.3 (2001), pp. 277–299.

- [155] H. Kawamoto, S. Horigoshi, and S. Saka. “Effects of side-chain hydroxyl groups on pyrolytic β -ether cleavage of phenolic lignin model dimer”. In: *Journal of Wood Science* 53.3 (2007), pp. 268–271.
- [156] T. Kishimoto, Y. Uraki, and M. Ubukata. “Chemical synthesis of β -O-4 type artificial lignin”. In: *Organic & Biomolecular Chemistry* 4.7 (2006), pp. 1343–1347.
- [157] T. Kotake, H. Kawamoto, and S. Saka. “Pyrolysis reactions of coniferyl alcohol as a model of the primary structure formed during lignin pyrolysis”. In: *Journal of Analytical and Applied Pyrolysis* 104 (2013), pp. 573–584.
- [158] T. Kotake, H. Kawamoto, and S. Saka. “Mechanisms for the formation of monomers and oligomers during the pyrolysis of a softwood lignin”. In: *Journal of Analytical and Applied Pyrolysis* 105 (2014), pp. 309–316.
- [159] T. Nakamura, H. Kawamoto, and S. Saka. “Condensation reactions of some lignin related compounds at relatively low pyrolysis temperature”. In: *Journal of wood chemistry and technology* 27.2 (2007), pp. 121–133.
- [160] C. P. Masuku. “Thermolytic decomposition of coniferyl alcohol”. In: *Journal of Analytical and Applied Pyrolysis* 23.2 (1992), pp. 195–208.
- [161] R. F. Service. “Battle for the Barrel”. In: *Science* 339.6126 (Mar. 22, 2013), pp. 1374–1379. DOI: 10.1126/science.339.6126.1374.
- [162] D. J. Hayes. “An examination of biorefining processes, catalysts and challenges”. In: *Catalysis Today* 145.1 (July 15, 2009), pp. 138–151. DOI: 10.1016/j.cattod.2008.04.017.
- [163] M. Wellisch et al. “Biorefinery systems - potential contributors to sustainable innovation”. In: *Biofuels, Bioproducts and Biorefining* 4.3 (2010), pp. 275–286. DOI: 10.1002/bbb.217.
- [164] M. G. Mandl. “Status of green biorefining in Europe”. In: *Biofuels, Bioproducts and Biorefining* 4.3 (2010), pp. 268–274. DOI: 10.1002/bbb.219.

- [165] M. McCoy et al. “Facts & Figures For The Chemical Industry, Production: Growth In Most Regions”. In: *Chem. and Eng. News* 83 (2005), pp. 67–76.
- [166] M. Bomgardner et al. “Facts & Figures For The Chemical Industry, Lackluster Year For Chemical Output”. In: *Chem. and Eng. News* 91 (2013), p. 41.
- [167] *Statistical Review of World Energy*. BP, 2013.
- [168] G. W. Huber, J. W. Shabaker, and J. A. Dumesic. “Raney Ni-Sn Catalyst for H₂ Production from Biomass-Derived Hydrocarbons”. In: *Science* 300.5628 (June 27, 2003), pp. 2075–2077. DOI: 10.1126/science.1085597.
- [169] S. K. Hanson et al. “Aerobic Oxidation of Pinacol by Vanadium(V) Dipicolinate Complexes: Evidence for Reduction to Vanadium(III)”. In: *Journal of the American Chemical Society* 131.2 (Jan. 21, 2009), pp. 428–429. DOI: 10.1021/ja807522n.
- [170] A. J. Crisci et al. “Acid-Functionalized SBA-15-Type Silica Catalysts for Carbohydrate Dehydration”. In: *ACS Catalysis* 1.7 (July 1, 2011), pp. 719–728. DOI: 10.1021/cs2001237.
- [171] J. E. Holladay et al. *Top Value-Added Chemicals from Biomass-Volume II-Results of Screening for Potential Candidates from Biorefinery Lignin*. Pacific Northwest National Laboratory (PNNL), Richland, WA (US), 2007.
- [172] F. Cherubini and A. H. Strmman. “Chemicals from lignocellulosic biomass: opportunities, perspectives, and potential of biorefinery systems”. In: *Biofuels, Bioproducts and Biorefining* 5.5 (2011), pp. 548–561. DOI: 10.1002/bbb.297.
- [173] H.-R. Bjrvik and F. Minisci. “Fine Chemicals from Lignosulfonates. 1. Synthesis of Vanillin by Oxidation of Lignosulfonates”. In: *Organic Process Research & Development* 3.5 (Sept. 1, 1999), pp. 330–340. DOI: 10.1021/op9900028.
- [174] A. G. Sergeev and J. F. Hartwig. “Selective, Nickel-Catalyzed Hydrogenolysis of Aryl Ethers”. In: *Science* 332.6028 (Apr. 22, 2011), pp. 439–443. DOI: 10.1126/science.1200437.

- [175] Z. Strassberger et al. “Catalytic cleavage of lignin β -O-4 link mimics using copper on alumina and magnesia-alumina”. In: *Green Chemistry* 15.3 (Feb. 25, 2013), pp. 768–774. DOI: 10.1039/C3GC37056A.
- [176] A. L. Jongorius et al. “CoMo sulfide-catalyzed hydrodeoxygenation of lignin model compounds: An extended reaction network for the conversion of monomeric and dimeric substrates”. In: *Journal of Catalysis* 285.1 (Jan. 2012), pp. 315–323. DOI: 10.1016/j.jcat.2011.10.006.
- [177] W. Xu et al. “Depolymerization and Hydrodeoxygenation of Switchgrass Lignin with Formic Acid”. In: *ChemSusChem* 5.4 (2012), pp. 667–675. DOI: 10.1002/cssc.201100695.
- [178] R. N. Olcese et al. “Aromatic Chemicals by Iron-Catalyzed Hydrotreatment of Lignin Pyrolysis Vapor”. In: *ChemSusChem* 6.8 (2013), pp. 1490–1499. DOI: 10.1002/cssc.201300191.
- [179] A. C. Atesin et al. “Etheric C-O Bond Hydrogenolysis Using a Tandem Lanthanide Triflate/Supported Palladium Nanoparticle Catalyst System”. In: *Journal of the American Chemical Society* 134.36 (Sept. 12, 2012), pp. 14682–14685. DOI: 10.1021/ja306309u.
- [180] Q. Song, F. Wang, and J. Xu. “Hydrogenolysis of lignosulfonate into phenols over heterogeneous nickel catalysts”. In: *Chemical Communications* 48.56 (June 18, 2012), pp. 7019–7021. DOI: 10.1039/C2CC31414B.
- [181] T. D. Matson et al. “One-Pot Catalytic Conversion of Cellulose and of Woody Biomass Solids to Liquid Fuels”. In: *Journal of the American Chemical Society* 133.35 (Sept. 7, 2011), pp. 14090–14097. DOI: 10.1021/ja205436c.
- [182] Q. Song et al. “Lignin depolymerization (LDP) in alcohol over nickel-based catalysts via a fragmentation-hydrogenolysis process”. In: *Energy & Environmental Science* 6.3 (Feb. 20, 2013), pp. 994–1007. DOI: 10.1039/C2EE23741E.

- [183] C. Li et al. “One-pot catalytic hydrocracking of raw woody biomass into chemicals over supported carbide catalysts: simultaneous conversion of cellulose, hemicellulose and lignin”. In: *Energy & Environmental Science* 5.4 (Mar. 21, 2012), pp. 6383–6390. DOI: 10.1039/C1EE02684D.
- [184] T. H. Parsell et al. “Cleavage and hydrodeoxygenation (HDO) of C-O bonds relevant to lignin conversion using Pd/Zn synergistic catalysis”. In: *Chemical Science* 4.2 (Jan. 2, 2013), pp. 806–813. DOI: 10.1039/C2SC21657D.
- [185] S. D. Mansfield, K.-Y. Kang, and C. Chapple. “Designed for deconstruction - poplar trees altered in cell wall lignification improve the efficacy of bioethanol production”. In: *New Phytologist* 194.1 (2012), pp. 91–101. DOI: 10.1111/j.1469-8137.2011.04031.x.
- [186] T. Parsell et al. “A synergistic biorefinery based on catalytic conversion of lignin prior to cellulose starting from lignocellulosic biomass”. In: *Green Chemistry* 17.3 (2015), pp. 1492–1499.
- [187] M. Selig, N. Weiss, and Y. Ji. *Enzymatic Saccharification of Lignocellulosic Biomass: Laboratory Analytical Procedure: Issue Date, 3/21/2008*. National Renewable Energy Laboratory, 2008.
- [188] Y. Kim et al. “Soluble inhibitors/deactivators of cellulase enzymes from lignocellulosic biomass”. In: *Enzyme and Microbial Technology* 48.4 (Apr. 7, 2011), pp. 408–415. DOI: 10.1016/j.enzmitec.2011.01.007.
- [189] E. I. Grbz and J. A. Dumesic. “Catalytic Strategies and Chemistries Involved in the Conversion of Sugars to Liquid Transportation Fuels”. In: *Catalysis for the Conversion of Biomass and Its Derivatives*. Ed. by M. Behrens and A. K. Datye. Ed. Open Access, Feb. 28, 2013, pp. 293–359.
- [190] G. W. Huber et al. “Production of Liquid Alkanes by Aqueous-Phase Processing of Biomass-Derived Carbohydrates”. In: *Science* 308.5727 (June 3, 2005), pp. 1446–1450. DOI: 10.1126/science.1111166.

- [191] N. D. Bonawitz and C. Chapple. “The Genetics of Lignin Biosynthesis: Connecting Genotype to Phenotype”. In: *Annual Review of Genetics* 44.1 (2010), pp. 337–363. DOI: 10.1146/annurev-genet-102209-163508.
- [192] R. Vanholme et al. “Metabolic engineering of novel lignin in biomass crops”. In: *New Phytologist* 196.4 (2012), pp. 978–1000. DOI: 10.1111/j.1469-8137.2012.04337.x.
- [193] R. Franke et al. “Modified lignin in tobacco and poplar plants over-expressing the Arabidopsis gene encoding ferulate 5-hydroxylase”. In: *The Plant Journal* 22.3 (2000), pp. 223–234. DOI: 10.1046/j.1365-313x.2000.00727.x.
- [194] S. Hama et al. “Dehydrogenation of Cycloalkanes by Suspended Platinum Catalysts”. In: *Chemistry Letters* 21.12 (1992), pp. 2463–2466. DOI: 10.1246/cl.1992.2463.
- [195] “Supported organoiridium catalysts for alkane dehydrogenation”. US8524963 B2. R. T. Baker, A. P. Sattelberger, and H. Li. Sept. 3, 2013.
- [196] C. L. Russell et al. “Catalytic Hydrocracking Reaction Pathways, Kinetics, and Mechanisms of n-Alkylbenzenes”. In: *Energy & Fuels* 8.6 (Nov. 1, 1994), pp. 1394–1400. DOI: 10.1021/ef00048a031.
- [197] S.-S. Chen and U. by Staff. *Styrene in Kirk-Othmer Encyclopedia of Chemical Technology*. John Wiley & Sons, Inc., 2000.
- [198] K. H. Chandawar, S. B. Kulkarni, and P. Ratnasamy. “Alkylation of benzene with ethanol over ZSM5 zeolites”. In: *Applied Catalysis* 4.3 (Nov. 15, 1982), pp. 287–295. DOI: 10.1016/0166-9834(82)80112-7.
- [199] J. Wallace and U. by Staff. *Phenol in Kirk-Othmer Encyclopedia of Chemical Technology*. John Wiley & Sons, Inc., 2000.
- [200] C. E. Wyman et al. “Comparative sugar recovery and fermentation data following pretreatment of poplar wood by leading technologies”. In: *Biotechnology Progress* 25.2 (2009), pp. 333–339. DOI: 10.1002/btpr.142.

- [201] A. Sluiter et al. *Determination of extractives in biomass: Issue Date, 7/17/2005*. Vol. 1617. National Renewable Energy Laboratory, 2005.
- [202] A. Broido. “Kinetics of solid-phase cellulose pyrolysis”. In: *Symposium on Thermal Uses and Properties of Carbohydrates and Lignins, San Francisco, Calif.(USA), 1976*. Academic Press. 1976.
- [203] H. M. Pilath et al. “Glucose reversion reaction kinetics”. In: *Journal of Agricultural and Food Chemistry* 58.10 (2010), pp. 6131–6140.
- [204] A. R. Teixeira et al. “Aerosol generation by reactive boiling ejection of molten cellulose”. In: *Energy & Environmental Science* 4.10 (2011), pp. 4306–4321.
- [205] A. D. Paulsen, M. S. Mettler, and P. J. Dauenhauer. “The role of sample dimension and temperature in cellulose pyrolysis”. In: *Energy & Fuels* 27.4 (2013), pp. 2126–2134.
- [206] K. G. Joback and R. C. Reid. “Estimation of pure-component properties from group-contributions”. In: *Chemical Engineering Communications* 57.1-6 (1987), pp. 233–243.
- [207] Y. Nannoolal, J. Rarey, and D. Ramjugernath. “Estimation of pure component properties: Part 3. Estimation of the vapor pressure of non-electrolyte organic compounds via group contributions and group interactions”. In: *Fluid Phase Equilibria* 269.1 (2008), pp. 117–133.
- [208] S. Kim et al. “Practical synthesis of KRN7000 from phytosphingosine”. In: *Synthesis* 6 (2004), pp. 847–850.
- [209] A. Pulsipher and M. N. Yousaf. “A renewable, chemoselective, and quantitative ligand density microarray for the study of biospecific interactions”. In: *Chemical Communications* 47.1 (2011), pp. 523–525.
- [210] F. Malz et al. “Synthesis of methyl 4'-O-methyl- β -d-cellobioside-13C 12 from d-glucose-13C 6. Part 2: Solid-state NMR studies”. In: *Carbohydrate Research* 342.1 (2007), pp. 65–70.

- [211] L. L. Lopez et al. “Automated strategies for obtaining standardized collisionally induced dissociation spectra on a benchtop ion trap mass spectrometer”. In: *Rapid Communications in Mass Spectrometry* 13.8 (1999), pp. 663–668. DOI: 10.1002/(SICI)1097-0231(19990430)13:8<663::AID-RCM538>3.0.CO;2-H.
- [212] X. Li et al. “The Growth Reduction Associated with Repressed Lignin Biosynthesis in *Arabidopsis thaliana* Is Independent of Flavonoids”. In: *The Plant Cell Online* 22.5 (May 1, 2010), pp. 1620–1632. DOI: 10.1105/tpc.110.074161.
- [213] R. S. Fukushima and R. D. Hatfield. “Extraction and Isolation of Lignin for Utilization as a Standard to Determine Lignin Concentration Using the Acetyl Bromide Spectrophotometric Method”. In: *Journal of Agricultural and Food Chemistry* 49.7 (July 1, 2001), pp. 3133–3139. DOI: 10.1021/jf010449r.
- [214] A. Sluiter et al. *Determination of sugars, byproducts, and degradation products in liquid fraction process samples: Issue Date, 12/08/2006*. National Renewable Energy Laboratory, 2006.
- [215] A. Sluiter et al. *Determination of structural carbohydrates and lignin in biomass: Issue Date, 7/8/2011*. National Renewable Energy Laboratory, 2008.

APPENDICES

A. SUPPORTING INFORMATION FOR ON-LINE MASS SPECTROMETRIC
METHODS FOR THE DETERMINATION OF THE PRIMARY PRODUCTS OF
FAST PYROLYSIS OF CARBOHYDRATES AND FOR THEIR GAS-PHASE
MANIPULATION

Below is the equation used to calculate the relative molar abundances of compounds that could not be ionized by chloride attachment but were ionized upon ammonium attachment.

$$\begin{array}{c} \boxed{\begin{array}{c} \text{Measured Relative} \\ \text{Abundance of Protonated} \\ \text{Ions of Selected m/z Value} \\ \text{from Pyrolysis} \\ \text{Ammonium Attachment} \end{array}} \times \begin{array}{c} \boxed{\begin{array}{c} \text{Ionization Bias in} \\ \text{Reference to Cellobiosan} \\ \text{for Direct Injection of} \\ \text{Model Compounds} \\ \text{Ammonium Attachment} \end{array}} + \begin{array}{c} \boxed{\begin{array}{c} \text{Measured Relative} \\ \text{Abundance of Ions Derived} \\ \text{from Cellobiosan from} \\ \text{Pyrolysis} \\ \text{Ammonium Attachment} \end{array}} \times \begin{array}{c} \boxed{\begin{array}{c} \text{Measured Relative} \\ \text{Abundance of Ions Derived} \\ \text{from Cellobiosan from} \\ \text{Pyrolysis} \\ \text{Chloride Attachment} \end{array}} - \begin{array}{c} \boxed{\begin{array}{c} \text{Calculated Relative Molar Abundance} \\ \text{of Protonated Ions of Selected m/z} \\ \text{Value from Pyrolysis in Relation to} \\ \text{Chloride Attached Ions} \\ \text{Chloride Attachment} \end{array}} \end{array} \quad (\text{A.1})$$

Example calculation for 5-hydroxymethylfurfural using above equation: $11 \pm 5\%$ (5-hydroxymethylfurfural + NH_4^+) $\times 1.33 \pm 0.02$ (ionization bias) $\div 52 \pm 6\%$ (cellobiosan + NH_4^+) $\times 26 \pm 3\%$ (cellobiosan + Cl^-) = $7 \pm 3\%$ (5-hydroxymethylfurfural + Cl^-)

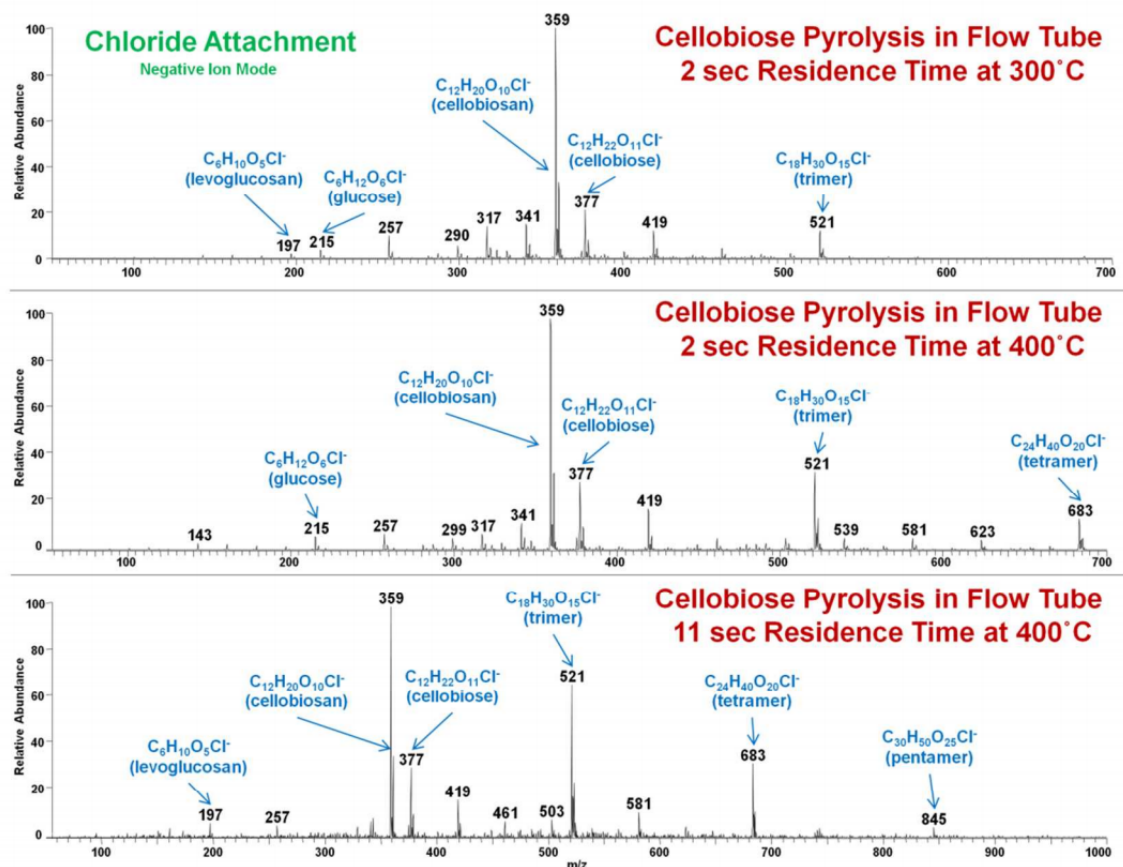


Figure A.1. Mass spectra collected after the primary products of fast pyrolysis of cellobiose were allowed to undergo reactions for 2 s at 300°C (top), 2s at 400°C (middle) and 11 s at 400°C (bottom) and ionized using chloride attachment in negative ion mode. All elemental compositions were determined using high resolution data collected in an LQIT/FT-ICR. All ions with m/z values lower than 170 correspond to deprotonated molecules.

B. SUPPORTING INFORMATION FOR HIGH-PRESSURE FAST-PYROLYSIS, FAST-HYDROLYSIS AND CATALYTIC HYDRODEOXYGENATION OF CELLULOSE: PRODUCTION OF LIQUID FUEL FROM BIOMASS

B.1 Screw feeder design

The purpose of the screw feeders is to introduce biomass or biomass model compounds into the reactor system at high pressures of up to 68 bar. The screw feeder consists of a feed hopper containing the solids, an auger tube with the screw and a feed chamber, which is a steel box on the right side of the screw feeder (as shown in Figure S.1). These different parts are connected using Conflat (CF) flanges. The material of construction of the screw feeder is stainless steel 316 except for the 1-in glass window attached to the feed chamber. The window has a maximum working pressure of 95 bar at room temperature. The feed hopper and the feed chamber can be purged with inert gas prior to any experiment. The screw feeder is driven by an Applied Motion M400 electric servo motor which is connected to the feeder via magnetic coupling and therefore isolated from the high pressure environment. The screw feeder is capable of feed rates in the range of 0.1 to $20 \text{ g} \times \text{min}^{-1}$.

B.2 High pressure reactor design

B.2.1 Fast-hydrolysis Reactor

A cross sectional view of the fast-hydrolysis reactor is shown in Figure S.2. The body of the cyclone reactor is machined from stainless-steel type-347 round bar and has an OD and ID maximum of 2.375-in and 1.69-in respectively, corresponding to schedule 160 pipe. At 650°C , the basic allowable stress for TP347 seamless pipe is 4.4 ksi (5.9 ksi at 600°C) which corresponds to an internal design pressure of 110 bar (or 145 bar at 600°C). The flange connection at the top of the reactor is a F316H 2-in

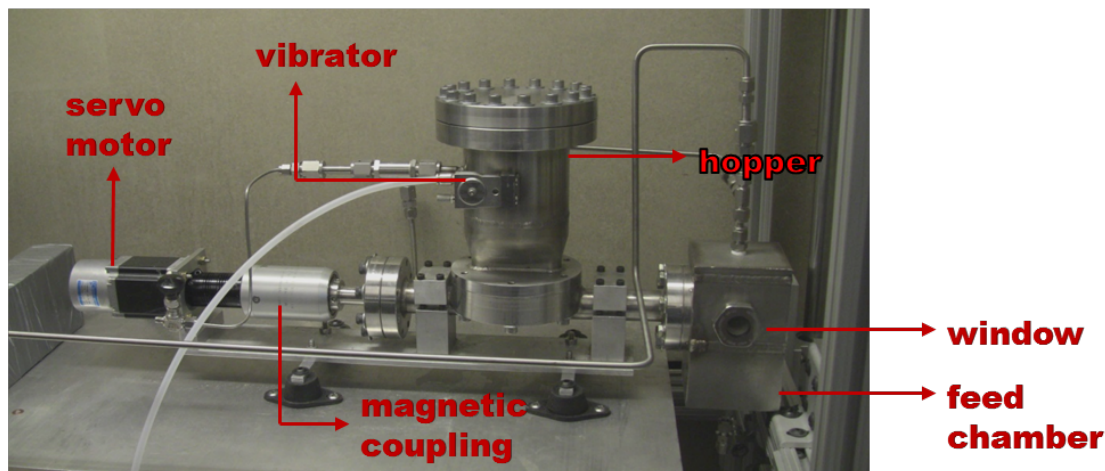


Figure B.1. Picture of high pressure biomass screw feeder.

2500 B16.5 flange which has a maximum working pressure of 106.5 bar at 650°C. At the bottom of the reactor, the OD and ID are 1.05-in and 0.614-in respectively which corresponds to schedule 160 pipe and has an internal design pressure of 179 bar. The bottom flange, which is used to connect to the char collector, is a F316H # 1500 $3/4$ -in B16.5 flange which has a maximum working pressure of 106 bar at 593°C.

The char collector was machined from stainless-steel type-316 round bar and has an OD of 3.5-in and an ID of 2.626-in, equivalent to schedule 160 pipe. At 315°C, the char collector body has an internal design gage pressure of 381 bar. The bottom of the collector uses F316H # 600 3-in B16.5 flanges for access to the inside of collector if needed. These have a maximum working pressure of 100 bar at 40°C.

B.2.2 Downstream fixed-bed vapor-phase hydrodeoxygenation (HDO) Reactor

The HDO reactor, shown in Figure S.3, itself is simply an empty tube with a porous metal frit that supports the catalyst bed. It is made from $1/2$ -in schedule 80 A312 TP316 piping and socket-welded to F316H # 1500 B16.5 flange connections. The pipe has an internal design gage pressure of 236 bar at 650°C. The flanges have

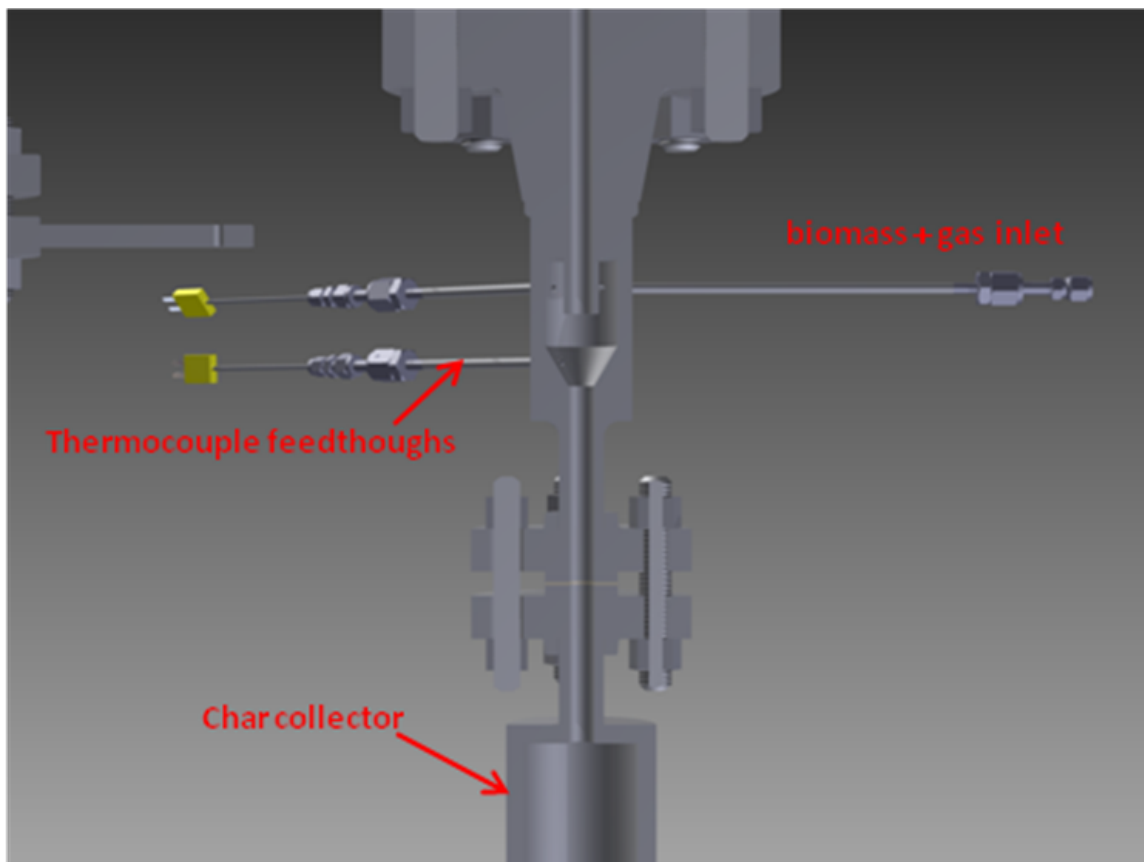


Figure B.2. Cross section view of high-pressure cyclone-type fast-hydrolysis reactor.

maximum working pressure of 106 bar at 593°C. The connector from the cyclone reactor to the secondary reactor is made from $\frac{1}{2}$ -in schedule 80 A312 TP316 piping and uses $\frac{1}{2}$ -in F316H # 1500 and 2-in F316H # 2500 B16.5 flange connections. Again, these flanges have a maximum working pressure of 132 and 106.5 bar at 650°C respectively.

B.2.3 Condenser and Gas/Liquid Separation

The purpose of this step is to cool and condense the pyrolysis vapors to 15-20°C and then separate them from the permanent gas stream. The vapor quenching system

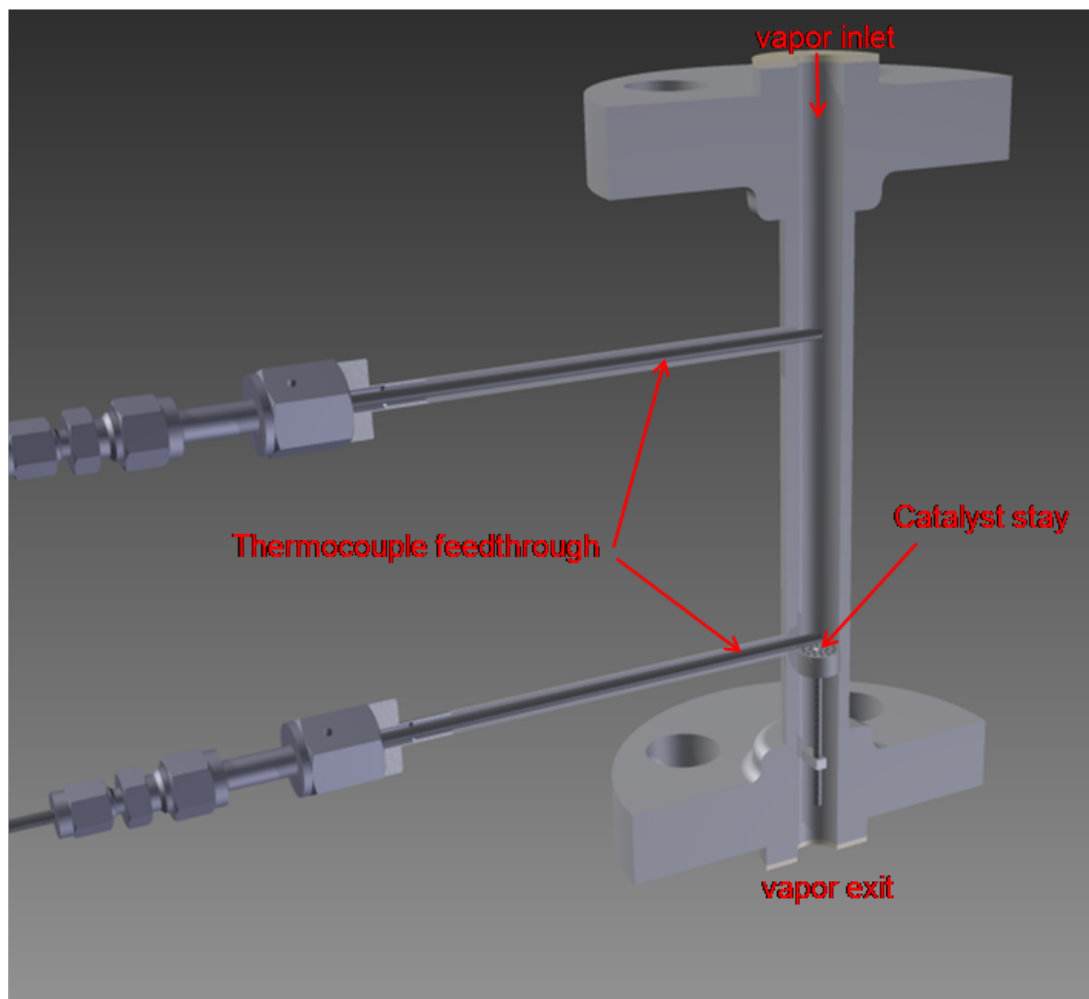


Figure B.3. Cross section view of downstream fixed-bed vapor-phase HDO reactor.

consists of a concentric-tube countercurrent condenser. Gas and vapors pass through the center tube which is cooled by circulation of 50/50 mixture of ethylene glycol and water at 5°C. The condensed vapors are separated from permanent gases in a Swagelok coalescence filter, which utilizes a glass fiber filter element to help coalesce liquids and is rated to 68 bar at ambient temperature. After passing through the filter, gases are passed through a stainless steel trap, which is cooled using ice-water mixture

to collect any remaining condensable liquids. The gas stream is then depressurized via a backpressure regulator and sent to exhaust and GC analysis streams.

The tube portion of the shell and tube condenser is made from schedule 80 A312 TP316 piping and connects to the secondary reactor or connector with a 1/2-in #1500 B16.5 flange. The pipe has an internal design gage pressure of 236 bar at 650°C. The flanges have maximum working pressure of 106 bar at 593°C. The exit of the condenser connects to the coalescence filter via 1/4-in A312 TP316 tube with a wall thickness of 0.028-in welded to a 1/4-in fVCR connector which has an allowable working pressure of 275 bar at 100°C

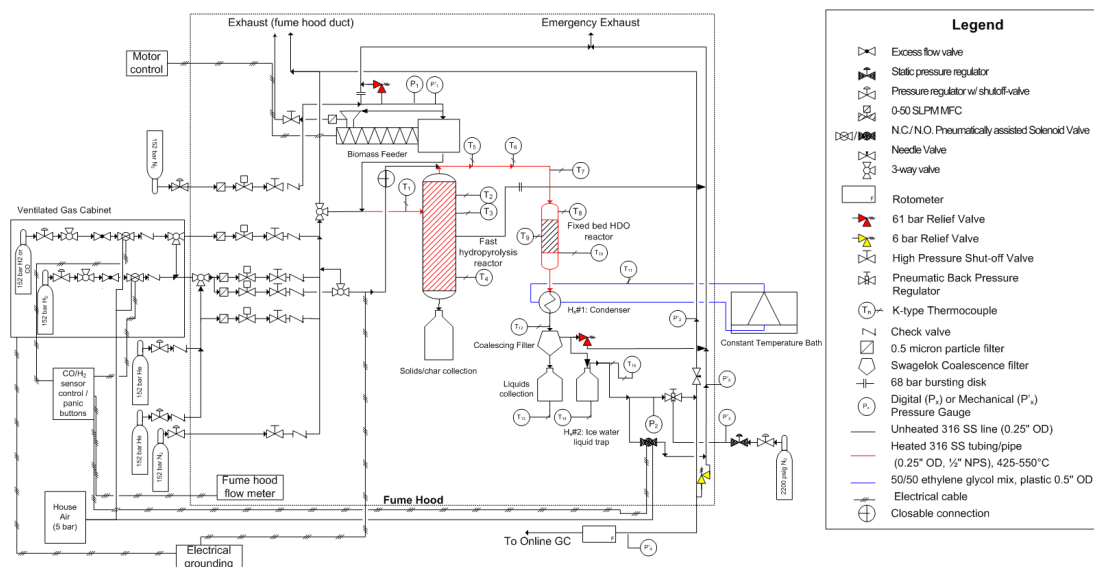


Figure B.4. Process flow diagram of the complete reactor system along with the hydrogen safety systems like hydrogen detectors, automatic shut-off valves, excess flow valves, redundant pressure relief and emergency exhaust.

Table B.1.
Chemical compounds identified and quantified for LC-MS analysis of liquid products from all experiments.

Chemical Compound	Retention Time / min	Calibration Range / $\text{g} \times$ L^{-1}
Cellobiosan	11.3	0 - 0.7
Levogalactosan	15.5	0 - 8.0
Levoglucosan	16.1	0 - 6.2
Glycolaldehyde	17	0 - 3.2
Formic Acid	18	0 - 6.1
Acetic Acid	19.3	0 - 3.2
1,6:2,3-Dianhydro-b- D-mannopyranose (DAMP)	20.9	0 - 2.0
Hydroxyacetone	21.5	0 - 1.9
Methanol	24.3	0 - 4.3
Acetone	26.9	0 - 2.8
Ethanol	27.6	0 - 2.0
Levoglucosenone	33.5	0 - 2.2
5-Hydroxymethyl- furfural (5-HMF)	33.9	0 - 1.0
Furfural	47.3	0 - 0.6

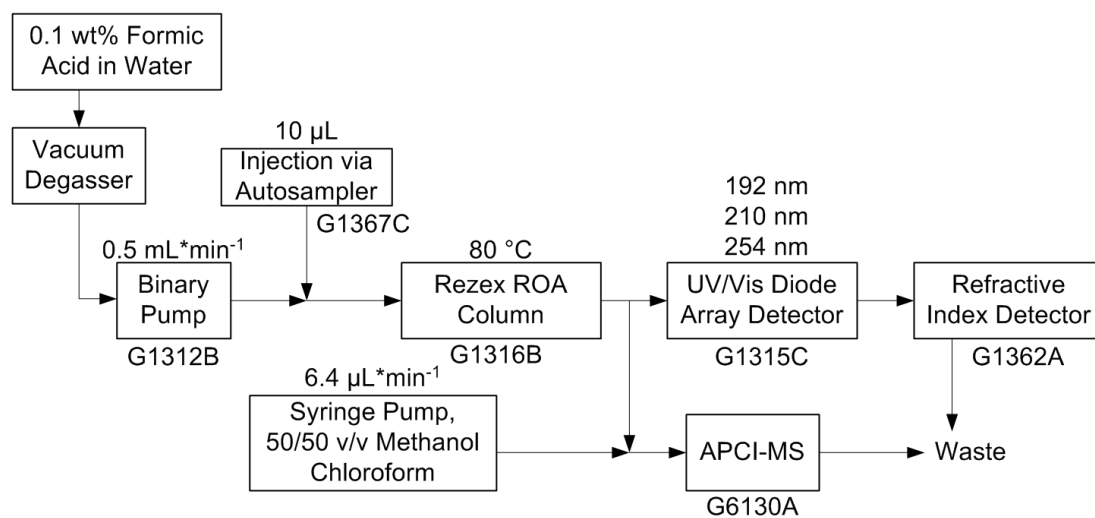


Figure B.5. Simplified schematic of the LC-MS setup for the analysis of liquid products from all experiments. Model numbers of the Agilent LC-MS modules are shown below each unit. Relevant analysis method parameters are shown above each unit.

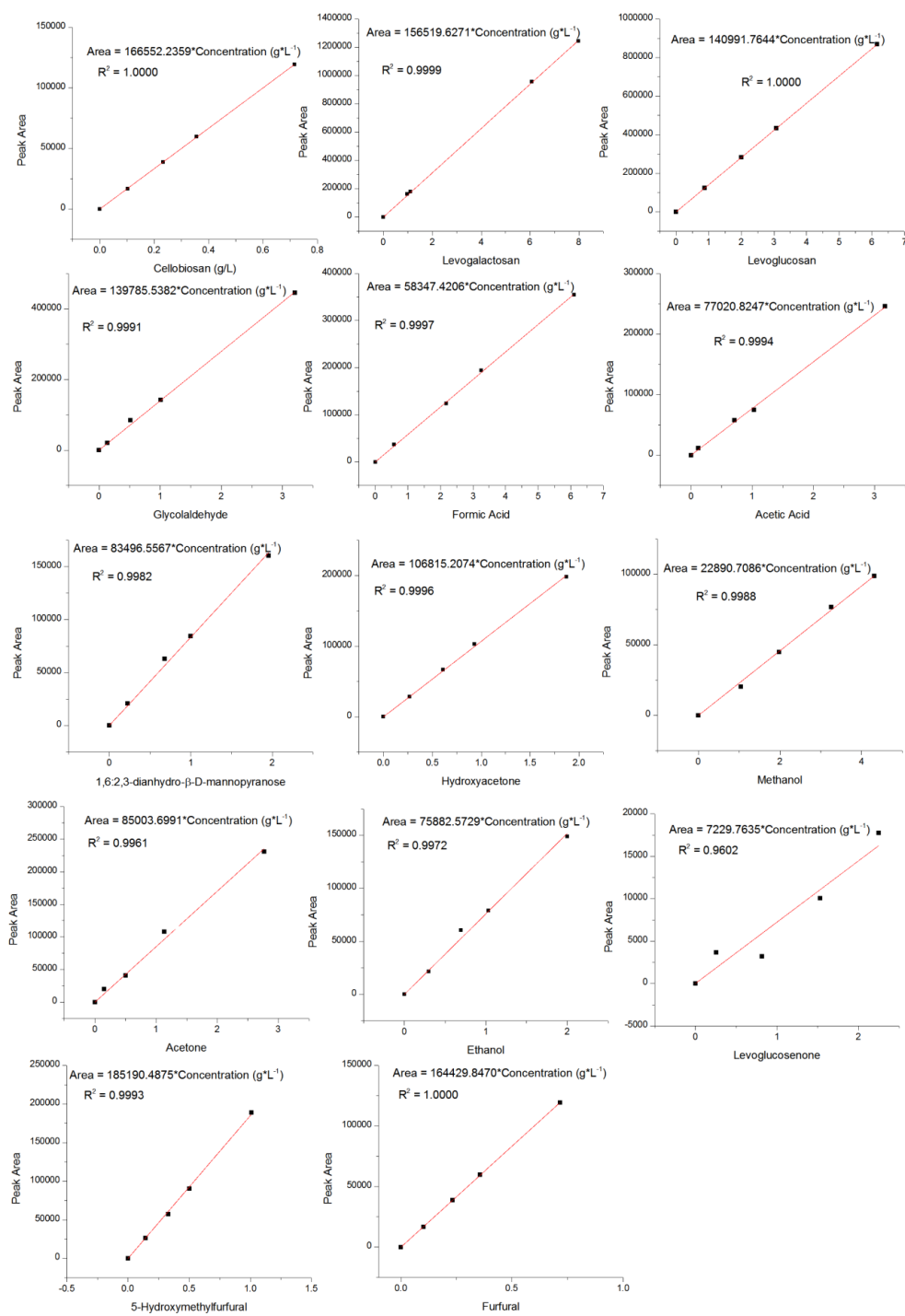


Figure B.6. LC-MS calibrations of the 14 chemical compounds used for quantification

C. SUPPORTING INFORMATION FOR MASS SPECTROMETRIC STUDIES OF FAST PYROLYSIS OF CELLULOSE

C.1 Pyrolysis Probe - Mass Spectrometer Residence Time Experimental

Ex-situ temperature measurements were done in order to measure the temperature of the platinum ribbon on the CDS Analytical Pyroprobe. A LASCON infrared pyrometer (Dr.Mergenthaler GmbH & Co.KG, Germany) was connected to the pyroprobe via a homebuilt triggering device that employs an optoisolator as shown in Figure C.1.

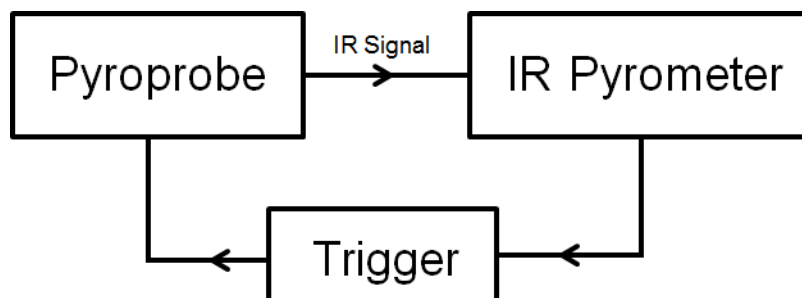


Figure C.1. A block diagram showing the set-up for ex-situ temperature measurements for the pyroprobe.

The residence time plus analysis time of pyrolysis products was measured as shown in Figure C.2. The IR pyrometer was used to trigger the pyroprobe, the oscilloscope (Tektronix, Beaverton, OR) and the LQIT mass spectrometer simultaneously. When the IR pyrometer was started, it triggered the pyroprobe and the oscilloscope via the optoisolator trigger used for ex-situ experiments. The mass spectrometer was triggered by the IR Pyrometer using an analog output configured for Transistor-Transistor Logic (TTL) operation. In order to have a high sampling rate, the Thermo Scientific (Chatham, MA) LTQ mass spectrometer was operated in the Turbo Scan

mode with Automatic Gain Control set to off and fill time set to 1 ms. Under these conditions, the mass spectrometer recorded data at the rate of 40 ms/scan. The ultra-fast scan rate comes with a price of lower mass resolution but provides a better estimate of the time point when inflection is observed in the total ion current.

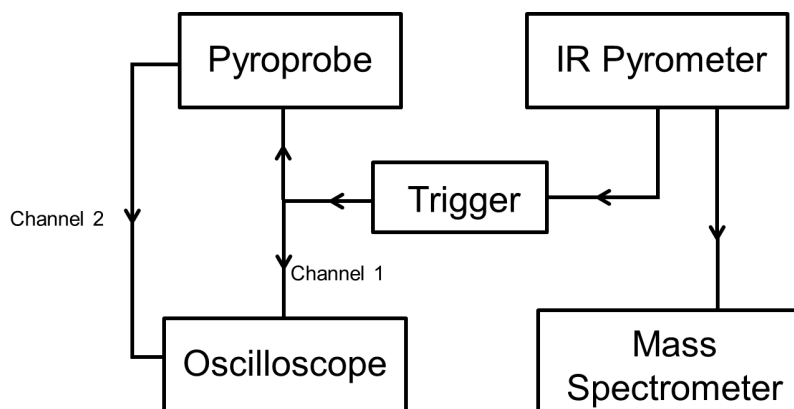


Figure C.2. A block diagram showing the set-up for in-situ residence plus analysis time measurements for the pyrolysis/MS setup.

Channel 1 was connected to the triggering device and was used to trigger the oscilloscope. Channel 2 connected to the oscilloscope measured the current passing through the pyroprobe filament, a spike in which represented the time at which the pyroprobe started heating. As soon as the IR pyrometer was started, the pyroprobe started the run cycle before heating up, and oscilloscope and mass spectrometer started collecting data immediately. The residence and analysis times were determined by measuring the time lag between when the pyroprobe reached 275°C (the lowest temperature at which pyrolysis products were reliably observed) and when the pyrolysis products were first seen in the mass spectrometer. A detailed schematic of the electronic setup used for the residence and analysis time measurement is available upon request.

C.2 Pyrolysis Probe - Gas Chromatograph / Mass Spectrometer

A modified Pyroprobe 5200 HP (CDS Analytical Inc.) was connected to an online GC/MS. In the case of the pyrolysis-GC/MS experiments, a resistively heated Pt coil was used as the heating source for pyrolysis of cellulose and cellotriosan. A known weight (0.2 - 0.7mg) of the reactant sample was loaded in a cylindrical quartz tube (O.D. = 2.52mm, I.D. = 1.91mm, L = 25.3mm) which was placed in the open end of the Pt coil. This assembly was placed in the pyroprobe interface which was flushed prior to pyrolysis with He to remove air. The pyrolysis probe interface was then heated to a temperature of 300°C, after which the Pt coil was heated to 600°C, at a heating rate of $1000^{\circ}\text{C} \times \text{s}^{-1}$. A stream of helium carrier gas carried the pyrolysis products from the quartz tube to the GC/MS inlet via a heat traced transfer line. All the vapor-phase products were analyzed with an online Agilent 7890N gas chromatograph with a HP-5ms (30m \times 250mm \times 0.25 μm) column connected to an Agilent 3-way splitter, which split the flow to a Flame Ionization Detector and an electron ionization Agilent 5975C Mass Spectrometer. The GC column was kept at 33°C for 10 minutes and then heated to 300°C at a heating rate of $10^{\circ}\text{C} \times \text{min}^{-1}$ and held at 300°C for 20 minutes providing optimum time for all observable products to elute. The pyrolysis products were quantified against standard calibration curves developed for compounds levoglucosan, glycolaldehyde, furfural, hydroxymethyl furfural (HMF), hydroxyacetone, and acetic acid. The permanent gases were quantified using the MS detector against calibration curves for CO and CO₂. The char was quantified by weighing the quartz tube three times during every experimental run: empty (1st), with sample (2nd) and after pyrolysis (3rd). The difference between the second and first weights was used to calculate the weight of the sample loaded, while that between the third and first weights were used to calculate the amount of char left behind after pyrolysis.

Table C.1.
Quantitative pyrolysis product distribution produced from the Pyrolysis-GC/MS reactor for pyrolysis of cellotriosan and cellulose.

Compound	Cellotriosan	Cellulose
6 carbons		
levoglucosan	45 ± 2.9	44 ± 2.6
other anhydrosugars	4.5 ± 0.75	5.5 ± 0.35
1,6-anhydroglucofuranose	1.5 ± 0.37	2.6 ± 0.23
ADGH	1.6 ± 0.42	2.7 ± 0.23
5-hydroxymethylfurfural	1.4 ± 0.08	1.4 ± 0.07
levoglucosenone	0.22 ± 0.05	0.19 ± 0.06
DAGP	0.22 ± 0.05	0.14 ± 0.02
HMCP	0.13 ± 0.01	n.d.
5 carbons		
1,2-cyclopentanedione	0.59 ± 0.20	0.3 ± 0.01
furfural	0.37 ± 0.01	0.44 ± 0.06
2-methyl-furan	0.13 ± 0.04	0.08 ± 0
1,3-cyclopentadiene	0.08 ± 0.02	0.06 ± 0.01
3 and 4 carbons		
methylglyoxal	2.4 ± 0.48	1.6 ± 0.08
1-hydroxy-2-propanone	0.58 ± 0.20	0.26 ± 0.01
methyl vinyl ketone	0.48 ± 0.07	0.42 ± 0.02
DHHF	0.20 ± 0.03	0.23 ± 0.01
2-propenal	0.14 ± 0.02	n.d.
Light oxygenates		
glycolaldehyde	6.6 ± 0.5	9.2 ± 1.2
acetaldehyde and glyoxal	0.4 ± 0.12	0.4 ± 0.02
formaldehyde	0.25 ± 0.06	0.17 ± 0.03
Permanent gases		
methane	0.15 ± 0.04	0.15 ± 0.02
carbon monoxide	3.5 ± 0.28	2.1 ± 0.11
carbon dioxide	4.8 ± 0.57	3.6 ± 0.18
Other		
water (assumed)	5	5
char	5.8 ± 0.35	11 ± 1.2
unidentified and minor	9	5.5
Total	95 ± 7.6	96 ± 6.5

Abbreviations: n.d., not detected; ADGH, 1,5-anhydro-4-deoxy-D-glycero-hex-1-en-3-ulose; DAGP, 1,4:3,6-dianhydro- α -D-glucopyranose; HMCP, 2-hydroxy-3-methyl-2-cyclopenten-1-on; DHHF, dihydro-4-hydroxy-2(3H)-furanone

D. SUPPORTING INFORMATION FOR FAST PYROLYSIS OF ^{13}C -LABELED CELLOBIOSSES: GAINING INSIGHTS INTO THE MECHANISMS OF FAST PYROLYSIS OF CARBOHYDRATES

In the process of synthesizing labeled the two labeled cellobioses, the following procedure was employed. Many ^1H and ^{13}C spectra were gathered to verify the structure of the intermediates. For the sake of brevity, those NMR spectra are not reproduced here, but are instead available from the published supporting information for Degenstein et. al. *J. Org. Chem.* 2015, 80 (3), 1909.[10] In the following text the references to these NMR figures are kept as (Figure) S1 through S18.[10] The online supporting information for this article also contains additional information on the DFT calculations performed including, for example, the geometries in xyz format for the optimized structures of reactants, products and transition states.[10]

D.1 Synthesis of Labeled Cellobioses.

3- ^{13}C - β -D-Glucose and [1- ^{13}C]glucopyranosylglucose were purchased from Omicron Bio-chemicals. The synthesized compounds (for the syntheses, see below) were purified by column chromatography on a Teledyne-ISCO CombiFlash system with a silica gel column. These compounds were characterized by ^1H and ^{13}C NMR spectroscopy and high-resolution mass spectrometry. The reactions were performed under an argon atmosphere if needed. Solvents were purified and/or predried as necessary. Analytical thin-layer chromatography (TLC) was used to monitor the reactions. Visualization was accomplished with UV light (254 nm) and by ethanol/ H_2SO_4 TLC stain. CDCl_3 , CDOD , and D_2O were used as NMR solvents. ^1H NMR spectra were acquired on a 400 MHz instrument, and the chemical shifts (δ) are reported relative to the residual solvent peak. ^{13}C NMR spectra were acquired on a 100 MHz instrument, and the

chemical shifts are reported in parts per million relative to the residual solvent peak. When reporting spectral data, the format chemical shift (integration, multiplicity, J value(s) in Hz, identification) was used with the following multiplicity abbreviations: s = singlet, d = doublet, t = triplet, q = quartet, m = multiplet. The elemental compositions were obtained using high-resolution mass spectrometry and ESI in positive-ion mode, and the measured m/z values are reported. The previously synthesized compound 2,3,4,6-tetra-O-benzyl-D-glucopyranosyl trichloroacetimidate (S7) was prepared from commercially available 2,3,4,6-tetra-O-benzyl-D-glucopyranose by following a literature procedure.[208] The synthesis of labeled cellobioses glucopyranosyl[3- ^{13}C]glucose (S9) and glucopyranosyl[5- ^{13}C]glucose (S17) are shown in Schemes 1 and 2, respectively.

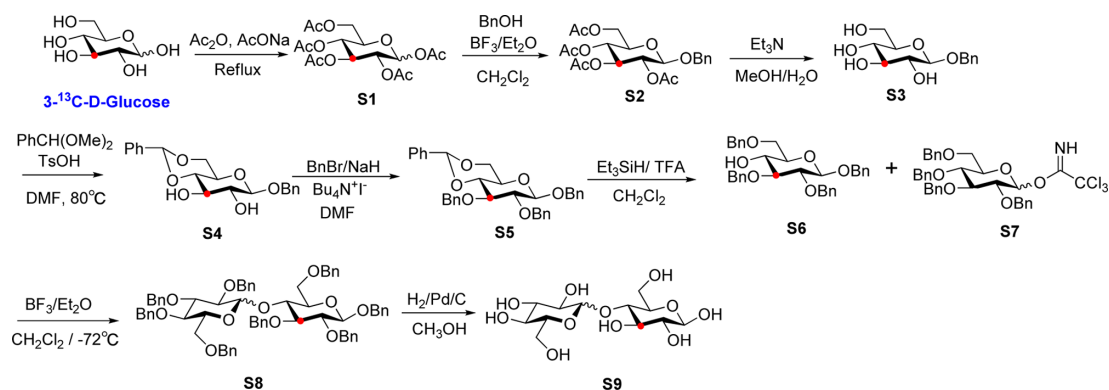


Figure D.1. Synthesis of Glucopyranosyl[3- ^{13}C]glucose

1,2,3,4,6-Penta-O-acetyl-3- ^{13}C - β -D-glucopyranoside (S1).[209] To a solution of acetic anhydride (6 mL) was added sodium acetate trihydrate (1.13 g, 8.3 mmol, 3 equiv). The mixture was refluxed at 90°C for 20 min, and then the labeled D-glucose (0.5 g, 2.8 mmol) was added. The resulting mixture was stirred for 4 h and then concentrated, dissolved in methanol, and recrystallized with cold water. A white solid was then filtered and dried to afford S2 (1.00 g, 92%). ^1H NMR (400 Hz, CDCl_3 , δ): 2.02, 2.03, 2.04, 2.09, and 2.12 (15H, s, CH_3), 3.84-3.87 (^1H , m, CH), 4.10-4.13 (^1H , m, CH_2), 4.28-4.32 (^1H , dd, $J_1 = 8, J_2 = 4$, CH), 5.04-5.09 (d, ^1H , $J = 8$, CH), 5.13-5.17

(m, ^1H , CH), 5.42-5.47 (m, ^1H , CH), 5.72-5.74 (d, ^1H , $J = 8$, CH). ^{13}C NMR (100 Hz, CDCl_3 , δ): 170.6, 170.1, 169.4, 169.2, 168.9, 91.7, 89.1, 74.0, 69.8, 67.8, 67.5, 61.5, 20.7. HRMS (ESI): calcd for $^{13}\text{CC}_{15}\text{H}_{22}\text{O}_{11}\text{Na}$ [$\text{M} + \text{Na}$] $^+$, 414.1093; measured, 414.1086.

Benzyl 2,3,4,6-Tetra-O-acetyl-3- ^{13}C - β -D-glucopyranoside (S2).[95] To a solution of penta-O-acetylglucose S1 (1.00 g, 2.56 mmol) and benzyl alcohol (0.61 mL, 5.60 mmol) in anhydrous CH_2Cl_2 (10 mL) was added $\text{BF}_3\cdot\text{Et}_2\text{O}$ (0.41 mL, 3.33 mmol). The reaction mixture was stirred at room temperature (RT) for 24 h and diluted with 5% aqueous NaHCO_3 (10 mL). The organic layer was separated, washed sequentially with aqueous NaHCO_3 (10 mL) and water (10 mL), dried over Na_2SO_4 , and concentrated. The crude product was recrystallized from EtOH to give S2 (0.55 g, 49%). ^1H NMR (400 Hz, CDCl_3 , δ): 7.39-7.27 (5H, m, Ar-H), 5.13-4.99 (3H, m, CH, H2, H3, and H4), 4.88 (^1H , d, $J = 12$, CH_2), 4.61 (^1H , d, $J = 12$, CH_2), 4.60 (^1H , d, $J = 8$, CH, H1), 4.30 (^1H , dd, $J = 12$, 4, CH, H6), 4.19 (^1H , dd, $J = 12$, 2, CH, H6), 3.67-3.64 (^1H , m, CH, H5), 2.09 (3H, s, CH_3), 2.00 (3H, s, CH_3), 1.99 (3H, s, CH_3), 1.98 (3H, s, CH_3). ^{13}C NMR (100 Hz, CDCl_3 , δ): 170.6, 170.2, 169.3, 169.2, 136.6, 128.4, 127.9, 127.8, 127.7, 99.2, 77.0, 76.7, 72.7, 71.7, 71.4, 70.6, 70.1, 69.7, 68.5, 68.1, 20.5. HRMS (ESI): calcd for $^{13}\text{CC}_{20}\text{H}_{26}\text{O}_{10}\text{Na}$ [$\text{M} + \text{Na}$] $^+$, 462.1424; measured, 462.1410.

Benzyl 3- ^{13}C - β -D-Glucopyranoside (S3).[95] A mixture of benzyl 2,3,4,6-tetra-O-acetyl- β -D-glucopyranoside (0.896 g, 2.50 mmol), MeOH (16 mL), triethylamine (2 mL), and H₂O (2 mL) was stirred for 5 h. The reaction was concentrated in vacuo, and the resulting residue was purified by chromatography (5:1 $\text{CH}_2\text{Cl}_2/\text{CH}_3\text{OH}$) to give S3 (0.44 g, 81%). ^1H NMR (400 Hz, CD_3OD , δ): 7.43-7.25 (5H, m, Ar-H), 4.78 (2H, ABq, $J = 16$, PhCH_2), 4.36 (^1H , d, $J = 8$ Hz, CH, H1), 3.89 (^1H , dd, $J = 12$, 2, CH, H6), 3.70 (^1H , dd, $J = 12$, 6, CH, H6), 3.35-3.15 (4H, m, CH, H2, H3, H4, and H5). ^{13}C NMR (100 Hz, CDCl_3 , δ): 139.1, 129.3, 129.2, 128.7, 103.3, 78.1, 75.1, 74.9, 74.1, 71.8, 71.4, 62.8. HRMS (ESI): calcd for $^{13}\text{CC}_{12}\text{H}_{18}\text{O}_6\text{Na}$ [$\text{M} + \text{Na}$] $^+$, 294.1030; measured, 294.0988.

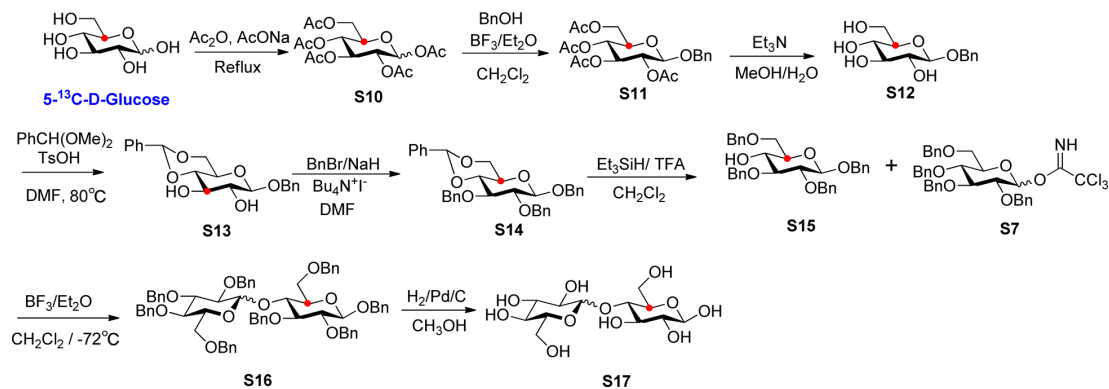


Figure D.2. Synthesis of Glucopyranosyl[5- ^{13}C]glucose

Benzyl 4,6-O-Benzylidene-3- ^{13}C - β -D-glucopyranoside (S4).[95] To a mixture of benzyl β -D-glucopyranoside (0.21 g, 0.78 mmol) and benzaldehyde dimethyl acetal (0.14 mL, 0.94 mmol) in dimethylformamide (DMF) (2 mL) at RT was added p-toluenesulfonic acid (TsOH:H₂O) (37 mg, 0.195 mmol). The reaction mixture was stirred for 5 min, heated to 80°C, and stirred for 2.5 h. The mixture was cooled to RT and subsequently concentrated at reduced pressure. The resulting residue was partitioned between CH₂Cl₂ (20 mL) and saturated Na₂CO₃ (20 mL). The layers were separated, and the aqueous layer was extracted with CH₂Cl₂ (3 × 10 mL). The combined organic layers were washed with water (2 × 10 mL) and brine (10 mL), dried over MgSO₄, and concentrated. Purification of the resulting residue by flash chromatography (1:1 EtOAc/hexanes) provided the desired product (0.21 g, 75%) as a white solid. ¹H NMR (400 Hz, CDCl₃, δ): 7.50-7.48 (2H, m, Ar-H), 7.37-7.29 (8H, m, Ar-H), 5.46 (1H, s, benzylidene CH), 4.88 (1H, d, J = 12, CH₂), 4.59 (1H, d, J = 12, CH₂), 4.53 (1H, d, J = 8, CH, H1), 4.31 (1H, dd, J = 8, 4, CH, H4), 3.59-3.76 (2H, m, CH, C₆, H₃), 3.63-3.58 (4H, m, CH, H6, H2, and 2OH), 3.35-3.30 (1H, m, CH, H5). ¹³C NMR (100 Hz, CDCl₃, δ): 137.0, 136.8, 129.2, 128.5, 128.1, 128.0, 126.3, 102.2, 101.8, 80.6, 80.2, 77.4, 77.0, 76.71, 74.6, 74.2, 73.0, 72.8, 71.2, 68.5, 66.2. HRMS (ESI): calcd for ¹³CC₂₀H₂₂O₆Na [M + Na]⁺, 382.1314; measured, 382.1310.

4,6-O-Benzylidene-1,2,3-tri-O-benzyl-3-¹³C-β-D-glucopyranoside (S5).[210] S4 (partially protected, 0.21 g, 0.58 mmol) was added to anhydrous DMF (2 mL), and the mixture was stirred at 0°C for 30 min. NaH in mineral oil (60%) (94 mg, 2.32 mmol) was then added under argon in small portions over 30 min, with the temperature being maintained at 0°C. Tetrabutylammonium iodide (54 mg, 0.14 mmol) was then added, and the mixture was stirred for a further 2 h at 0°C. Benzyl bromide (0.21 mL, 1.74 mmol) was then added slowly. The reaction mixture was stirred at 0°C for a further 30 min, allowed to warm to room temperature, and stirred for 24 h. Methanol was added slowly to destroy the excess NaH, and the solvents were then removed in vacuo. The residue was subjected to column chromatography with 3:2 hexane/ethyl acetate to furnish S5 as a pale-yellow oil (0.3 g, 81%). ¹H NMR (400 Hz, CDCl₃, δ): 7.48-7.34 (20H, m, Ar-H), 5.65 (¹H, s, CH, H7), 5.04-4.71 (8H, m, CH, CH₂), 4.48-4.44 (¹H, dd, J = 8, 4, CH, H4), 3.92-3.76 (2H, m, CH, H6, H3), 3.66-3.60 (2H, m, CH, H6, H2), 3.53-3.48 (¹H, m, CH, H5). ¹³C NMR (100 Hz, CDCl₃, δ): 138.5, 137.1, 129.0, 128.3, 127.6, 126.0, 103.2, 101.1, 80.9, 80.7, 77.4, 76.8, 75.4, 75.1, 71.6, 68.8, 66.1. HRMS (ESI): calcd for ¹³CC₃₃H₃₄O₆Na [M + Na]⁺, 562.2253; measured, 562.2227.

1,2,3,6-Tetra-O-benzyl-3-¹³C-β-D-glucopyranoside (S6).[210] Triethylsilane (0.27 mL, 1.68 mM) and trifluoroacetic acid (0.13 mL, 1.68 mmol) were added to a solution of S5 (0.3 g, 0.56 mmol) in anhydrous CH₂Cl₂ (10 mL) at 0°C. The solution was stirred at RT for 6 h. The reaction mixture was diluted with EtOAc (approximately 20 mL), neutralized with saturated aqueous NaHCO₃ and brine, dried over Na₂SO₄, and evaporated to dryness. The residue was purified by flash column chromatography (3:10 EtOAc/hexane) to get S6 (0.2 g, 60%) as a colorless oil. ¹H NMR (400 Hz, CDCl₃, δ): 7.45-7.29 (20H, m, Ar-H), 5.02-4.64 (8H, m, CH₂), 4.58 (¹H, d, J = 8, CH, H1), 3.86-3.48 (6H, m, CH, CH₂, ring CH), 2.60 (¹H, s, OH). ¹³C NMR (100 Hz, CDCl₃, δ): 138.6, 138.3, 137.5, 128.1, 127.8, 102.5, 84.3, 84.1, 83.8, 82.5, 81.7, 81.4, 77.3, 77.0, 76.7, 75.2, 74.7, 74.1, 73.6, 71.7, 71.3, 71.1, 70.2. HRMS (ESI): calcd for ¹³CC₃₃H₃₆O₆Na [M + Na]⁺, 564.2433; measured, 564.2465.

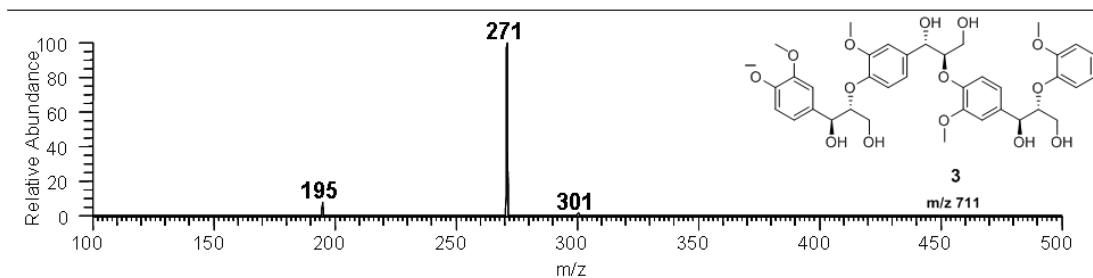
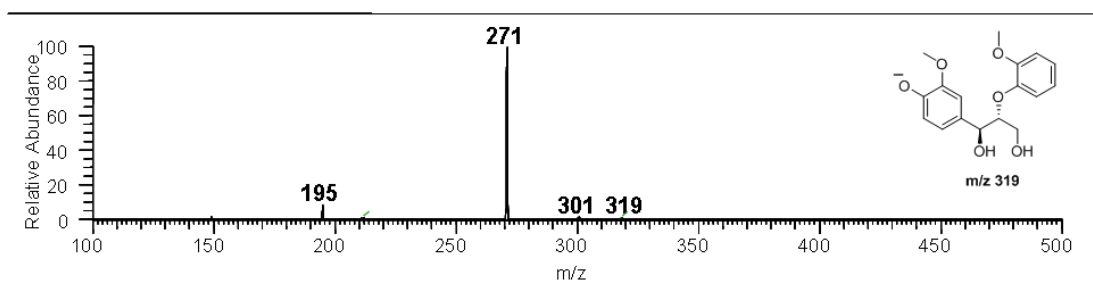
2,3,4,6-Tetra-O-benzyl- β -D-glucopyranosyl-(1-4)-tetra-O-benzyl-3- ^{13}C - β -D-glucopyranoside (S8).[210] To a solution of S6 (0.1 g, 0.18 mmol) and S7 (0.12 g, 0.18 mmol) in anhydrous CH_2Cl_2 (5 mL) was added $\text{BF}_3\cdot\text{Et}_2\text{O}$ (3 μL , 0.018 mmol) at -72°C . After the solution was stirred at -72°C for 1 h, the reaction mixture was neutralized with triethylamine. The residue was purified by flash column chromatography (1:8 EtOAc/hexane) to give S8 as a 1:3 mixture of α and β isomers (0.12 g, 55%) as a colorless syrup. ^1H NMR (400 Hz, CDCl_3 , δ): 7.42-7.19 (40H, m, Ar-H), 5.15-4.46 (18H, m, CH, PhCH_2 , H1, H1'), 3.92-3.35 (12H, m, CH, CH_2 , ring CH). ^{13}C NMR (100 Hz, CDCl_3 , δ): 139.3, 138.6, 137.6, 128.3, 127.8, 127.5, 102.4, 84.8, 83.1, 78.0, 77.3, 76.7, 75.5, 74.9, 73.2, 70.9, 69.0, 68.2. HRMS (ESI): calcd for $^{13}\text{CC}_{68}\text{H}_{70}\text{O}_{11}\text{Na}$ $[\text{M} + \text{Na}]^+$, 1086.4849; measured, 1086.4846.

Glucopyranosyl[3- ^{13}C]glucose (S9).[210] A solution of S8 (0.12 g, 1.15 mmol) in MeOH (10 mL) was hydrogenated in the presence of 10% Pd/C (15 mg) at atmospheric pressure at RT for 36 h. After the catalyst was filtered off, the reaction mixture was evaporated to give S9 ($\alpha:\beta = 1:3$, 34 mg, 87%) as a colorless solid. ^1H NMR (400 Hz, D_2O , δ): 4.56 (^1H , d, $J = 8$, CH, H1'), 4.41 (^1H , d, $J = 8$, CH, H1), 3.83- 3.15 (12H, m, CH, CH_2 , ring CH). ^{13}C NMR (100 Hz, D_2O , δ): 103.1, 96.3, 92.4, 76.8, 76.6, 76.1, 75.4, 74.9, 74.6, 73.8, 72.1, 70.7, 70.0, 61.0, 60.5. HRMS (ESI): calcd for $^{13}\text{CC}_{11}\text{H}_{22}\text{O}_{11}\text{Na}$ $[\text{M} + \text{Na}]^+$, 366.1060; measured, 366.1068.

Glucopyranosyl[5- ^{13}C]glucose (S17).[210] The same synthesis strategy as described above for S9 was employed for the synthesis of glucopyranosyl[5- ^{13}C]glucose (S17). A solution of S16 (0.12 g, 1.15 mmol) in MeOH (10 mL) was hydrogenated in the presence of 10%Pd/C (15 mg) at atmospheric pressure at RT for 36 h. After the catalyst was filtered off, the reaction mixture was evaporated to give S17 ($\alpha:\beta = 1:3$, 34 mg, 87%) as a colorless solid. ^1H NMR (500 MHz, D_2O , δ): 4.56 (^1H , d, $J = 5$, CH, C_1'), 4.41 (^1H , d, $J = 5$, CH, C_1), 3.83-3.15 (12H, m, CH, CH_2 , ring CH). ^{13}C NMR (125 MHz, D_2O , δ): 102.5, 95.6, 91.7, 78.8, 78.5, 78.3, 75.9, 75.4, 74.7, 74.2, 73.8, 71.7, 71.2, 71.1, 70.0, 69.4, 60.5, 60.1, 59.9. HRMS (ESI): calcd for $^{13}\text{CC}_{11}\text{H}_{22}\text{O}_{11}\text{Na}$ $[\text{M} + \text{Na}]^+$, 366.1060; measured, 366.1066.

E. SUPPORTING INFORMATION FOR DETERMINATION OF THE PRIMARY
FAST PYROLYSIS PRODUCTS OF SYNTHETIC G-LIGNIN OLIGOMERS
WITH β -O-4 LINKAGES VIA ON-LINE MASS SPECTROMETRY

Direct Inject of dimer – Ionization – Isolation m/z 319- CAD on m/z 319



Pyrolysis of 3 – Ionization – Isolate ion of m/z 319 - CAD

Figure E.1. The CAD pattern of m/z 319 isolated from the pyrolysis spectrum of 3 is the same as the CAD pattern of authentic dimer using direct inject.

Table E.1.

All major tetrameric, trimeric, dimeric and monomeric pyrolysis product ions of 1-3 with m/z , relative abundances and fragment sequences. Water (W) and formaldehyde (F) losses are also indicated. Ions in bold are parent fragment ions.

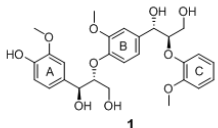
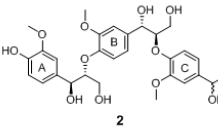
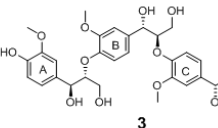
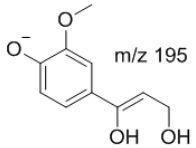
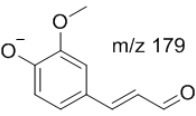
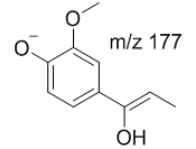
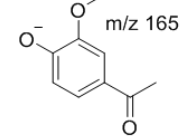
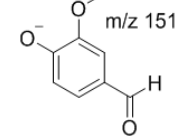
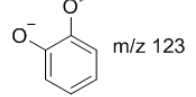
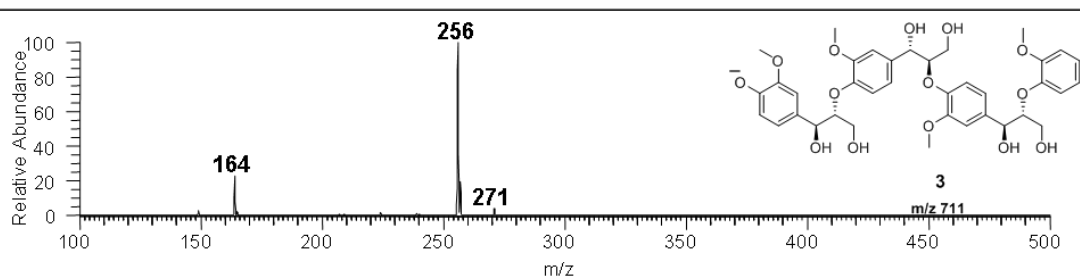
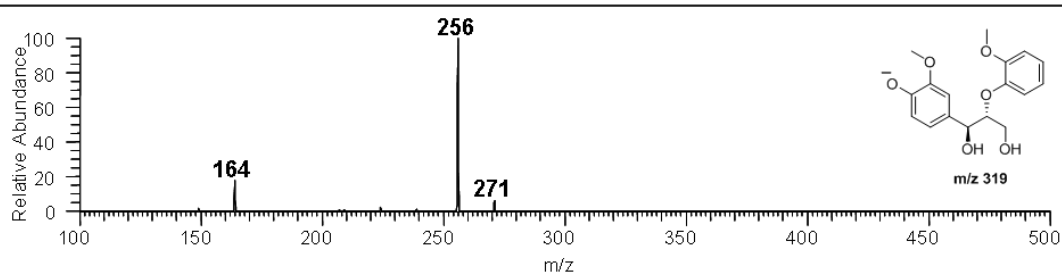
			
Tetrameric Fragment ions	----	----	m/z 711 (23%), ABCD, [M-H] ⁻ m/z 663 (6%), ABCD, [711-W-F] ⁻ m/z 615 (2%), ABCD, [663-W-F] ⁻
Trimeric Fragment ions	m/z 515 (34%), ABC, [M-H] ⁻ m/z 467 (5%), ABC, [515-W-F] ⁻	m/z 589 (5%), ABC, [M-H] ⁻ m/z 541 (3%), ABC, [589-W-F] ⁻	m/z 515 (100%), BCD, [M-H-A] ⁻ m/z 467 (18%), BCD, [515-W-F] ⁻ m/z 419 (15%), BCD, [467-W-F] ⁻ m/z 587 (2%), ABC, [M-H-D] ⁻
Dimeric Fragment ions	m/z 319 (100%), BC, [M-H-A] ⁻ m/z 271 (24%), BC, [319-W-F] ⁻ m/z 256 (2%), BC, [271-CH ₃] ⁻ m/z 391 (3%), AB, [M-H-C] ⁻ m/z 373 (5%), AB, [391-W] ⁻ m/z 355 (2%), AB, [373-W] ⁻ m/z 343 (1%), AB, [373-F] ⁻ m/z 325 (3%), AB, [373-W-F] ⁻	m/z 393 (100%), BC, [M-H-A] ⁻ m/z 375 (3%), BC, [393-W] ⁻ m/z 357 (15%), BC, [375-W] ⁻ m/z 345 (25%), BC, [375-F] ⁻ m/z 327 (23%), BC, [375-W-F] ⁻ m/z 391 (5%), AB, [M-H-C] ⁻ m/z 373 (18%), AB, [391-W] ⁻ m/z 355 (13%), AB, [373-W] ⁻ m/z 343 (7%), AB, [373-F] ⁻ m/z 325 (20%), AB, [373-W-F] ⁻	m/z 319 (100%), CD, [M-H-AB] ⁻ m/z 271 (20%), CD, [319-W-F] ⁻ m/z 391 (20%), AB or BC, [M-H-CD or AD] ⁻ m/z 373 (45%), AB or BC, [391-W] ⁻ m/z 355 (5%), AB or BC, [373-W] ⁻ m/z 343 (15%), AB or BC, [373-F] ⁻ m/z 325 (13%), AB or BC, [373-W-F] ⁻
Monomeric Fragment ions	m/z 195 (50%) m/z 179 (100%) m/z 177 (30%), m/z 165 (10%) m/z 164(4%) m/z 151 (15%) m/z 123 (35%)	m/z 197 (30%) m/z 195 (10%) m/z 179 (100%) m/z 177 (25%), m/z 165 (10%) m/z 164(2%) m/z 151 (12%)	m/z 195 (80%) m/z 179 (100%) m/z 177 (70%), m/z 165 (33%) m/z 164(5%) m/z 151 (55%) m/z 123 (28%)

Table E.2.
CAD of small lignin products produced upon pyrolysis of β -O-4 G-Lignin tetramer along with proposed structures.

Proposed Structure	MS ²	MS ³	MS ⁴
 m/z 195	195—CH ₃ (180) 5% 195—CH ₂ O(165) 100%	165—CH ₃ (150) 100%	150—CO(122) 100%
 m/z 179	179—CH ₃ (164) 67% 179—H ₂ O (161) 100% 179—CH ₃ & H ₂ O (146) 27%	146—CO(118) 100%	
 m/z 177	177—CH ₃ (162) 100% 177—CH ₃ OH(145) 3%	162—CO(134) 100% 162—CHO(133) 24% 162—C ₂ H ₂ O(120) 10% 162—CO ₂ (118) 12% 162—C ₃ H ₄ O(106) 12%	
 m/z 165	165—CH ₃ (150) 100%	150—CO(122) 100% 150—CHO(121) 16%	
 m/z 151	151—CH ₃ (136) 100%	136—CO(108) 22% 136—CO ₂ (92) 100%	
 m/z 123	123—CH ₃ (108) 100%	No further losses observed upon CAD of m/z 108	

**Direct Inject of dimer – Ionization – Isolation m/z 319- CAD on m/z 319
- Isolation m/z 271-CAD on m/z 271**



Pyrolysis of 3 – Ionization – Isolate ion of m/z 271 - CAD

Figure E.2. The CAD pattern of m/z 271 isolated from the pyrolysis spectrum of 3 is the same as the CAD pattern of m/z 271 from authentic dimer using direct inject.

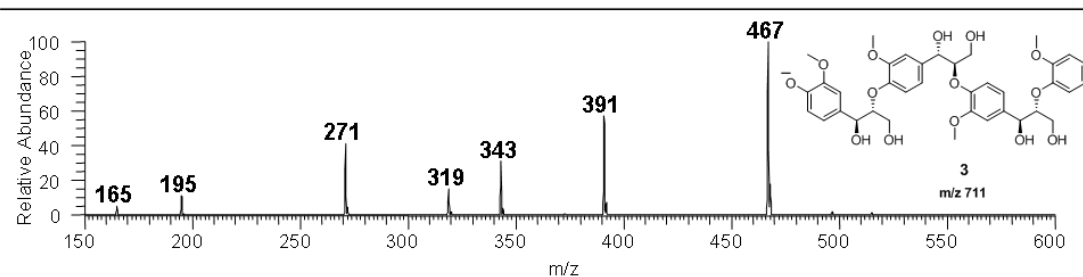
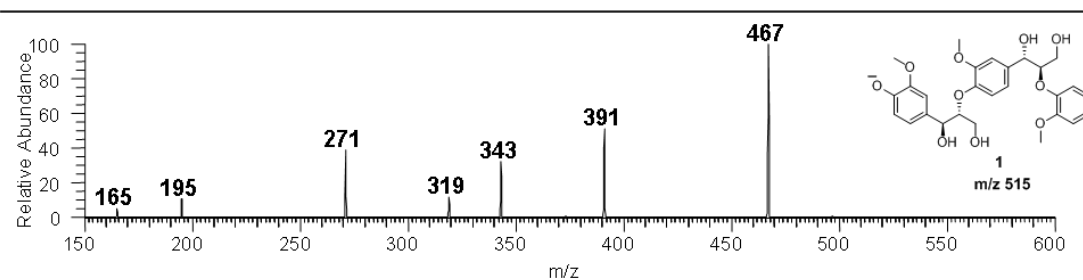
Direct Inject of 3 – Ionization – Isolation m/z 515- CAD on m/z 515**Pyrolysis of 3 – Ionization – Isolate ion of m/z 515 - CAD**

Figure E.3. The CAD pattern of m/z 515 isolated from the pyrolysis spectrum of 3 is the same as the CAD pattern of m/z 515 from authentic 1 using direct inject.

F. SUPPLEMENTARY INFORMATION FOR FAST PYROLYSIS OF GUAIACYL LIGNIN MODEL COMPOUNDS WITH β -O-4 LINKAGES

F.1 Estimation of Lights, CO, and CO₂

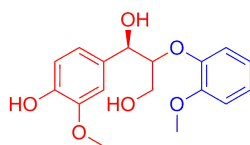
It was not possible to estimate CO and CO₂, since it was not detected in the FID. The column used for analysis of lignin pyrolysis products is a shortened HP-5ms column and as a result is not suitable for separating the light molecules. As a consequence, it was not possible to achieve baseline separation for the peaks of formaldehyde, acetaldehyde and other minor lights which are expected from pyrolysis of the lignin model compounds. Additionally CO and CO₂ also eluted along with the broad lights peaks, however their contribution to the FID signal can be considered negligible since CO has a very low response factor and CO₂ cannot be detected. Additionally, in the mass spectrometer, the major ion fragments from CO₂ and acetaldehyde overlap making it difficult to estimate CO₂ by calibrating for m/z 44 signal in the mass spectrometer for CO₂. Preliminary estimations from m/z 44 and m/z 28 indicate no more than 1% of the contribution from CO and CO₂.

F.2 Estimation of Water

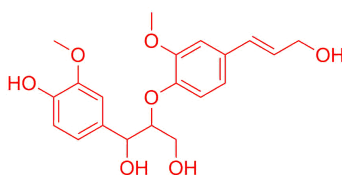
Estimation of water was performed taking into account the amount of oxygen lost from the monomeric species (depending the structures identified) as compared to their precursors in the model compound. For polymer 5 and trimer 4 it was estimated to be 4-5% depending on the residence time. For all other model compounds it was <4%.

F.3 Char Yield versus Coniferyl Alcohol

Figure F.3 shows the char yield and the coniferyl alcohol fraction in vapor phase pyrolysis products as a function of the degree of polymerization. Coniferyl alcohol was used since it was the most abundant monomeric species bearing a $C\alpha=C\beta$ bond, however it was not the only compound with $C\alpha=C\beta$ bond in the product distribution. Other species having $C\alpha=C\beta$ bonds are expected to be a part of the dimer fraction (i.e. dimer 6), but they could not be identified due to experimental limitations. These species are expected to be a part of polymer 5 to a greater extent as compared to model compounds 1-3 due to nature of end group, and hence a higher proportion of aromatic rings with alkyl substituents. It should be kept in mind that although, $C\alpha=C\beta$ bond bearing molecules have been shown to be prone to char formation via condensation reactions, it is not the only factor contributing to char formation. The fact that coniferyl alcohol pyrolysis produced less char than tetramer 3, trimer 4, and polymer 5 also indicated presence of other contributing factors which have been mentioned previously.



Dimer 1



Dimer 6

Figure F.1. Structure of lignin model compound Dimer 1 and predicted lignin fragment Dimer 6.

Table F.1.

Predicted boiling point of the lignin model compounds aim to show the relative volatility of the model compounds. Boiling point predicted via Joback fragmentation method modified by S.E. Stein.

Lignin Model compound	°C
Dimer 1	469
Trimer 2	693
Tetramer 3	917
Trimer 4	804
Dimer 6	551

Table F.2.

Weight percentage of monomeric species based on the number of carbon atoms in the molecule.

Compounds	Dimer 1	Trimer 2	Tetramer 3	Trimer 4	Polymer 5
C ₇ -C ₉ monomers	10.7	10.7	13.2	13.8	14.7
C ₁₀ monomers	89.3	89.3	86.8	86.2	85.3

Table F.3.

Elution time for dimer 1 for each of the different columns tested.

Column #	Solid phase volume / mm³	Dimer 1 elution time / min
Column 1	37.4	35.0
Column 2	3.8	40.0
Column 4	0.3	23.0

Table F.4.

Quantified lumped pyrolysis product distribution from coniferyl alcohol in wt% of the reactant.

	Wt% of starting model compound
Lights	3.1
Monomers	58.5
Other Dimers	27.3
Char	10.0
Total	98.9

Table F.5.

Quantified pyrolysis product distribution from dimer 1 as a function of the vapor phase residence time in wt% of the reactant.

Residence time (s)	0.5	0.5	1.6	1.6	3.1
Lights	2.0	3.0	2.9	2.4	3.3
Monomers	25.3	27.9	41.6	40.9	51.5
Dimer	63.4	59.3	42.8	44.9	23.5
Other Dimers	7.2	7.9	11.3	9.3	16.9
Char	<u>n.d</u>	<u>n.d</u>	<u>n.d</u>	<u>n.d</u>	<u>n.d</u>
Total	97.9	98.1	98.6	97.6	95.2

Table F.6.
Quantified pyrolysis product distribution from polymer 5 as a function of the vapor phase residence time in wt% of the reactant.

Residence time (s)	0.5	0.5	1.6
Lights	7.5	7.4	7.7
Monomers	41.4	38.9	46.9
Other Dimers	18.6	19.0	13.5
Char	25.0	27.0	24.3
Total	92.5	92.3	92.5
Water *	4.35	3.94	4.92
Total	96.8	96.2	97.4

* Water is estimated based on the total moles of oxygen lost from the observed monomeric species

Table F.7.

Detailed pyrolysis product distribution produced from dimer 1 as a function of the vapor phase residence time in wt% of the reactant fed.

Residence time	0.5	0.5	1.6	1.6	3.1
Light Oxygenated Hydrocarbons (C₁-C₃)	2.0	3.0	2.9	2.4	3.3
Monomeric species					
<u>guaiacol</u> (2-methoxy-phenol)	12.1	12.7	18.7	18.8	24.7
2-methoxy-benzaldehyde	0.4	0.5	0.9	0.8	0.7
2-methoxy-4-vinylphenol	0.1	0.2	0.3	0.3	0.4
4-hydroxy-3-methoxybenzaldehyde	0.5	0.5	0.9	1.1	1.2
1-(4-hydroxy-3-methoxyphenyl)ethan-1-one	0.6	0.4	0.8	1.3	1.6
1-(4-hydroxy-3-methoxyphenyl)prop-2-en-1-one	1.5	2.8	4.5	4.9	5.4
4-(3-hydroxyprop-1-en-1-yl)-2-methoxyphenol	0.6	0.5	0.6	0.7	0.7
3-(4-hydroxy-3-methoxyphenyl) <u>acrylaldehyde</u>	0.3	0.5	0.7	0.7	0.6
4-(3-hydroxyprop-1-en-1-yl)-2-methoxyphenol	5.9	5.2	7.4	7.7	10.2
<u>Coniferyl alcohol</u> (3-hydroxy-1-(4-hydroxy-3-methoxyphenyl)propan-1-one)	1.8	1.3	1.2	1.1	2.5
<i>Other monomeric species</i>	1.5	3.3	5.6	3.5	3.5
Dimeric species					
Dimer 1	63.4	59.3	42.8	44.9	23.5
2-methoxy-4-(2-(2-methoxyphenoxy)vinyl)phenol	1.2	3.8	5.3	5.1	11.2
<i>Other dimeric species</i>	6.0	4.2	6.0	4.3	5.7
Total	97.9	98.1	98.5	97.6	95.2

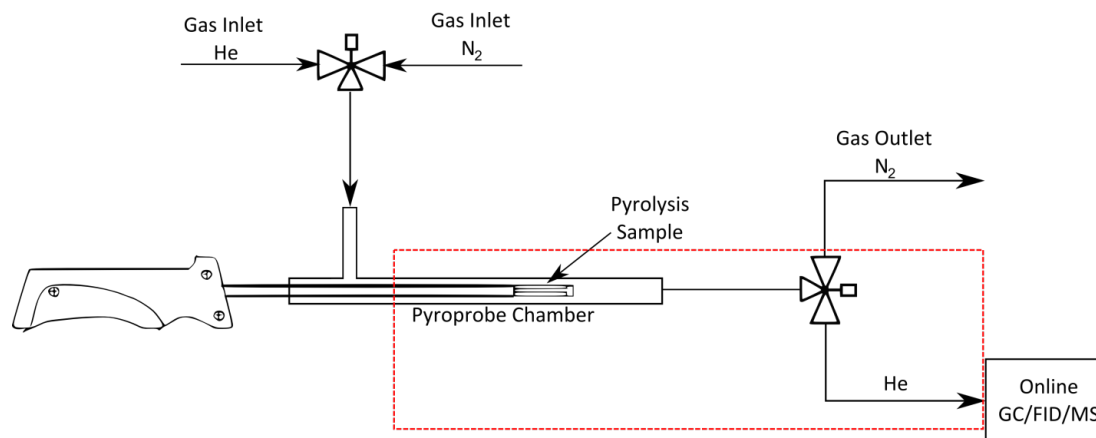


Figure F.2. Schematic of experimental setup (Py-GC/MS) for pyrolysis studies with Lignin model compounds. Red box indicates the heated zone ($T=300^{\circ}\text{C}$).

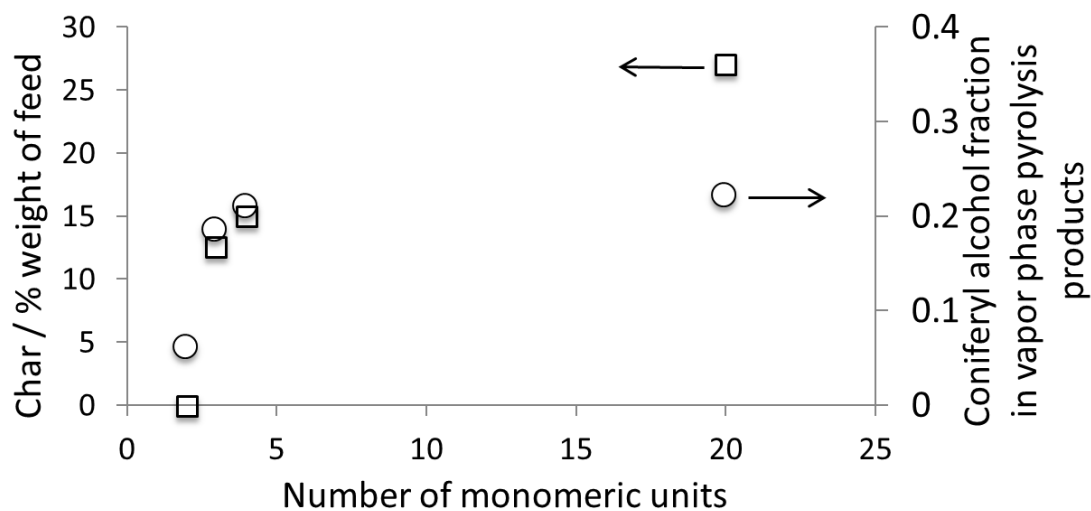


Figure F.3. Char yield and coniferyl alcohol fraction in the vapor phase pyrolysis products as a function of the degree of polymerization of the lignin model compounds.

G. SUPPLEMENTARY INFORMATION FOR A SYNERGISTIC BIOREFINERY BASED ON CATALYTIC CONVERSION OF LIGNIN PRIOR TO CELLULOSE STARTING FROM LIGNOCELLULOSIC BIOMASS

G.1 HPLC/MS Analysis

G.1.1 Instrumentation

All analyses were performed using a Thermo Scientific linear quadrupole ion trap (LQIT)-Fourier transform ion cyclotron resonance (FT-ICR; 7 T magnet) mass spectrometer coupled with a Surveyor Plus HPLC. The HPLC system consisted of a quaternary pump, autosampler, thermostatted column compartment, and photodiode array (PDA) detector. The LQIT was equipped with an ESI source. HPLC eluent (flow rate of 500 $\mu\text{L}/\text{min}$) was mixed via a T connector with a 10 mg/mL sodium hydroxide water solution (flow rate of 0.1 $\mu\text{L}/\text{min}$) and connected to the ion source. This allows for efficient negative ion generation by ESI.[126] The LQIT-FT-ICR mass spectrometer was operated using the LTQ Tune Plus interface. Xcalibur 2.0 software was used for HPLC/MS data analysis. Automated gain control was used to ensure a stable ion signal. A nominal pressure of 0.65×10^{-5} Torr, as read by an ion gauge, was maintained in the higher pressure LQIT vacuum manifold and 2.0×10^{-10} Torr in the FT-ICR vacuum manifold, as read by an ion gauge.

G.1.2 High-performance liquid chromatography/high-resolution tandem mass spectrometry

All samples were introduced into the HPLC/MS via an autosampler as a full-loop injection volume (25 μL) for high reproducibility. 1 mg/L ammonium formate in water (A) and 1 mg/mL ammonium formate in acetonitrile (B) were used as the mobile-phase solvents. Ammonium formate was used to encourage negative ion production.

Table G.1.
HPLC/MS quantitation of all soluble aromatic/phenolic products from
lignin conversion and HDO over Zn/Pd/C catalyst in MeOH.

Biomass Type	Methylparaben (mg) [†]	2,6-Dimethoxy-4-propylphenol (mg)	Dihydroeugenol (mg)	Removed Oxygen (mg) [‡]
Poplar WT-717	5.4	49.4	21.9	2.3
Poplar WT-717 Microporus Cage	9.0	41.6	29.2	2.3
-Recycled Cage Reaction 1	3.5	47.1	23.3	2.3
-Recycled Cage Reaction 2	2.3	29.6	15.0	1.4
-Recycled Cage Reaction 3	2.3	22.0	11.6	1.0
Poplar NM-6	6.7	62.5	30.5	3.0
Poplar WT-LORRE	26.2	56.1	46.0	3.3
Poplar 717-F5H (High S Poplar)	3.2	59.4	12.1	2.3
Lodgepole Pine WT	n/a	n/a	56.5	1.8
White Birch WT	n/a	54.0	26.3	2.6
Eucalyptus WT	n/a	80.0	34.5	3.7
Poplar WT-LORRE no ZnCl ₂	6.8	8.3	6.6	0.5
Poplar WT-LORRE no Pd/C	15.2	0	0	0
Poplar WT-LORRE no H ₂	8.4	1.4	3.7	0.15

A nonlinear, two-slope gradient was used (35% A and 65% B at 30.0 min to 5% A and 95% B at 55.0 min). The column was placed in a thermostatted column compartment that maintained the column at a temperature of 30°C to increase the reproducibility of the retention times and peak widths. The PDA detector for HPLC was set at 280 nm. The exact conditions used for ionization of the analytes and injection of the ions into the mass spectrometer were optimized using a stock solution of 2-methoxy-4-propylphenol in a 0.15 mg/mL NaOH 50:50 acetonitrile/water solution. All ion optics were optimized using the automated tuning features of the LTQ Tune Plus interface. The ESI probe position was optimized manually for optimal signal. The following ESI conditions were used: sheath gas pressure 60 (arbitrary units), auxiliary gas pressure 30 (arbitrary units), sweep gas pressure 0 (arbitrary units), and spray voltage 3.50 kV. For the analysis of lignin conversion products, data-dependent scans were used. Data-dependent scanning involves the instrument automatically selecting the most abundant ions from the ion source, one after another, for further experiments. This allows for separate MS acquisitions to be performed simultaneously for the same ions in the two different mass analyzers of the LQIT-FT-ICR wherein the higher duty-cycle LQIT performs tandem mass spectral acquisitions for the selected ions, while the lower duty-cycle FT-ICR carries out high-resolution measurements for elemental composition determination for the same ions. A resolving power of 400,000 at m/z 400 was used in the FT-ICR. The MS² experiments involve the isolation (using a mass/charge ratio window of 2 Th) and fragmentation of selected ions formed upon negative ion-mode ESI spiked with NaOH. The ions were kinetically excited and allowed to undergo collisions with helium target gas for 30 ms at a q value of 0.25 and at normalized collision energy [211] of 40%. The most abundant product ion formed in the MS² experiments was subjected to a further stage of ion isolation and fragmentation (MS³). See example data in Figure G.1.

Table G.2.
Reaction mass balance after catalytic cleavage and HDO of WT poplar
lignin over Zn/Pd/C catalyst.

Organic Liquid Phase

Ether soluble

dihydroeugenol	4.9%
2,6-dimethoxy-4-propylphenol	6.0%
methylparaben	2.8%
unknown	11%

Water soluble

glucose	1.3%
xylose	5.8%
arabinose	0.4%

Solid Residue

glucan	46%
xylan	6.0%
arabinan	0.4%
unknown	13.9%
TOTAL	98.5%

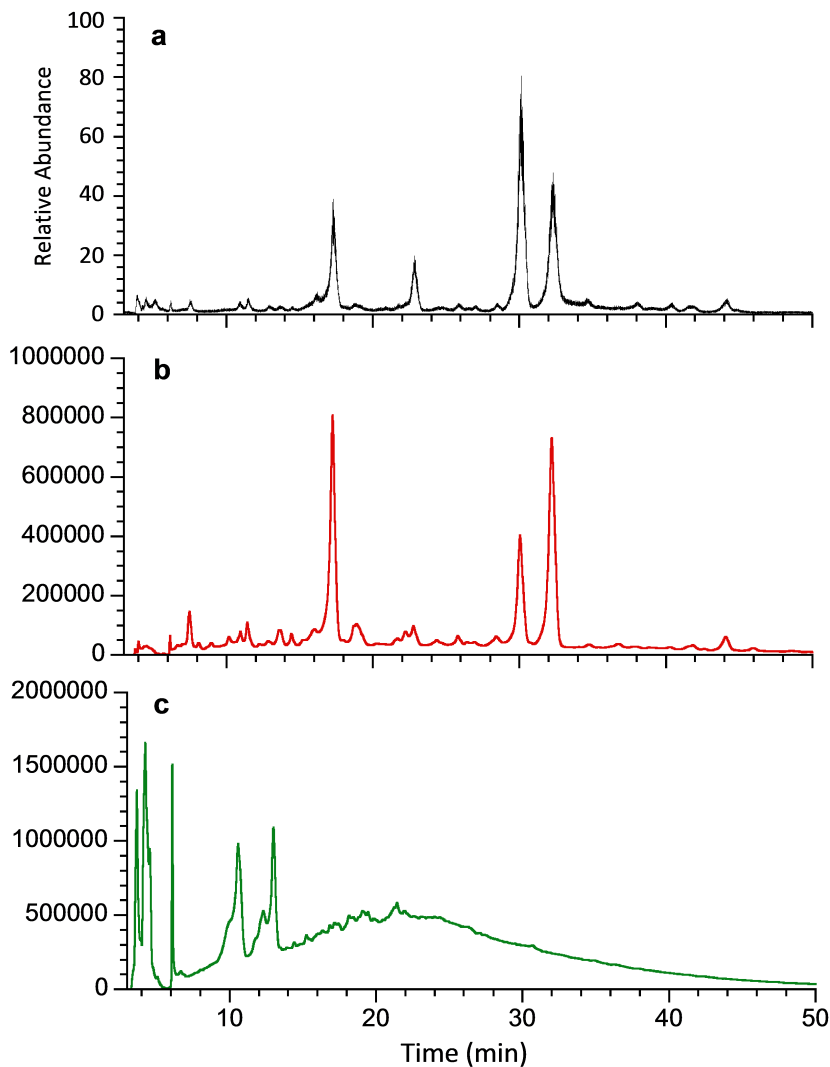


Figure G.1. (a) HPLC/MS and (b) HPLC/UV spectra of poplar WT-LORRE 225°C and 500 psig H₂ in MeOH for 12 hours (c) HPLC/UV spectra of organosolv poplar.

G.1.3 Quantitation of aromatic products from lignin conversion

Standard solutions, each consisting of, dihydroeugenol, 2,6-dimethoxy-4-propylphenol, and methylparaben, were made from 1.0 mM stock solutions and diluted to a final volume of 1.0 mL with the following final concentrations: 0.005, 0.010, 0.050, 0.10, and 0.15 mM. Vanillyl alcohol was used as the internal standard (0.1 mM) and

Table G.3.
DFRC analysis of lignin composition for each of the biomass samples.

Lignin Type	Poplar WT-717	Poplar WT-NM-6	Poplar WT-LORRE	Poplar 717-F5H	WT-Lodgepole Pine	WT-White Birch	WT-Eucalyptus
H (mg)	9.64	8.98	7.34	17.80	5.17	12.58	2.51
G (mg)	80.15	84.20	90.93	48.65	118.99	75.66	117.71
S (mg)	92.88	115.41	86.72	182.38	0.00	84.44	225.99

was added into each of the five standard solutions. A full-loop injection was performed for each standard solution; thus, a total volume of 25 μL was injected onto the column. After separation, selected ion chromatograms for deprotonated dihydroeugenol, 2,6-dimethoxy-4-propylphenol, methylparaben, and vanillyl alcohol were extracted from measured mass spectrometric data by Thermo Xcalibur Quan Browser software and used to create calibration curves.

G.2 Determination of Lignin Content in Washed Biomass

DFRC (Derivatization Followed by Reductive Cleavage). Composition of lignin was determined by DFRC analysis as previously reported.³ Briefly, 15 mg of cell-wall samples were resuspended in 20% acetyl bromide solution, containing 4,4'-ethylidene-bisphenol dissolved in acetic acid as an internal standard. The dissolved lignin solution was dried down, dissolved in 2 mL of dioxane/acetic acid/ water (5/4/1, v/v/v) and reacted with 50 mg of Zn dust for 25 minutes. The reaction products were purified with C-18 SPE columns (Supelco), and acetylated with pyridine/acetic anhydride (2/3, v/v). The lignin derivatives were analyzed by gas chromatography/flame ionization detection (GC-FID) (Model 7890A, Agilent Technologies, Santa Clara, CA) using response factors relative to the internal standard of 0.80 for p-coumaryl alcohol peracetate, 0.82 for coniferyl alcohol peracetate, and 0.74 for sinapyl alcohol peracetate (see Table G.3).

Table G.4.
Acetyl bromide soluble lignin content analysis (ABSL).

Biomass Type	mg ABSL/g CW	% ABSL
Poplar WT-717	160	19
Poplar NM-6	159	18
Poplar WT-LORRE	172	19
Poplar 717-F5H (High S Poplar)	174	20
Lodgepole Pine WT	283	31
White Birch WT	136	16
Eucalyptus WT	215	24

G.2.1 Acetyl Bromide Soluble Lignin (ABSL)

Lignin content was determined by the acetyl bromide method.[212, 213] The dried samples (between 2 and 5 mg) were added to a 10-mL glass tube with 2.5 mL of 25% acetyl bromide in acetic acid. The tubes were tightly sealed with Teflon lined caps. Tubes were stirred overnight at room temperature until the wall tissue completely dissolved. The samples were transferred to a 50-mL volumetric flasks containing 2 mL 2 M NaOH. The tubes were rinsed with acetic acid to complete the transfer. 0.35 mL of 0.5 M freshly prepared hydroxylamine hydrochloride was added to the volumetric flasks which were then made up to 50 mL with acetic acid and inverted several times. The absorbance of the solutions was recorded at 280 nm with UV/Vis spectrophotometer (Model DU730, Beckman Coulter, Brea, CA). (see Table G.4)

Table G.5.
Sugar content of the MeOH fraction after extraction of phenolic products from lignin.

Biomass Type	Glucans (mg)	Xylans (mg)	Arabinans (mg)	Total Sugar (mg)
Poplar WT-717	17	52	8	77
Poplar NM-6	23	78	5	106
Poplar WT-LORRE	12	55	4	71
Poplar 717-F5H (High S Poplar)	16	68	5	89
<u>Lodgepole</u> Pine WT	30	85	5	118
White Birch WT	24	42	4	70
Eucalyptus WT	38	44	3	85

G.3 Determination of Carbohydrates

G.3.1 Liquid Fraction

To determine sugar content in the methanol fraction, 20 mL of H₂O was added to 10 mL methanol and the resulting solution extracted 3 times with 20 mL of Et₂O in each extraction to remove small organic fragments and aromatics (Table G.5). The methanol was then removed under reduced pressure. The carbohydrates in the water layer were quantified by HPLC following the sulfuric acid digestion using a method previously developed by Sluiter et al.[214]

G.3.2 Solid Residue

The remaining cellulosic residue for each biomass was collected on filter paper then dried (Table G.6). The moisture content of each sample was measured and the carbohydrates in the samples were quantified via HPLC after sulfuric acid digestion following the method previously developed by Sluiter et al.[215] HPLC analysis was

Table G.6.
Sugar content of the remaining cellulosic solid residue after lignin conversion over Zn/Pd/C as determined via acid hydrolysis with HPLC analysis.

Biomass Type	Residue Mass (mg)[*]	Glucan (mg)	Xylan (mg)	Arabinan (mg)	Total Sugars (mg)	Total Sugar %
Poplar WT-717	555	383	29	4	416	75
Poplar WT-LORRE	627	433	57	4	494	79
Poplar 717-F5H (High-S Poplar)	572	430	49	4	483	84
Poplar WT-NM-6	477	261	21	4	286	60
Lodgepole Pine WT	546	398	22	4	424	78
White Birch WT	475	365	0	4	369	78
Eucalyptus WT	506	429	0	4	433	86

* Mass of the residue excluding Pd/C catalyst and moisture.

performed using an Aminex HPX-87H 300 × 7.8 mm column (Bio-Rad Laboratories, Hercules, CA) with a refractive index detector (model 2414, Waters Corporation, Milford, MA) in an Alliance Waters 2695 Separations Module (Waters Corporation, Milford, MA). Column temperature was maintained at 65 °C. The mobile phase was 5 mM H₂SO₄ at a flow rate of 0.6 mL/min.

G.4 Enzymatic Hydrolysis

G.4.1 Pd/C free solid residue

Using compositional analysis data, biomass samples equal to the equivalent of 0.1g cellulose were added to plastic vials (Table G.7). Added to each vial was 5.0 ml of citrate buffer (0.1 M, pH 4.8, containing 2% NaN₃). CTEC cellulase was added to the vials at a concentration of 60 fpu (filter paper units), and the total volume was brought to 10 ml with distilled water. Reaction controls for the biomass contained buffer, water, and the identical amount of biomass in 10 ml volume. Cellulase controls

Table G.7.
Enzymatic Hydrolysis of Pd/C free biomass residue after reaction under catalytic HDO conditions.

Biomass	Dry Residue Mass (g)	Cellulose Mass (g)	Cellulose by mass (%)	Glucose Yield at 76 hours (%)	Avg.	Std. Dev.
WT-717 Poplar	0.2310	0.0952	41	12.67		
WT-717 Poplar	0.2292	0.0944	41	8.82	10.75	2.72
Wt-717 Poplar Residue	.1201	0.0940	78	94.55		
WT-717 Poplar Residue	.1224	0.0958	78	96.38	95.47	1.29

were prepared with CTEC cellulase, buffer, and water in 10 ml volume. Samples were sealed and agitated 50°C for 76 hours. After 76 hours, the glucose concentration in each sample was analyzed by HPLC. The low concentrations of glucose detected in control reactions were subtracted from the yields of the corresponding biomass reactions.

G.5 Pyrolysis of the Cellulosic Solid Residue from the Biomass

Pyrolysis experiments were performed using a Pyroprobe 5200 HP supplied by CDS Analytical (Oxford, PA). The pyroprobe is equipped with a resistively heated platinum coil surrounding a quartz tube capable of heating at up to 20,000°C/s. Sample was loaded on the inside of the quartz tube and then pyrolyzed with a heating rate of 1,000°C/s at a temperature of 600°C for 3 seconds. The pyrolysis was performed inside the atmospheric chemical ionization (APCI) source of a Thermo Scientific (Waltham, MA) LTQ linear quadrupole ion trap (LQIT). The pyrolysis products evaporating from the probe were immediately quenched in a 100°C region where they were ionized via either positive or negative mode APCI (see example data in Figure G.2). The corona discharge was operated at 3,000 V with a discharge current of 4 μ A. Ionization of pyrolysis products was achieved with the aid of dopants infused into the APCI source through the APCI probe. In both positive and negative mode APCI, a 50:50 (v/v) solution of ammonium hydroxide:water was co-fed through

a T connector with a 50:50 (v/v) solution of methanol:water. In positive mode APCI, the flow rates were 3 $\mu\text{L}/\text{min}$ for the ammonium hydroxide:methanol solution and 300 $\mu\text{L}/\text{min}$ for the methanol:water solution. With positive mode APCI, analytes were ionized either by protonation ($[\text{M}+\text{H}^+]$) or ammoniation ($[\text{M}+\text{NH}_4^+]$). In negative mode APCI, the flow rates were 1 $\mu\text{L}/\text{min}$ for the ammonium hydroxide:methanol solution and 300 $\mu\text{L}/\text{min}$ for the methanol:water solution. With negative mode APCI, the analytes are deprotonated ($[\text{M}-\text{H}]^-$).

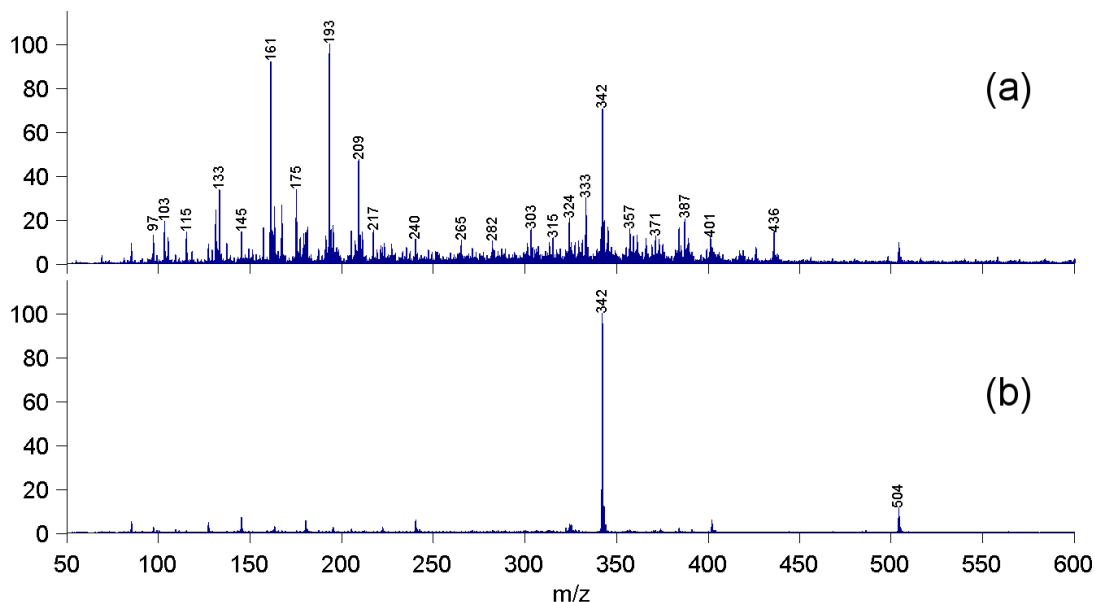


Figure G.2. Pyrolysis of unreacted raw eucalyptus WT (a) and eucalyptus WT residue (b) in Ammonium Positive Attachment mode.

G.6 Hydrodeoxygenation Reaction of Dihydroeugenol to Hydrocarbons, Propylcyclohexane and Propylbenzene - Continuous Vapor-Phase Reactor

G.6.1 Calculating % Yield

The % yield of products is based on the total mass of the products and removed O divided by the mass of the lignin content of each sample as shown in the following equation.

$$\% \text{ yield} = \frac{\text{dihydroeugenol (mg)} + \text{2,6-dimethoxy-4-propyl phenol (mg)} + \text{removed O (mg)}}{\text{initial weight of biomass (mg)} \times \text{ABSL Lignin \%} \times 100} \quad (\text{G.1})$$

The hydrodeoxygenation reaction of 2-methoxy-4-propylphenol (dihydroeugenol) was conducted in a high-pressure, vapor-phase, fixed-bed, plug-flow, continuous, stainless-steel reactor at 300°C and a total pressure of 350 psig. During reaction, the hydrogen (Praxair UHP) partial pressure was 342.4 psig, 2-methoxy-4-propylphenol (Sigma-Aldrich >99%) partial pressure was 1.1 psig, and Argon (used as an internal standard, 99.997%) partial pressure was 6.5 psig. The weight hourly space velocity (WHSV, gram dihydroeugenol.gram catalyst-1.h-1) was 5.1.

The catalyst used was a bimetallic PtMo with a 5 wt% Pt loading and a 1:1 atomic Pt:Mo ratio using multi-walled carbon nanotubes (MWCNT) (Cheaptubes, Inc.) as the support. The catalyst was prepared via sequential incipient wetness impregnation of the MWCNT support. First, an aqueous solution of tetraammineplatinum(II) nitrate ($\text{Pt}(\text{NH}_3)_4(\text{NO}_3)_2$, Sigma-Aldrich) was added and the 5% Pt/MWCNT was dried overnight at 60°C in air. Then, an aqueous solution of ammonium heptamolybdate ($(\text{NH}_4)_6\text{Mo}_7\text{O}_{24} \cdot 4\text{H}_2\text{O}$, Sigma-Aldrich) was added, and the 5% PtMo(1:1)/MWCNT catalyst was dried overnight at 120°C in air. The catalyst was reduced at 200 psig in situ in 50 sccm H₂ and 75 sccm He at 450°C for 2 hours. The catalyst loading in the reactor was 110 mg, with the catalyst bed diluted with quartz powder in a 10:1 quartz to catalyst ratio.

All gas- and vapor-phase products were analyzed with an online Agilent 6890N gas chromatograph with a Carboxen-1000 column connected to a thermal conductivity detector and a SPB-1 capillary column connected to an Agilent Deans Switch 3-way splitter which split the flow to a Flame Ionization Detector and Agilent 5973N Mass Spectrometer. Mass balances closed to 100% ± 5%.

Under these conditions, the product propylcyclohexane was produced in >97% yield, as can be seen in Table G.8. Yield is defined as:

Table G.8.

(a) Product yields of the high-pressure, vapor-phase hydrodeoxygenation reaction of 2-methoxy-4-propylphenol (dihydroeugenol) at 100% conversion in the continuous reactor. (b) Comparison of product yields of the high-pressure, vapor-phase hydrodeoxygenation reaction of dihydroeugenol, 2,6-dimethoxy-4-propylphenol and a 50:50 mixture at 100% conversion in the micro-scale pulse reactor and the continuous reactor.

Product	Yield at 100% conversion of Dihydroeugenol	Yield at 100% Conversion			
		Micro-scale pulse reactor			Continuous reactor
		Dihydroeugenol	2,6-dimethoxy-4-propylphenol	50:50 mixture	Dihydroeugenol
Propylcyclohexane	97.8	97.8	97.5	98.0	97.8
Propylbenzene	0.2	0.5	0.7	0.6	0.2
Propylcyclopentane	0.7	0.6	0.6	0.5	0.7
Methyl-propylcyclopentane	0.5	0.1	0.0	0.0	0.6
Other Products	0.8	1.0	1.2	0.9	0.8

Reaction Conditions: 300 °C, 350 psi, 0.06 mL/min dihydroeugenol, 2.65 L/min H₂, 50 ml/min Ar, 110 mg 5% PtMo(1:1)/MWCNT catalyst

$$\frac{\text{Moles of Ring Product}}{\text{Moles of Dihydroeugenol Converted}} \times \text{Conversion of Dihydroeugenol} \quad (\text{G.2})$$

Ring products include all compounds that contain a ring structure (i.e., all products except methanol, methane, and water that are produced from removal of the oxygenated ring substituents).

G.7 Hydrodeoxygenation Reaction of Dihydroeugenol and 2,6-Dimethoxy-4-propylphenol to Hydrocarbons, Propylcyclohexane and Propylbenzene - Micro-Scale Pulse Reactor

The hydrodeoxygenation reaction of 2-methoxy-4-propylphenol (dihydroeugenol) and 2,6-dimethoxy-4-propylphenol was conducted in a pulsed, high-pressure, fixed-bed reactor at 300°C and a total pressure of 350 psig (24 bar). The pulse reactor used is a modified Pyroprobe 5200 HP, manufactured by CDS Analytical, Inc. A known amount of reactant was loaded in the quartz tube and placed in a chamber at 350 psig pressure of hydrogen. The quartz tube was heated using the Pt coil to vaporize the

reactant, which was carried to the fixed-bed reactor as a pulse by the flowing hydrogen gas. During reaction, a pulse of the reactant (dihydroeugenol (Sigma-Aldrich >99%) and/or 2,6-dimethoxy-4-propylphenol) in hydrogen (Praxair UHP) at a pressure of 350 psig was passed over a catalyst and analyzed using a downstream GC-FID-MS detector.

The catalyst used was a bimetallic PtMo with a 5 wt% Pt loading and a 1:1 atomic Pt:Mo ratio using multiwalled carbon nanotubes (MWCNT) as the support. The preparation and reduction procedure has been described in the earlier section of the document.

All gas- and vapor-phase products were analyzed with an online Agilent 7890N gas chromatograph with a DB1701 column connected to an Agilent Deans Switch 3-way splitter which split the flow to a Flame Ionization Detector and an Agilent 5975C Mass Spectrometer. Mass balances closed to 100% \pm 5%.

Under these conditions, the product propylcyclohexane was produced in >97% yield, as can be seen in Table G.8. Yield is defined as:

$$\frac{\text{Moles of Ring Product}}{\text{Moles of Dihydroeugenol Converted}} \times \text{Conversion of Dihydroeugenol} \quad (\text{G.3})$$

Ring products include all compounds that contain a ring structure (i.e., all products except methanol, methane and water which are produced from removal of the oxygenated ring substituents). Table G.7 shows the comparison of the product yields in the micro-scale pulse reactor and the continuous reactor. Table G.7 shows that >97% yield is obtained for the product propylcyclohexane with either reactant dihydroeugenol or 2,6-dimethoxy-4-propylphenol, or with a 50:50 (V:V) mixture of dihydroeugenol and 2,6-dimethoxy-4-propylphenol.

VITA

VITA

John Charles Degenstein was born on May 28th, 1987 to Joel Alec Degenstein and Rachel Renee Degenstein in Midland, Texas. He has 3 siblings, Kate, Ann and Nick. John grew up in The Woodlands, Texas a suburban neighborhood north of Houston. He graduated from The Woodlands High School in 2005. During high school, John participated in the varsity swimming team and in string orchestra. After high school, John studied Chemical Engineering with a Math minor at the University of North Dakota, graduating *magna cum laude* with his B.S. in 2009. John stayed at the University of North Dakota to work on his Master of Science degree in Chemical Engineering, graduating in 2011. He was advised by Prof. Yun Ji with his Master's thesis topic being related to conversion of lignocellulosic biomass via pretreatment and enzymatic saccharification. John next moved to begin his doctoral studies at Purdue in August of 2011 working under Profs. Rakesh Agrawal, W. Nicholas Delgass, and Fabio H. Ribeiro studying pyrolysis of biomass. John graduated with his Ph. D. in chemical engineering in 2016. During his time in college and graduate school, John won several awards including the Two Time Highest GPA on Men's Swimming and Diving Team (North Dakota, 2007 and 2008), the Ross Fellowship (Purdue, 2011), the Univ. of North Dakota Distinguished Thesis Award for Master's Degree Work (2013), and the Award for Multidisciplinary Research from C3Bio a Dept. of Energy EFRC (2013). Upon graduation, John will join Three Cities Research (TCR, based in New York City, New York) and work for TCR in San Antonio, Texas.